Role of lysosomes in oxidative stress induced regulated cell death

By

Nagakannan Pandian

A thesis submitted to the Faculty of Graduate Studies of

The University of Manitoba

in partial fulfilment of the requirements of the degree of

DOCTOR OF PHILOSOPHY

Department of Physiology and Pathophysiology

University of Manitoba

Winnipeg, Canada

Abstract

Oxidative stress caused either due to overproduction of reactive oxygen species (ROS) or failure of endogenous antioxidants leads to damage of cellular macromolecules and intracellular organelles, which if remain uncontrolled may lead to cell death. Lysosomes play a vital role in maintaining cellular homeostasis by acting as the terminal degradative organelles in autophagic process. Autophagy is a highly regulated pro-survival pathway that delivers the toxic cellular debris and damaged organelles to the highly acidic lysosomes for digestion. Any impairment in lysosomal function can lead to inhibition of autophagic process and protein accumulation. Importantly, due to the presence of potent hydrolyzing enzymes within its lumen, any compromise in lysosomal membrane integrity can lead to severe cellular damage and cell death. Several factors including ROS has been shown to contribute to lysosomal membrane permeabilization (LMP); however, the molecular mechanisms involved in the induction of cell death by LMP during uncontrolled oxidative stress is poorly understood.

In this thesis, I demonstrate that excessive oxidative stress induced by inactivation of endogenous thiol antioxidants such as thioredoxin (Trx) and glutathione (GSH) systems promote oxidative damage of lysosomes and results in activation of apoptotic and non-apoptotic cell death mechanisms. Inactivation of Trx system led to blockade of autophagic process and protein accumulation, which was attributed to loss of lysosomal proteolytic ability and acidity. On further exploration, I discovered that inhibition of Trx system caused oxidative inactivation of cathepsin L, a pro-autophagic lysosomal protease and LMP resulting in the induction of apoptotic pathway. Using small molecule inhibitor screening, cathepsin B was found to be the executioner of apoptotic cell death in this model.

Complementary studies in another model of a recently identified non-apoptotic cell death mechanism known as ferroptosis further confirms cathepsin B as a major executioner of cell death under oxidative stress conditions. Iron mediated lipid peroxidation is a major player in ferroptosis. GSH and glutathione peroxidase 4 (GPX4) are required for proper scavenging of lipid peroxides and hence depletion of GSH or deletion of GPX4 results in ferroptosis. Using pharmacologic and gene-knockout approaches, cathepsin B was identified as the cell death executioner in ferroptosis which was confirmed in primary fibroblasts derived from cathepsin B knockout (*Ctsb*$^{-/-}$) mice. Accordingly, inhibition of cathepsin B also attenuated several markers of cell death and preserved the integrity of mitochondrial and lysosomal membranes. Using inhibitor screening and knockout cell lines, cathepsin B was found to act as a histone H3 protease during ferroptosis that was not previously recognized in any physiological or pathological settings.

Taken together, this thesis establishes that cathepsin B acts as an executioner of cell death induced by LMP following failure of intracellular redox balance. These findings can have implications in several disease conditions including traumatic injuries, neurodegenerative diseases and cancers where oxidative stress plays a key role in occurrence and development of pathologies.

Acknowledgements

Foremost, I am immensely grateful to my supervisor Dr. Eftekhar Eftekharpour for having faith in me and giving me an opportunity to be a part of his research team. This thesis would have been impossible without his continuous guidance, encouragement and support over the years. More than a supervisor, Dr. Eftekharpour has been a good friend of mine and has been instrumental in improving my scientific thinking, communication and writing skills.

I would like to sincerely thank my advisory committee members Dr. Soheila Karimi-Abdolrezaee, Dr. Saeid Ghavami and Dr. Sanjiv Dhingra. I am indebted to your constructive feedbacks, constant support and encouragement. I cannot thank you enough for writing the letters of support, which helped me get many research awards and scholarships. Most importantly, I thank you very much for listening to my loooong presentations with patience.

I would also like to thank my past and present lab mates Ariff, Imam, Albert, Affan, Alennie, Khuong and Shakila and my colleagues at the Regenerative Medicine Program Hardeep, Arsalan, Chris, Scott, Santhosh, Vasu, Robby and Vichy for their critical feedbacks, stimulating discussions and constant support.

I would like to extend my gratitude to Ms. Gail McIndless and Ms. Judith Olfert for their constant help and support over these years.

I thank my friends in Winnipeg Bhavya, Niketa, Glen, Manoj, Anjali, Nivedita and Raghu for their best wishes and motivation.

I owe my special thanks to my past mentors Dr. Thippeswamy and Dr. Veerapur, who have always cared for me and supported constantly throughout my academic years.

I thank all the funding agencies that supported my research over these six years: Research Manitoba, Will-to-Win Foundation, Manitoba Paraplegic Foundation, Health Sciences Centre Foundation, Wings for Life Foundation and the University of Manitoba. I am also thankful to the travel awards provided by Faculty of Graduate Studies – University of Manitoba, Canadian Oxidative Stress Consortium, Society for Redox Biology and Medicine, Nick Shepel Travel Award and Nancy Hettie Clark Travel award from Manitoba Neuroscience Network.

Finally, I would have not come this far without the support and unconditional love from my family. I would like to dedicate this work to my parents Mr. K. Pandian and Mrs. P. Mallika and my brother Dr. Manjunathan Pandian and thank them for having confidence in me and being my source of inspiration.

Table of Contents

List of Tables

List of Figures

List of Abbreviations

3-MA	3-methyl adenine
AIF/AIFM1	apoptosis inducing factor mitochondria associated 1
AL	autolysosome
AMC	7-Amino-4-methylcoumarin
AMS	4-acetamido-4'-maleimidylstilbene-2,2'-disulfonic acid
AP	autophagosome
ATG	autophagy related
Au	auranofin
Baf A1	bafilomycin A1
Bcl-2	B-cell lymphoma 2
BSO	L-buthionine sulfoximine
CA074	L-3-trans-(propylcarbamyl)oxirane-2-carbonyl)-L-isoleucyl-L-proline
CA074-me	CA074 methyl ester
CCK-8	cell counting kit-8
CMA	chaperone mediated autophagy
CQ	chloroquine
CTSB	cathepsin B
CTSD	cathepsin D
CTSL	cathepsin L
CysC	cystatin C
cyto C	cytochrom C
DFO	deferoxamine

DIDS	4,4′-Diisothiocyanatostilbene-2,2′- disulfonate
DMEM	Dulbecco's modified eagle medium
DMSO	dimethyl sulfoxide
DPPH	2,2-diphenyl-1-picrylhydrazyl
DTNB	5,5'-dithiobis-(2-nitrobenzoic acid)
DTT	dithiothreitol
FBS	fetal bovine serum
Fer-1	ferrostatin-1
GAPDH	glyceraldehyde-3-phosphate dehydrogenase
GFP	green fluorescent protein
γ-GCSc	γ-glutamylcysteine synthetase catalytic subunit
γ-GCSm	γ-glutamylcysteine synthetase modifier subunit
GSH	glutathione
GPX4	glutathione peroxidase 4
H_2O_2	hydrogen peroxide
IAA	iodoacetic acid
IAM	iodoacetamide
ITS	insulin-transferrin-selenium
LAMP	lysosomal-associated membrane protein
LPO	lipid peroxidation
LY	lysosome
MAP1LC3B/LC3	microtubule associated protein 1 light chain 3 beta
MCB	monochlorobimane

MDA	malondialdehyde
MEF	mouse embryonic fibroblasts
MMP	mitochondrial membrane permeability
ΔΨm	mitochondrial membrane potential
NAC	N-acetyl-L-cysteine
NADPH	nicotinamide adenine dinucleotide phosphate
NEM	N-ethylmaleimide
Nrf2	nuclear factor erythroid 2–related factor 2
PARP	poly (ADP-ribose) polymerase
PBS	phosphate-buffered saline
Pep-A	pepstatin-A
Prx	peroxiredoxin
qPCR	quantitative real-time polymerase chain reaction
RFP	red fluorescent protein
RFU	relative fluorescence unit
rh-CTSB	recombinant human cathepsin B
rh-CTSL	recombinant human cathepsin L
ROS	reactive oxygen species
S.E.M	standard error of mean
SCR	scramble
SD	serum deprivation
SQSTM1/p62	sequestosome 1
TCA	trichloroacetic acid

TEM	transmission electron microscopy
TMRM	tetramethylrhodamine methyl ester
TRKD	TrxR1 knockdown
Trx	thioredoxin
TrxR	thioredoxin reductase
VDAC1	voltage dependent anion channel 1
WST-1	water soluble tetrazolium-1
WT	wild type
x_c^-	system x_c^- cystine/glutamate antiporter
Z-FY-CHO	benzyl N-[1-[[1-(4-hydroxyphenyl)-3-oxopropan-2-yl]amino]-1-oxo-3-phenylpropan-2-yl] carbamate

List of Copyrighted Materials

Below is the list of manuscripts that I have published/submitted from this thesis work. Chapters 2 and 3 and a portion of chapter 1 were published in the journal *Free Radical Biology and Medicine*, which belongs to Elsevier group. As per Elsevier policy, authors of original work do not require formal permission to use the article in part or full in a dissertation/thesis. Part of chapter 4 was published in *Cellular and Molecular Neurobiology* (Springer Nature group) for which copyright permission has been obtained.

1. **Pandian Nagakannan**, Mohamed Ariff Iqbal, Albert Yeung, James A. Thliveris, Mojgan Rastegar, Saeid Ghavami, Eftekhar Eftekharpour. Perturbation of redox balance after thioredoxin reductase deficiency interrupts autophagy-lysosomal degradation pathway and enhances cell death in nutritionally stressed SH-SY5Y cells. *Free Radical Biology and Medicine 2016;101:53-70.*
2. **Pandian Nagakannan** and Eftekhar Eftekharpour. Differential redox sensitivity of cathepsin B and L holds the key to autophagy-apoptosis interplay after Thioredoxin reductase inhibition in nutritionally stressed SH-SY5Y cells. *Free Radical Biology and Medicine 2017;108:819-831*.
3. **Pandian Nagakannan**, Md. Imamul Islam, Soheila Karimi-Abdolrezaee, Eftekhar Eftekharpour. Inhibition of VDAC1 protects ggainst glutamate-induced oxytosis and mitochondrial fragmentation in hippocampal HT22 cells. *Cellular and Molecular Neurobiology 2019;39(1):73-85*.
4. **Pandian Nagakannan,** Parisa Tabeshmehr, Eftekhar Eftekharpour. Oxidative Damage of Lysosomes in Regulated Cell Death Systems: Pathophysiology and Pharmacologic Interventions. *Free Radical Biology and Medicine 2020;157:94–127.*

Chapter 1

Introduction

Portions of this chapter has been included in the following published review:

Pandian Nagakannan, Parisa Tabeshmehr, Eftekhar Eftekharpour. Oxidative Damage of Lysosomes in Regulated Cell Death Systems: Pathophysiology and Pharmacologic Interventions. *Free Radical Biology and Medicine 2020;157:94–127.*

1.1 Reactive oxygen species

Reactive Oxygen Species (ROS) are continuously formed as a byproduct of cellular respiration and metabolism. Basal or low concentration of ROS mediates various intracellular signaling pathways either through activation of ROS sensors, oxidative modifications of several signaling components and/or modifying the activity of transcription factors (Apel and Hirt, 2004). However, accumulation of ROS either due to increased production or failure of ROS eliminating mechanism/s can lead to a condition called as "oxidative stress", which inflicts detrimental effects on the cellular macromolecules and eventually tissue damage (Lushchak, 2014; Sies, 2015). ROS including oxygen free radical superoxide ($O_2^{\bullet}$), hydroxyl radical ($^{\bullet}OH$), hydroperoxyl ($HO^{\bullet}_2$), hydrogen peroxide (H_2O_2), singlet oxygen ($^1O_2$), nitric oxide ($NO^{\bullet}$) and peroxynitrites ($ONOO^-$) are implicated in the development and progression of numerous pathological conditions. Although mitochondria are the major source of cellular ROS, other organelles including endoplasmic reticulum, peroxisome and lysosomes do generate ROS (Lushchak, 2014; Reczek and Chandel, 2015).

Under physiological conditions, several endogenous antioxidants, either through enzymatic or non-enzymatic reactions, limit the accumulation of ROS to prevent any cellular damage. As illustrated in Fig.1.1, superoxide dismutase (SOD) catalyzes the conversion of $O_2^{\bullet}$ to H_2O_2, which in turn is decomposed to H_2O and O_2 by catalase. Peroxidases like glutathione peroxidases and peroxiredoxins can also catalytically breakdown H_2O_2 (Wood et al., 2003; Valko et al., 2007). H_2O_2 in the presence of transition metals like Fe^{2+} and Cu^+ can generate a highly unstable and extremely reactive $^{\bullet}OH$ (and hydroxyl anion (OH^-)) through a process called as "Fenton Reaction" (Valko et al., 2007). The spontaneous reaction between H_2O_2 and $O_2^{\bullet}$ can also produce $^{\bullet}OH$ (and molecular oxygen) through Haber-Weiss reaction (Kehrer, 2000). Moreover, $O_2^{\bullet}$ can react with

$NO^{\bullet}$ to form $ONOO^{-}$, which in turn can generate nitrogen dioxide ($NO_2^{\bullet}$) and $^{\bullet}OH$ (Radi, 2018). Unlike H_2O_2 and $O_2^{\bullet}$, which have half-lives of 10^{-5} s and 10^{-6} s respectively, $^{\bullet}OH$ are comparatively short lived with a half-life of 10^{-9} s (Giorgio et al., 2007). Due to relatively long half-life, H_2O_2 can diffuse readily across biological membranes and exert its actions further away from its site of production (Kohen and Nyska, 2002). In contrast, due to its negative charge, $O_2^{\bullet}$ is unable to pass through the membranes and hence can react with its substrates only in its immediate environment. Similarly, due to short half-life (limiting its diffusion capacity) and indiscriminate reactivity, $^{\bullet}OH$ can modify biological molecules only in proximity of its site of production (D'Autreaux and Toledano, 2007).

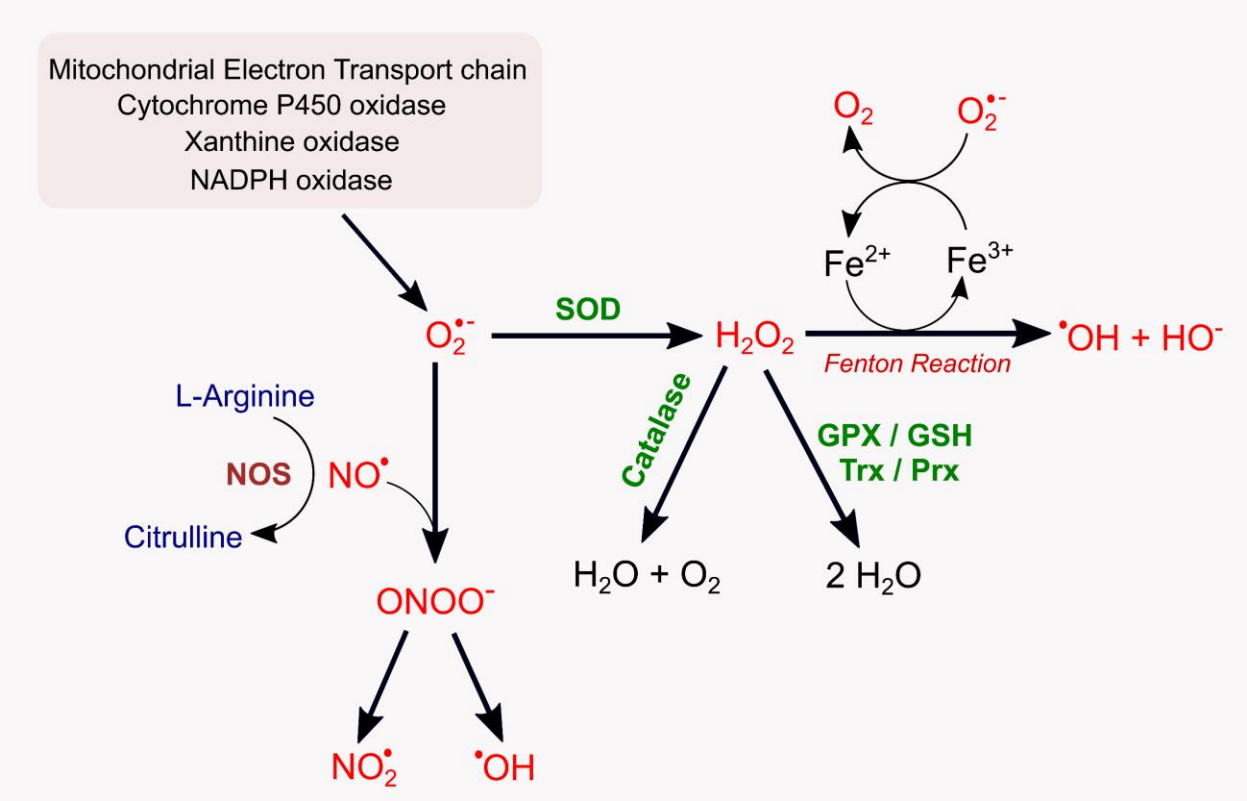

Figure 1.1. **Production of ROS and antioxidant defense systems.** O_2, molecular oxygen; $O_2^{\bullet}$, superoxide radical; H_2O_2, hydrogen peroxide; $^{\bullet}OH$, hydroxyl radical; OH^{-}, hydroxyl anion; $NO^{\bullet}$, nitric oxide; $ONOO^{-}$, peroxynitrites; $NO_2^{\bullet}$, nitrogen dioxide; Fe^{2+}, ferrous ion; Fe^{3+}, ferric ion; SOD, superoxide dismutase; GSH, glutathione; GPX, glutathione peroxidase; Trx, thioredoxin; Prx, peroxiredoxin; NOS, nitric oxide synthase.

1.2 Oxidative damage of biomolecules

ROS, when uncontrolled, can modify the cellular biomolecules including RNA, DNA, proteins and lipids either through oxidation or nitrosylation. These oxidative modifications can cause changes in structure, integrity, solubility, activity and/or susceptibility to degradation (Berlett and Stadtman, 1997; Jung and Grune, 2008; Thanan et al., 2015).

1.2.1 Protein oxidation

ROS can cause direct damage to the proteins by attacking the polypeptide backbone or amino acid side chains resulting in fragmentation, structural changes, loss of function or activity of proteins (Stadtman and Levine, 2000; Grimm et al., 2012). While oxidation of amino acids including aspartate, glutamate and proline residues can lead to cleavage of peptide backbone, protein carbonyls are formed due to oxidation of lysine, arginine, histidine, and proline (Mirzaei and Regnier, 2006; Costa et al., 2007). The secondary oxidation products of other biomolecules including lipids, carbohydrates and nucleic acids can also cause protein oxidation through formation of protein adducts (Bau et al., 2002; Kurbanyan et al., 2003; Grimsrud et al., 2008; Gentile et al., 2009). Reversible oxidation of amino acids as observed in cellular signaling events are revoked by the intracellular antioxidants. Conversely, when the proteins undergo irreversible oxidative damage beyond repair due to the formation of hydroxyl, carbonyl, sulfinic and sulfonic derivatives, the oxidized proteins are cleared by the cellular protein degradation machineries, the ubiquitin proteasome system and autophagy-lysosomal system. However, when these oxidized proteins are not degraded, this can lead to further severe oxidation of amino acid residues, cross-linking to other proteins and accumulation of protein aggregates (Costa et al., 2007; Jung and Grune, 2008; Pajares et al., 2015). Accumulation of oxidatively modified proteins like protein carbonyls and protein-adducts including ceroid, lipofuscin, advanced aged glycation end products

and α-synuclein have been documented during natural aging and many pathological conditions like neurodegenerative and cardiovascular diseases, muscular dystrophy, arthritis, atherosclerosis, cataracts and diabetes mellitus (Yin, 1996; Dalle-Donne et al., 2003; Martinez et al., 2010; Reeg and Grune, 2015).

The sulfur containing amino acids, cysteine and methionine, are highly prone to oxidative changes and are most frequently oxidized (Hoshi and Heinemann, 2001b). These thiol (-SH) amino acids contribute to the preservation of structural integrity, functionality of many enzymes and redox cycling of endogenous antioxidants such as glutathione (GSH) and thioredoxin (Trx) (Levine et al., 2000). As shown in Fig. 1.2, oxidation of cysteine can generate sulfenic acid (-SOH), sulfinic acid ($-SO_2H$) and sulfonic acid ($-SO_3H$). While sulfenylation can be reversed by thioredoxin or GSH-dependent reductases, sulfinylation can only be reduced by a specialized enzyme, sulfiredoxin. Sulfonylation, on the contrary, is an irreversible oxidation which can cause permanent structural and functional changes in proteins. Similarly, NO• radical can react with the thiol group of cysteine to form a reversible post-translation modification, S-nitrosothiol (-SNO). Reactive cysteine residues in proteins can also be modified by hydrogen sulfide (H_2S) through a process called protein sulfhydration resulting in the conversion of thiol group of cysteine to persulfide group (-SSH) (Chung et al., 2013; Nakamura et al., 2013). Apart from oxidative/nitrative changes, cysteine residues can also undergo lipid modifications such as palmitoylation, prenylation, farnesylation and geranylgeranylation (Farnsworth et al., 1994; Zhang and Casey, 1996; Rodenburg et al., 2017). Likewise, oxidation of methionine produces methionine sulfoxide, which can undergo further oxidation to from methionine sulfone. While methionine sulfoxide can be reduced by methionine sulfoxide reductases, methionine sulfone is an irreversible modification (Drazic and Winter, 2014; Reeg and Grune, 2015) (Fig. 1.3).

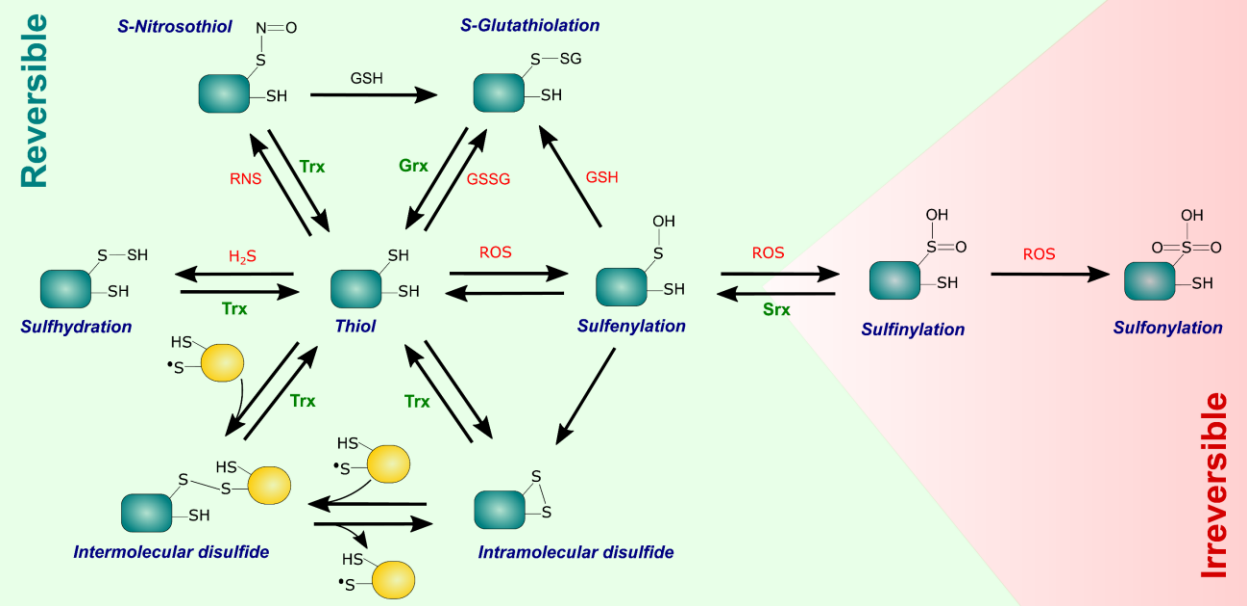

Figure 1.2. **Reversible and irreversible oxidative modifications of cysteine**. ROS, Reactive Oxygen Species; RNS, Reactive Nitrogen Species; GSH, reduced glutathione; GSSG, oxidized glutathione; Grx, glutaredoxin, Trx, thioredoxin; Srx, sulfiredoxin; H_2S, hydrogen sulfide.

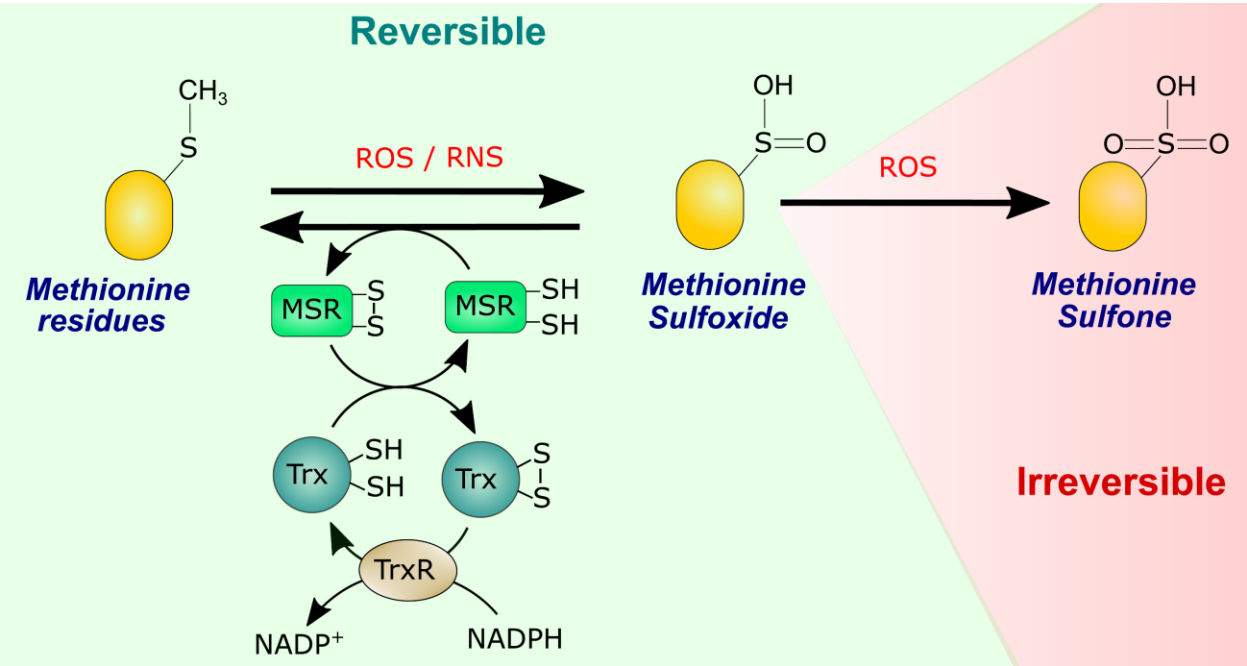

Figure 1.3. **Reversible and irreversible oxidative modifications of methionine.** ROS, reactive oxygen species; RNS, reactive nitrogen species; MSR, methionine sulfoxide reductase; Trx, thioredoxin; TrxR, thioredoxin reductase; NADPH, nicotinamide adenine dinucleotide phosphate (reduced); $NADP^+$, nicotinamide adenine dinucleotide phosphate (oxidized).

1.2.2 Lipid peroxidation

Lipid peroxidation is a process in which free radicals extract an electron from lipid molecules in the cell membrane resulting in the generation of primary oxidizing intermediates such as lipid peroxyl radicals (LOO$^{\bullet}$) and lipid hydroperoxides (LOOH) and secondary products including propanal, hexanal, and 4-hydroxynonenal (4-HNE) and malondialdehyde (MDA) leading to the loss of membrane properties. Unsaturated phospholipids, glycolipids and cholesterols are the major targets of lipid peroxidation (Girotti, 1998; Yin et al., 2011; Ayala et al., 2014). Lipid peroxidation can occur by both enzymatic and non-enzymatic processes. ROS like $^{\bullet}$OH, HO$^{\bullet}_2$ and $ONOO^-$ are potent inducers of lipid peroxidation and could initiate a lipid oxidation chain reaction resulting in membrane damage (Bielski et al., 1983; Schneider et al., 2008). Similarly, enzymes including cyclooxygenases, lipoxygenases and cytochrome P450 catalyzes the peroxidation of poly unsaturated fatty acids (PUFA) or arachidonic acid to generate various metabolites including stable hydroxides and lipid hydroperoxides. These metabolites are further processed by several other enzymes to generate respective biologically active signaling molecules such as prostaglandins, leukotrienes or thromboxanes (Girotti, 1998; Smith et al., 2011; Ayala et al., 2014; Gruber et al., 2015). However, few reactive metabolites formed in the process can oxidize other lipids initiating a chain reaction or form adducts with proteins and nucleic acids. For example, Leukotriene A4 (LTA4), a conjugated triene epoxide is formed as an intermediate by 5-lipoxygenase from arachidonic acid during the generation of biologically active leukotrienes B4 and C4. LTA4, due to its high reactivity can form adducts with nucleosides and nucleotides in DNA and RNA (Reiber and Murphy, 2000; Hankin et al., 2003). Similarly, other highly reactive lipid hydroperoxide metabolites including 9,12-dioxo-10(E)-dodecenoic acid (DODE), 4,5-epoxy-2(E)-decenal (EDE), 4-HNE and MDA can form adducts with DNA and proteins (Slatter et al.,

2004; Lee et al., 2005; Williams et al., 2007; Pizzimenti et al., 2013). The biological effects of secondary lipid peroxidation metabolites such as MDA and 4-HNE are well studied and are implicated in aging and many pathological conditions including inflammation, atherosclerosis, neurodegenerative, cardiovascular, renal and hepatic diseases, diabetes and cancer (Negre-Salvayre et al., 2008; Iacobini et al., 2009; Garcia et al., 2013).

The reactive lipid hydroperoxides are mainly metabolized by glutathione peroxidase 4 (GPX4) to corresponding lipid alcohols using GSH as electron donor (Brigelius-Flohe, 1999). It is also known as phospholipid hydroperoxide glutathione peroxidase (PHGPx) due to its unique ability to reduce hydroperoxides in phospholipids and cholesterol in mammalian cells (Imai and Nakagawa, 2003). GPX4 is widely distributed and can be found in cytosol, mitochondrial and nuclear compartments (Schneider et al., 2009). Failure of the hydroperoxide neutralization can lead to increase in membrane permeability, organelle damage and cell death (Wong-Ekkabut et al., 2007). For instance, cardiolipin, a phospholipid exclusively present in inner and outer mitochondrial membrane is highly prone to peroxidation (Lesnefsky and Hoppel, 2008; Paradies et al., 2009). Cardiolipin oxidation can cause loss of mitochondrial integrity and function. More importantly, cytochrome c (cyto C) strongly binds with cardiolipin but not cardiolipin hydroperoxide. Hence, oxidation of cardiolipin can result in induction of intrinsic apoptotic cascade due to the rapid release of cyto C into the cytosol. Overexpression of mitochondrial GPX4 was shown to efficiently inhibit cardiolipin oxidation and its consequences (Nomura et al., 2000). Very recently, lipid peroxidation has been found to play the central role in the induction of ferroptosis, a novel iron dependent cell death mechanism. This is characterized by massive accumulation of lipid peroxidation products and can be induced by either depletion of GSH or inhibition / deletion of GPX4. Approaches such as iron chelation, lipoxygenase inhibition and lipophilic antioxidants such

as vitamin E, all of which target the buildup of lipid peroxides, can mitigate ferroptotic cell death (Dixon et al., 2012; Conrad et al., 2018; Shah et al., 2018). Similarly, Trx dependent peroxidase, peroxiredoxins, can also metabolize lipid hydroperoxides and protect the phospholipids of cellular membranes (Luo et al., 2010; Zuo et al., 2018). Knockout of members of peroxiredoxin family has been shown to cause severe lipid peroxidation and cell death (Baskin-Bey et al., 2005; Tran et al., 2018). Recently, peroxiredoxin 6 was demonstrated to negatively regulate ferroptosis by inhibiting excessive lipid peroxidation (Lu et al., 2019).

1.2.3 Oxidative damage to nucleic acids

ROS like $^1O_2$, $^{\bullet}OH$, $HO^{\bullet}_2$ and $ONOO^-$ are shown to readily react with purine and pyrimidine bases of DNA and RNA producing over 80 different varieties of oxidatively modified DNA lesions including diastereomers and unstable hydroperoxide precursors (Cadet et al., 2003; Wagner and Cadet, 2010; Cadet et al., 2011). Due to low redox potential, guanine is highly prone to oxidative attack by ROS and nitrating species generating 8-oxoguanine (8-oxoG), 8-hydroxydG (8-OHdG) and 8-nitroguanine (8-nitroG) (Steenken and Jovanovic, 1997). These oxidative changes can cause single strand and double strand DNA breaks, which may lead to mutagenesis, if not repaired. DNA lesions including 8-oxoG, 8-OHdG and thymine glycol are used as reliable biomarkers of oxidative stress in several pathologies including neurodegeneration and carcinogenesis (Kikuchi et al., 2002; Dedon and Tannenbaum, 2004; Fukae et al., 2005; Kryston et al., 2011). Repair mechanisms such as base excision repair (BER) and nucleotide excision repair (NER) process the oxidatively generated DNA lesions stress (Kryston et al., 2011). Inactivation of DNA repair mechanism due to oxidative damage or failure of antioxidant defense system can also cause DNA lesions. In melanoma cells and human skin fibroblasts, depletion of GSH retarded the BER of oxidative purine modifications induced by radiation (Eiberger et al., 2008). A similar impairment in BER

was observed in Trx deficient cells and inactivation of Trx by overexpression of TXNIP was associated with enhanced oxidative DNA damage (Kim et al., 2013a; Oberacker et al., 2018).

1.3 Cellular antioxidants

The redox status of the cell is determined by the balance between ROS and its counteractive molecules called antioxidants, which nullify the effects of ROS through either enzymatic and non-enzymatic actions. Several studies have demonstrated that the absence / inactivation of these antioxidants can cause severe oxidative stress and have detrimental impact on the cellular growth, proliferation and survival (Ho et al., 2004; Turanov et al., 2010; Watanabe et al., 2014a; Muri et al., 2018). As shown in Fig. 1.1, several enzymatic antioxidants such as SOD, catalase, peroxidases such as glutathione peroxidase and thioredoxin / peroxiredoxin system modulate the free radical chain reactions and neutralize ROS. Similarly, non-enzymatic antioxidants such as glutathione, vitamin A, C and E, α-lipoic acid, metal binding proteins, uric acid, bilirubin and melatonin rapidly inactivate ROS and thereby terminating the free radical chain reaction and prevent further oxidative cellular damage (Aslani and Ghobadi, 2016; Mironczuk-Chodakowska et al., 2018). As discussed above, ROS can reversibly / irreversibly oxidize the cellular macromolecules and thus rendering them inactive or reactive, which may cause further oxidative damage to the cell. These oxidative modifications can occur on enzymes, carriers or transcription factors in the cytosol, mitochondria, nucleus or plasma membrane. Endogenous reductants like GSH or Trx functions mainly by reducing the oxidized biomolecules directly or indirectly by acting as a recycler / co-factor for the enzymatic / non-enzymatic ROS decomposer and thus ensures normal physiology of the cells (Ren et al., 2017).

1.3.1 Thioredoxin system

Thioredoxin (Trx) and its reducing enzyme Thioredoxin reductase (TrxR) together with NADPH constitute the Thioredoxin system. There are mainly three isoforms identified in mammalian cells, Trx1 and TrxR1 in cytoplasm, Trx2 and TrxR2 in mitochondria and a third isoform in testis, Trx3 and TrxR3. Trx is a small (12 kDa) multifunctional protein expressed ubiquitously and was first identified as a hydrogen donor for ribonucleotide reductase in *Escherichia coli*. Trx functions by catalyzing the dithiol / disulfide oxido-reduction with the help of the conserved cysteine residues in their active site (-Cys^{32}-Gly-Pro-Cys^{35}-) and in this process gets oxidized (Trx-S_2). TrxR is a NADPH dependent selenocysteine containing enzyme that catalyzes the transfer of electrons from NADPH to Trx-S_2, reducing it to Trx-SH_2, the active form (Laurent et al., 1964; Holmgren, 1985; Nishiyama et al., 2001; Holmgren and Lu, 2010) (Fig. 1.4). In addition to the two active site cysteine residues, human Trx also contains three structural cysteine moieties at Cys^{62}, Cys^{69}, and Cys^{73}. These structural cysteine residues also play a critical role in regulating the catalytic activity of Trx. An intermolecular Cys^{73}-Cys^{73} homodimer disulfide linkage can cause loss of catalytic activity of Trx. This Cys^{73} homodimer of Trx was found to be inaccessible by TrxR (Gasdaska et al., 1996). Likewise, formation of a second disulfide bond between Cys^{62} and Cys^{69}, in addition to the active site disulfide, was shown to inactivate Trx (Watson et al., 2003). Interestingly, this Cys^{62} and Cys^{69} disulfide linkage can be reduced by glutaredoxin, but not TrxR (Du et al., 2013). Similarly, S-nitrosylation of Cys^{69} and Cys^{73} can also inhibit the oxido-reductase activity of Trx and make it inaccessible to TrxR (Hashemy and Holmgren, 2008).

Trx in its reduced form (Trx-SH_2) can effectively reduce cysteine modifications such as sulfenylation, S-nitrosylation, S-sulfhydration and disulfide bond formation and rescue the protein function (Spector et al., 1988a; Wu et al., 2011; Ju et al., 2016) (Fig. 1. 2). Trx also plays a crucial

role in methionine reduction reactions by recycling Methionine sulfoxide reductase, which gets oxidized and inactivated in the process of reducing methionine sulfoxide to methionine (Reeg and Grune, 2015) (Fig. 1.3). Trx, by its oxidoreductase activity, recycles Peroxiredoxins (Prx-S_2 to Prx-SH_2), which in turn decomposes H_2O_2, organic hydroperoxides and $ONOO^-$ (Dubuisson et al., 2004; Trujillo et al., 2007).

Trx expression is induced by various oxidative stimuli through antioxidant responsive element (ARE) by activation of Nuclear factor erythroid 2-related factor 2 (NRF2) (Kim et al., 2003). Trx interacts with a number of target proteins and modulates several physiological processes inside the cell including maintaining reducing environment, controlling cell cycle, inhibiting apoptosis and inflammation, enhancing transcription of other antioxidants such as superoxide dismutase, promote vasculogenesis and increase neural stem cell proliferation (Nishiyama et al., 2001; Samuel et al., 2010; Song et al., 2011; Tian et al., 2014). While genetic knockdown of either Trx1 or Trx2 is lethal at embryonic stage, their overexpression has been shown to increase life span in mice (Matsui et al., 1996; Nonn et al., 2003; Perez et al., 2011; Pickering et al., 2017). The protective effects of Trx and TrxR proteins are well studied in the context of cancer cells. Upregulation of Trx system in some cancers has been linked to their enhanced resistance to anti-tumor treatments and therefore pharmacological and molecular inhibition of Trx system to inhibit cancer growth is routinely pursued (Gorrini et al., 2013a). Overexpression of Trx in experimental models of neuronal, cardiac and renal ischemic injuries had shown better tissue preservation and improved functional recovery (Takagi et al., 1999; Kasuno et al., 2003; Shao et al., 2014).

The cytoprotective effect of Trx is mediated by its capacity to inhibit the activation of apoptosis signal kinase 1 (Ask1). Under normal conditions, Trx binds to ASK1 and inhibits apoptosis, however during severe oxidative stress conditions, Trx get oxidized and dissociates from ASK1.

Once dissociated, ASK1 can get activated by either phosphorylation or by multimerization through formation of disulfide bonds, which further activates the JNK and p38 MAP kinase pathways to induce cell death (Tobiume et al., 2001; Nadeau et al., 2007) (Fig. 1.4). Trx can also modulate the protease function of caspases -3, -6 and -8 and impact the progression of apoptosis through oxidation, transnitrosylation and denitrosylation (Mitchell and Marletta, 2005; Mitchell et al., 2007; Sengupta et al., 2010; Islam et al., 2019).

Trx is inactivated mainly by two ways – oxidation of cysteines or by binding with a natural inhibitor called Thioredoxin Interacting Protein (TXNIP) through formation of a disulfide bond between Cys247 in Txnip and Cys32 in Trx1 (Zhou and Chng, 2013; Hwang et al., 2014). The binding of TXNIP to Trx is dependent on the redox status of Trx; TXNIP neither binds to oxidized nor mutant Trx, proving that a reduced Trx active site is essential for TXNIP action (Hwang et al., 2014; Shalev, 2014).

In many cases, the binding of Trx to TXNIP appears to mutually inhibit each other's cellular functions. For instance, ROS induced dissociation of Trx from TXNIP was shown to facilitate the interaction of TXNIP to NLRP3 (nucleotide binding domain leucine-rich-containing family, pyrin domain containing 3) inflammasome resulting in the activation of caspase-1 and production of pro-inflammatory cytokines such as Interleukin – 1beta (IL-1β) and IL-18 (Zhou et al., 2010; Chen et al., 2017) (Fig. 1.4). Similarly, TXNIP can translocate to mitochondria in response to oxidative stress, where TXNIP binds to Trx2 leading to dissociation and activation of Ask1 and resulting in mitochondrial pathway mediated cell death (Chen et al., 2008a; Saxena et al., 2010).

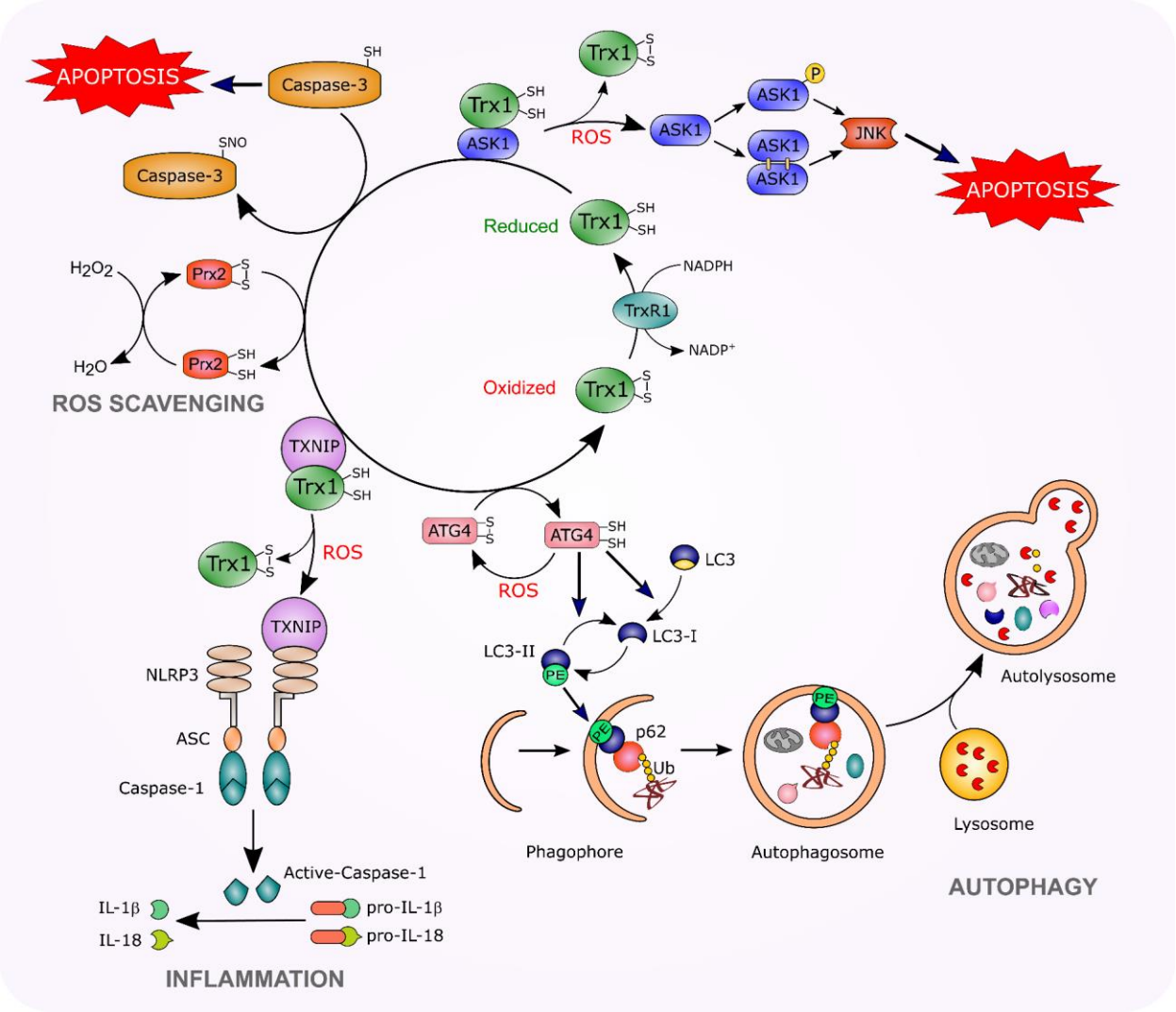

Figure 1.4. **Cellular functions of thioredoxin**. Trx1 in its reduced state mediates the reduction of several oxidized target proteins including ATG4 and peroxiredoxins (Prx). ATG4 is a major component of autophagy system and mediates the conversion of LC3 to LC3-I facilitating the addition of phosphatidylethanolamine (PE) to form LC3-PE (LC3-II), which allows it to bind to the autophagosome membrane. Trx participates in the decomposition of H_2O_2 by acting as a redox recycler of Prx. Oxidation of Trx1 in response to oxidative stress leads to dissociation of TXNIP, which can bind and activate NLRP3 inflammasome resulting in secretion of pro-inflammatory cytokines such as IL-1β and IL-18. Similarly, dissociation of ASK1 from Trx leads to the activation of ASK1 and activation of downstream intermediaries such as JNK signaling resulting in apoptosis. Additionally, Trx1 also controls apoptosis by mediating the S-nitrosylation of active site cysteine residues in Caspase-3 rendering them inactive. Oxidatively inactivated Trx is rejuvenated by the action of TrxR which transfers electrons from NADPH to Trx.

1.3.2 Glutathione system

Glutathione (GSH, L-γ-glutamyl-L-cysteinyl-glycine) is the most abundant non-protein sulfhydryl and acts as an important reservoir of amino acid cysteine in the cells (Franco and Cidlowski, 2009). GSH is a tripeptide molecule made up of amino acids – cysteine, glycine and glutamate. GSH is synthesized by a two-step reaction catalyzed by γ-glutamylcysteine synthase (γ-GCS) and GSH Synthetase. γ-GCS, also known as glutamate-cysteine ligase (GCL), is a heterodimer composed of a modulatory subunit (γ-GCSm or GCLM) and a catalytic subunit (γ-GCSc or GCLC). In the first step, γ-GCS catalyzes the ATP dependent rate limiting reaction by adding glutamate to cysteine to create L-γ-glutamyl-L-cysteine. GSH Synthetase, a homodimer, then adds glycine to L-γ-glutamyl-L-cysteine to generate GSH (Dickinson and Forman, 2002; Aslani and Ghobadi, 2016) (Fig. 1.5).

GSH can directly scavenge free radicals including $^{1}O_2$, $O_2^{\bullet}$, $^{\bullet}OH$ and DNA radicals and also acts as an essential co-factor for the selenium dependent enzyme GPX, which detoxifies peroxides such as H_2O_2, LOO• and $ONOO^-$. In the process of neutralizing ROS, directly or indirectly, GSH is oxidized to form GSSG (dimer), which is then reduced to GSH by the action of glutathione reductase with the utilization of NADPH. The increase in the ratio of GSSG to GSH has been recognized as an index of severity of oxidative stress (Franco and Cidlowski, 2009; Aslani and Ghobadi, 2016). Indeed, oxidation of GSH to GSSG has been shown to precede DNA damage and apoptosis (Esteve et al., 1999). Consistently, depletion of GSH causes increased oxidative stress, mitochondrial dysfunction, apoptosis through both intrinsic and extrinsic pathways and necrosis (Canals et al., 2001; Armstrong et al., 2002; Higuchi, 2004; Franco et al., 2007; Franco et al., 2008; Franco et al., 2014). Recently, GSH depletion was shown to cause Ferroptosis, a novel iron dependent cell death mechanism initiated by the accumulation of lipid peroxides due to the failure

of GSH/GPX4 machinery (Dixon et al., 2012; Conrad et al., 2018). Similarly, increasing the intracellular GSSG content also have been shown to cause cell death (Park et al., 2009). High levels of GSH and GPX has been shown to confer resistance against various forms of cell death and DNA damage (Friesen et al., 2004; Cazanave et al., 2007; Dannenmann et al., 2015).

GSH is also involved in the removal of xenobiotics and toxic metabolites by the action of glutathione-S-transferase (GST) leading to the formation of GSH adducts as in the case of detoxification of lipid peroxidation product, 4-HNE (Balogh and Atkins, 2011). GSH can also form an adduct with NO generating S-nitrosoglutathione (GSNO), which acts as a reservoir for NO thereby facilitating S-nitrosylation of proteins (Keszler et al., 2010; Broniowska et al., 2013). GSNO is the most abundant low molecular weight S-nitrosothiol (SNO) and plays a significant role in NO dependent regulatory mechanisms including smooth muscle relaxation and inhibition of platelet aggregation (Debelder et al., 1994). GSNO reductase (also known as alcohol dehydrogenase 3), using NADH as a cofactor, reduces GSNO to GSSG and ammonia (NH_3) (Jensen et al., 1998).

GSH and GSSG can react with protein thiols to form mixed disulfides by a process known as protein glutathionylation to regulate the protein function. This process can proceed either by the reaction of a sulfenylated protein with GSH or disulfide exchange reaction with GSSG or addition of GSH to S-nitrosylated cysteine residue (Xiong et al., 2011) (Fig. 1.2). Protein S-glutathionylation has been shown to amplify apoptotic signals (Di Stefano et al., 2006; Anathy et al., 2009). Contrastingly, glutathionylation can also cause inactivation of caspases-3 (Huang et al., 2008). Glutaredoxins (Grx) are oxidoreductases that act in conjunction with GSH and NADPH dependent glutathione reductase to catalyze the reduction of reversible protein mixed disulfides and S-glutathionylated proteins. Grx deglutathionylates the proteins through a thiol / disulfide

exchange reaction. Grx initially reacts with the S-glutathionylated protein and forms an intermediate, Grx-S-SG. The oxidized Grx or the Grx intermediate is then reduced by GSH yielding Grx-SH_2 (reduced Grx) and GSSG, which is reduced by glutathione reductase to GSH (Xiong et al., 2011). Four isoforms of Grxs are expressed in human: Grx1, Grx2, Grx3, and Grx5 (Aslani and Ghobadi, 2016). Certain members of Grx family, Grx1 and Grx2, can also promote S-glutathionylation of proteins such as actin and GAPDH (Gallogly et al., 2008). Apart from removal of GSH from proteins, Grx has been shown to play an important role in maintaining redox homeostasis through reactivating Trx by reducing the non-active site disulfide of Trx, which cannot be reduced by TrxR (Du et al., 2013). Conversely, components of Trx system can also act as backup for few Grxs. During conditions when reactivation of Grx by GSH is substantially decreased due the increase in GSSG/GSH ratio, Grx2 was shown to be reactivated using the reducing equivalents from TrxR (Johansson et al., 2004). In addition, Grx can also act as an alternative recycling mechanism for peroxiredoxin 2 by reducing the mixed disulfides formed between GSH and the active site cysteine moieties of Prx (Rahantaniaina et al., 2013; Peskin et al., 2016).

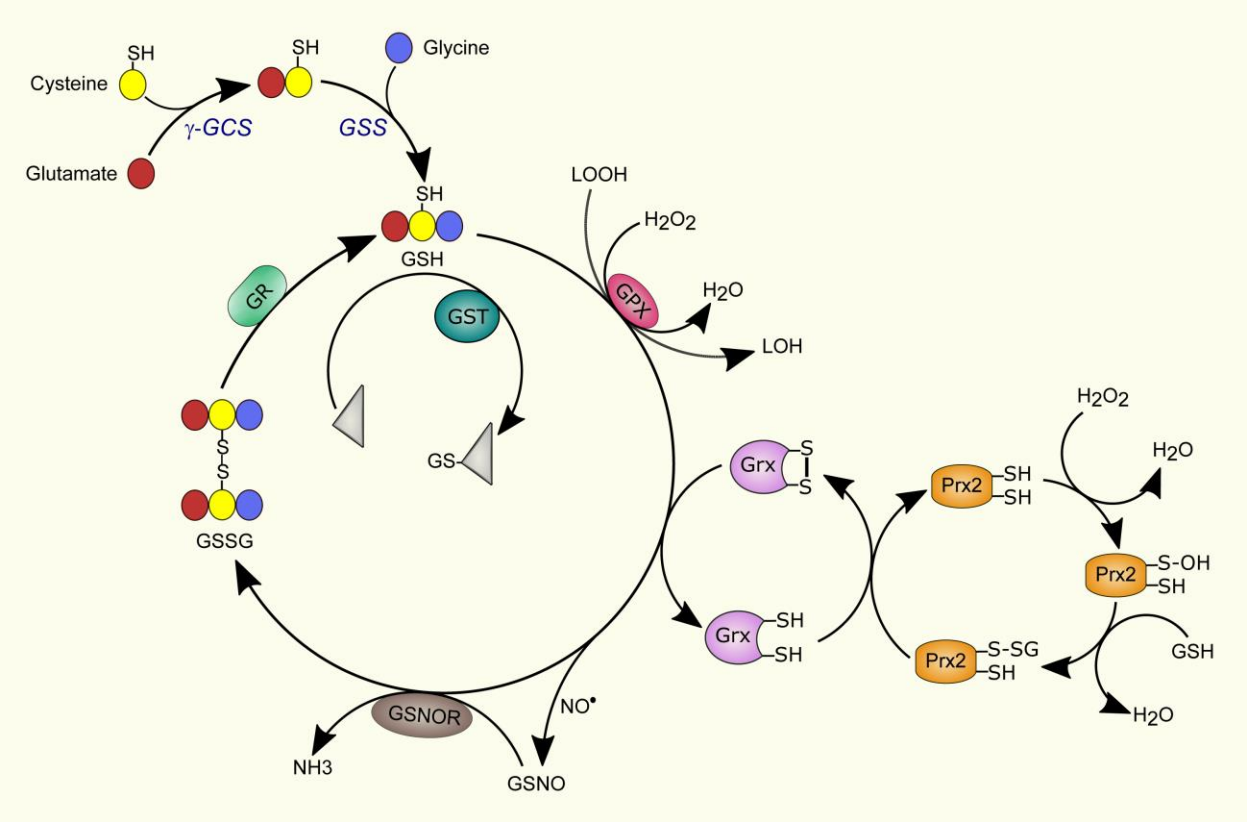

Figure 1.5. **Synthesis and cellular functions mediated by GSH.** GSH is synthesized by the conjugation of three amino acids – glutamine, cysteine and glycine. GSH acts as an essential cofactor for multiple enzymes involved in (1) detoxification of peroxidases (GPX), (2) deglutathionylation reactions (Grx), (3) reducing S-nitrosoglutathione or GSNO (GSNOR) and (4) detoxification of xenobiotics (triangular structure). During these processes GSH is oxidized to GSSG, which is reduced by GR. GSSG, oxidized glutathione; GPX, glutathione peroxidase; Grx, glutaredoxin; GST, glutathione-S-transferase; GSNOR, S-nitrosoglutathione reductase; GR, glutathione reductase; Prx2, peroxiredoxin 2; γ-GCS, γ-glutamylcysteine synthase; GSS, glutathione synthetase; LOOH, lipid hydroperoxide; LOH, lipid alcohol; H_2O_2, hydrogen peroxide; $NO^{\bullet}$, nitric oxide; triangle-GS, xenobiotic conjugated with GSH.

1.4 Protein degradation systems

Degradation of misfolded, oxidatively damaged and aggregated proteins is accomplished by two intracellular proteolytic systems: the ubiquitin proteasome system and autophagy-lysosomal system. Mammalian cells do have other proteolytic systems such as caspases and Ca^{2+} activated calpains, which can cleave their substrates and cause destruction of intracellular constituents during apoptosis, necrosis and other tissue injuries (Lecker et al., 2006; Feng et al., 2014).

1.4.1 Ubiquitin proteasome system

The ubiquitin proteasome system (UPS) is responsible for degrading majority of short-lived proteins including transcription factors, signal transducers and misfolded, mutated and defective proteins (Laney and Hochstrasser, 1999; Kruger et al., 2001). Proteasomes are multi-subunit catalytic protease complexes found in cytosolic and nuclear compartments. Eukaryotic cells contain two major pathways of UPS: 26S proteasome complex and the 20S "core" proteasome (Scherrer and Bey, 1994; Jung et al., 2009b; Jung et al., 2014). The 20S proteasome along with a regulatory subunit called 19S forms the 26S proteasome complex. While the 20S proteasome can actively recognize and eliminate the misfolded and oxidized proteins in an ATP and ubiquitin independent manner, proteins that are targeted to 26S proteasome requires the substrates to be tagged with poly-ubiquitin tail so that it can be recognized by the ATP-dependent 19S regulator (Davies, 2001; Ciechanover and Stanhill, 2014; Lefaki et al., 2017). To facilitate the recognition of target proteins by 26S proteasome, a cascade of four enzymes namely, E1 (ubiquitin-activating enzyme), E2 (ubiquitin-conjugating enzyme), E3 (ubiquitin ligase) and E4 (ubiquitin-prolongation enzyme) covalently attach ubiquitin to the substrate proteins (Hershko and Ciechanover, 1998; Koegl et al., 1999). The mono-ubiquitinated and poly-ubiquitinated substrates are recognized by 19S proteasome, which deubiquitinates and unfolds the target proteins and threads them into the

proteolytic chamber of 20s catalytic subunit (Strickland et al., 2000; Finley, 2009; Rousseau and Bertolotti, 2018).

Both 20S and 26S proteasomes are susceptible to oxidative modifications, but to varying degrees, which can impact their function and cause accumulation of defective, misfolded and oxidized proteins (Reinheckel et al., 1998; Reinheckel et al., 2000; Ishii et al., 2005). Multiple studies have demonstrated that 26S proteasome is highly susceptible to oxidative inactivation resulting in disassembly of the proteasomal complex and accumulation of ubiquitinated proteins (Wang et al., 2010; Haratake et al., 2016; Wang et al., 2017). Moreover, oxidative stress can also cause inactivation of ubiquitin conjugating (E1 and E2) enzymes, which are essential for ubiquitinating the substrates (Shang and Taylor, 1995). In contrast, 20S proteasome is comparatively resistant to oxidative stress and can degrade the oxidized proteins under mild to moderate oxidative stress conditions (Reinheckel et al., 1998; Reinheckel et al., 2000; Aiken et al., 2011). Interestingly, proteins that undergo irreversible oxidation like carbonylation were shown to be not preferentially ubiquitinated (Kastle and Grune, 2011). In fact, 20S proteasome was found to be the major proteolytic system in degradation of oxidatively modified proteins, while 26S complex turned out to be the main pathway for removal of native proteins and not very effective in clearing oxidized proteins (Grune et al., 1996; Davies, 2001). However, severe oxidative stress can cause extensive protein oxidation, cross-linking, protein aggregation and adduct formation with lipid peroxidation products such as 4HNE and lipofuscin making them resistant to proteolytic digestion. These accumulated protein aggregates and adducts can bind to 20S proteasome and inhibit it irreversibly (Friguet et al., 1994; Friguet and Szweda, 1997; Sitte et al., 2000; Verhoef et al., 2002). And, defective protein clearance due to dysfunctional UPS are associated with the buildup of abnormal protein aggregates especially in neurodegenerative diseases including Alzheimer's, Huntington's

and Parkinson's (Lowe et al., 1988; McNaught and Jenner, 2001; Bedford et al., 2008; Tai et al., 2012).

1.4.2 Autophagy – lysosomal system

Autophagy is a highly regulated catabolic process involved in the digestion and recycling of damaged cellular components to maintain cellular homeostasis. Three main types of autophagy that are morphologically and mechanistically distinct have been identified: macroautophagy, microautophagy and Chaperone mediated autophagy (CMA) (Settembre et al., 2013). Macroautophagy (here after referred to as autophagy) involves an isolation membrane that engulfs the cellular debris and dysfunctional organelles destined for digestion by autophagy to form a double layered vesicle called autophagosome. The autophagosome then fuses with the highly acidic lysosome forming the autolysosome, where the lytic enzymes digest the cargo and monomers such as amino acids and free fatty acids are generated for reutilization. In microautophagy, the soluble cytosolic substrates are directly sequestered through lysosomal or endosome membrane invagination. Unlike yeast cells, where three forms of selective autophagy (micropexophagy, piecemeal microautophagy of the nucleus and micromitophagy) are found, mammalian cells undergo non-selective microautophagy (Li et al., 2012). CMA involves internalization of cytosolic proteins tagged with the CMA targeting pentapeptide motif (KFERQ) into the lysosomal lumen for degradation. The cytosolic chaperone HSC70 (Heat Shock cognate 70) recognizes the CMA targeting motif and targets the substrate proteins to the surface of the lysosomes where the lysosomal transporter LAMP-2a (lysosome-associated membrane protein type 2a) interacts with the substrates and transfers the substrate into the lysosomal lumen (Orenstein and Cuervo, 2010).

Around 38 autophagy related genes (ATGs) regulating various stages of autophagy have been identified by genetic screening in yeast, many of which are highly conserved across eukaryotes. Among these, 18 core autophagic machinery genes (ATG1–10, ATG12–14, ATG16–18, ATG29, and ATG31) are essential for autophagosome formation (Mizushima et al., 2011; Lippai and Low, 2014b; Cohen-Kaplan et al., 2016). Various factors can induce autophagy, of which the most effective inducing signal being starvation/deprivation of nutrients and/or growth factors. These signals converge at the nutrient sensing protein kinase, mTOR (mechanistic Target of Rapamycin), which at well-fed state interacts with ULK1 (Unc51-like serine/threonine kinase) complex consisting of ULK1, Atg13, FIP200 (focal adhesion kinase family interacting protein of 200 kDa) and Atg101 and keeps the complex inhibited by phosphorylating ULK1 and ATG13. Under mTOR inhibition, either due to nutritional stress or rapamycin (mTOR inhibitor) treatment, ULK1 and ATG13 are dephosphorylated leading to ULK1 activation, which in turn phosphorylates ATG13 and FIP200 leading to the initiation of phagophore nucleation (Ganley et al., 2009; Hosokawa et al., 2009; Jung et al., 2009a; Mercer et al., 2009). The central metabolic sensor of the cell, AMPK (5' AMP-activated protein kinase) plays a key role in initiation of autophagy during nutritional stress. AMPK, which gets activated in response to low ATP or high AMP levels as observed during nutrient depletion or hypoxia, can suppress mTOR activity by multiple pathways. AMPK can phosphorylate and activate TSC2 (tuberous sclerosis complex 2), a GTPase-activating protein, resulting in the suppression of Rheb (GTPase Ras homolog enriched in brain), which is essential for the activation of mTOR (Inoki et al., 2003b; Inoki et al., 2003a; Li et al., 2004). AMPK can also directly phosphorylate mTOR at Ser722 and Ser792 and inactivate mTOR signaling (Gwinn et al., 2008; Hindupur et al., 2015). Alternatively, AMPK can promote autophagy by direct activation of ULK1 by phosphorylating serine residues at 317 and 777 (Kim et al., 2011).

The activated ULK1 complex then triggers phagophore nucleation by interacting with class III PI3K (phosphoinositide 3-kinase) complex consisting of vacuolar protein sorting 15 and 34 (VPS15 and 34), Beclin-1, AMBRA1 (activating molecule in Beclin-1-regulated autophagy protein 1) and ATG14. Phosphorylation of Beclin-1 (at Ser14 and Ser30) and ATG14 (at Ser29) by ULK1 enhances the recruitment and lipid kinase activity of class III PI3K (VPS34), which converts phosphatidylinositol to phosphatidylinositol-3-phosphate (PI3P) (Russell et al., 2013; Wold et al., 2016; Park et al., 2018). ULK1 can also phosphorylate AMBRA1, which anchors the class III PI3K complex to cytoskeleton by binding to Beclin-1. Phosphorylation of AMBRA1 by ULK1 has been suggested to facilitate the dissociation of class III PI3K complex from cytoskeleton and enable translocation of the complex to autophagy initiation sites (Di Bartolomeo et al., 2010; Mizushima et al., 2011). The anti-apoptotic Bcl-2 family proteins such as Bcl-2, Mcl-1 and Bcl-xl can also regulate autophagy induction by its interaction with Beclin-1, which disrupts the binding of Beclin-1 with VPS34 (Pattingre et al., 2005; Erlich et al., 2007). Competitive disruption of Bcl-2-Beclin-1 interaction by BH3 only proteins like Bad or BH3 mimetic were demonstrated to induce autophagy (Maiuri et al., 2007b). Similarly, phosphorylation of Beclin-1 by death associated protein kinase (DAPK) and phosphorylation of Bcl-2 by JUN N-terminal kinase-1 (JNK1) can reduce the inhibitory interaction between Beclin-1 and Bcl-2 and induce autophagy (Wei et al., 2008a; Zalckvar et al., 2009). Furthermore, Bcl-2 can also interact with AMBRA1 and inhibit autophagy initiation (Strappazzon et al., 2011).

PI3P generated from phosphatidylinositol at the phagophore nucleation site then recruits the PI3P effectors, double-FYVE-containing protein 1 (DFCP1) and WD-repeat domain phosphoinositide-interacting proteins (WIPIs) to the phagophore. This enables WIPIs to recruit the ATG12–ATG5–ATG16 complex, which facilitates the elongation and expansion of phagophore through

conjugation of ATG8 family proteins (Mizushima et al., 2011). Microtubule-associated protein light chain 3 (LC3), a ATG8 family member, is an ubiquitin like protein that is synthesized as pro-LC3 with additional sequences at C-terminal. The cysteine protease ATG4 processes pro-LC3 to LC3-I, which exposes the glycine residue at the C-terminal that is essential for their conjugation to phosphatidylethanolamine (PE). This proteolytically processed LC3-I is further activated by E1-like enzyme ATG7 in an ATP dependent manner. An E2-like enzyme ATG3 conjugates PE to activated LC3-I to form LC3-ATG3 conjugate which interacts with the E3-like complex, ATG12–ATG5–ATG16, to generate the lipidated form LC3-II (Ichimura et al., 2000; Fujita et al., 2008; Dikic and Elazar, 2018). LC3-II incorporates into both the inner and outer surfaces of the expanding phagophore membrane, where it binds to different adaptor proteins and facilitates the sequestration of cargo for degradation (Glick et al., 2010). Following the closure of the double layered autophagosomal membrane, the outer lipid bilayer membrane of the autophagosome fuses with the lipid bilayer membrane of lysosomes to form autolysosome. This process is regulated by multiple factors including small GTPases like Rab7 (Ras-associated binding 7), SNARE (soluble N-ethylmaleimide-sensitive factor attachment protein receptors) proteins and tethering factors like HOPS (homotypic fusion and protein sorting) complex and ATG14L, phospholipids and ATG8-family proteins (Nakamura and Yoshimori, 2017; Dikic and Elazar, 2018; Lorincz and Juhasz, 2019). Importantly, ATG4 deconjugates LC3-PE on the outer membrane of autophagosomes, which facilitates the interaction and fusion of the autophagosome with lysosomes (Kirisako et al., 2000; Yu et al., 2012). Once fused, the lysosomal acid hydrolases digest the sequestered autophagic cargo and the salvaged metabolites are released into the cytosol to be reused by the cell (Dikic and Elazar, 2018; Lorincz and Juhasz, 2019).

Selective sequestration of cargo is achieved by the adaptor proteins like sequestosome-1/ubiquitin binding protein p62, which bind to their substrates through an ubiquitin-binding domains and dock to LC3-II via their LC3-interacting region (LIR) and hence target the cargo to autophagosomes (Pankiv et al., 2007; Lamark et al., 2009). In addition to ubiquitin mediated autophagy, substrates can also be delivered to autophagosome independently of ubiquitin, especially in selective autophagy. Other adaptor proteins that can bind to the substrates in a ubiquitin dependent and/or independent manner and channel them to the autophagic degradation include NBR1 (Neighbor of BRCA1 protein) (Deosaran et al., 2013), optineurin (Wong and Holzbaur, 2014), NDP52 (Nuclear Dot Protein 52 kDa) (Thurston et al., 2009), Tax1BP1 (Tax1-Binding Protein 1) (Tumbarello et al., 2015), Tollip (Toll interacting protein) (Lu et al., 2014), NCAO4 (Nuclear receptor Coactivator 4) (Mancias et al., 2014), BNIP3 (BCL2 19 kDa-Interacting Protein 3) (Quinsay et al., 2010) and SMURF1 (Smad-Ubiquitin Regulatory Factor 1) (Orvedahl et al., 2011).

1.5 Redox regulation of autophagy and cell death mechanisms

1.5.1 Redox regulation of autophagy

ROS induced modifications including oxidation and S-nitrosylation plays a crucial role in several steps of autophagy including initiation and sustaining the autophagic process. Many studies have demonstrated that induction of autophagy by starvation or chemical inducers caused a corresponding increase in ROS production; similarly, addition of exogenous ROS can also induce autophagy (Kissova et al., 2006; Kim et al., 2007; Kunchithapautham and Rohrer, 2007; Scherz-Shouval et al., 2007b). Further confirming the role of ROS in regulation of autophagic process, treatment with antioxidants were shown to inhibit autophagy induction (Bridges, 1987; Underwood et al., 2010). ROS like $O_2^{\bullet}$ and H_2O_2 has been suggested to induce autophagy through activation of AMPK or JNK1 pathways (Li et al., 2013a; Zhang et al., 2013). Activation of AMPK,

as observed during starvation, can induce autophagy by either activating ULK1 (Kim et al., 2011) or suppressing mTOR activity (Alexander et al., 2010; Hindupur et al., 2015). The serine/threonine kinase JNK1 induces autophagy by interrupting the inhibitory interaction of Bcl-2 with Beclin-1 by phosphorylating Bcl-2 (Wei et al., 2008a). Interestingly, NO (by S-nitrosylation of JNK1) was shown to inhibit JNK1 dependent Bcl-2 phosphorylation and enhance Bcl-2-Beclin-1 interaction thereby suppressing autophagy. Additionally, NO can also negatively regulate autophagy by activating mTOR through phosphorylation of AMPK, which in turn is due to NO mediated S-nitrosylation of IKKβ (inhibitor of kappa B kinase) (Sarkar et al., 2011).

Notably, ROS induced cysteine oxidation plays a major role in autophagy progression through regulation of cysteine protease ATG4, which generates mature LC3-I from pro-LC3. H_2O_2 mediated reversible oxidation of Cys81 residue was shown to inactivate ATG4, thereby preventing delipidation of LC3-II and thus facilitating the autophagosome elongation (Scherz-Shouval et al., 2007b; Fernandez and Lopez-Otin, 2015). Interestingly, ATG4 is active during the maturation of autophagy and cleaves PE from LC3-II to recover LC3 from the mature autophagosomes facilitating the autophagosome-lysosomal fusion (Kirisako et al., 2000; Yu et al., 2012). Although the differential susceptibility of ATG4 to ROS oxidation at initiation and maturation stage of autophagy is still poorly understood, recent studies have demonstrated that Trx has redox control over ATG4. In these experiments, competitive inhibition of Trx using a mutant form of Trx1 was shown to result in enhanced autophagy and the fine tuning of ATG4 by the intracellular redox status was suggested to regulate the autophagosome formation (Perez-Perez et al., 2014). Additionally, a pro-oxidant complex comprising of REDD1 (regulated in development and DNA damage responses 1) and TXNIP was shown to suppress ATG4 activity and induce autophagy. Importantly, Trx activity was substantially increased in both *Redd1*$^{-/-}$ and *Txnip*$^{-/-}$ MEF cells, which

was associated with decreased cytosolic ROS and defective induction of autophagy in both normal and hypoxic conditions confirming the key regulatory role of Trx system in autophagy (Qiao et al., 2015). Similarly, changes in the ratio of GSH to GSSG can also modulate macro or selective autophagy (mitophagy). Depletion or oxidation of GSH was shown to change the intracellular environment to more oxidizing conditions, which facilitated oxidation of thiols like Prxs and primed the cells for autophagy commitment (Deffieu et al., 2009; Desideri et al., 2012; Sun et al., 2018).

1.5.2 Redox regulation of cell death mechanisms

Disturbed intracellular redox status is a well-known trigger for induction of cell death. Several redox sensitive proteins, transcription factors and other signaling molecules are involved in the regulation of cell death. The functions of apoptotic mediators such as cyto C, Bcl-2, caspases can be directly or indirectly altered by cellular ROS (Trachootham et al., 2008). For instance, the interaction between cardiolipin and cyto C is essential for the anchorage of cyto C to the inner mitochondrial membrane (Kagan et al., 2009). However, under oxidative stress conditions, excessive ROS accumulation can activate the peroxidase activity of cyto C-cardiolipin complex resulting in the peroxidation of cardiolipin. This leads to the dissociation of cyto C-cardiolipin complex and release of cyto C into the cytosolic compartment through the mitochondrial permeability transition pore (mPTP) initiating the activation of apoptosis (Kagan et al., 2005). Equally, many of the components of mPTP such as voltage-dependent anion channel (VDAC), adenine nucleotide translocase (ANT) and cyclophilin D (CypD) are subject to redox regulation. Nitrosylation of essential tyrosine residues in VDAC and ANT (Aulak et al., 2001; Vieira et al., 2001; Yang et al., 2019b) and oxidation induced intramolecular disulfide bridge formation in CypD (Linard et al., 2009; Nguyen et al., 2011) are suggested to contribute to mPTP opening

resulting in the release of mitochondrial contents into cytosol. The MOM can as well be permeabilized by the pro-apoptotic Bcl-2 family members including Bax and Bak, which can form oligomeric complexes and induce pore formation in MOM or can interact with mPTP to increase the permeability (Dewson and Kluck, 2009; Suh et al., 2013). Moreover, cysteine oxidation induced disulfide bridge formation was shown to promote dimerization, translocation and insertion of Bax into the mitochondrial membrane (D'Alessio et al., 2005; Nie et al., 2008; Brustovetsky et al., 2010).

Likewise, the redox status of the active site cysteine residues in both initiator and executioner caspases are crucial for their function. Oxidative modifications such as disulfide formation, S-nitrosylation and S-glutathionylation can affect the proteolytic activities of caspases. For example, Trx was shown to activate and inactivate caspases by S-nitrosylation and denitrosylation reactions, respectively, suggesting that nitrosylation reactions can act as a redox switch in modulating caspase activities. While Trx (Cys69 or Cys73) mediated S-nitrosylation of active site cysteine (Cys163) of caspase-3 suppressed the proteolytic activity and apoptosis, nitrosylation of the same cysteine moiety by Trx (Cys32) was shown to enhance its enzymatic activity and promote cell death (Mitchell and Marletta, 2005; Mitchell et al., 2007; Benhar et al., 2008). Additionally, other caspases such as -8 and -9 were also demonstrated to be regulated by the transnitrosylating and denitrosylating activities of Trx (Sengupta et al., 2010; Zhang et al., 2016a). In the same way, S-glutathionylation of pro-caspase-3 was shown to suppress TNF-α induced apoptosis as the glutathionylated pro-caspase-3 was resistant to proteolytic cleavage induced activation by initiator caspase-8 (Pan and Berk, 2007; Trachootham et al., 2008).

1.5.3 Cross talk between autophagy and cell death mechanisms

Autophagy, though been activated to clear the damaged proteins and organelles in an attempt to maintain a healthy intracellular environment, sustained or over-activation of autophagic process can deplete the cells of essential intracellular elements including mitochondria and other critical proteins and trigger cell death (Nemchenko et al., 2011). In fact, due to the observation that dying cells often display accumulation of autophagic vesicles, autophagy was initially classified as type II programmed cell death or "autophagic cell death" (Kroemer and Levine, 2008). In support of this postulate, several studies have demonstrated that inhibition of autophagy by chemical inhibition or genetic knockdown of key autophagic proteins like ATG5 and ATG7 can block cell death (Kim et al., 2013b; Kim et al., 2014b; Molaei et al., 2015; Shan et al., 2016; Guo et al., 2017).

There are common mediators like JNK and Bcl-2 family proteins that can regulate multiple catabolic processes like autophagy and apoptosis and can switch a cellular stress response from pro-survival to cell death inducing signal. Activation of JNK by nutrient deprivation or ROS induces both autophagy and apoptosis through phosphorylation of Bcl-2. This leads to the dissociation of Bcl-2-Beclin-1 complex inducing autophagy and also decreases Bcl-2-Bax interaction resulting in apoptosis (Wei et al., 2008a; Wei et al., 2008b). Bcl-2 was shown to maintain its anti-apoptotic function even when it was bound to Beclin-1, which was suggested to be due to the weak affinity between Beclin-1 and Bcl-2 proteins as compared to the interaction between Bax and Bcl-2 (Pattingre et al., 2005; Ciechomska et al., 2009; Gordy and He, 2012). Accordingly, sequestering Bcl-2/Bcl-xl by enhancing their binding to Beclin-1 was shown to induce apoptosis in a Bax-dependent manner. The pro-apoptotic kinase, Mst-1 (Mammalian Ste20-like kinase-1) was shown to phosphorylate the threonine residue of Beclin-1 at 108 thereby

enhancing its interaction with Bcl-2/Bcl-xl and inhibiting autophagy. Simultaneously, this improved interaction between Bcl-2/Bcl-xl with Beclin-1 lead to the activation of Bax and induction of apoptosis (Maejima et al., 2013).

Although autophagy is mechanistically distinct from other cell death pathways, autophagy can be influenced by factors that govern cell death processes and vice versa is also true. Apoptosis mediators like caspases can inhibit autophagy by cleaving the essential component of autophagic machinery. Beclin-1 was shown to be proteolytically cleaved by caspases including caspase-3 and -8 (Wirawan et al., 2010; Zhu et al., 2010; Li et al., 2011). Likewise, caspase and calpain were shown inactivate AMBRA1 and ATG5 by proteolysis thereby inhibiting the activation of pro-survival autophagy (Yousefi et al., 2006; Pagliarini et al., 2012).

Autophagy, due to its degradative function, can cause similar attenuation of apoptosis by selectively sequestering certain intracellular pro-apoptotic mediators. Autophagic degradation of active-caspase-8 was shown to promote resistance to apoptosis (Hou et al., 2010). Also, NOXA, a pro-apoptotic and pro-necrotic factor, was demonstrated to be eliminated by autophagic pathway thereby blocking apoptotic progression (Wang et al., 2018b).

Autophagy can act as an inducer of cell death by depleting the endogenous pro-survival proteins. As an example, autophagy was shown to degrade the enzymatic antioxidant catalase thereby inducing abnormal ROS accumulation and necrotic cell death (Yu et al., 2006). In ferroptosis, autophagic degradation of ferritin plays a key role in cell death induction. Ferritin is a metalloprotein that serves principally to store iron. Autophagic degradation of ferritin by NCOA4 mediated selective autophagy leads to excessive accumulation of iron in the cytosol which results in lipid peroxidation and ultimately ferroptotic cell death (Tang et al., 2018). Autophagy can also induce cell death independent of its degradative functions. As in the case of caspase-8 self-

processing, where autophagosomal membrane can act as a platform for the assembly of intracellular DISC, which leads to the activation of caspase-8 and subsequent induction of apoptosis through caspase-3 activation (Young et al., 2012). Likewise, autophagy was also shown to promote necroptosis by facilitating the assembly of necrosome on autophagosomal membrane by ATG5 mediated recruitment of receptor-interacting protein 1 and 3 (RIP1 and RIP3) and FADD (Fas Associated Via Death Domain) (Basit et al., 2013).

Alternatively, lysosomes, the digestive component of autophagy can also act as an inducer of cell death. Due to the presence of hydrolytic enzymes that are capable of digesting most cellular macromolecules, any damage to the lysosomes can be potential harmful to the cells (Boya and Kroemer, 2008). Various factors, including ROS and proteases, that are discussed in the following sections can cause permeabilization of lysosomes, which can initiate various types of cell death pathways depending on the extent of lysosomal damage.

1.6 Lysosomes

Lysosomes are dynamic membrane-bound subcellular organelles that were originally discovered by Christian de Duve in 1955 (de Duve, 2005). Apart from playing a key role in maintaining cellular homeostasis by facilitating the digestion and recycling of cellular macromolecules, lysosomes are also involved in a plethora of other cellular processes including differentiation, immune response, nutrient sensing and cell death. Around 80 acid hydrolases including nuclease, proteases, lipases, phosphatases, glycosidases and sulfatases are present within the lysosomal lumen in a highly acidic environment (pH 4.5-5). The acidic lumen facilitates the degradation of macromolecules as most of the lysosomal hydrolases exhibit optimal activity at acidic pH but are inactivated at the neutral pH (7.4) of cytosol. The vacuolar ATPase (v-ATPase) residing in the lysosomal membrane maintains the acidic luminal interior by pumping protons from the cytoplasm

into the lysosomal lumen against their electrochemical gradient by harnessing the energy generated from ATP hydrolysis (Yamashima and Oikawa, 2009; Appelqvist et al., 2013). In addition to the acidic pH, a healthy supply of reducing equivalents is required for reduction of disulfide bonds in proteins for their optimal digestion by lysosomal enzymes. The reducing equivalents are also vital for appropriate activation of some enzymes (Ewanchuk and Yates, 2018). The limiting membrane of the lysosome is composed of a single lipid-bilayer and proteins. The internal (luminal) lysosomal perimeter is lined by a glycoprotein coat called "glycocalyx' protecting the lumen from the acidic environment (Settembre et al., 2013). The heavily glycosylated structural proteins including Lysosome-Associated Membrane Protein 1 (LAMP1) and 2 (LAMP-2) present in the lysosomal membrane resists the proteolytic destruction of lysosomal membrane (Kundra and Kornfeld, 1999).

1.6.1 Lysosomal biogenesis

Lysosomal biogenesis involves a complex process, much of which is still unknown. Transcription factor EB (TFEB), belonging to the microphthalmia-associated transcription factor (MITF) family proteins, is known as the master regulator of lysosome biogenesis. Nutrient sufficiency inactivates and retains TFEB in the cytoplasm, whereas extreme stimulus including starvation causes TFEB to translocate into nucleus and induce an array of genes involved in lysosome biogenesis. The phosphorylation status of TFEB governs its subcellular localization and activity (Yang et al., 2018). Under nutrient rich conditions, TFEB is inactivated by phosphorylation of serine residues at 142 and 211 by mTORC1 and/or ERK2. Remarkably, the phosphorylation at Ser211 acts as the docking site for the molecular chaperone 14-3-3, which prevents the nuclear translocation of TFEB by sequestering it in the cytoplasm (Settembre et al., 2011; Martina et al., 2012; Roczniak-Ferguson et al., 2012). Conversely, inactivation of mTORC1 during nutrient starvation or

lysosomal stress alleviates TFEB phosphorylation promoting TFEB to translocate to nucleus. In addition, starvation concomitantly induces the efflux of lysosomal Ca^{2+} through Ca^{2+} transporter, mucolipin 1 (MCOLN1) belonging to the transient receptor potential channel family (TRPML1) to activate the calcium and calmodulin-dependent protein phosphatase calcineurin, which dephosphorylates TFEB at Ser142 and Ser211, preventing the binding of 14-3-3 thereby enabling TFEB to translocate to nucleus (Tong and Song, 2015). Interestingly, MCOLN1 is a redox sensitive channel and can be activated by Reactive Oxygen Species (ROS) triggering lysosomal Ca^{2+} release leading to calcineurin-dependent nuclear translocation of TFEB (Zhang et al., 2016b). TFEB, once accumulated in the nucleus, binds and activates Coordinated Lysosomal Expression and Regulation (CLEAR) network to promote the transcription of target genes (Appelqvist et al., 2013).

The lysosomal acid hydrolases are synthesized in the rough endoplasmic reticulum and are transported to the trans-Golgi network (TGN). The lysosomal hydrolases contain a carbohydrate tag, mannose-6-phosphate (M6P), to distinguish them from other secretory proteins and to enable accurate recognition and lysosomal targeting. The M6P tag is precisely added to the N-linked oligosaccharide chains of the acid hydrolase during their passage through TGN. The cation-dependent and / or independent M6P receptors present in TGN recognizes and binds to the M6P tagged hydrolases and packs them in clathrin-coated carriers that bud from TGN. These carrier vesicles subsequently deliver their contents to the endosomes and then to lysosomes. Once, the endosomes fuse to vesicles to form lysosomes, the acidic luminal pH triggers the dissociation of M6P receptors from the lysosomal enzymes and the M6P receptors are recycled back to TGN (Coutinho et al., 2012a; Progida and Bakke, 2016). Thus, M6P receptors are used to distinguish lysosomes from endosomes, since M6P receptors are absent in lysosomes, but are found in TGN,

endosomes and the plasma membrane. Other soluble enzymes as well as non-enzymatic lysosomal proteins are sorted for lysosomal trafficking by an M6P-independent route using other receptors such as lysosomal integral membrane protein (LIMP-2) and sortilin (Coutinho et al., 2012b). For example, the lysosomal enzyme β-glucocerebrosidase uses LIMP-2 (Reczek et al., 2007) and lysosomal proteases such as cathepsins D and H uses sortilin (Canuel et al., 2008) as transport receptors. LIMP-2 may be involved in regulation of lysosomal membrane integrity as loss of its homologue protein SCAV-3 in *Caenorhabditus elegans* results in lysosomal rupture and affects its longevity (Li et al., 2016b).

Lysosomes can also contain few highly heterogeneous membranous bodies within the lumen called as intraluminal vesicles. These vesicles are formed by invagination of limiting membrane in the endocytic pathway and is involved in sorting and delivery of cargos, especially lipids and membranes to lysosomes for degradation (Piper and Katzmann, 2007; Appelqvist et al., 2013).

1.6.2 Cathepsins: the major class of lysosomal proteases

Cathepsins are a major class of lysosomal proteases involved in protein processing machinery in the context of a wide variety of physiological and pathological processes. These include protein degradation, prohormones activation, antigen presentation, bone resorption and remodeling, keratinocyte differentiation, mammary gland involution, osteoarthritis, atherosclerosis, pulmonary arterial hypertension and tumor progression and invasion (Burke et al., 2003; Turk et al., 2012; Chang et al., 2019). Cathepsins are categorized based on their structure and catalytic mechanisms into three subtypes: serine, aspartic and cysteine proteases. The serine proteases include Cathepsins A and G, aspartic proteases include Cathepsins D and E while Cathepsins B, C, F, H, K, L, O, S, V, X and W belong to cysteine proteases (Reiser et al., 2010; Turk et al., 2012). Almost all the cathepsins require an acidic environment to exhibit their optimal activity with few

exceptions including cathepsins K and S, which can maintain stable activities at pH 7 and 8 (Cirman et al., 2004; Wilder et al., 2011). Also, cathepsins such as B, D and L, which are widely implicated in lysosomal membrane permeabilization (LMP) mediated cell death, remain active and degrade their substrates at neutral pH (Boya and Kroemer, 2008). The optimal activity of cysteine cathepsins is maintained by an acidic yet reducing condition. The source of reducing equivalents required for cysteine cathepsins activity is not currently known; It has been postulated that thioredoxin reductase might be the reducing system using NADPH that provides the reducing capacity for phagolysosomes and lysosomes (Ewanchuk and Yates, 2018). Supporting this notion, our lab has shown that inhibition of thioredoxin reductase using pharmacological inhibitors and genetic manipulation severely impairs lysosomal activity (Nagakannan et al., 2016) . The reducing enzyme for activation of cysteine cathepsins is γ-interferon-inducible lysosomal thiol reductase (GILT) (Balce et al., 2014). This enzyme is regulated by γ-interferon which in turn is regulated transcriptionally by thioredoxin (Kang et al., 2008).

Cathepsins are not limited to the acidic environment of the cell. For example, cathepsin B was found to be localized in extrafollicular space in thyroid carcinomas, where cathepsin B was suggested to facilitate invasiveness and metastasis through extracellular matrix degradation (Shuja et al., 1999). Similarly, variants of Cathepsin B and V were found in the nucleus of thyroid carcinoma HTh74 cells (Tedelind et al., 2010). The nuclear variant of cathepsin L was found to be involved in cell cycle progression through cleavage of Cut Like Homeobox 1 (CUX1) transcription factor (Goulet et al., 2004; Goulet et al., 2006) and embryonic stem cell differentiation through histone H3 cleavage (Duncan et al., 2008). Cathepsins can degrade a wide variety of substrates including cell adhesion molecules like fibronectin, laminin, tenascin, collagen, receptors like epidermal growth factor receptor and ephrin type A receptor 2 (Guinec et al., 1993; Sobotic et al.,

2015), and intracellular pro- and anti-apoptotic proteins (Cirman et al., 2004; Droga-Mazovec et al., 2008).

Loss of cathepsins or their functions are associated with severe abnormalities or defective functioning of organs indicating their vital role in several physiological functions. Loss of lysosomal functions seems to affect nervous system the most. Deletion of both cathepsin B and L in mice display neuronal degeneration in cerebellum and cerebral cortex, severe hypotrophy and motility defects resulting in lethality by fourth week of life (Felbor et al., 2002; Sevenich et al., 2006; Stahl et al., 2007). Similarly, deficiency or mutation of cathepsin D was found to cause lysosomal storage disease associated with ceroid lipofuscinoses and neurodegeneration (Tyynela et al., 2000; Koike et al., 2003). Mice deficient of cathepsin D were found to die before fourth postnatal week displaying extensive intestinal necrosis accompanied by thromboembolism (Saftig et al., 1995). Various endogenous inhibitors of cathepsins have been identified including cystatins, thyropins and serpins, which prevent the cathepsins form binding to their substrates. Among these, cystatins form the major class of inhibitors which constitutes three subfamilies: Type-1 cystatins (Stefin A and B), type-2 cystatins (cystatins C, D, E and F) and type-3 cystatins (Kininogens) (Stoka et al., 2016; Pogorzelska et al., 2018). Cystatins, especially cystatin C, functions as endogenous neuroprotective agent by preventing neuronal cell death and promoting neurogenesis (Pirttila et al., 2005; Xu et al., 2005; Watanabe et al., 2014b). Deficiency of cystatins has been shown to enhance cathepsin activity and is implicated in many disease conditions. Unverricht–Lundborg disease (ULD) or progressive myoclonic epilepsy type 1 (EPM1) is an inherited neurodegenerative disorder caused due to loss-of-function mutation of cystatin B (Rinne et al., 2002). Knockout of cystatin B in mice (which mimics the clinical symptoms of ULD) augmented cathepsin B and D activities and lead to neuronal loss in cerebellum and cerebral cortex. These

effects were rescued when cystatin B knockout mice were crossbred with cystatin C overexpressing mice, while crossbreeding of cystatin B knockout and cystatin C knockout mice exacerbated the clinical symptoms, cerebral atrophy and neuronal loss (Kaur et al., 2010). Similarly, reduction in cystatin C levels was associated with enhanced cathepsin S activity in tears obtained from patients with Sjögren's Syndrome, a systemic autoimmune disease that is characterized by dryness of eyes and mouth (Edman et al., 2018). Moreover, cystatin C acts as a pro-survival factor by inducing autophagy through mTOR inhibition during cellular stress (Tizon et al., 2010).

1.6.3 Lysosomal membrane permeabilization

LMP is characterized by the leakage of the lysosomal contents including the catabolic enzymes like cathepsins into the cytosol due to rupture of lysosomal membrane. The extent of lysosomal membrane damage decides the cellular outcome. While partial LMP results in translocation of lysosomal contents, including cathepsins like B and D, to the cytoplasm triggering the activation of several effectors leading to apoptosis or autophagic cell death (Karch et al., 2017; Wang et al., 2018a), complete LMP causes loss of lysosomal proton gradient and massive leakage of lysosomal contents into the cytosol leading to increased cytosolic acidification and widespread hydrolytic damage of cellular components resulting in necrosis (Brunk et al., 1997; Boya and Kroemer, 2008). Additionally, acidification of cytosolic compartment has been shown to cause mitochondrial acidification, resulting in mitochondrial depolarization and impaired Ca^{2+} handling (Gursahani and Schaefer, 2004) and can also act as an effector mechanism for recruitment of Bax onto the mitochondrial membrane triggering apoptosis (Gursahani and Schaefer, 2004). Besides, acidification of the cytosolic compartment also facilitates certain the lysosomal proteases like cathepsin D to maintain their enzymatic activity to cause proteolytic degradation of key cellular

proteins during apoptosis (Nilsson et al., 2006; Mrschtik and Ryan, 2015). Causes and consequences of LMP are depicted as schematic in Figure 1.6.

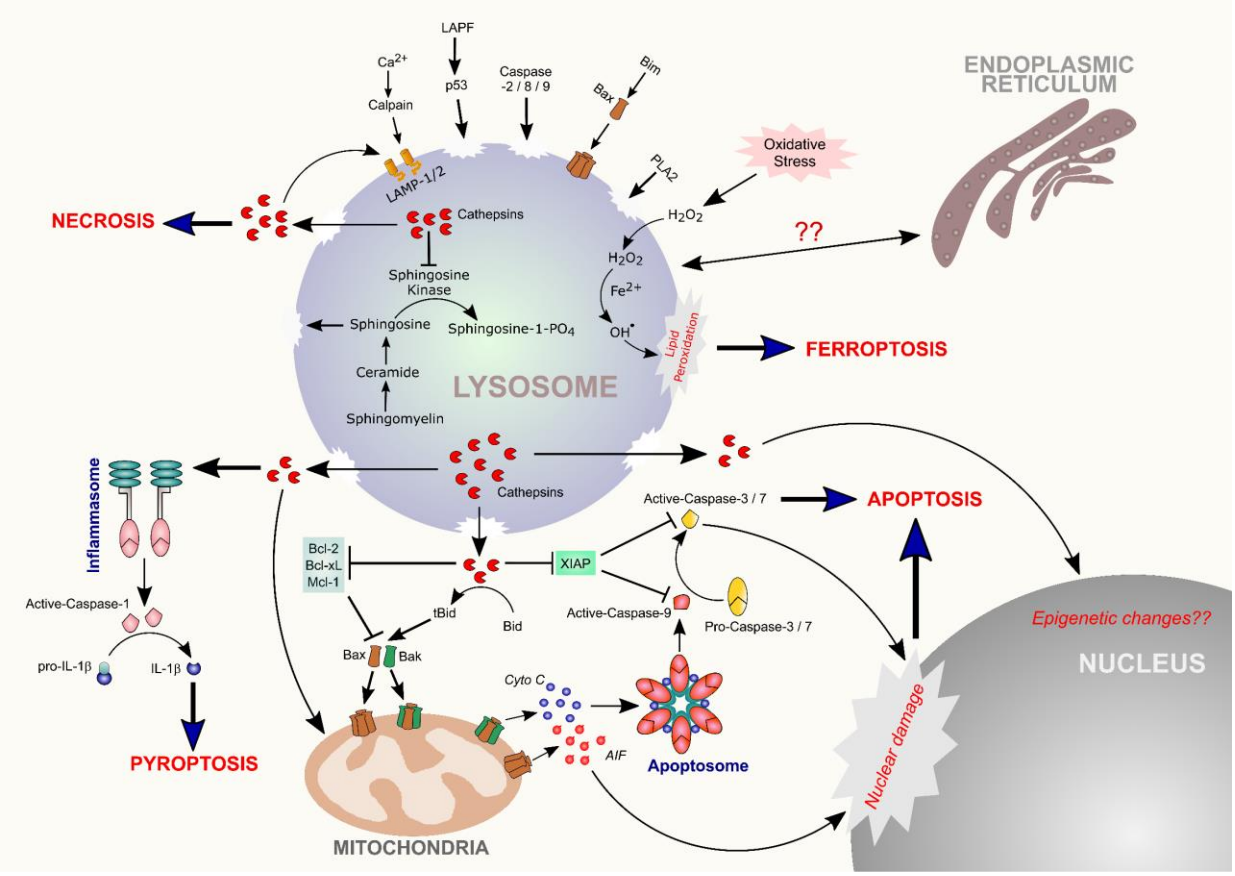

Figure 1.6. Causes and consequences of lysosomal membrane permeabilization (LMP). Number of factors like hydroxyl radicals produced by Fenton reaction (using Fe^{2+}), p53, apoptotic regulatory protein Bax, proteases such as calpain, caspases and cathepsins, and the natural sphingolipid sphingosine which acts as a lysosomotropic detergent can cause lysosomal membrane rupture. The consequences of LMP in particular interest on the role of cathepsins is highlighted. The cathepsins discharged into the cytosolic compartment can cause proteolytic degradation / activation of several cytosolic substrates (Bcl-2, Bcl-xL, Mcl-1, XIAP and Bid), cause direct or indirect organelle damage (mitochondria and nucleus) and trigger / execute various forms cell death. Bcl-2: B-cell lymphoma 2; Bcl-xL: B-cell lymphoma-extra-large; Mcl-1: myeloid cell leukemia 1; BIM: Bcl-2-interacting mediator of cell death; Bak: Bcl-2 homologous antagonist/killer; Bax: Bcl-2-associated X protein; Bid: BH3 interacting-domain death agonist; tBid: truncated p15 BID; XIAP: X-linked inhibitor of apoptosis protein; LAPF: lysosome associated and apoptosis inducing protein containing PH and FYVE domains; Ca^{2+}: Calcium; Fe^{2+}: Ferrous Iron; H_2O_2: Hydrogen peroxide; $OH^{\bullet}$: Hydroxyl radical; PLA2: Phospholipases A2; Cyto C: Cytochrome C; AIF: Apoptosis Inducing Factor; IL-1β: Interleukin 1β; LAMP 1 / 2: Lysosomal-associated membrane protein 1 or 2.

1.6.3.1 Causes of lysosomal membrane permeabilization

1.6.3.1.1 Oxidative stress and reactive oxygen species

Increased production of ROS can lead to disruption of lysosomal membrane integrity by peroxidation of lysosomal membrane lipids (Fong et al., 1973; Myers et al., 1993). Exogenous oxidizing insults like photosensitization and H_2O_2 are shown to induce LMP (Zdolsek et al., 1990; Vanden Berghe et al., 2010). Several studies have demonstrated that scavenging ROS can inhibit lysosomal dependent cell death by preserving lysosomal integrity contents further exemplifying the role of ROS in LMP process (Roberg and Ollinger, 1998; Yu et al., 2004; Windelborn and Lipton, 2008; Huai et al., 2013; Oku et al., 2017). Lysosomes can produce ROS inside the lysosomal lumen through Fenton reaction that is catalyzed by iron and can lead to LMP (Kurz et al., 2010). ROS, either in the form of $O^{2\bullet}$ or H_2O_2 are generated from different sources including plasma membrane (NADPH oxidase), peroxisomes, mitochondria and endoplasmic reticulum and accumulate in the cytosol. Superoxide dismutase converts the highly unstable $O_2^{\bullet}$ to relatively stable H_2O_2 increasing the cytosolic concentration of H_2O_2, which is then eliminated by the action of catalase, glutathione peroxidase and peroxiredoxin maintaining the cellular redox balance (Lushchak, 2014; Reczek and Chandel, 2015). Inhibition of antioxidants is sufficient to induce regulated cell death mechanisms. Depletion of glutathione has been extensively used as an anti-cancer treatment (Marengo et al., 2008). Although different cells may respond differently to this stress, inhibition of GSH synthesis by L-buthionine-*S*,*R*-sulfoximine (BSO) leads to exacerbation of oxidative stress as shown by increased ROS including lipid hydroperoxides and induction of apoptosis, which is mediated by activation of calpains and caspases (Marengo et al., 2008). This could be effectively inhibited by administration of vitamin C or inhibition of NADPH oxidase, confirming the involvement of oxidative stress in this model.

During oxidative stress, a portion of excessive H_2O_2 can escape dismutation, and diffuse into lysosomes, that lack any hydrogen peroxidase enzymes. Lysosomes are important storage organelle of labile redox-active iron, as they are the terminal degradative organelles in autophagy process and digest many iron-containing macromolecules including cytosolic enzymes with iron co-factors, iron binding protein ferritin, metallothioneins and iron rich mitochondrial components (Terman and Kurz, 2013). In high acidic and reducing environment within the lysosomes, the unchelated ferric iron (Fe3+) is reduced to ferrous (Fe^{2+}). The diffused H_2O_2 can react with Fe^{2+} resulting in the formation of extremely reactive $^{\bullet}OH$ or the similarly reactive oxo-iron species such as ferryl or perferryl radicals (Kurz et al., 2008). The $^{\bullet}OH$ radicals are highly reactive and can cause peroxidation of membrane lipids by abstracting electron form the unsaturated fatty acids, which in turn creates an unstable lipid radical initiating a self-propagating chain reaction of lipid peroxidation (Radi, 2018). This results in lysosomal membrane rupture and leakage of lysosomal contents into the cytosol causing damage to other intracellular organelles and cell death. The role of labile iron in LMP is further substantiated by the finding that iron chelators completely protect against oxidative stress induced LMP and cell death (Persson et al., 2003; Lin et al., 2010). Additionally, HSP70, a molecular chaperone, can prevent LMP by scavenging the intra-lysosomal redox active iron, thus protecting against ROS induced LMP dependent cell death (Doulias et al., 2007).

1.6.3.1.2 Other factors

Although the discharge of cathepsins from lysosomes into cytosol is a consequence of LMP, numerous studies have shown that once in cytosol, cathepsins can also cause lysosomal membrane damage, further propagating LMP (Werneburg et al., 2002; Feldstein et al., 2004; Guicciardi et al., 2007; Jacobson et al., 2013; Katsnelson et al., 2016). For instance, hepatocytes derived from

cathepsin B deficient mice were found to be resistant to TNF-α and lysosomotropic detergent sphingosine induced LMP. (Werneburg et al., 2002). Similarly, caspases such as caspase 2, -8 and -9 were shown to cause LMP directly or indirectly (Guicciardi et al., 2000; Werneburg et al., 2004; Gyrd-Hansen et al., 2006). Likewise, members of the pro-apoptotic Bcl-2 family proteins, which are known to permeabilize mitochondria initiating apoptosis, are also suggested to cause LMP by forming proteolipid pores in the lysosomal membranes (Werneburg et al., 2012). In an *in-vitro* set up, recombinant Bax was able to trigger cathepsin release from purified lysosomes (Kagedal et al., 2005; Johansson et al., 2010). Moreover, on induction of apoptosis by various stimuli, Bax was found to translocate to lysosomal membrane and induce LMP, which was attenuated by downregulation of Bax (Feldstein et al., 2004; Kagedal et al., 2005; Feldstein et al., 2006; Castino et al., 2009; Bové et al., 2014).

In addition, the lipid composition of lysosomal membrane plays a major role in the susceptibility to LMP. Compared to other cellular membranes, lysosomal membrane contains lower concentrations of cholesterol and sphingolipids (Hamer et al., 2012). In contrast, bis (monoacylglycerol) phosphate (BMP), a negatively charged glycerophospholipid is found to be highly concentrated in the inner lysosomal membranes. However, in comparison to the limiting membrane, the intraluminal vesicular membranes are enriched in cholesterol and BMP (Kobayashi et al., 1998; Kobayashi et al., 2002; Mobius et al., 2003; Schulze et al., 2009). Implicating the essential role of cholesterol in lysosomal membrane integrity, depletion of lysosomal cholesterol using methyl-β-cyclodextrin, a cholesterol sequestering agent, was shown to sensitize lysosomes to osmotic stress (Hao et al., 2008) leading to membrane destabilization and permeability to potassium ions and protons (Deng et al., 2009). In contrast, addition of cholesterol to isolated lysosomes were shown to reduce permeability (Fouchier et al., 1983), and therefore, increasing

lysosomal cholesterol content in *in-vitro* experiments protects against membrane permeabilizing agents and attenuates cell death (Appelqvist et al., 2011; Reiners et al., 2011; Appelqvist et al., 2012a; Gutierrez et al., 2016). Similarly, the oxidative metabolites of cholesterol, formed either due to free radical attack or enzymatic reactions, called "Oxysterols" are known to permeabilize membranes allowing ions and small polar molecules to pass through (Holmes and Yoss, 1984; Olsen et al., 2012). Recently, an oxysterol 27-Hydroxycholesterol was shown to induce pyroptosis through LMP, implicating the impact of cholesterol oxidation products on lysosomal membrane (Chen et al., 2019).

Lysosomal membranes were shown to undergo lipid peroxidation in response to free radicals in an *in-vitro* setup (Fong et al., 1973). End products of lipid peroxidation such 4-hydrononenal (4-HNE) and malondialdehyde are increased after oxidative damage of cellular membrane lipids that can impair cellular functions. Accumulation of 4-HNE in lysosomes is shown during oxidative stress which can cause LMP and cell death in neurons. Most importantly, 4-HNE was able to permeabilize isolated lysosomes indicating its direct membrane destabilizing effect on lysosomes (Hwang et al., 2008).

Similarly, sphingolipid catabolism acts as a major trigger for LMP. Sphingosine, an amino alcohol containing a long unsaturated hydrocarbon chain, forms the backbone of sphingolipid sphingomyelin. Sphingomyelin is degraded by enzyme sphingomyelinase to generate ceramide and phosphocholine. Ceramide is further converted to sphingosine by ceramidase. Being the most abundant sphingolipid in mammalian cells, sphingomyelin metabolism is vital for maintaining membrane homeostasis (Gault et al., 2010); however, increased hydrolysis of sphingomyelin and accumulation of the breakdown products, particularly sphingosine, has been found to induce LMP and cell death (Ullio et al., 2012). Sphingosine is accumulated in lysosomes due to the protonation

of their free amino group, which promotes lysosomal membrane disruption by acting as a detergent. A dose dependent response to sphingosine has been reported for lysosomal membrane; at low dose of sphingosine induces partial LMP and apoptosis whereas, high dose sphingosine leads to extensive lysosomal membrane rupture resulting in necrosis (Kagedal et al., 2001). Remarkably, inhibition of sphingosine kinase-1, which catalyzes the conversion of sphingosine to sphingosine-1-phosphate, was sufficient to trigger LMP and cell death in glioma cells (Mora et al., 2010). Sphingosine kinase-1 is also a cathepsin B substrate (Taha et al., 2005; Taha et al., 2006) and administration of sphingosine failed to induce LMP in hepatocytes obtained from Cat $B^{-/-}$ mice (Werneburg et al., 2002).

1.6.3.2 Consequences of lysosomal membrane permeabilization

1.6.3.2.1 LMP and apoptosis

Lysosomal proteases released in LMP can induce apoptosis by either caspase dependent or independent mechanisms. Cathepsins such as B and D once released from the lysosomes into the cytoplasm, can cleave the pro-apoptotic protein Bid to t-Bid (Cirman et al., 2004; Droga-Mazovec et al., 2008; Appelqvist et al., 2012b), which then translocates to mitochondria and interacts with Bax/Bak to form oligomers. This process facilitates creating pores in the mitochondrial outer membrane leading to cyto C release, assembly of apoptosome and eventual activation of caspase cascade and induction of apoptosis (Eskes et al., 2000; Wei et al., 2000). Furthermore, lysosomal cathepsins can enhance the mitochondrial destabilization and cell death by degrading the anti-apoptotic members of Bcl-2 family, Bcl-2, Bcl-xl and Mcl-1, which prevent apoptosis by antagonizing the actions of pro-apoptotic proteins such as Bax and Bak (Droga-Mazovec et al., 2008; Brunelle and Letai, 2009). Cathepsins can also cause direct caspase activation by proteolytic cleavage as shown for Caspase-2, which can directly induce mitochondrial permeabilization and

apoptosis, after activation by cathepsin B in TNF-α induced hepatocyte apoptosis (Guicciardi et al., 2005). Cathepsin L was shown to induce caspase-3 cleavage (Ishisaka et al., 1999; Hishita et al., 2001) and caspase 8 is a known substrate of cathepsin D (Conus et al., 2008). Additionally, cathepsins were also found to facilitate caspase activation by degrading XIAP (X-linked inhibitor of apoptosis) (Droga-Mazovec et al., 2008; Taniguchi et al., 2015), an endogenous inhibitor of caspases-3, -7 and -9 (Srinivasula et al., 2001; Paulsen et al., 2008). Alternatively, cathepsins can also induce caspase-independent apoptosis by triggering the translocation of Apoptosis Inducing Factor (AIF) from mitochondria to nucleus (Chen et al., 2005; Yuste et al., 2005; Sevrioukova, 2011).

1.6.3.2.2 LMP and necrosis

The intensity of LMP is an important factor in method of cell death. Massive LMP is known to induce necrotic cell death characterized by cellular swelling and loss of plasma membrane integrity (Brunk et al., 1997). One of the earliest reports to identify the role of lysosomal membrane damage in necrosis was in 1966 by Allison and Dingle (Allison and Dingle, 1966), where necrosis of rat adrenal cortical cells caused by 7,12-Dimethylbenz(a)anthracene (DMBA), a carcinogenic hydrocarbon, was shown to be due to leakage of lysosomal enzymes. Lysomotrophic detergents such as O-methyl-serine dodecylamide hydrochloride (MSDH), Leu-Leu-OMe (LLOMe) and sphingosine induce necrosis at higher concentrations which otherwise cause apoptotic cell death at lower concentrations (Li et al., 2000; Kagedal et al., 2001; Talukdar et al., 2016). Similarly, cathepsins were shown to mediate necrotic cell death caused by lysosomal disrupting adjuvants alum and LLOMe. Interestingly, inhibition of cathepsins not only inhibited necrosis but also further lysosomal destabilization (Jacobson et al., 2013).

1.6.3.2.3 LMP and necroptosis

Necroptosis is a regulated form of necrosis identified by cellular swelling, plasma membrane rupture and moderate chromatin condensation (Tang et al., 2019). It involves the activation of receptor-interacting kinases-1 (RIPK1) and 3 (RIPK3), resulting in the activation of pseudokinase mixed-lineage kinase domain-like protein (MLKL) by phosphorylation. The phorpshorylated MLKL forms oligomers and locates to the intracellular and plasma membrane ultimately leading to loss of membrane integrity and cell death (Gudipaty et al., 2018). Compromise in lysosomal membrane integrity was suggested to precede plasma membrane disruption during necroptosis (Vanden Berghe et al., 2010). The necroptosis inducers RIPK1 and RIPK3 are proposed to be degraded in lysosomes, as inhibition of lysosomal function led to the accumulation of these two kinases. Necroptosis ensues in the absence of apoptosis. Interestingly, the combination of bafilomycin and pan-caspase inhibitor was sufficient to induce necroptosis, which otherwise requires the addition of TNF-α with pan-caspase inhibitor to cause necroptotic cell death (Liu et al., 2018). Similarly, granulysin, a cytotoxic protein released by T cells and Natural Killer cells was shown to cause LMP and release of cathepsin B during necroptosis (Zhang et al., 2009).

1.6.3.2.4 LMP and pyroptosis

Pyroptosis is a inflammasome mediated programmed cell death pathway triggered by various stimuli including invading pathogens, hypoxic insults and trauma (Bortolotti et al., 2018; Cheng et al., 2019). Most of the inflammatory danger signals induce inflammasome assembly by causing lysosomal rupture. The lysosomal proteases such as cathepsins once released from the ruptured lysosomes can activate NLRP3 (nucleotide binding domain leucine-rich-containing family, pyrin domain containing 3) inflammasomes and lead to the secretion of pro-inflammatory cytokines. Silica crystals and aluminum salts were shown cause NLPR3 inflammasome activation through

lysosomal rupture, where inhibition of lysosomal acidification with Bafilomycin completely blocked the silica induced IL-1β secretion. Interestingly, the activation of caspase-1 and secretion of IL-1β was found to be dependent on Cathepsin B. Further confirming the essential role of lysosomal destabilization in inflammasome activation, sterile LMP induced by lysosomotropic agent Leu-Leu-OMe (L-leucyl-L-leucine methyl ester) was shown to be sufficient to induce cytokine secretion in wild type, but not in NLRP3 or ASC deficient bone marrow–derived macrophages (Hornung et al., 2008). Similarly, Amyloid β was shown to induce NLPR3 activation and the consequent caspase-1 activation and interleukin secretion through LMP and cathepsin B. Interestingly, cathepsins D and L were found have no role in inflammasome activation (Halle et al., 2008). NLRP3 inflammasome was suggested to mediate the inflammatory response observed in atherosclerosis. Cholesterol crystals, as observed in atherosclerosis, was shown to elicit acute inflammation in mice when injected intraperitoneally. However, mice deficient of cathepsin B was found to be resistant to induction of inflammation indicating the crucial role of lysosomes in cholesterol crystals induced inflammasome activation (Duewell et al., 2010). Interestingly, one of the major cholesterol oxidation product, 27-hydroxycholesterol, was shown to cause lysosomal destabilization and pyroptosis, which was partially prevented by the cathepsin B inhibitor, CA-074-me, demonstrating the key role of lysosome and lysosomal protease in the execution of pyroptotic cell death (Chen et al., 2019).

1.6.3.2.5 LMP and ferroptosis

Lysosomes are mainly implicated in ferroptosis due to their essential role in autophagy and cellular iron homeostasis. Lysosomes forms a major source of free iron due to the degradation of iron binding protein ferritin in lysosomes during the process called ferritinophagy, which is mediated by the cargo receptor Nuclear receptor coactivator 4 (NCOA4) (Hou et al., 2016). Addition of iron

chelators like deferoxamine or desferrioxamine, which are known to accumulate exclusively in acidic organelles such as lysosomes (Cable and Lloyd, 1999; Persson et al., 2003), was shown to abrogate lysosomal ROS generation and ferroptotic cell death (Kubota et al., 2010; Torii et al., 2016). Further evidence of involvement of iron levels and lysosomes in ferroptosis has been revealed by inhibition of lysosomal acidity and proteases using respective inhibitors. These approaches effectively decreased the labile iron pool by preventing the degradation of ferritin and ROS generation in lysosomes and ameliorate cell death induced by ferroptotic inducers (Kubota et al., 2010; Gao et al., 2016; Torii et al., 2016).

Therapeutic initiation of ferroptosis is an effective approach for induction of cell death. Salinomycin is an antibacterial compound, which is currently used in experimental studies for its breast cancer stem cell killing property. Salinomycin and its derivative Ironomycin, were shown to cause ferroptotic cell death by sequestering iron in the lysosomes, triggering degradation of ferritin and increasing lysosomal ROS production. This was rescued by iron chelator deferoxamine and cathepsin B inhibitor illustrating the role of lysosomes in ferroptosis (Mai et al., 2017). Similarly, a recent report showed that ferroptosis is mediated by permeabilization of lysosomes after administration of cisplatin, a platinum based antitumor agent in human renal proximal tubular epithelial cell line HK-2 (Deng et al., 2019). Despite the importance of LMP in execution of ferroptosis, the potential existence of an executioner molecule and the underlying mechanisms in ferroptosis remains unknown.

The contribution of lysosomes to induction of ferroptosis is not merely a passive action mediated by their rupture; in fact, lysosome may actively contribute to ferroptosis by degradation of few endogenous anti-ferroptotic proteins including Glutathione Peroxidase 4 (GPX4). This endogenous antioxidant enzyme is involved in the neutralization of lipid peroxides and plays a

central role in preventing ferroptosis. Genetic depletion or inhibition of GPX4 activity using specific inhibitors like RSL3 or by depleting GSH can induce ferroptosis (Friedmann Angeli et al., 2014; Gaschler et al., 2018). Recently, GPX4 was shown to be degraded through the lysosomal autophagic process CMA in response to ferroptosis induction by erastin. Inhibition of the molecular chaperone HSP90 was able to prevent GPX4 degradation and ferroptosis. Importantly, lysosomal acidification inhibitors such as Bafilomycin A1, chloroquine and ammonium chloride were shown to prevent erastin induced degradation of GPX4 and ferroptotic cell death (Wu et al., 2019). Similarly, ARNTL (aryl hydrocarbon receptor nuclear translocator-like protein 1), is a core circadian clock protein that is degraded in lysosomes during ferroptosis. Inhibition of lysosomal acidification using chloroquine inhibited ARNTL degradation in human tumor cell lines, Calu-1 and HT1080 (Yang et al., 2019a).

The possibility of LMP in ferroptosis was suggested by us (Nagakannan and Eftekharpour, 2017a) and others (Gao et al., 2018). We showed that ferroptotic induction was associated with the leakage of lysosomal cathepsin B into the cytosolic compartment. Inhibition of cathepsin B was able to mitigate cell death induced by various ferroptotic inducing agents. Inhibition of CTSB synthesis was also effective in prevention of ferroptosis (Gao et al., 2018).

1.7 Thesis overview

1.7.1 Study rationale

Oxidative stress has been identified as a common phenomenon in almost all disease conditions including trauma, degenerative diseases, and numerous cancers. Oxidative modifications of biomolecules, especially proteins and lipids, by ROS is a common process during normal cellular metabolism. Cellular thiols, including glutathione (GSH) and thioredoxin (TRX) are cellular rheostat for regulation of ROS levels. However, overproduction of ROS or depletion of cellular antioxidants can result in oxidative stress, which can cause severe oxidative damage of macromolecules impairing their functions. As highlighted in the above section, lysosomes play a key role in autophagic process and are crucial for maintaining cellular homeostasis. Disruption of lysosomal integrity is highly lethal due to its highly acidic content and hydrolytic enzymes capable of digesting most of the cellular macromolecules. Previous reports have identified that several factors can destabilize lysosomes leading to cell death. However, the impact of uncontrolled ROS generated due to the inactivation or depletion of endogenous antioxidants on lysosomal integrity and status of lysosomal cathepsins needs further investigation. A potential link between lysosomal-autophagy pathway and the novel non-apoptotic cell death mechanism, ferroptosis, has been shown previously; however, the underlying mechanism is not clear.

1.7.2 General hypothesis and research objectives

The overall goal of my PhD thesis was to investigate the potential involvement of cellular thiols in lysosome-mediated cell death during oxidative stress and identify the key molecular players.

1.7.3 Hypotheses:

1. Severity of oxidative stress dictates the crosstalk between autophagy and apoptosis
2. Lysosomal destabilization and differential regulation of lysosomal cathepsins mediate the interplay between autophagy to apoptosis
3. Lysosomal cathepsins mediate the execution of lipid peroxidation induced non-apoptotic cell death, ferroptosis.

1.7.4 Specific research objectives:

1. To determine the effect of oxidative stress induced by inactivation of endogenous antioxidant system on autophagy and apoptosis.
2. To investigate the role of lysosomes and lysosomal cathepsins in the crosstalk between autophagy to apoptosis.
3. To investigate the status of lysosomes and cathepsins in ferroptosis.

Chapter 2

Perturbation of redox balance after thioredoxin reductase deficiency interrupts autophagy-lysosomal degradation pathway and enhances cell death in nutritionally stressed SH-SY5Y cells

Contents of this chapter has been included in the following published article:

Pandian Nagakannan, Mohamed Ariff Iqbal, Albert Yeung, James A. Thliveris, Mojgan Rastegar, Saeid Ghavami, Eftekhar Eftekharpour. Perturbation of redox balance after thioredoxin reductase deficiency interrupts autophagy-lysosomal degradation pathway and enhances cell death in nutritionally stressed SH-SY5Y cells. *Free Radical Biology and Medicine 2016;101:53-70.*

Author Contributions: My contributions in this work includes conceptualization, experimental design, collection and interpretation of data. Dr. Eftekhar Eftekharpour performed confocal microscopy and image analysis. Mohamed Ariff Iqbal was responsible for lentiviral work and Albert Yeung analyzed ROS levels in immunostained images (Suppl. Fig. 2.1). Dr. James Thliveris performed electron microscopy. Dr. Mojgan Rastegar provided training and technical expertise for the lentiviral work. Dr. Saeid Ghavami gave experimental suggestions and provided ATG7 knockout adenovirus. I prepared the manuscript under the guidance of my supervisor.

Acknowledgement: Authors would like to acknowledge the support provided by Government of Manitoba for research funding through the Spinal Cord Injury Research Council (SCIRC), the Health Sciences Centre Foundation, and the University of Manitoba (EE). PN and MAI received studentships from Research Manitoba. We would like to acknowledge the technical expertise provided by Mr. Robby M. Zachariah and Mr. Khuong Le.

2.1 Abstract:

Oxidative damage and aggregation of cellular proteins is a hallmark of neuronal cell death after neurotrauma and chronic neurodegenerative conditions. Autophagy and ubiquitin protease system are involved in degradation of protein aggregates, and interruption of their function is linked to apoptotic cell death in these diseases. Oxidative modification of cysteine groups in key molecular proteins has been linked to modification of cellular systems and cell death in these conditions. Glutathione and thioredoxin systems provide reducing protons that can effectively reverse protein modifications and promote cell survival. The central role of Thioredoxin in inhibition of apoptosis is well identified. Additionally, its involvement in initiation of autophagy has been suggested recently. We therefore aimed to investigate the involvement of Thioredoxin system in autophagy-apoptosis processes. A model of serum deprivation in SH-SY5Y was used that is associated with autophagy and apoptosis. Using pharmacological and RNA-editing technology we show that Thioredoxin reductase deficiency in this model enhances oxidative stress and interrupts the early protective autophagy and promotes apoptosis. This was associated with decreased protein-degradation in lysosomes due to altered lysosomal acidification and accumulation of autophagosomes as well as impairment in proteasome pathway. We further confirmed that the extent of oxidative stress is a determining factor in autophagy- apoptosis interplay, as upregulation of cellular reducing capacity by N-acetylcysteine prevented impairment in autophagy and proteasome systems thus promoted cell viability. Our study provides evidence that excessive oxidative stress inhibits protein degradation systems and affects the final stages of autophagy by inhibiting autolysosome maturation: a novel mechanistic link between protein aggregation and conversion of autophagy to apoptosis that can be applicable to neurodegenerative diseases.

2.2 Introduction:

Macroautophagy, commonly referred to as autophagy, is a protective mechanism responsible for sequestration of old/damaged proteins and organelles by lysosomal proteases. This process (Feng et al., 2014) involves initiation and formation of phagophore vesicles to engulf the damaged proteins/organelles and formation of autophagosome. The autophagosome then fuses with lysosomes to form autolysosome in which proteases like cathepsins are activated and digest the cargo. Disruption of autophagy at any stage during this process has been shown to induce cell death and therefore it has been a hot research topic as a potential therapeutic approach that can induce or prevent cell death in different conditions.

Extensive research on the involvement of Reactive Oxygen Species (ROS) in regulation of autophagy indicate the importance of a balanced ROS-antioxidant ratio in autophagy progression: Low levels of ROS is required for basal autophagy(Scherz-Shouval and Elazar, 2007; Li et al., 2013b) and application of antioxidant molecules under normal conditions has been shown to be detrimental for autophagy process(Underwood et al., 2010). Increased ROS levels such as those observed in starvation (Scherz-Shouval et al., 2007a; Li et al., 2013b), neurodegenerative diseases (ND) (Ghavami et al., 2014; Walter et al., 2016), and injury (Tang et al., 2014; Wang et al., 2014) enhances autophagy-mediated protein degradation and excessive levels of ROS results in cell death (Chen et al., 2008b). Application of antioxidants has proven to be protective in these conditions by regulation of autophagy (Cabet et al., 2015). These reports indicate that maintaining the cellular redox balance is a critical factor for protective autophagy.

The redox balance of the cell is regulated by the availability of cellular thiol systems including Glutathione (GSH) and Thioredoxin (Trx). Numerous lines of evidence suggest that reversible oxidation of cysteines in key signaling molecules is used as a molecular switch in many redox

regulated processes including autophagy (Levonen et al., 2014). Cysteine residues are found in many proteins including the autophagy related proteins (ATG), however the only direct evidence for regulatory role of ROS on autophagy has been shown for ATG4 (Scherz-Shouval et al., 2007a). This group showed that ATG4 is directly oxidized by H_2O_2, a critical step for formation of autopohagosomes(Scherz-Shouval et al., 2007a). A more recent report (Perez-Perez et al., 2014) indicated that ATG4 activity might be specifically regulated by Trx1 redox status, although this remains to be confirmed in mammalian systems. Trx1 redox status has also been shown to be involved in regulation of apoptosis(Ahsan et al., 2009; Zeldich et al., 2014) through inhibition of apoptosis signal kinase-1 by reduced Trx(Liu et al., 2000; Shao et al., 2015). These reports may suggest a key central role for Trx system in autophagy-apoptosis interplay.

Based on these reports, we employed a model of serum deprivation (SD) in SH-SY5Y neuroblastoma cells that has been previously used to study autophagy(Xu et al., 2013), and apoptosis(Bar-Am et al., 2005). The redox regulatory role of Trx1 is directly dependent upon the availability of its reduced form and its redox buffering capacity is disabled after oxidation. Thioredoxin reductase (TrxR) is a selenocysteine oxidoreductase and the most commonly known enzyme involved in reduction of oxidized Trx (Mustacich and Powis, 2000), although a more recent report suggested that glutathione and glutaredoxin systems can act as back up mechanism for Trx1 reduction(Du et al., 2012). Genetic knockout of heart specific mitochondrial TrxR (Kiermayer et al., 2015) results in dysregulation of autophagy; however, the underlying cellular mechanism remains unknown. In the present study, we employed Auranofin (Au), a well-studied pharmacological inhibitor of TrxR, and a small hairpin RNA editing approach to downregulate TrxR activity in SH-SY5Y neuroblastoma cells. This model was used to examine the underlying mechanisms of autophagy and apoptosis progression in nutritionally stressed SH-SY5Y cells.

2.3 Materials and methods

2.3.1 Reagents

The following reagents were used in this study: Auranofin and Puromycin (Tocris Bioscience, UK), Bafilomycin A1, Thioredoxin reductase 1 assay kit (Cayman chemical, USA), 3-Methyladenine, Chloroquine, N-Acetyl-L-cysteine, Iodoacetic acid, tertiary butyl hydroperoxide (Sigmaaldrich, Canada), CellROX Deep Red Reagent, Lysotracker Red DND-99, DQ Red BSA (Molecular Probes, USA), Insulin, Insulin-Transferrin-Selenium (ITS) and Halt Protease and phosphatase inhibitor cocktail (Thermo Scientific, USA), Iodoacetamide (abcam, USA). All other chemicals used in this study were of analytical grade.

2.3.2 Cell culture

The human neuroblastoma cell line SH-SY5Y was a kind gift from Dr. Jun-Feng Wang, University of Manitoba. The cells were grown in Dulbecco's modified Eagle's medium (DMEM) containing high glucose (4.5 g/L) supplemented with 4 mM glutamine, 1 mM Sodium Pyruvate and 10% heat inactivated Fetal Bovine Serum in a humidified incubator containing 5% CO_2 at 37°C. Pre-confluent cells (70-80% confluence) between passages 5-16 were used for these experiments.

2.3.3 Serum deprivation, treatments and measurement of cell viability

To induce serum deprivation, cells were washed once with warm serum free DMEM medium (SD medium) and were then incubated with fresh SD medium for specified time points. Auranofin (Au) was diluted in SD or complete growth medium to reach the indicated concentrations in culture medium. In experiments involving addition of autophagy inhibitors, cells were incubated with the indicated concentrations of inhibitors for 30 min in complete growth medium prior to induction of SD followed by co-treatment for the experimental time duration in SD medium with or without (Au). All inhibitors were dissolved in DMSO and were diluted in growth medium. The final

concentration of DMSO in the culture medium was less than 0.01% to avoid any solvent effects. N-Acetylcysteine (NAC) was prepared in DMEM at a stock concentration of 0.5 M. A final concentration of 2.5 mM was used in culture conditions. This did not cause any significant change in pH (pH=7.4±0.1). Any modification in the treatment protocols are described in the figure legends.

Cell viability was determined using Water Soluble Tetrazolium-1 reagent (WST-1, Roche Diagnostic GmbH, Mannheim, Germany) or Cell Counting Kit-8 (CCK-8) kit (Dojindo Molecular Technologies, Japan) according to the manufacturer's instructions. Briefly, SH-SY5Y cells were seeded in 96 well plates at a density of 15,000 cells/well in 100 µl culture medium and incubated for 24 - 48 hr for adhesion and then subjected to appropriate treatment conditions. At the end of experimental period, 10 µl of WST-1 or CCK-8 reagent was added to each well and incubated for further 4 hr. The absorbance was measured at 450 nm with background correction at 650 nm using Synergy H1 Hybrid Reader (BioTeK Instruments, USA). Cell viability was expressed as percentage of control.

2.3.4 Generation of TrxR1 knockdown and ATG7 knockout cell lines

Knockdown of TrxR1 in SH-SY5Y cells was achieved by lentiviral transfection of anti-TrxR1 shRNA. Lentiviral particles were produced by co-transfecting HEK293T cells with the packaging plasmids (GAG, VSVG, REV and TAT) and shRNA (Origene, USA), as shown previously (Rastegar et al., 2009). Medium containing viral particles was harvested 48 hr post transfection, centrifuged, filtered and diluted with fresh media and added to SH-SY5Y cells to downregulate TrxR1 using polybrene as transfection reagent.

To deplete ATG7, Cells were transfected with either control or ATG7 shRNA using adenoviral particles for 24 hr (Santa Cruz Biotechnolgies, USA). The cells were selected by growing in the presence of 1 µg/ml puromycin containing media(Ghavami et al., 2015).

2.3.5 Thioredoxin Reductase enzyme assay

TrxR activity was measured by end point assay according to the method described by Holmgren (Holmgren, 1979b) with slight modifications. Briefly, 20 µg of total cell lysate was incubated with the reaction mixture containing 5 µM of rhTrx, Insulin (250 µM) and NADPH (700 µM) in TE Buffer (50 mM Tris-HCl and 1 mM EDTA, pH 7.5) for 30 min at 37°C. After incubation, the reaction was terminated by addition of 1 mM DTNB / 8 M Guanidine HCl in 0.2 M Tris-Cl, pH 8.0 and the final absorbance was measured at 412 nm.

2.3.6 Measurement of reactive oxygen species

Cells were grown on glass coverslips were treated appropriately and incubated with 2.5 µM CellROX deep red reagent for 30 min at standard conditions. After the incubation period, media was discarded and cells were washed twice with PBS and fixed with 3% paraformaldehyde in PBS; to visualize the nuclei, cells were stained with DAPI (1:10000). The emitted far red fluorescence from CellROX was imaged using a LSM710 Zeiss confocal microscope (Zeiss, Germany) and the mean fluorescence intensity was measured using Image J software (NIH, version 1.49v)

2.3.7 Lysotracker red staining

SH-SY5Y cells grown on glass coverslips were treated as described above and were incubated with Lysotracker red reagent (250 nM) for 30 min at 37°C. After the incubation, the cells were washed twice with PBS and fixed with 3% paraformaldehyde in PBS. The coverslips were then used for double labelling for other protein/s as mentioned in figure legends, counterstained for nuclear marker DAPI and examined using confocal microscope. For imaging, Zen 2011 software

(Zeiss, Germany) was used; an imaging profile was optimized using control samples for baseline exposure time and intensity. This profile was then applied in random microscopic fields for all experimental conditions. Co-localization module in Zen software was used and an observer blinded to experimental conditions evaluated the co-localization of Lysotracker and LAMP2 in a minimum of 150 cells/condition.

2.3.8 DQ-BSA staining

Cells were incubated with 10 µg/ml DQ-BSA Red reagent for 4 hr at 37°C. After the incubation period, the cells were washed 3 times with PBS prior being subjected to the specified treatments in figure legends. At the termination of experiments, cells were washed with PBS and fixed with 3% paraformaldehyde in PBS and counterstained for nuclei using DAPI. The cells were imaged using confocal microscope using similar imaging conditions for all samples and the red fluorescence intensity was analyzed by Image J software.

2.3.9 Quantitative PCR

Total RNA from SH-SY5Y cells was extracted using Purelink RNA mini kit (Invitrogen). 1 µg of extracted RNA was linearly amplified and converted to cDNA using Superscript VILO cDNA synthesis kit (Invitrogen) according to manufacturer's instructions. Quantitative PCR was performed using 500 ng of cDNA with SYBR green (Molecular Probes) as the fluorescent reporter. GAPDH was used as housekeeping gene to normalize the values.

The primer sequences used were as follows: p62-F: 5'-AAGCCGGGTGGGAATGTTG-3'; p62-R: 5'-GCTTGGCCCTTCGGATTCT-3'; GAPDH-F: 5'-CTGACTTCAACAGCGACACC-3'; GAPDH-R: 5'-TGCTGTAGCCAAATTCGTTGT-3'.

2.3.10 Antibodies:

The following antibodies at specified dilutions were used in this study: LC3 (1:2500, Sigma) cleaved Caspase-3 (1:1000), cleaved Caspase-9 (1:1000), PARP-1 (1:1000), ATG7 (1:1000), ATG5 (1:1000), ubiquitin (1:1000), and rabbit IgG HRP-conjugated secondary antibody were obtained from Cell signaling Technologies, USA; Trx1 (1:1000), TrxR1 (1:1000), SQSTM1 (p62, 1:1000) and β-actin (1:4000) were obtained from Santa Cruz Biotechnologies, USA; Proteasome 20S (1:1000) and GAPDH (1:5000) were purchased from abcam, USA and LAMP2 (0.5 µg/ml) was purchased from Developmental Studies Hybridoma Bank, University of Iowa, USA. All Alexa flour labelled secondary antibodies used for immunocytochemistry were purchased from Molecular Probes, USA.

2.3.11 Western blot analysis

Cells were scrapped and collected by centrifugation at 4000 rpm for 5 min. The cell pellets were washed once with ice cold PBS and lysed in NP-40 lysis buffer (50 mM Tris HCl pH 8, 150 mM NaCl, 5 mM EDTA, 1% NP-40) with protease and phosphatase inhibitors by sonicating (3 x 5 sec) on ice and centrifuged at 10,000g for 15 min at 4°C to obtain the supernatant. Protein concentration in the cell extracts was measured using Pierce BCA Protein Assay Kit.

Western blotting was done according to routine protocols (Mahmood and Yang, 2012). Equal amount of proteins was resolved in SDS-PAGE and transferred to PVDF membrane. After blocking for 1 hr with 5% non-fat milk in Tris-buffered saline containing 0.2% Tween 20 (TBS-T), membrane was probed with primary antibodies overnight at 4°C, and HRP-conjugated secondary antibody for 1 hr at room temperature. Proteins were detected using ECL prime detection reagent (GE Healthcare Life Sciences). To assess equal loading, membranes were striped in 0.2 N NaOH for 15 min at room temperature and re-probed with β-actin or GAPDH antibody.

Densitometry measurements were done using AlphaEaseFC (version 6.0.0, Alpha Innotech) or Image J software.

2.3.12 Redox western blot

The redox status of Trx was assessed as described previously (Bersani et al., 2002). Briefly, cells were collected by scrapping, washed with PBS and lysed in TEU buffer (8 M Urea in 50 mM Tris–HCl, pH 8.2, 1 mM EDTA) containing 30 mM iodoacetic acid (IAA) and incubated for 30 min at 37°C. To remove the excess IAA, the proteins were precipitated with ice cold Acetone: 1 N HCl (98:2, v/v), washed two more times with ice cold Acetone: 1 N HCl and centrifuged at 13,000 x g for 10 min at 4°C. The pellet was dissolved in TEU buffer containing 3.5 mM DTT and incubated at 37°C for 30 min to reduce the disulfides and the newly reduced thiols were amidomethylated with 10 mM iodoacetamide (IAM) at 37°C for 15 min. Equal amount of proteins was subjected to native Urea PAGE on 8% gels and transferred to PVDF membrane followed by detection of bands using standard western blot protocol.

2.3.13 Immunocytochemistry

Cells were cultured on coverslips and after appropriate treatments, were washed in PBS and fixed with 3% paraformaldehyde in PBS. After permeabilization of cells with 0.3% Triton-X-100, coverslips were incubated with appropriate primary antibodies overnight at 4°C followed by PBS washes three times and incubated with secondary antibody for 1 hr at room temperature. After washing with PBS twice, nuclei were counterstained with DAPI and the coverslips were mounted on glass slides. Immunofluorescence images were acquired by confocal microscope.

2.3.14 Electron microscopy

Cells were pelleted after trypsinization, rinsed with PBS and fixed with 3% glutaraldehyde in 0.1 M phosphate buffer followed by 1% osmium tetroxide. Samples were embedded in Epon-812 and

stained with uranyl acetate and lead citrate and imaged using Phillips CM-10 electron microscope (Philips Electronics, Eindhoven, The Netherlands) (Luft, 1961)

2.3.15 Statistical analysis

All values were expressed as mean ± S.E.M. The statistical analysis was carried out by one-way analysis of variance (ANOVA) to compare multiple groups followed by Tukey's post-hoc test while two tailed unpaired student t-test was used for comparing two groups. For multiple comparisons where TrxR1 knockdown cells were used, data were analyzed by two-way ANOVA followed by Tukey's post-hoc test. *p* values less than 0.05 were considered as significant.

2.4 Results

2.4.1 Neuronal serum starvation induces an early induction of autophagy and apoptosis

Serum deprivation (SD) is a widely used stimuli for induction of autophagy (Bao et al., 2009) and apoptosis(Joza et al., 2001), providing a useful tool to identify underlying mechanisms governing the interplay between these two processes. In the present study, SH-SY5Y neuronal cells were starved in serum free DMEM-high glucose medium for 6, 24 and 48 hr. We observed a significant time dependent cell death starting as early as 6 hr after induction of SD, which was further enhanced up to 48 hr (Fig. 2.1A). We next confirmed a time dependent increase in caspase-3 and 9 cleaved products with cleaved PARP-1 protein levels indicating that SD induces apoptosis through classical caspase dependent pathway (Fig. 2.1B). We next assessed the progression of autophagy in this model. During the progression of autophagy, the cytosolic form of microtubule associated protein LC3 (LC3-I) is lipidated to form LC3-phosphatidyl-ethanolamine conjugate (LC3-II). LC3-II is localized on autophagosome and autolysosomal membranes, and is used as an important marker of autophagy induction(Son et al., 2012). An increase in LC3-II protein levels was observed at early hours of starvation (6 hr); however, the levels were returned to near normal level at the later time point (48 hr) (Fig. 2.1C-D) indicating that autophagy is an early event in cellular response to SD. Autophagy progression was further confirmed with time dependent increase in ATG12-ATG5 conjugate formation, and ATG7 levels and a decrease in p62 levels (Fig. 2.1C-D). Induction of autophagy and apoptosis was further confirmed using transmission electron microscopy (TEM) in starving SH-SY5Y cells at 6 and 24 hr. Autophagosomes (AP), as markers of autophagy were identified by a double-layer membrane vesicle which is reduced to one layer after fusion with primary lysosomes (LY) and formation of autolysosomes (AL) (Fig. 2.1E). At 6 and 24 hr of SD, we found marked accumulation of autophagosome and lysosomes confirming

an ongoing autophagy process. Apoptotic cells were identified by nuclear condensation only at later time points (24 hr) (Fig. 2.1 E4 and E5).

Figure 2.1. Serum deprivation (SD) results in activation of autophagy and apoptosis in SH-SY5Y cells.

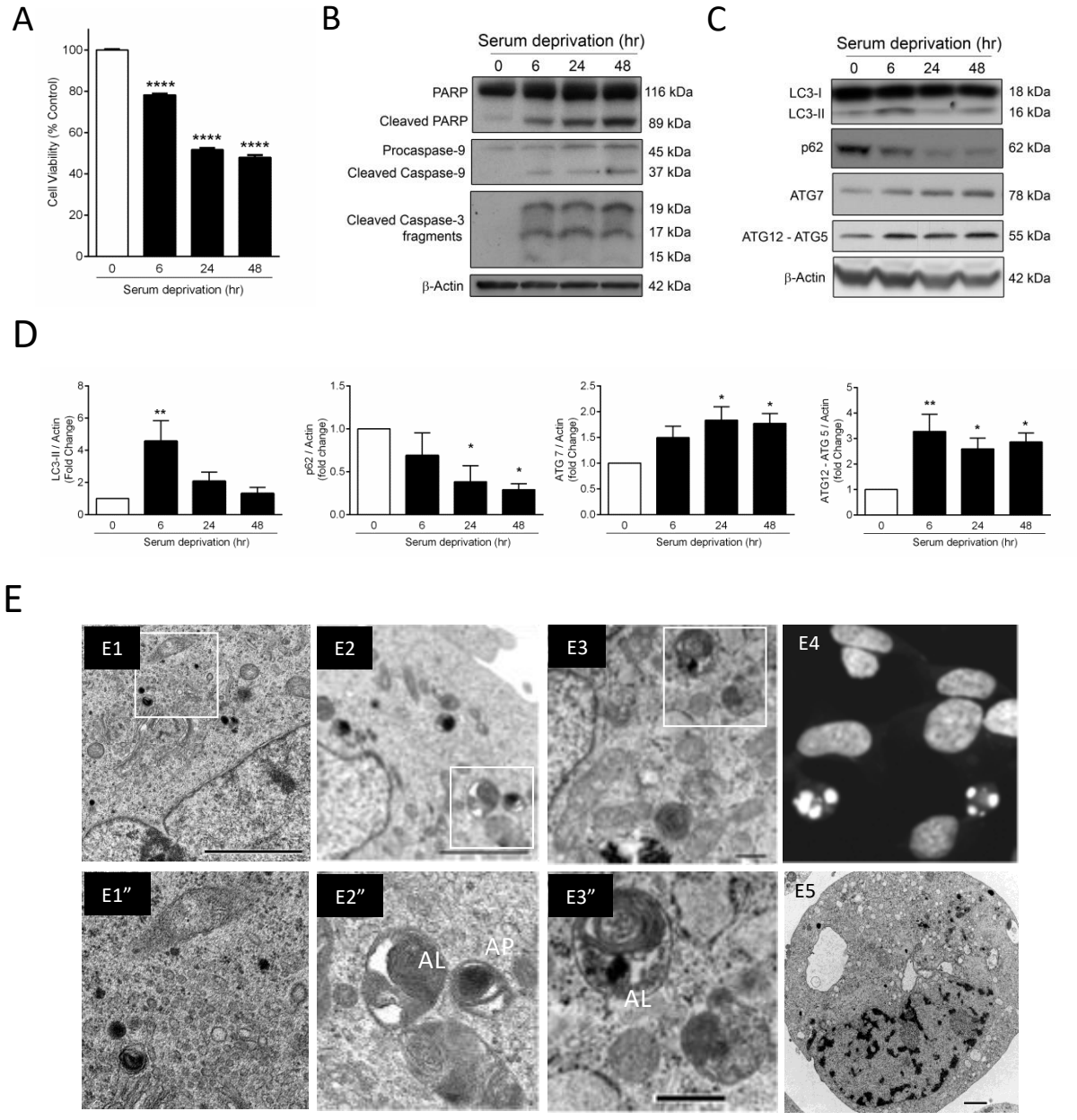

Figure 2.1. Serum deprivation (SD) results in activation of autophagy and apoptosis in SH-SY5Y cells. (A) SH-SY5Y cells were nutritionally stressed by depriving fetal bovine serum (FBS, 10%) for the indicated time periods and cell viability was assessed using Cell Counting Kit-8 assay. Values are expressed as mean ± S.E.M., $n \geq 6$; ****$p<0.001$. SH-SY5Y cells were harvested after indicated time durations of SD for western blot analysis of apoptotic **(B)** and autophagic markers **(C)**. Densitometric analysis of autophagy related proteins are summarized as bar graphs in **D.** Values are expressed as mean ± S.E.M., $n \geq 3$; *$p<0.05$, **$p<0.01$ Vs FBS control (0 hr). **(E)** Ultrastructural changes in normal and serum deprived cells using electron microscopy; Representative electron microscopy images of SH-SY5Y cells in normal growth condition **(E1)**, serum deprived for 6 hr **(E2)** and 24 hr **(E3)** are shown here. **E4** shows the fragmented apoptotic nuclei after 24 hr serum deprivation. Higher magnification images of the inserts in **E1, E2** and **E3** are shown as **E1", E2"** and **E3"**. TEM image of condensed nuclei after 24 hr serum deprivation is shown in **E5**.

2.4.2 Serum deprivation induces Thioredoxin reductase 1 upregulation

Thioredoxin (Trx) and thioredoxin reductase (TrxR) are well recognized molecules that are induced during cellular adaptive response to stressful conditions (Eftekharpour et al., 2000; Andoh et al., 2002) and in tissue samples in ND (Lovell et al., 2000). We therefore examined the levels of Trx related proteins in our model (Fig. 2.2A). Western blotting showed a non-significant increase in Trx1 protein level at 6, 24 and 48 hr after SD (Fig. 2.2A and B); however, a significant increase in TrxR1 protein level (2 fold) was observed at 6 hr which was maintained throughout the experimental duration (Fig. 2.2A and C). Insulin reductase activity was used to investigate the correlation of TrxR protein levels and its enzymatic activity. We observed that the increase in TrxR protein level at 6 hr was associated with a significant increase in TrxR enzymatic activity. However, TrxR enzymatic activity returned to basal levels in 24 and 48 hrs SD samples, despite the elevated levels of TrxR protein (Fig. 2.2C). This may indicate the importance of TrxR enzymatic activity during the early time points of starvation-induced oxidative stress in these cells. Our data suggest that the ongoing oxidative stress in these conditions may lead to inactivation of TrxR activity which coincides with autophagy exit and promotion of apoptosis.

2.4.3 Pharmacological inhibition of TrxR enhanced cell death in serum-deprived SH-SY5Y cells

To investigate the involvement of TrxR in cell survival, we employed Auranofin (Au), a well-characterized inhibitor of TrxR (Marzano et al., 2007). Au has been studied extensively to induce cell death in cancer cells where increased Trx levels has been linked to resistance to chemotherapeutic treatments (Lu et al., 2007). An effective dose of Au (0.5uM) was chosen to decrease the TrxR activity by 50% under SD conditions (IC50) (Fig. 2.2D). This was associated with significant cell death in these cells (Fig. 2.2E). Interestingly, this dose of Au caused a significant increase in TrxR enzymatic activity in normal condition (Fig. 2.2D) but did not cause

any significant changes in cell viability (Fig. 2.2E). We and others have previously shown that TrxR activity and protein levels is upregulated after addition of electrophiles (Eftekharpour et al., 2000; Hintze et al., 2003), indicating that TrxR is regulated by antioxidant response element (Brigelius-Flohe et al., 2012).

To investigate the underlying mechanism of enhanced cell death after pharmacological inhibition of TrxR, we used western blotting for apoptosis markers. Our data indicated that administration of Au further exacerbated the expression of apoptotic markers in a dose dependent fashion (Fig. 2.2F). Au treatment at 0.25 and 0.5uM increased PARP cleavage and activation of caspases 3 and 9 in comparison with their untreated timed match controls. This confirms that loss of TrxR activity during nutritional stress further aggravates cell death. Our observations confirm previous reports that Trx system, in particular TrxR, plays an essential role in survival of cells during stressful conditions (Cox et al., 2008).

Figure 2.2. Pharmacological inhibition of Thioredoxin Reductase enhances apoptosis in serum deprived (SD) SH-SY5Y cells.

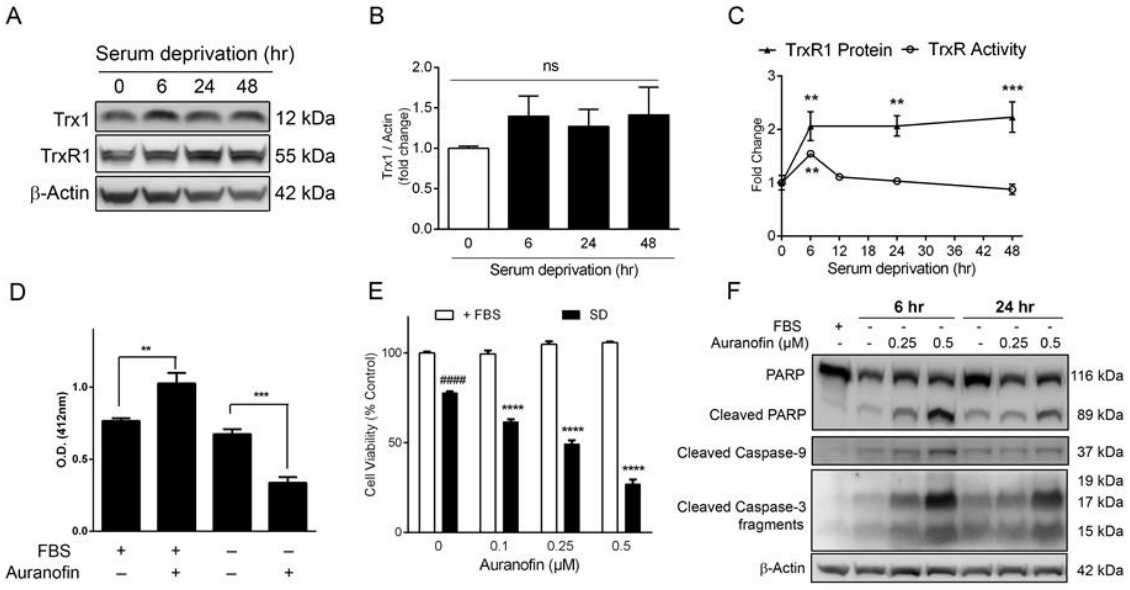

Figure 2.2. Pharmacological inhibition of Thioredoxin Reductase enhances apoptosis in serum deprived (SD) SH-SY5Y cells. **(A)** SH-Y5Y cells were subjected to increasing durations of serum deprivation and assessed for the levels of Thioredoxin 1 and Thioredoxin reductase 1 by western blotting. Quantification of Trx1 protein levels is shown as bar graph **(B)** and TrxR1 protein and TrxR activity are shown as line graph **(C).** TrxR activity was measured by Insulin reduction assay (described in materials and methods section). Values are expressed as mean ± S.E.M., n≥6 for protein and n=3 for TrxR activity; **p<0.01, ***p<0.001 Vs FBS control. **(D)** SH-SY5Y cells were incubated with auranofin (0.5μM) in complete growth condition (10% FBS media) or serum free media for 24 hr and thioredoxin reductase activity in whole cell lysate was estimated by Insulin reduction assay. Values are expressed as mean ± S.E.M. n=3; **p<0.01 and ***p<0.001. **(E)** Cell viability was assessed using WST-1 assay in SH-SY5Y cells exposed to indicated concentrations of auranofin in complete growth medium (10% FBS) or serum free medium (SD) for 24 hr. Values are expressed as mean ± S.E.M., n=9; #### p<0.0001 Vs 10% FBS Control, **** p<0.0001 Vs SD Control. **(F)** Representative western blots showing markers of apoptosis in lysates extracted from SH-SY5Y cells incubated with indicated concentrations of auranofin during different durations of SD.

2.4.4 Pharmacological inhibition of TrxR enhances oxidative stress and protein ubiquitination

The involvement of Trx system in maintaining the redox balance has been attributed to the direct interaction of Trx with peroxides or as a substrate for peroxiredoxin-mediated ROS scavenging (Hanschmann et al., 2013). Trx is oxidized in these reactions and therefore the availability of TrxR activity is essential for maintaining Trx in its active form. We therefore examined the effect of TrxR inhibition on ROS levels and Trx oxidation. CellRox is a cell permeable reagent that is oxidized by ROS and produces a strong fluorescence detectable microscopically. We observed that SD enhances the endogenous ROS levels in SH-SY5Y cells, this was significantly intensified after addition of Au to these cells (Suppl. Fig. 2.1A). Increased levels of ROS has been linked to increased protein ubiquitination after SD (Cernotta et al., 2011). Therefore, ubiquitinated proteins were assessed by western blotting, using an antibody that detects all ubiquitinated proteins; although we did not detect any significant changes in SD-treated cells after 6hr of SD, a prominent rise in the level of ubiquitinated proteins was detected after inhibition of TrxR using Au (Suppl. Fig. 2.1B) suggesting a failure in cellular proteolytic mechanisms as a consequence of aggravated oxidative stress.

2.4.5 TrxR inhibition blocks autophagy by impairing autophagic clearance of aggresomes

Recent reports have indicated that pharmacological inhibition of TrxR induces cell death in cancer cells by triggering autophagy (Shao et al., 2015) leading to accumulation of autophagosomes and cell death (Lin et al., 2015), however the underlying mechanisms have not been adequately investigated. We therefore examined whether autophagy is interrupted in this model. Using western blotting for autophagy markers, a significant increase in LC3-II levels (3.6-fold change) was observed at 6 hr of SD in SH-SY5Y cells. Although addition of Au (0.5μM) to SD-treated cells caused an increase in LC3-II levels when compared to control cells (2.02-fold change), this

increase was significantly lower than SD alone; this indicates that TrxR inhibition decreases the autophagy rate at early time point. By 24 hr after SD/ SD+Au treatment, the increase in LC3-II levels of Au-treated cells was not significantly different when compared to SD-treated cells (Fig. 2.3A, C and D). Additionally, no significant change observed in ATG12-ATG5 conjugate levels in comparison with their relevant SD controls.

Evidence of autophagy interruption in Au-treated cells is also shown in Figure 2.3A. A reliable marker of autophagy progress is the disappearance of p62 in normal autophagy. p62, also known as ubiquitin binding protein p62 or sequestosome-1, is an adaptor protein involved in selective degradation of ubiquitinated autophagy substrates. Accumulation of p62 is a well-recognised marker for autophagy interruption and has been well studied in context to ND, where accumulation of protein aggregates is prominent (Lippai and Low, 2014a). Immunocytochemical analysis revealed that Au-treatment enhances p62 protein accumulation as early as 3 hr after induction of stress, which was further intensified at 6 hr. This was associated with accumulation of enlarged autophagosomes in Au-treated cells (Fig. 2.3B) at 6 hr. The increase in p62 protein levels was also confirmed using western blotting at 6 and 24 hr after stress. The SD-treated cells displayed a notable decrease in p62 protein levels indicating a normal autophagy progression, whereas addition of Au to the SD-treated cells resulted in a significant increase in p62 levels at 6 ($p<0.001$) and 24 hr ($p<0.01$) when compared to their time matched SD-treated cells (Fig. 3C, D). The increase in p62 levels can be resulted from two processes: 1) in situ synthesis in response to activation of antioxidant response element (Haga et al., 2014), and 2) autophagy interruption/inhibition(Korolchuk et al., 2009). We therefore used real time PCR which revealed a significant increase of p62 mRNA levels (Fig. 2.3E) in SD+Au treated cells, indicating that increased transcription of p62 is partly responsible for p62 accumulation. The contribution of

autophagy inhibition was assessed using western blotting for LC3-II levels in cultures of SH-SY5Y cells subjected to SD with or without Au in the presence or absence of bafilomycin A1 (Baf A1), an inhibitor of autophagy maturation. Following the standard protocols (Rubinsztein et al., 2009), LC3-II levels were normalized to actin and then were compared in the presence and absence of BafA1. In SD-treated cells, LC3-II levels were significantly increased with BafA1 treatment, indicating a normal autophagy flux. However, addition of BafA1 in SD+Au-treated cells, did not cause any significant increase in LC3-II levels indicating an interruption of autophagy flux after inhibition of TrxR activity (Suppl. Fig. 2.2). To ensure that Baf A1 has efficiently blocked the lysosomal function in these experiments, a high dose of Baf A1 (100nM) was added during the last 4 hr of the experiment and the LC3-II levels were quantified. Similar results to the Baf A1 low-dose experiments were observed after administration of 100nM Baf A1 (Fig. 2.4A and B). Evidence of autophagy flux inhibition was further shown by accumulation of autophagosomes in Au-treated cells using TEM (Suppl. Fig. 2.3). These results confirms the previous report on TrxR role in modulation of autophagy (Lin et al., 2015).

To demarcate the exact stages of autophagy that are affected by TrxR inhibition, we employed two approaches: administration of chemical inhibitors of autophagy and genetic knockdown of autophagy related protein 7 (ATG7). Application of 3-Methyl adenine (3-MA, 5mM), Chloroquine (CQ, 20μM) and Bafilomycin A1 (BafA1, 10nM) enhanced the SD-mediated cell death at 24 hr, suggestive of the protective effect of autophagy during starvation. Inhibition of TrxR by Au, significantly ($p<0.0001$) sensitized the serum starved cells to the cytotoxic effects of the above-mentioned autophagy inhibitors as shown by enhanced cell death (Fig. 2.4C), indicating that TrxR inhibition promotes apoptosis through interruption of autophagy. Likewise, other autophagy inhibitors such as Spautin-1 and LY294002 (PI3 kinase inhibitor) also enhanced cytotoxicity of

Au under SD condition, further supporting the above findings (data not shown). A similar effect was observed in autophagy compromised cells where addition of Au significantly ($p<0.05$) increased cell death at 6 hr in ATG7 knockdown cells in comparison to normal cells (Fig. 2.4D). These results suggest that inhibition of TrxR could be inhibiting the progression of protective autophagy at multiple steps.

Figure 2.3. Pharmacological inhibition of Thioredoxin Reductase inhibits serum deprivation (SD) induced autophagy in SH-Y5Y cells.

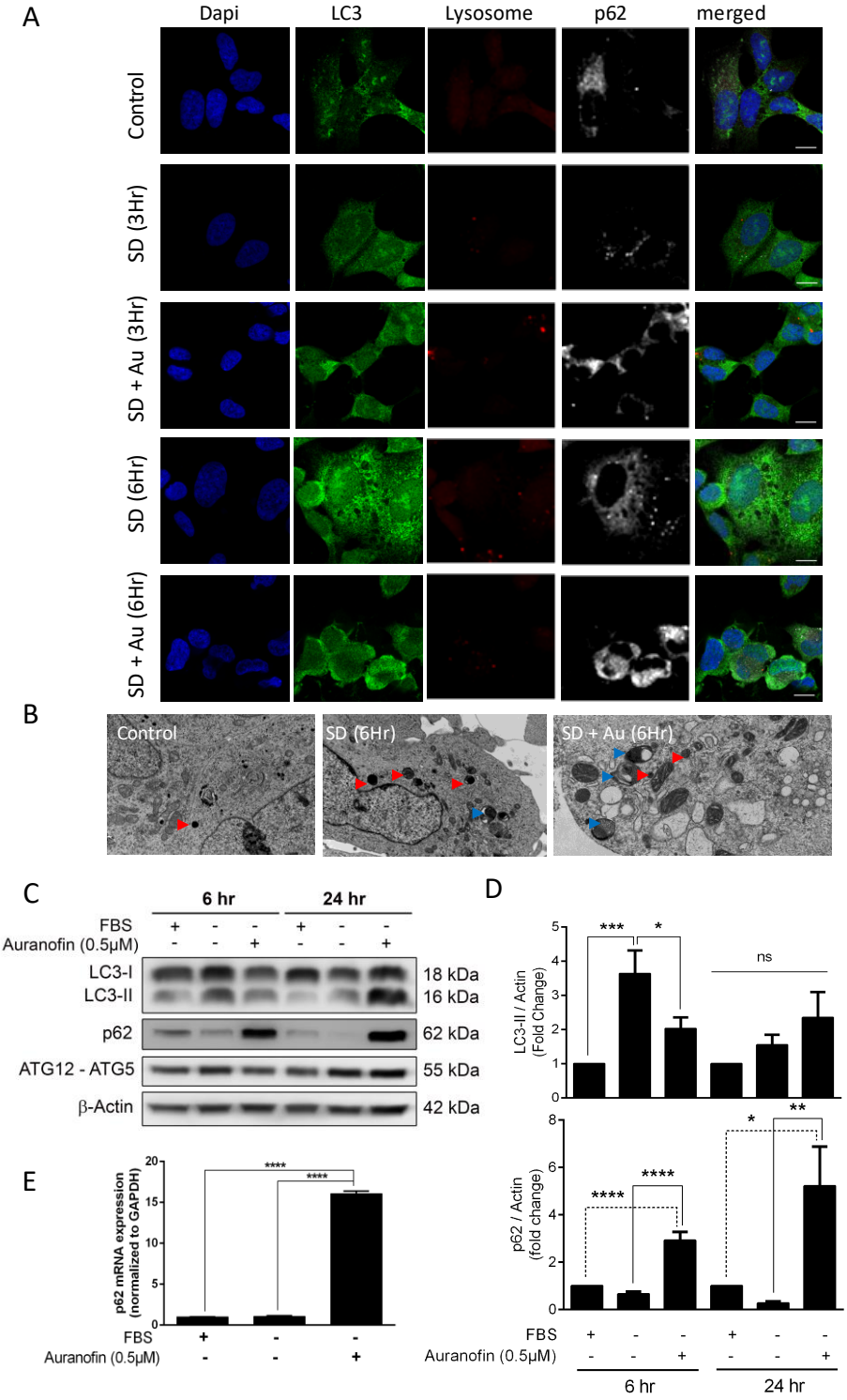

Figure 2.3. Pharmacological inhibition of Thioredoxin Reductase inhibits serum deprivation (SD) induced autophagy in SH-Y5Y cells. (A) Immunofluorescence images showing the effect of auranofin (Au) on SD induced autophagy. SH-SY5Y cells were deprived of serum for either 3 or 6 hr and incubated with or without Au (0.5μM) and the cells were labeled for lysosomes with lysotracker red reagent (red) and stained for LC3 (green) and p62 (white); nuclei were stained with DAPI (blue). **(B)** Ultrastructural changes in normal and serum deprived SH-SY5Y cells treated with or without Au (0.5μM) analysed by electron microscopy. Arrow heads identify Autophagosomes (blue) and lysosomes (red). **(C)** Au inhibits autophagy. Representative western blot showing autophagy related protein levels in SH-SY5Y cell lysates subjected to SD in the presence or absence of Au. **(D)** Quantification of LC3-II and p62 protein expressions are shown as bar graphs. Values are expressed as mean ± S.E.M., n≥6; *p<0.05, **p<0.01, ***p<0.001, ****p<0.0001 Vs FBS control. **(E)** Au upregulates p62 mRNA levels in serum deprived SH-SY5Y cells. Total RNAs were prepared from cells that were subjected to 6 hr of SD in the presence or absence of Au and p62 mRNA levels were quantified using qPCR. Values are expressed as mean ± S.E.M., n=3; ****p<0.0001 Vs FBS control.

Figure 2.4. Inhibition of Thioredoxin Reductase affects autophagy flux in serum deprived (SD) SH-SY5Y cells.

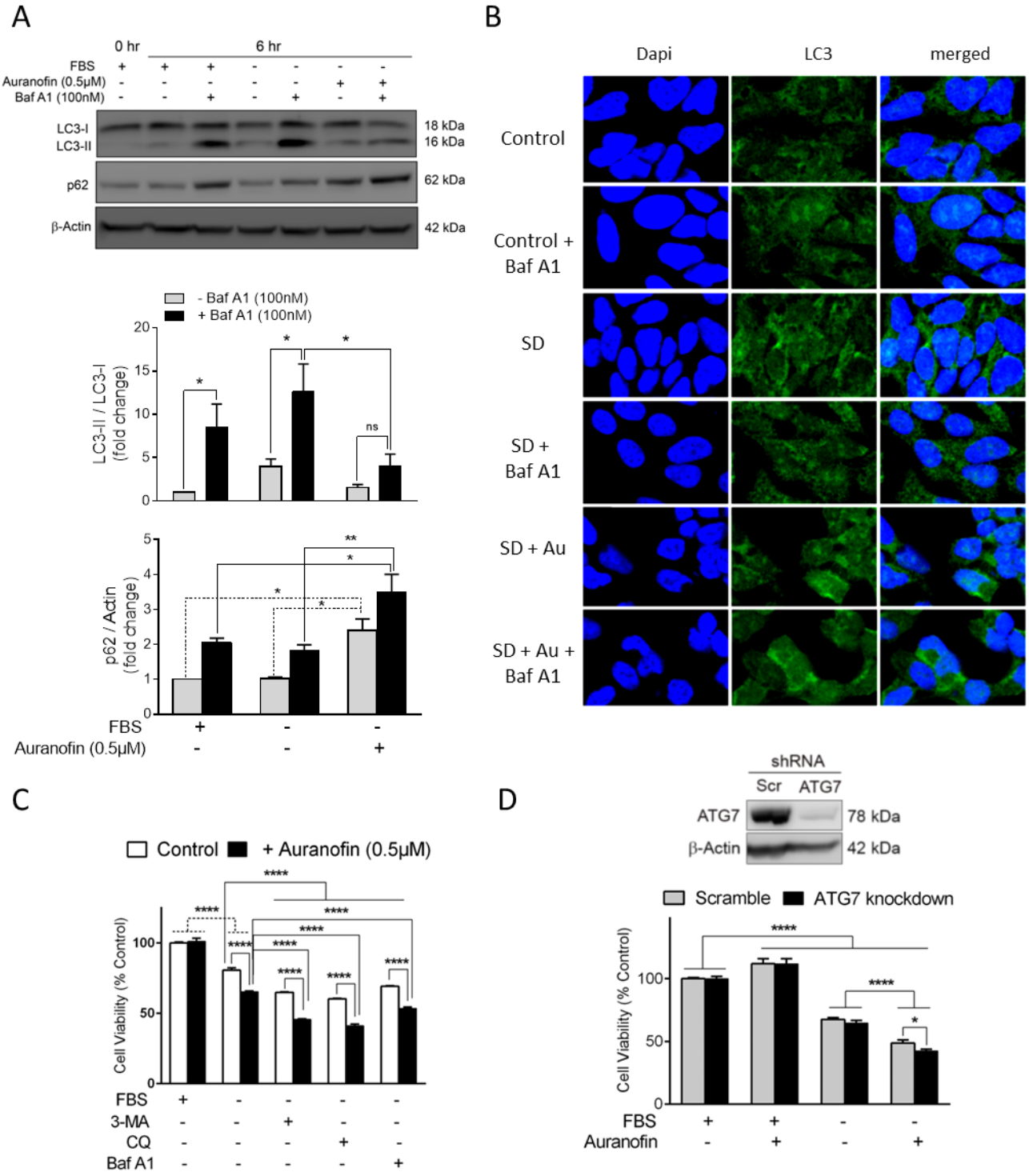

Figure 2.4. Inhibition of Thioredoxin Reductase affects autophagy flux in serum deprived (SD) SH-SY5Y cells. Au decreases autophagy flux. **(A)** Representative western blot showing LC3 and p62 protein levels in lysates extracted from SH-SY5Y cells subjected to serum deprivation for 6 hr in the presence or absence of Au (0.5μM) or Baf A1 (100 nM) or both; Baf A1 was added during the last 4 hr of SD. Quantification of LC3-II and p62 protein expressions are shown as bar graph. Values are expressed as mean ± S.E.M., n≥3; *p<0.05, **p<0.01. **(B)** Immunofluorescence images of LC3 (green) in SH-SY5Y cells subjected to SD for 6 hr in the presence or absence of Au (0.5μM) with or without Baf A1 (10nM). **(C)** SH-SY5Y cells were subjected to SD for 24 hr with or without auranofin (0.5μM) in the presence or absence of the following autophagy inhibitors: 3-methyladenine (3-MA, 5mM), Chloroquine (CQ, 20μM) and Bafilomycin (Baf A1, 10nM) and assessed for cell viability using WST-1 assay. Values are expressed as mean ± S.E.M., n=3; ****p<0.0001. **(D)** ATG7 was downregulated using adenovirus mediated shRNA delivery. Cell survival in scramble or ATG7 knockdown cells subjected to SD in the presence or absence of auranofin (0.5μM) for 6 hr was measured using cell Counting Kit-8 assay. Values are expressed as mean ± S.E.M., n≥4; *p<0.05, ****p<0.0001.

2.4.6 Defective lysosomal activity underlies autophagy interruption during TrxR deficiency

To investigate whether protein degradation systems are affected after TrxR inhibition, we focused on the lysosome machinery and ubiquitin proteasome system. Intracellular proteins destined for degradation are tagged by ubiquitination for recycling by the proteasome system, but long-lived proteins and autophagy-destined old organelles are additionally tagged and chaperoned by p62 to autophagosomes. These will eventually fuse with lysosomes to form active autolysosomes and recycle the p62-labelled cargo (Lippai and Low, 2014a). Any interruption of lysosomal function will result in accumulation of ubiquitinated proteins and consequently cell death (Gu et al., 2005). To confirm if TrxR deficiency impairs lysosomal activity, we measured the protein degradation capacity of lysosomes. DQ-BSA is a compound that is taken up by lysosomes through endocytosis and produces a bright red fluorescent signal after degradation in acidic environment of lysosomes. With 6 hr of SD, a significant increase ($p<0.0001$) in red fluorescence was observed indicating a rise in lysosome-mediated degradation of DQ-BSA. Addition of Au to the serum starved cultures caused a significant reduction ($p<0.0001$ vs SD) in DQ-BSA fluorescence indicating an impaired lysosomal degradative capacity (Fig. 2.5A).

To further confirm changes in lysosomal activity, we used Lysotracker, a fluorescent stain that labels acidic active lysosomes in live cells (Zhou et al., 2013). A prominent increase in number of lysotracker-positive vesicles was observed after 6 hr in SD conditions (Fig. 2.5B). This reflects the normal increase in lysosomal activity during serum deprivation, and is in agreement with previous reports (Zhou et al., 2013). On the contrary, addition of Au during SD caused a substantial decrease in lysotracker-positive lysosomes. To ensure the Lysotracker signal specificity to lysosomes, we assessed LAMP2-Lysotracker colocalization by using the co-localization probe in

Zen software. This approach has been previously used to examine proper acidification of lysosomes and autolysosomes (Lee et al., 2010). A significant decrease in lysosomal acidification was detected by a decrease in colocalization co-efficiency ($p<0.0001$) in serum starved cells treated with Au, indicating a diminished acidification of LAMP2-positive vesicles (Fig. 2.5C). This was visualized further using the Profile probe in Zen software (Fig. 2.5C"). The signal intensity for Lysotracker staining shows a prominent increase in lysosomal number and Lysotracker signal in SD-treated cells (Fig. 2.5C2") in comparison to the normal controls (Fig. 2.5C1"). The Au-treated cells contained enlarged LAMP2-positive clusters and did not show any detectable Lysotracker signal confirming that Au-mediated inhibition of TrxR is associated with a defective lysosome acidification (Fig. 2.5C3").

Figure 2.5. Thioredoxin reductase deficiency causes defective lysosomal activity.

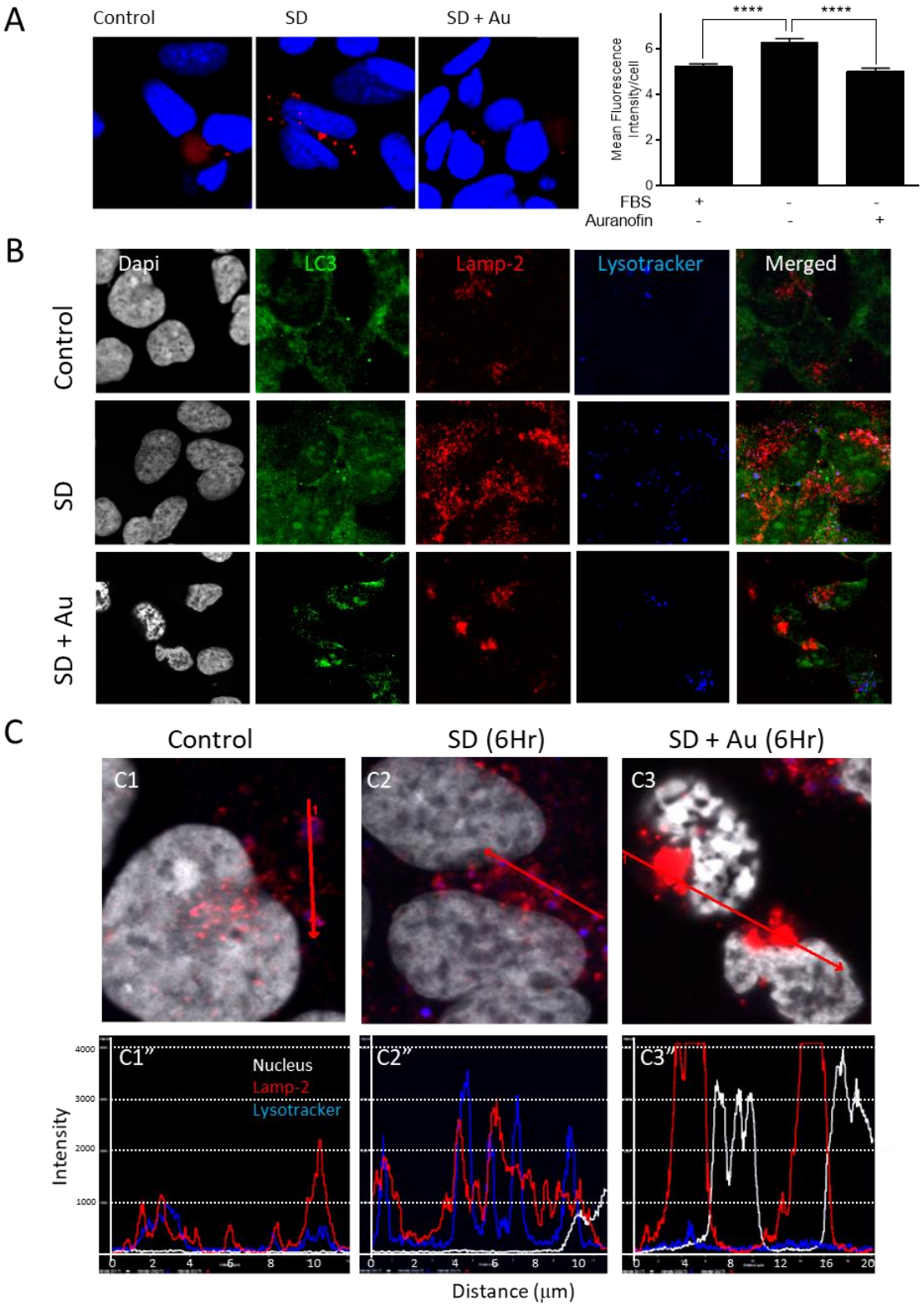

Figure 2.5. Thioredoxin reductase deficiency causes defective lysosomal activity. (A) SH-SY5Y cells were loaded with DQ-BSA Red (10µg/ml) and the cells were subjected to SD for 6 hr in the presence or absence of Auranofin (Au, 0.5µM). Representative images showing degradation of DQ-BSA (as red fluorescence) and quantification of DQ-BSA fluorescence normalized to per cell are shown. Values are expressed as mean ± S.E.M. n≥60 cells. ****p<0.0001. **(B)** Active (acidic) lysosome/autolysosomes were labelled using Lysotracker. SH-SY5Y cells were treated as described and the cells were incubated with the Lysotracker for 30min before termination of experiment. Cells were then washed and fixed with PFA as described in Materials and Method. Anti-LAMP2 antibody was used for identification of autophagosomes and lysosomes. Representing confocal microscopy images are depicted here. **(C1-C3)** Confocal images of SH-SY5Y cells showing immunolabelled LAMP2 (Red) and Lysotracker (blue) were used for quantification of signal intensity using profile analysis tool in Zen 2011 software (Zeiss). **(C1"-C3")** depicting the signal intensity along the red arrow in their respective microscopic field. Colocalization of LAMP2-Lysotracker was also assessed using the Colocalization analysis tool in Zen 2011 software. We observed that Au-treated cells displayed a significantly lower colocalization co-efficient than their SD counterparts. (0.379±0.012 in SD vs. 0.303 ±0.013 in Au-treated, p<0.0001).

2.4.7 Enhancement of cell reducing capacity prevents Au-mediated impairment of autophagy and ubiquitin proteasome system and improves cell survival under serum deprived conditions

To investigate whether alleviating oxidative stress by antioxidant treatment can translate into better proteolysis, we examined the efficiency of NAC (2.5mM) in reverting the diminished proteolytic activity during TrxR inhibition. Evidence of improved autophagy was observed after co-incubation of Au treatment with NAC. This approach significantly reduced the accumulation of p62 (Fig. 2.6A) and poly-ubiquitinated proteins (Fig. 2.6B) in Au treated starving SH-SY5Y cells. To address the possibility whether accumulation of poly-ubiquitinated proteins after Au-treatment is due to inhibition of proteasome system, the level of proteasome 20s subunits was assessed using western blotting. Serum deprivation alone caused a modest increase in proteasome 20s levels indicating the activation of Ubiquitin Proteasome System (UPS) during oxidative stress. However, addition of auranofin significantly reduced the levels of proteasome 20s when compared to SD alone indicating an inhibition of UPS system under TrxR deficient state which was prevented with the addition of NAC (Fig. 2.6C). Of note, we observed that our anti-proteasome 20s antibody detected a high molecular weight band (~80kDa) in 24hr-Au treated cells that may suggest a proteasome 20s dimer/oligomer formation or a defective proteasome processing under oxidative stress conditions. NAC treatment completely dissolved this high molecular weight band. The protective roles of NAC on cell viability has been related to increased glutathione and decrease ROS levels (You et al., 2015) in Au-toxicity. Similarly, we observed a significant increase in cell viability (Fig. 2.6D and E) in Au-treated cells which was co-treated with NAC. These results further reiterate that loss of TrxR impairs the cellular redox balance and affects protein aggresome clearance, eventually leading to cell death.

Figure 2.6. N-Acetyl-L-Cysteine (NAC) prevents the proteolytic dysfunction after TrxR deficiency and promotes cell survival in starving SH-SY5Y cells.

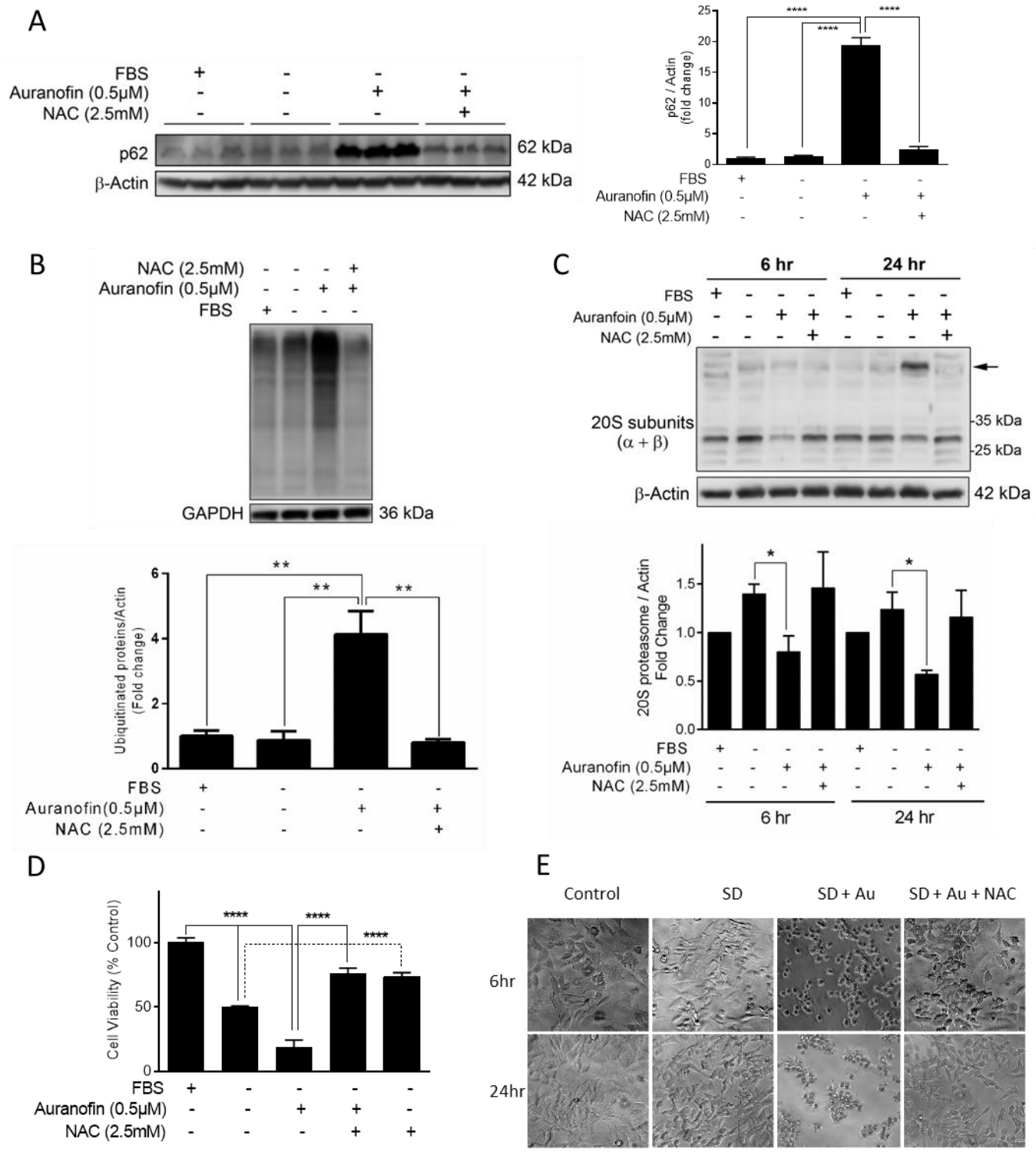

Figure 2.6. N-Acetyl-L-Cysteine (NAC) prevents the proteolytic dysfunction after TrxR deficiency and promotes cell survival in starving SH-SY5Y cells (A) SH-SY5Y cells were subjected to 6 hr of SD with or without auranofin or in combination with NAC and the cell lysates were subjected to western blot analysis. Densitometric analysis of p62 normalized to β-actin is shown. Values are expressed as mean ± S.E.M., n=3; ****p<0.0001. **(B)** Representative western blot and densitometric analysis showing poly-ubiquitinated proteins in cell extracts from SH-SY5Y cells were subjected to serum free conditions alone or in combination with auranofin and/or NAC or both for 6 hr. Values are expressed as mean ± S.E.M., n=3; **p<0.01. **(C)** SH-SY5Y cells were incubated with indicated treatments for either 6 or 24 hr. Western blot and densitometric analysis for proteasome 20s subunits are shown. Values are expressed as mean ± S.E.M., n ≥ 3; *p<0.05. **(D)** Cell viability was measured after 24 hr of respective treatments using Cell-counting kit-8 assay. Values are expressed as mean ± S.E.M., n ≥ 10; ****p<0.0001. **(E)** Phase contrast micrographs of SH-SY5Y cells exposed to serum free media in the presence of absence of auranofin (Au, 0.5μM) for 6 and 24 hr is shown. Note the recovery effect with the addiction of NAC (2.5mM).

2.4.8 Gene knockdown of TrxR1 mimics Au-mediated effects after serum deprivation

To confirm the involvement of TrxR in regulation of autophagy, we opted to generate a stable knock-down of cytosolic TrxR1 in SH-SY5Y cells. A commercially available lentiviral delivery of short hairpin RNA for TrxR1 was used in this study. The knockdown efficiency was assessed by western blotting (Fig. 2.7A), and measurement of TrxR enzymatic activity by insulin reduction assay (Holmgren, 1979a) (Fig. 2.7B). A 78% decrease in TrxR activity and TrxR1 protein (70% decrease) was observed in comparison with scramble (SCR) shRNA treated cells. TrxR1 knockdown (TRKD) cells displayed a significant decrease in cell viability at 24 hr in our SD model ($p<0.0001$) (Fig. 2.7C), which was further exacerbated after inhibition of autophagy by 3-MA (5mM). This confirmed our findings that inhibition of autophagy aggravates cell death in the absence of TrxR1. Cell viability in TRKD cells was further decreased with increasing duration of SD at 48 and 72 hr (data not shown).

TRKD cells demonstrated a pronounced activation of apoptosis as evidenced by 2.8 fold increase in cleaved caspase-3 levels and 1.65 fold increase in cleaved PARP levels in comparison to SCR cells; similarly at 24 hr, a 2.1 fold increase in cleaved caspase-3 and 1.8 fold increase in cleaved PARP was detected (Fig. 2.7D). This further supports our observations with pharmacological inhibition of TrxR using Au. Overall, TrxR1 deficiency in these experiments resulted in higher sensitivity to oxidative stress induced cell death evidenced by a significant increase in caspase-3 cleaved fragments in TRKD cells when compared to SCR cells as early as 3 hr after induction of SD (Suppl. Fig. 2.4).

To investigate the effect of downregulated TrxR1 levels in autophagy process, selected markers of autophagy were measured using western blotting. Despite a higher basal level of LC3-I in knockdown cells, we did not detect any significant difference in LC3-II levels. TRKD cells also

contained higher levels of p62 protein (1.6-fold) than their control counterparts, which is partially related to increased p62 gene expression (Fig 2.7D-G). When the cells were grown under serum free media (SD) for 6 hr, a significant increase in LC3-II/LC3-I ratio was observed in SCR ($p<0.05$) but not in TRKD cells, indicating a defective autophagy under TrxR1 deficiency, confirming our findings in Au-mediated TrxR inhibition. However, we did not see any apparent difference in clearance of p62 protein between TRKD and SCR cells as confirmed by western blotting (6 and 24 hr) and immunostaining at 3 and 6 hr after SD (Fig. 2.7D-F).

Under SD conditions in our study, cells were exposed to a serum-free DMEM medium which contains normal glucose levels but is devoid of essential growth factors and selenium. These experiments showed that SD in this medium is associated with induction of autophagy and apoptosis, we then asked whether minimizing/inhibition of protective autophagy will affect apoptosis. This will show if inhibition of TrxR1 will sufficiently induce apoptosis under minimal stress conditions. We therefore used a chemically defined medium consisting of DMEM supplemented with 1% ITS (Insulin-transferrin-selenium) that minimizes autophagy induction. In a sharp contrast to the SD model in DMEM media (Fig. 2.7D, Lanes 3 and 4), the ITS-treated SCR cells displayed no indication of intrinsic apoptosis at 6 hr in SCR (Fig 2.7D, Lane 5) and evidence of apoptosis progression was delayed to late time points (24 hr) (Fig 2.7D, Lane 11). The TRKD cells were prominently more sensitive to SD treatment in ITS-media as evidenced by high levels of Caspase-3 and PARP-1 at 6 and 24 hr after induction of SD when compared to the SCR cells (Fig. 2.7D, Lane 6 and 12). These experiments showed that decreased levels of TrxR1 in TRKD cells interrupts autophagy induction and enhances their sensitivity to apoptosis.

Figure 2.7. Gene knockdown of Thioredoxin reductase 1 (TrxR1) enhances apoptosis and inhibits autophagy during nutritional stress in SH-SY5Y cells.

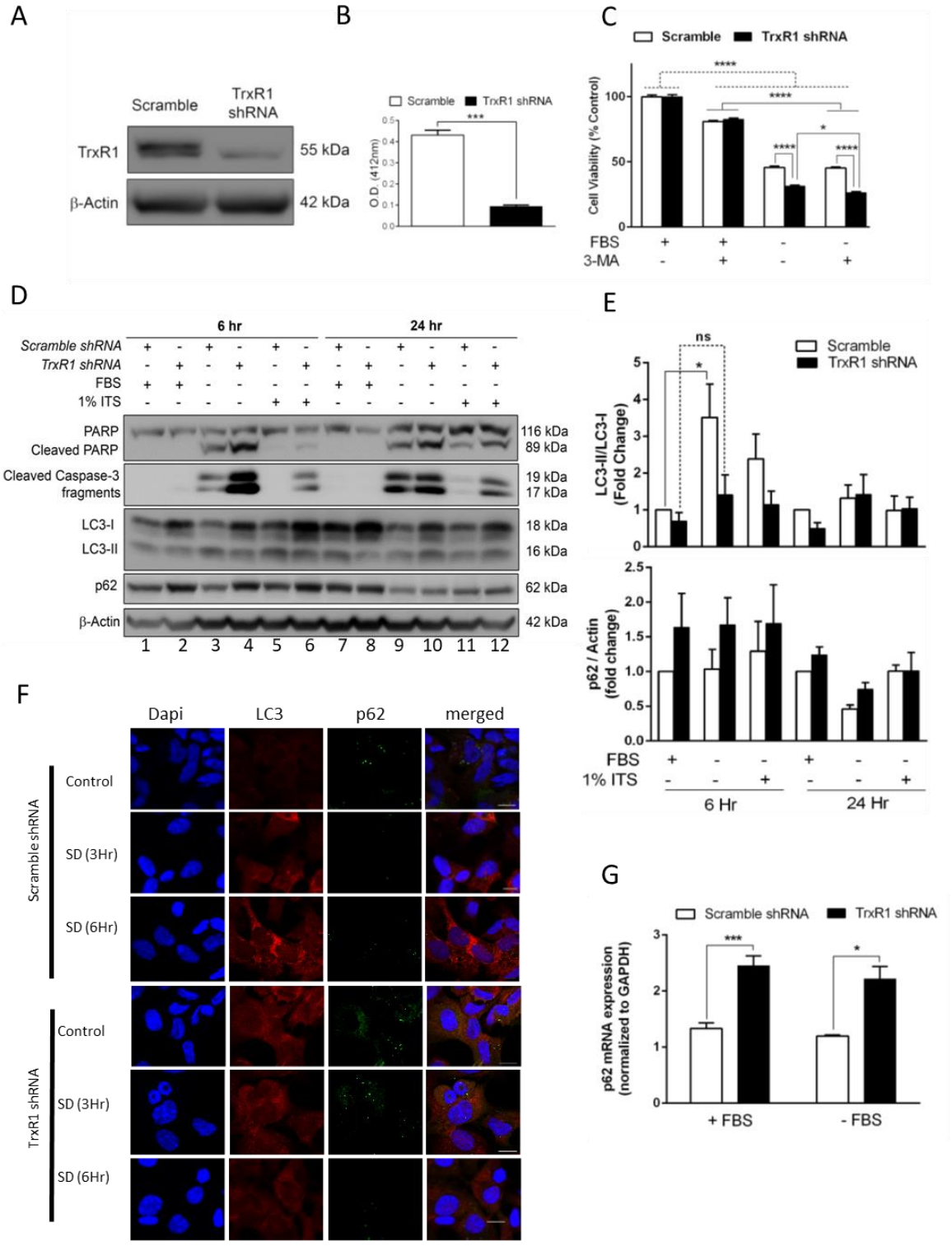

Figure 2.7. Gene knockdown of Thioredoxin reductase 1 (TrxR1) enhances apoptosis and inhibits autophagy during nutritional stress in SH-SY5Y cells. (A) Representative western blot showing TrxR1 protein expression in SH-SY5Y cells transfected with scramble or TrxR1 shRNA. **(B)** Thioredoxin reductase activity measured by insulin reduction assay. Values are expressed as mean ± S.E.M., n=8; ***p<0.001. **(C)** TrxR1 knockdown and scramble control cells were subjected to 24 hr of serum deprivation (SD) in the presence or absence of autophagy inhibitor, 3-Methyladenine (3MA, 5mM) and the cell viability was measured using Cell counting kit-8. Values are expressed as mean ± S.E.M., n≥4; *p<0.05, ****p<0.0001. **(D)** TrxR1 knockdown interrupts autophagy and enhances apoptosis in serum deprived SH-SY5Y cells. Representative western blot showing apoptotic and autophagic markers in scramble and TrxR1 knockdown cells incubated with complete growth medium or serum free media or 1% ITS media for indicated durations. Note the increase in cleaved PARP and caspase 3 fragments at an early period of starvation (6 hr). Quantification of autophagic markers are shown as bar graphs **(E)**. Values are expressed as mean ± S.E.M., n=3; *p<0.05, **p<0.001. **(F)** Representative immunofluorescence images of scramble and TrxR1 knockdown cells subjected to 3 or 6 hr serum deprivation (SD) and stained for autophagic markers. Note the accumulation of p62 (green) proteins in TrxR1 knockdown cells in comparison to scramble cells. DAPI was used to stain the nuclei (blue). **(G)** TrxR1 knockdown upregulates p62 mRNA levels in serum deprived SH-SY5Y cells. Total RNAs were prepared from Scramble or TrxR1 knockdown cells that were subjected to 6 hr of SD and p62 mRNA levels were quantified using qPCR. Values are expressed as mean ± S.E.M., n=3; *p<0.05, ***p<0.001.

2.4.9 TrxR1 downregulation blocks autophagy flux

Similar to the results obtained with Au-treatment, addition of BafA1 significantly increased the level of LC3-II/LC3-I ratio in both SCR and TRKD cells in normal and SD conditions in comparison to their untreated controls ($p<0.0001$). Autophagy flux was assessed using the LC3-II/LC3-I ratio in the presence and absence of BafA1 (Rubinsztein et al., 2009). As expected, addition of BafA1 to SCR cells after SD led to a significant increase in LC3-II/LC3-I ratio in comparison to BafA1 treated FBS control, indicating a normal autophagy flux ($p<0.0001$). On the contrary, the increase in LC3-II/LC3-I ratio in TRKD cells subjected to SD + BafA1 was not significantly different from Baf A1 treated control. Additionally, p62 accumulation was significantly increased in TRKD cells upon inhibition of autophagosome maturation by BafA1 during SD, confirming an impairment of autophagy flux and protein degradation in TrxR1 deficient cells (Fig 2.8A and B). Accumulation of autophagosomes was observed using TEM micrographs at 6 and 24 hr after SD in TRKD, but not in SCR cells (Suppl. Fig. 2.5).

Figure 2.8. Downregulation of Thioredoxin reductase 1 (TrxR1) impairs autophagy flux.

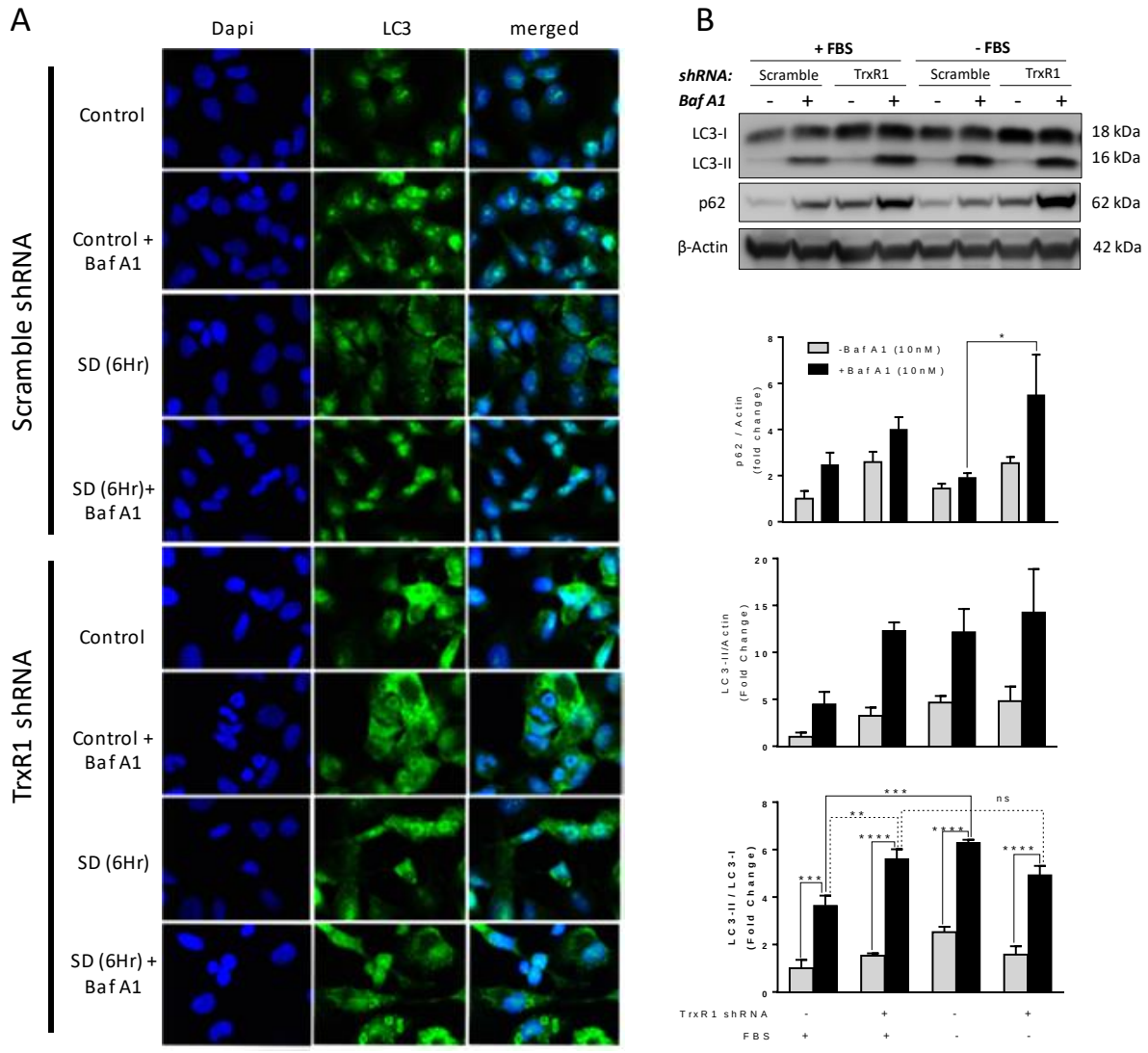

Figure 2.8. Downregulation of Thioredoxin reductase 1 (TrxR1) impairs autophagy flux. (A) Immunofluorescence of LC3 (green) in scramble and TrxR1 knockdown SH-SY5Y cells subjected to serum deprivation (SD) for 6 hr with or without Baf A1 10nM. **(B)** Representative western blot showing LC3 and p62 protein levels in lysates extracted from scramble and TrxR1 knockdown SH-SY5Y cells subjected to normal or serum free condition for 6 hr in the presence or absence of Baf A1 (10 nM). Quantification of LC3-II and p62 protein expressions are shown as bar graphs. Values are expressed as mean ± S.E.M., n=3; *p<0.05, **p<0.01, ***p<0.001, ****p<0.0001.

2.4.10 Aggravation of oxidative stress, protein ubiquitination and lysosomal deficiency after downregulation of TrxR1 in SH-SY5Y cells

Enhanced basal level of oxidative stress in TRKD cells was evident by a significant increase in CellRox staining in comparison with the SCR cells (Fig. 2.9A). TRKD also displayed higher levels of protein ubiquitination at 6 and 24 hr after SD (Fig. 2.9B). These findings directly support our results with pharmacological inhibition of TrxR by Au.

Trx1 reducing capacity is mainly dependent on the availability of TrxR (Mustacich and Powis, 2000), although a recent report indicated that glutathione and glutaredoxin may be alternative reducing system for Trx (Du et al., 2012). To examine whether inhibition/ downregulation of TrxR will affect Trx levels or its oxidative status, we used conventional and redox western blotting. A marked upregulation of Trx1 protein was observed in TRKD cells which was further increased with SD (Fig. 2.9C), indicating a compensatory Trx synthesis by these cells. This prompted us to use redox western blotting for analysing redox status of Trx1 in these cells. Iodoacetic acid/Iodoacetamide method was employed to separate the reduced and oxidized Trx1 using Urea PAGE (Bersani et al., 2002; Du et al., 2012). We found enhanced oxidation of Trx1 as evidenced by increased levels of semi-oxidized and fully oxidized Trx1 in TRKD cells. Minimal levels of Trx1 oxidation was observed in SCR cells only after SD (Fig. 2.9D). The effect of TrxR1 downregulation on lysosomes was assessed by DQ-BSA lysosomal protein degradation assay. On subjecting to 6 hr of SD, SCR cells showed a significant increase in DQ-BSA degradation ($p<0.0001$), whereas TRKD cells did not show any change in comparison to FBS control; this suggests that TrxR1 deficiency decreases lysosomal proteolytic activity (Fig. 2.9E) as confirmed by our pharmacological inhibition of TrxR.

Figure 2.9. Downregulation of Thioredoxin reductase 1 (TrxR1) increase oxidative stress, accumulation of polyubiquitinated proteins and lysosomal dysfunction in serum starved (SD) SH-SY5Y cells.

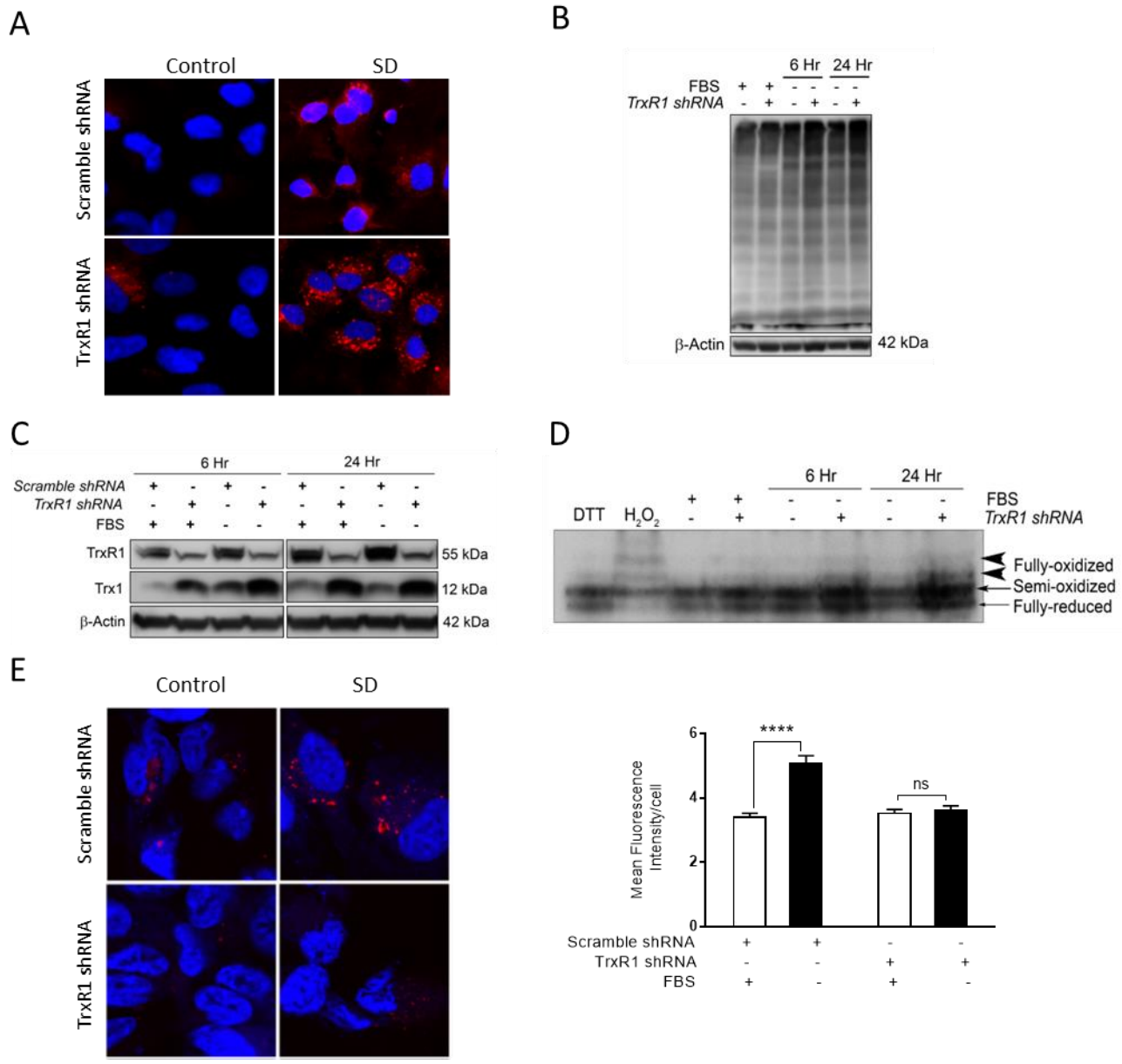

Figure 2.9. Downregulation of Thioredoxin reductase 1 (TrxR1) increase oxidative stress, accumulation of polyubiquitinated proteins and lysosomal dysfunction in serum starved (SD) SH-SY5Y cells. (A) Scramble and TrxR1 knockdown cells were exposed to 6 hr of serum deprivation (SD) and stained with CellROX deep red reagent (red); DAPI was used to identify nuclei (blue). Representative western blot showing increased polyubiquinated proteins **(B)** and thioredoxin 1 **(C)** levels in scramble and TrxR1 knockdown SH-SY5Y cells subjected to SD. **(D)** TrxR1 downregulation increases oxidized thioredoxin 1 levels. Scramble and TrxR1 knockdown cells were exposed to 6 and 24 hr of SD and then assessed for Trx redox status using Iodoacetic acid (IAA) and Iodoacetamide (IAM) method by Urea PAGE. Cells treated with Dithiothreitol (DTT, 5mM) or Hydrogen Peroxide (H_2O_2, 0.5mM) for 30 minutes were used as controls. **(E)** Scramble and TrxR1 knockdown cells were subjected to 6 hr of SD after DQ-BSA loading and the mean fluorescence intensity/cell was quantified. Values are expressed as mean ± S.E.M. $n \geq 60$ cells. ****$p<0.0001$.

2.4.11 The impact of oxidative stress severity on autophagy-apoptosis interplay in nutritionally stressed SH-SY5Y cells

Our cumulative results from pharmacological inhibition and genetic downregulation of TrxR, a major cellular antioxidant system, suggested that exacerbation of oxidative stress may play a key role in transition of autophagy to apoptosis. We therefore aimed to assess whether the severity of oxidative stress can affect the autophagy and apoptosis progression. For these experiments we exposed the SH-SY5Y cells to an increasing gradient (25-200μM) of tertiary butyl hydroperoxide (tBHP) in serum free media. Addition of tBHP caused a significant increase in ROS generation in starving SH-SY5Y cells, which was significantly reduced by NAC treatment confirming the induction of oxidative stress (Fig. 2.10A). Cells were harvested at 6 hr and markers of autophagy and apoptosis were assessed by western blotting. A dose response increase in both LC3II and p62 protein levels were detected in response to increasing concentrations of tBHP indicating accumulation of aggregated proteins and an interrupted autophagic process. We also observed an enhanced expression of apoptotic markers including cleaved PARP-1, and cleaved caspase 3 (Fig. 2.10B). These results confirm our hypothesis that increased severity of oxidative stress interrupts autophagy and are in agreement with our findings in Au-treated and TRKD cells.

Figure 2.10. Increasing oxidative stress levels using tBHP affects autophagy-apoptosis conversion.

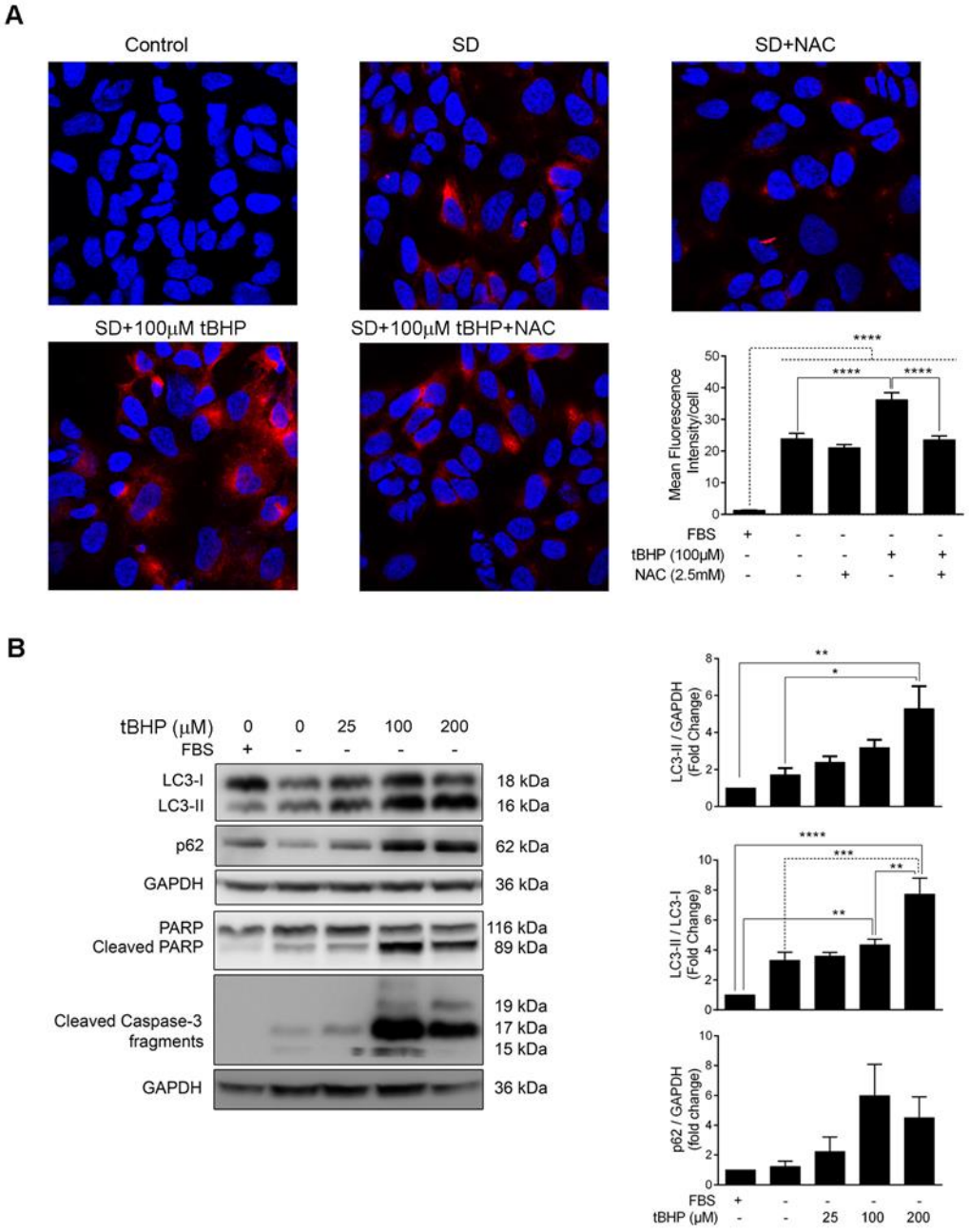

Figure 2.10. Increasing oxidative stress levels using tBHP affects autophagy-apoptosis conversion. **A)** SH-SY5Y cells were exposed to SD as well as SD+100μM tBHP and were processed for detection of ROS levels using CellROX Deep Red at 6hr. To confirm the protective effect of NAC under oxidative stress conditions, SD and tBHP treated cultures were co-incubated with 2.5mM NAC. Cultured were fixed and processed for ROS quantification as described in material and method section. Representative confocal micrographs shown here were taken using a 63x objective lens. Values are expressed as mean ± S.E.M. n≥200 cells. ****p<0.0001. **B)** Expression of autophagic and apoptotic markers were assessed in cultures exposed to SD with without increasing concentrations of tBHP. Quantification of LC3-II normalized to GAPDH, LC3-II/LC3-I ratio and p62 is depicted here. Values are expressed as mean ± S.E.M., n=5; *p<0.05, **p<0.01, ***p<0.001, ****p<0.0001.

2.5 Discussion

Oxidative stress is a well-known inducer of autophagy, but tight regulation of ROS is essential for its efficient progression. Aggravated oxidative stress enhances autophagy to clear damaged proteins; however, these increased stress levels also affect several regulatory proteins. A balanced cellular redox state is central for proper progression of autophagy and is maintained by fine tuning of oxidized and reduced forms of GSH and Trx. These thiols can donate protons to reduce the cysteine groups in oxidized proteins and modify their function. Despite the advances in redox biology, so far ATG4 is the only proposed target for Trx system whose activity is regulated by Trx system. Other potential redox sensitive proteins in the process of autophagy are proposed to contain cysteine groups in their key molecular domains, however these remain to be identified. In this study we aimed to identify the role of Trx system in regulation of autophagy progression. We used serum deprivation, a widely used model of in vitro oxidative stress (Pandey et al., 2003; Pirkmajer and Chibalin, 2011). Upon SD, cells undergo autophagy which is later replaced by apoptosis. This model provides an excellent model to study the underlying molecular systems involved in autophagy-apoptosis interplay. We observed that SD induces ROS levels during the early hours leading to autophagy that was replaced with aopotosis. To investigate the role of Trx system in this process, we used Au-treatment for acute inhibition of TrxR or used shRNA for its stable downregulation. These approaches enhanced oxidative stress as shown by elevated level of ROS and Trx oxidation and blocked autophagy flux that was accompanied by lysosomal dysfunction. Although glutathione and glutaredoxin systems can potentially contribute to Trx1 reduction to compensate for TrxR deficiency in these experiments as suggested previously (Du et al., 2012), our results imply that such system was not effective in these conditions.

2.5.1 Severity of oxidative stress determines cellular autophagic response

In this study, we showed that serum deprivation increases autophagy and lysosomal activity, however further elevation of oxidative stress led to diminished autophagic process in TrxR deficient state, as well as in response to increasing concentration of peroxides. This was supported by significant decrease in autophagy and proteasome marker levels and impaired clearance of damaged proteins.

Our results clearly show the impact of oxidative stress severity in regulation of autophagy and apoptosis. Our findings are in agreement with a recent report (Shao et al., 2015) that showed inhibition of TrxR using b5, a curcumin-derived compound resulted in apoptotic cell death that was attenuated by NAC treatment. They suggest that TrxR inhibition in a normal growth medium, induces oxidative stress that results in induction of autophagy at 48hr. This is in agreement with our findings that spontaneous inactivation of TrxR at 24 and 48hr, as observed under SD-mediated oxidative stress, is associated with a late induction of autophagy in this model as shown by a significant increase of Atg-7 and ATG5-12 conjugate at 48 hr (Fig. 2.1). We further proved that pharmacologic inhibition or genetic downregulation of TrxR in existing oxidative stress conditions (SD) exacerbated oxidative stress and cell death that was due to inhibition of autophagy. This indicates that severity of oxidative stress is a determining factor in autophagy progress; while low oxidative stress is required for promotion of normal autophagy, excessive oxidative stress inhibits the early protective autophagy.

2.5.2 Delineating the role of thiol antioxidants in autophagy-lysosome system

Considering the complex network of antioxidant systems and their overlapping and often compensatory behavior for maintaining the redox homeostasis of the cell, we recognize that the current experimental setting may not be able to exactly delineate the underlying role of antioxidant

systems in autophagy-lysosomal processes. GSH, as the most abundant cellular thiol molecule, has recently been shown to play a modulatory role in autophagy. Desideri *et al.* elegantly showed that a decreased GSH level after starvation is mediated by GSH oxidation and efflux through ABCC1 (ATP-binding cassette, subfamily C1) (Desideri et al., 2012). This ensures that an oxidized environment for autophagy progress is maintained. Our study further supports their findings as SD resulted in production of ROS which induced autophagy and a counter induction of TrxR as a redox defence mechanism. However, inactivation of TrxR under prolonged state of SD resulted in excessive oxidative stress which interrupted autophagy. Similarly, excessive aggravation of oxidative stress was shown to be detrimental for autophagy; as pharmacologic inhibition and downregulation of TrxR promoted apoptosis. We further showed that improving the reducing capacity of the cell using NAC treatment improved cell viability and reduced protein aggregation. Despite common findings, other fundamental differences exists between the two studies: Hela and HepG2 cells used in Desideri *et al*. study express high levels of ABCC1 which is essential for GSH efflux (Uhlen et al., 2015), but SH-SY5Y cells are amongst the cells with the lowest ABCC1 levels(Uhlen et al., 2015), and therefore maintaining an autophagy inducing redox balance in these cells may be regulated differently than Hela and HepG2 cells. Overall, although our study and the report by Desideri *et al* have looked at different thiol systems, both studies indicate the importance of a balanced redox state for autophagy progression.

In this study, we have identified lysosome deficiency as an outcome of aggravated oxidative stress and a cause of cell death after TrxR deficiency, however, it must be noted that perturbation of cellular redox balance will have a global effect on cellular signaling systems and organelles such as endoplasmic reticulum, Golgi and mitochondria. While these organelles are equipped with their own antioxidant regulating systems, a change in redox balance in one cellular compartment can

affect the health of others. In fact the protective effect of Trx system in prevention of endoplasmic reticulum stress has been previously shown in diabetes(Oslowski et al., 2012). In this disease a natural inhibitor of Trx system, thioredoxin inhibiting protein (Txnip), is upregulated which can directly bind to the cytoplasmic Trx as well as its mitochondrial counterpart. Therefore, Txnip interaction with Trx impedes its redox regulatory role in mitochondria and cytoplasm. Similarly, a previous record (Bai et al., 2007) showed that cytoplasmic Trx can have protective effect for both mitochondrial and endoplasmic reticulum compartment in a model of Parkinson disease(Bai et al., 2007). Our study showed that Trx1 is oxidized after TrxR deficiency which can in turn affect the other cellular components. The effect of TrxR inhibition on mitochondria and endoplasmic reticulum in our model remains to be examined.

2.5.3 Application of our findings to human diseases

The concept of autophagy to apoptosis conversion is an underlying mechanism in many diseases and conditions. In vitro models of oxygen and glucose deprivation, growth factor withdrawal and nutritional deprivation converge on induction of oxidative stress which leads to initiation of autophagy. Prolonged stressful condition or exacerbation of oxidative stress can interrupt autophagy and promote cell death often in an apoptotic fashion. Therefore, our findings that inhibition of TrxR under stress condition results in lysosomal deficits, accumulation of damaged proteins in autophagosomes and cell death can be applicable to many diseases including, stroke, spinal cord injury, neurodegenerative diseases and diabetes. Interestingly, down regulation of Trx and TrxR protein has been shown in human post-mortem Parkinson disease brains (Arodin et al., 2014) and in substantia nigra of a mouse model of this disease (Liu et al., 2013). This indicates the potential implication of our findings for neurodegenerative diseases.

The involvement of oxidative stress in conditions such as neurodegenerative diseases has inspired the use of antioxidants as a therapeutic approach during the last few decades, yet these approaches have generally failed in clinical trials. Our findings suggest that improving lysosomal-mediated autophagy can be an alternative therapeutic practice. Enhancement of autophagy using pharmacological reagents such as Rapamycin has been shown to improve functional recovery in models of neurotrauma (Sekiguchi et al., 2012; Zhou et al., 2015).

In summary, our study identifies a novel redox based mechanism in the regulation of autophagy; as most of the earlier reports emphasize the involvement of antioxidants on the induction of autophagy, our study shows that defects in oxidative stress-mediated lysosomal autophagy can also affect autophagosome-autolysosome maturation by redox dependent processes. Future experiments will focus on the role of redox balance on lysosome-autophagosome interactions and may provide additional information on redox sensitive processes in autophagy-apoptosis interplay. This can have potential therapeutic application in the field of neurodegenerative diseases.

2.6 Supplementary Materials

2.6.1 Supplementary Figures

Supplemental Figure 2.1. Inhibition of thioredoxin reductase causes increased oxidative stress and accumulation of poly-ubiquitinated proteins.

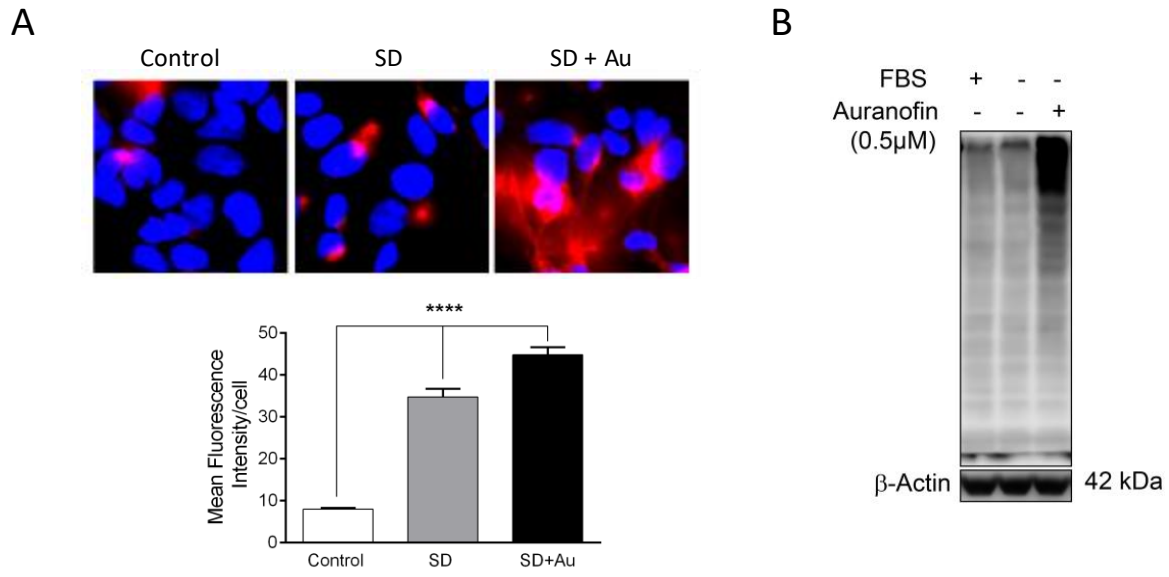

Supplemental Figure 2.1. Inhibition of thioredoxin reductase causes increased oxidative stress and accumulation of poly-ubiquitinated proteins. (A) Representative immunofluorescence images showing increased reactive oxygen species levels (CellROX, red) in SH-SY5Y cells treated with auranofin (Au, 0.5μM) during 6 hr of SD. Nuclei were stained with DAPI (blue). Quantification of ROS fluorescence intensity is shown as bar graph. Values are expressed as mean ± S.E.M., n≥100 cells; ****p<0.0001. **(B)** Representative western blot showing polyubiquinated proteins in lysates extracted from SH-SY5Y cells subjected to 6 hr SD with or without auranofin.

Supplemental Figure 2.2. Inhibition of Thioredoxin Reductase impairs autophagy flux in serum deprived (SD) SH-Y5Y cells.

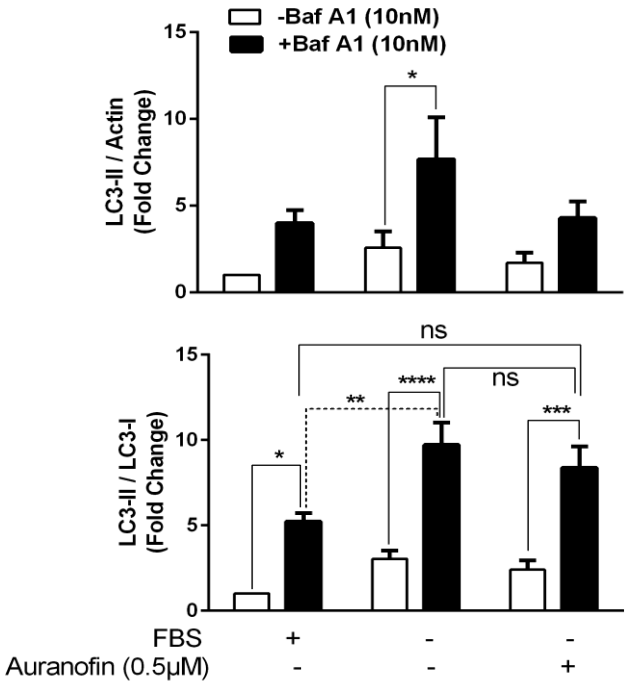

Supplemental Figure 2.2. Inhibition of Thioredoxin Reductase impairs autophagy flux in serum deprived (SD) SH-Y5Y cells. SH-SY5Y cells were serum deprived for 6 hr in the presence or absence of Au (0.5μM) or Baf A1 (10 nM) or both. Quantification of LC3-II normalized to actin and LC3-II/LC3-I ratio is shown here. Values are expressed as mean ± S.E.M., n=5; *p<0.05, **p<0.01.

Supplemental Figure 2.3. Electron micrographs depicting SH-SY5Y neuronal cells in SD and after inhibition of TrxR by Auranofin.

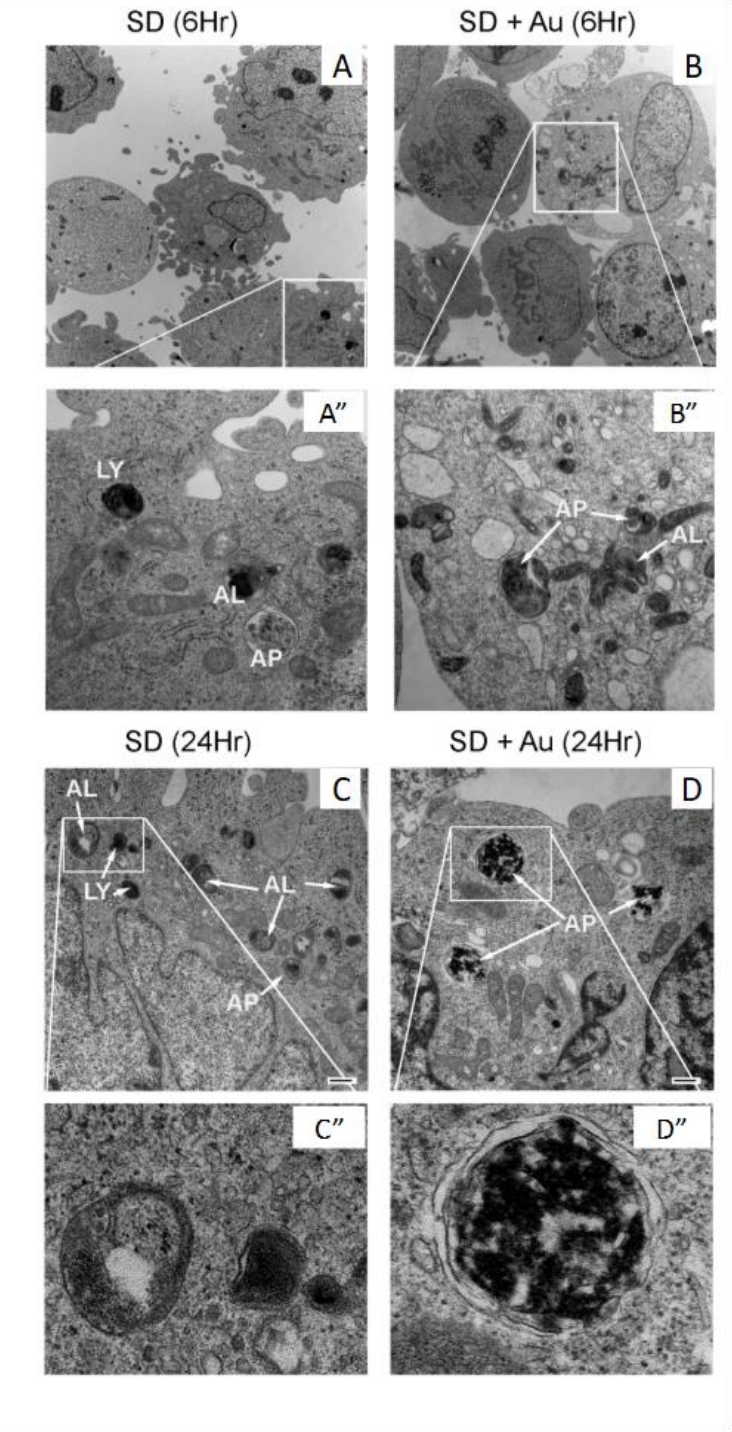

Supplemental Figure 2.3. Electron micrographs depicting SH-SY5Y neuronal cells in SD and after inhibition of TrxR by Auranofin. SH-SY5Y were treated as described (Control, SD, SD+Au) and cells were harvested for TEM. **(A)** Low magnification (4600x) of neuronal cells at 6 hr after SD, and (B) after SD+Au (6 hr). Evidence of early cell death is shown (*) as early as 6 hr after Au treatment. **(A")** and **(B")** are higher magnification (19000x) of selected areas in **A** and **B**. Accumulation of autophagosomes (AP) is observed at this early time point after inhibition of TrxR. **(C)** Cells deprived of serum (SD) for 24 hr display evidence of autophagy progress as shown by formation of Autophagosomes (AP), autolysosomes (AL) and primary lysosomes (LY). **(D)** Enlarged autophagosomes, and scarcity of lysosomes are observed at 24 hr after Au-treatment. Higher magnification (19000x) of autolysosome and autophagosome is shown in **C"** and **D".** Scale bar is shown in **C** and **D** (500nm) for comparative purposes.

Supplemental Figure 2.4. Genetic knockdown of Thioredoxin Reductase 1 sensitizes SH-SY5Y cells to serum deprived (SD) induced apoptosis.

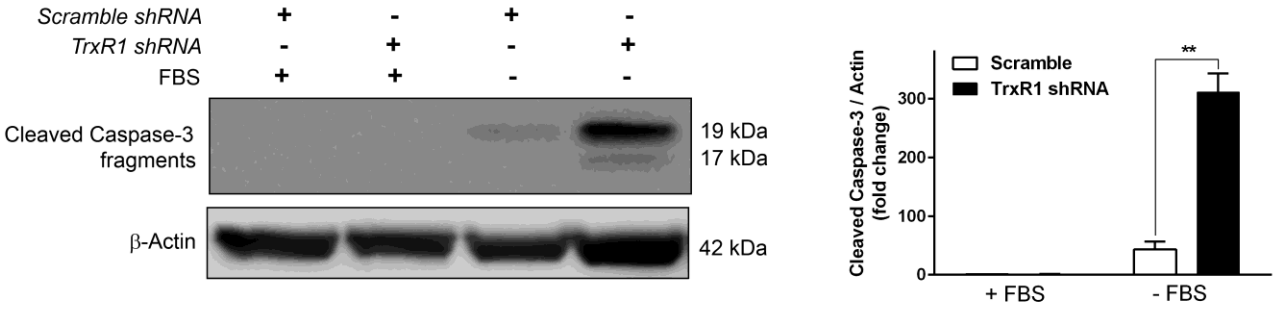

Supplemental Figure 2.4. Genetic knockdown of Thioredoxin Reductase 1 sensitizes SH-SY5Y cells to serum deprived (SD) induced apoptosis. SH-SY5Y cells transfected with scramble or TrxR1 shRNA were exposed to serum deprivation for 3 hr and the cell lysates were subjected to western blot analysis. Representative blot showing cleaved caspase-3 and the corresponding quantification are shown here. Values are expressed as mean ± S.E.M., n=2; **p<0.01.

Supplemental Figure 2.5. Electron micrographs depicting control (SCR-shRNA) and TRKD SH-SY5Y neuronal cells under SD conditions.

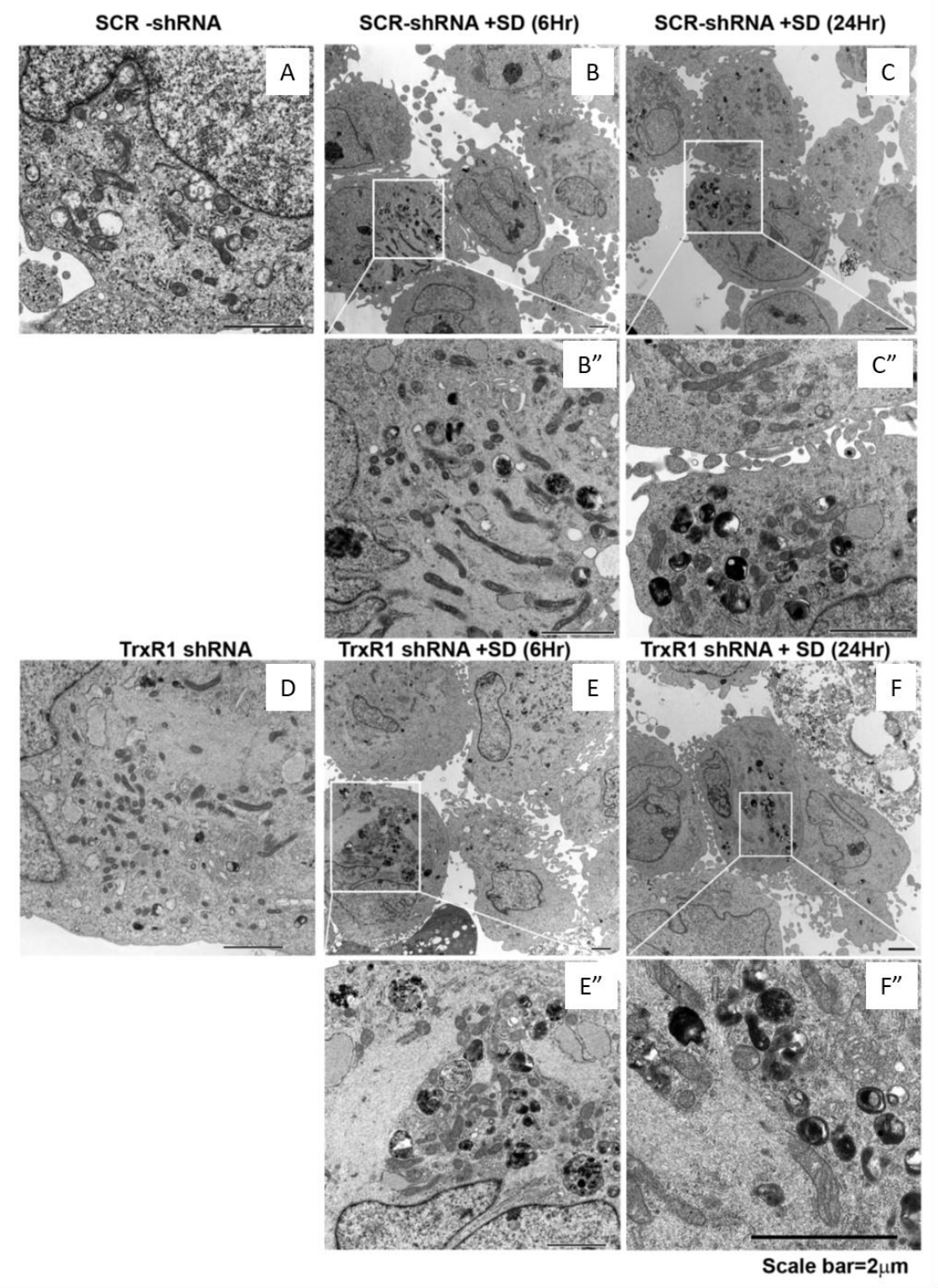

Supplemental Figure 2.5. Electron micrographs depicting control (SCR-shRNA) and TRKD SH-SY5Y neuronal cells under SD conditions. (A) Control SCR-cells in normal growth medium, **(B)** in SD (6 hr), and **(C)** after 24 hr. Insets depict enlarged area of cells undergoing autophagy. **(B")** Autophagophore formation is indicated by (*) and lysosomes and autophagosomes are seen throughout this cell. **(C")** SCR-cells at 24 hr after SD, many normal autolysosomes are seen indicating increased autophagy in these cells. **(D)** TRKD cells in normal growth medium (in comparison to SCR-cells) displayed increased levels of autophagy evidenced by the presence of autophagosomes and autolysosomes. **(E)** and **(F)**, TRKD cells at 6 and 24 hr after SD. Insets (**E"** and **F"**) show accumulation of autophagosomes. (Scale bar=2μm).

Chapter 3

Differential redox sensitivity of cathepsin B and L holds the key to autophagy-apoptosis interplay after Thioredoxin reductase inhibition in nutritionally stressed SH-SY5Y cells

Contents of this chapter has been included in the following published article:

Pandian Nagakannan and Eftekhar Eftekharpour. Differential redox sensitivity of cathepsin B and L holds the key to autophagy-apoptosis interplay after Thioredoxin reductase inhibition in nutritionally stressed SH-SY5Y cells. *Free Radical Biology and Medicine 2017;108:819-831*.

Author Contributions: My contributions in this work includes conceptualization, experimental design, collection and interpretation of data. I prepared the manuscript under the guidance of my supervisor.

3.1 Abstract:

Reactive oxygen species (ROS) are essential for induction of protective autophagy, however unexpected rise in cellular ROS levels overpowers the cellular defense and therefore promotes the programmed apoptotic cell death. We recently reported that inhibition of thioredoxin reductase (TrxR) in starving SH-SY5Y cells interrupted autophagy flux by induction of lysosomal deficiency and promoted apoptosis. (Free Radic Biol Med. 2016: 101:53-70). Here, we aimed to elucidate the underlying mechanisms during autophagy-apoptosis interplay and focused on regulation of cathepsin B (CTSB) and L (CTSL), the pro-apoptotic and pro-autophagy cathepsins respectively. Inhibition of TrxR by Auranofin, caused lysosomal membrane permeabilization (LMP) that was associated with a significant upregulation of CTSB activity, despite no significant changes in CTSB protein level. Conversely, a significant rise in CTSL protein levels was observed without any apparent change in CTSL activity. Using thiol-trapping techniques to examine the differential sensitivity of cathepsins to oxidative stress, we discovered that Auranofin-mediated oxidative stress interferes with CTSL processing and thereby interrupts its pro-autophagy function. No evidence of CTSB susceptibility to oxidative stress was observed. Our data suggest that cellular fate in these conditions is mediated by two concurrent systems: while oxidative stress prevents the protective autophagy by inhibition of CTSL processing, concomitantly, apoptosis is induced by increasing lysosomal membrane permeability and leakage of CTSB into cytoplasm. Inhibition of CTSB in these conditions inhibited apoptosis and increased cell viability. To our knowledge this is the first report uncovering the impact of redox environment on autophagy-apoptosis interplay in neuronal cells.

3.2 Introduction:

Redox signaling is mediated by interaction of reactive oxygen species (ROS) with cellular signaling machinery resulting in transient oxidation of these molecules and initiation of appropriate cellular signaling pathways. These temporarily oxidized proteins must be quickly reduced by cellular antioxidant thiols such as glutathione and thioredoxin to ensure their availability for further participation in cellular vital activities. Depletion of reducing equivalents will result in disruption of an ever-expanding list of cellular processes that may lead to cell death (Navarro-Yepes et al., 2014). *Protective* lysosomal-mediated autophagy is a major cellular process in normal and pathologic conditions. This process is essential for the turnover of long lived or damaged cellular proteins and organelles and ensures recycling of cellular macromolecules(Feng et al., 2014). The importance of ROS for normal autophagy has been shown previously as administration of antioxidant molecules perturbs this process (Underwood et al., 2010). An extensive review of the redox sensitivity of autophagy in neuronal cells has been recently published(Hensley and Harris-White, 2015). We also showed that perturbation of redox state of the cells affects autophagy rate and promotes apoptosis (Nagakannan et al., 2016), however the molecular mechanisms regulating the conversion of autophagy to apoptosis remains elusive. Understanding these mechanisms expands our knowledge in redox regulating systems and may lead to identification of novel therapeutic approaches for many diseases that are associated with altered lysosomal activity including neurodegenerative diseases.

The essential role of lysosomes in successful execution of autophagy is well documented. These organelles pack a variety of different hydrolytic enzymes including proteases, glycosidases and lipases (Turk et al., 2012). Disruption of lysosomal membrane integrity and spillage of these enzymes into cytoplasm will result in cell death; a process, known as lysosomal membrane

permeabilization (LMP) (Serrano-Puebla and Boya, 2016). The extent of LMP determines the cell death mode, as partial LMP in mild oxidative stress has been linked to activation of apoptosis while unregulated/severe LMP initiates necrotic cell death(Hampton and Orrenius, 1997). Cathepsins are a major group of lysosomal proteases that are synthesized as zymogens or pre-procathepsins, containing an N-terminal signal that is removed as zymogen enters the endoplasmic reticulum and forms the procathepsin isoform. Procathepsin is further processed in the endoplasmic reticulum lumen and is transferred into the lysosomes/endosomes. The acidic environment of lysosomes activate the mature cathepsin by removing the propeptide sequence (Turk et al., 2012). Cathepsins have a general papain-related structure and are involved in a variety of cellular functions including intracellular signaling pathways that modulate many cellular functions from proliferation to differentiation and cell death. Eleven different types of cathepsins have been identified that are responsible for protein degradation. Their abundance in number may suggest their functional redundancy, however these enzymes show restricted tissue localization or specialized function (Turk et al., 2001). The impact of cathepsins in the outcome of LMP has been shown by the moderate cell protective effect of cathepsin inhibitors under stressful conditions (Oberle et al., 2010). These inhibitors have made it possible to identify specific roles for members of cathepsin family as executioners of cell death. Amongst these enzymes, cathepsin B (CTSB) is mainly recognized as a pro-apoptotic enzyme and its involvement in activation of apoptosis through activation of Bid (de Castro et al., 2016)or trypsin (Sendler et al., 2016) has been described. Additionally CTSB has been shown to negatively regulate lysosomal function as its absence increases autophagy and lysosomal activity (Man and Kanneganti, 2016). Cathepsin L (CTSL) is known for its role in promotion of autophagy (Kaasik et al., 2005; Pucer et al., 2010; Sun et al., 2013; Wei et al., 2013). These enzymes play vital function in normal cell physiology,

and inhibition of these enzymes in intact cells causes lysosomal dysfunction and apoptotic cell death (Jung et al., 2015).

A recent report from our laboratory showed that oxidative stress after inhibition of thioredoxin reductase (TrxR) is responsible for autophagy-apoptosis conversion in a model of serum deprivation (SD) in SH-SY5Y cells (Nagakannan et al., 2016). We further showed that enhancement of cellular reducing capacity using N-acetylcysteine prevented autophagy disruption and improved cell viability. In this study, we aimed to further investigate the response of lysosomal cathepsins to oxidative stress. We hypothesized that interruption of autophagy and promotion of apoptosis may be mediated through differential regulation of CTSL and CTSB. Although activation of different cathepsins has been linked to autophagy and apoptosis in different models, the potential impact of oxidative stress in cathepsin processing and its contribution to this cross talk has not been previously shown.

3.3 Materials and Methods

3.3.1 Reagents

Auranofin was purchased from Tocris Bioscience, UK; Pepstatin A was from Cayman chemical, USA; N-Acetyl-L-cysteine (NAC), CA-074 methyl ester (CA-074-me) and Acridine orange were obtained from Sigma Aldrich, USA; Cathepsin L Inhibitor II (Z-FY-CHO) was from Calbiochem, USA; N-ethylmaleimide (NEM), 4-Acetamido-4'-Maleimidylstilbene-2,2'-Disulfonic Acid (AMS) and Halt Protease and phosphatase inhibitor cocktail were from Thermo Scientific, USA; human Cystatin C was purchased from Cedarlane, Canada. Cell Counting Kit-8 (CCK-8) was from Dojindo Molecular Technologies, Japan. Cathepsin B activity assay kit (ab65300) and cathepsin L activity assay kit (ab65306) were purchased from abcam, USA.

3.3.2 Cell culture, treatments and cell viability assay

Human neuroblastoma cell line SH-SY5Y was kindly provided by Dr. Jun-Feng Wang, University of Manitoba. The cells were cultured at 37°C and 5% CO_2 in a humidified incubator in DMEM (Dulbecco's modified Eagle's medium) containing 4.5 g/L glucose supplemented with 4mM glutamine, 1mM Sodium Pyruvate and 10% heat inactivated Fetal Bovine Serum.

On reaching 70-80% confluency, the cells were washed and incubated with SD (serum deprivation) medium for the specified time durations. To inhibit TrxR, Auranofin (Au) at a concentration of 0.5 µM was added to cultures based on our previous report (Nagakannan et al., 2016). This concentration induced ~70% cell death after 24 hr. In experiments where specific cathepsins were inhibited, the cells were pretreated overnight with following inhibitors: CA-074-me (15 µM), Z-FY-CHO (10 µM) or pepstatin A (50 µM) and then were treated with Au. Cystatin C (1.25 µM) was co-treated with Au. NAC was prepared as 0.5 M stock in DMEM and was added during Au addition at a final concentration of 2.5 mM to prevent ROS generation. We previously

showed the efficacy of this dose of NAC on ROS levels and efficient cell protection in this model (Nagakannan et al., 2016).

To determine cell viability, Cell Counting Kit-8 (CCK-8) (Dojindo Molecular Technologies, Japan) reagent was added in the culture medium (10% final concentration) at the end of treatment period. After incubation at 37°C for 4 hr, absorbance was measured at 450 nm using Synergy H1 Hybrid Reader (BioTeK Instruments, USA). Absorbance at 650 nm was used for background correction and the percentage of cell viability relative to control is presented.

3.3.3 Acridine orange staining

After appropriate treatments, cells were incubated with medium containing 2µg/ml Acridine orange for 15 min at 37°C (Kondratskyi et al., 2014). After the incubation period, the cells were washed twice with PBS and the cells were imaged under LSM710 Zeiss confocal microscope (Zeiss, Germany). The green fluorescence intensity was analyzed by Image J software (NIH, version 1.49v). An imaging protocol was optimized for the control samples and then applied for all the samples to ensure consistency in imaging parameters for all the samples.

3.3.4 Subcellular fractionation

Cells were collected by scrapping and centrifuged at 2000g to pellet the cells and washed twice with PBS. The following protocol was used as shown previously (Huang et al., 2012). The cells were lysed in subcellular fractionation buffer (250 mM sucrose, 20 mM HEPES, 10 mM KCl, 1.5 mM $MgCl_2$, 1 mM EDTA, 1 mM EGTA, pH 7.4) containing protease and phosphatase inhibitors by passing through a 25 G needle 10-15 times using a 1 ml syringe and incubated on ice for 20 min. Nuclei were pelleted by centrifugation at 1000 x g for 10 min at 4°C and the pellet was re-suspended in RIPA lysis buffer (50mM Tris HCl pH 8, 150 mM NaCl, 1 mM EGTA, 1% NP-40, 0.1% SDS, 0.5% sodium deoxycholate,5% glycerol and protease and phosphatase inhibitors) and

used as nuclear fraction. Supernatant was centrifuged at 10,000g for 10 min to pellet out mitochondria and the supernatant was transferred to fresh tubes. The supernatant was further spun at 21,000g for 2 hr and the supernatant was collected and labeled as cytosolic fraction. The resultant pellet was re-suspended in RIPA lysis buffer and designated as lysosomal enriched fraction.

3.3.5 Western blot analysis

Western blotting was performed using our laboratory routine procedure (Nagakannan et al., 2016). Briefly, following treatments, cells were collected by scrapping in their culture medium and washed once with ice cold PBS. The cell pellets were lysed in NP-40 lysis buffer (50mM Tris HCl pH 8, 150 mM NaCl, 5mM EDTA, 1% NP-40) containing protease and phosphatase inhibitors by sonication (3 x 5 sec) on ice. Cell extracts were collected by centrifugation at 10,000g for 15 min at 4°C and the protein concentration was determined using Pierce BCA Protein Assay Kit.

Equal amount of proteins was resolved on SDS-PAGE and transferred to PVDF membrane. After blocking with 5% non-fat milk, the membranes were probed with the following primary antibodies against: LC3 (1:2500, #L7543) from Sigma; cleaved caspase-3 (1:000, #9664), PARP-1 (1:1000, #9542), cathepsin B (1:1000, #31718), Nrf2 (1:1000, #12721) and ubiquitin (1:1000, #3936) from Cell signaling Technologies, USA; SQSTM1 (p62, 1:1000, #sc-28359), Prx2 (1:1000, #sc-515428), Lamin B1 (1:1000, #sc-377000) and cytochrome C (1:1000, #sc-13156) from Santa Cruz Biotechnologies, USA; cathepsin L (0.25µg/ml, AF952) and cystatin C (1µg/ml, #AF1196) from R & D systems, USA; LAMP-1 (0.5µg/ml, #H4A3) and LAMP2 (0.5 µg/ml, H4B4) from Developmental Studies Hybridoma Bank, University of Iowa, USA. After overnight incubation with primary antibodies, the membranes were then probed with appropriate HRP-conjugated secondary antibodies followed by detection using Clarity™ and Clarity Max™ Western ECL

Blotting Substrates (Bio-Rad Laboratories, USA). The membranes were striped using 0.2N NaOH for 15 min at room temperature and probed with GAPDH-HRP (1:5000, #ab185059, abcam, USA) or β-Actin-HRP (1:5000, #sc-47778, Santa Cruz Biotechnologies, USA) antibodies to confirm equal protein loading. Band densities of target proteins were measured using AlphaEaseFC (version 6.0.0, Alpha Innotech) and were normalized to GAPDH or β-Actin. The values are expressed as mean ± S.E.M of fold change.

3.3.6 Determination of oxidative modification of cathepsins

This method was used as has been described previously (Schwertassek et al., 2014). After appropriate treatments, cells were washed once with ice cold PBS containing 10 mM NEM (N-ethylmaleimide) to block free thiols and scrapped in 10% TCA and incubated on ice for 10 min. Proteins precipitates were pelleted by centrifugation at 16,000g for 15 min and the pellet was washed with 100% ice cold acetone. The dried pellet was dissolved in lysis buffer (50 mM Tris, pH 6.8, 1% SDS) containing 40 mM NEM by sonication and incubated at room temperature for 10 min. Equal amount of proteins were subjected to non-reducing SDS-PAGE and transferred to PVDF membrane followed by detection of bands using cathepsin L antibody (R & D systems, USA).

Additionally, AMS thiol trapping method was employed to confirm the results (Jakob et al., 1999). Cells were washed with ice cold PBS and incubated with ice cold 10% trichloroacetic acid (TCA) at 4°C for 20 min to denature the proteins. Protein precipitates were collected by scrapping and centrifuged at 16,000g for 2 min followed by washing with 100% Acetone. The protein pellet was solubilized by sonication in derivatization buffer (100mM Tris-HCl, pH 8.0, 1% SDS) containing 15mM AMS (4-acetamide-40-maleimidylstilbene-2,20-disulphonic acid). After incubation at room temperature for 1 hr, samples were mixed with non-reducing loading buffer and subjected to

non-reducing SDS-PAGE and western blotting using antibody against cathepsin L (1:500, #sc-6498) or cathepsin B (1:500, #sc-13985, Santa Cruz Biotechnologies, USA).

3.3.7 Immunocytochemistry

Cells were cultured on glass coverslips and treated appropriately. Subsequently, the cells were washed with PBS, paraformaldehyde fixed, permeabilized with 0.3% Triton-X-100 and incubated with primary antibody overnight at 4°C or for 4 hr at room temperature. Following PBS washes, the coverslips were incubated with Alexa flour conjugated secondary antibodies (Molecular Probes, USA) for 1 hr at room temperature. Finally, the coverslips were washed with PBS, counterstained for nuclear marker (DAPI) and mounted on to glass slides. The cells were imaged using confocal microscope.

3.3.8 Biochemical assessments

Enzymatic activities of cathepsin B and L were measured by fluorometric method using commercially available kits (abcam) according to the manufacturer's instructions. To measure the reduced glutathione levels at the specified time points, cells were incubated with 50 µM monochlorobimane (MCB) in the dark for 30 min at 37°C. Then the cells were scraped, washed once with PBS and lysed in NP-40 lysis buffer (50mM Tris HCl pH 8, 150 mM NaCl, 5mM EDTA, 1% NP-40). The cell lysates obtained after centrifuging at 12,500g for 15 min at 4°C were transferred to a black walled 96-well plate (Baxter et al., 2015). The GSH-MCB fluorescence was measured with excitation and emission wavelengths of 380 and 480nm, respectively, using Synergy H1 Hybrid Reader (BioTeK Instruments, USA) and were normalized to protein content, which was measured using Pierce BCA protein assay kit.

3.3.9 Quantitative Real Time PCR (RT-qPCR) analysis

Quantitative real time PCR was performed as described previously (Nagakannan et al., 2016). Purelink RNA mini kit and Superscript Master Mix were from Invitrogen, SYBR green was from Molecular Probes. List of primer sequences used in this study is provided in Table 3.1.

Table 3.1: List of primer sequences used in this study

CTSB-F	5’- CTC TATG AAT CCC ATG TAG GGT GC-3’	(Pucer et al., 2010)
CTSB-R	5’-CCT GTT TGT AGGTCG GGC TG-3’	
CTSL-F	5’-TCA GGA ATA CAG GGA AGG GAA A-3’	(Pucer et al., 2010)
CTSL-R	5’-TCC TGGGCT TAC GGT TTT GA-3’	
Nrf2-F	5′-GAGAGCCCAGTCTTCATTGC-3′,	(Reichard et al., 2007)
Nrf2-R	5′-TGCTCAATGTCCTGTTGCAT-3′	
p62-F	5’-AAGC CGGGTGGGAATGTTG-3’;	(Nagakannan et al., 2016)
P62-R	5’-GCTTGGCCCTTCGGATTCT-3’	
GAPDH	5’-CTGACTTCAACAGCGACACC-3’	(Nagakannan et al., 2016)
GAPDH	5’-TGCTGTAGCCAAAT-TCGTTGT-3’	

3.3.10 Statistical analysis

Data are represented as mean ± S.E.M. Statistical differences between the groups were evaluated by one-way analysis of variance (ANOVA) followed by Tukey’s post-hoc test (version 6.07, GraphPad Prism, La Jolla, California, USA). p values < 0.05 were considered as significant.

3.4 Results:

3.4.1 Lysosomal deficiency after TrxR inhibition is associated with lysosomal membrane permeabilization in serum deprived SH-SY5Y cells

Recently we reported that oxidative stress after inhibition of TrxR by Au during SD in SH-SY5Y cells caused autophagy dysfunction accompanied by lysosomal deficiency, which led to impairment in protein degradation and cell death. To examine the underlying mechanism/s involved in lysosomal dysfunction, we first tested whether lysosomal deficiency was associated with any changes in lysosomal-associated membrane proteins: LAMP-1 and LAMP-2. Our results indicated that LAMP-1 was not affected significantly between controls and treatments, however administration of Au significantly increased the LAMP-2 protein ($p<0.05$) after 24 hr SD (1.64-fold) (Fig. 3.1A). This indicates that inhibition of TrxR during energy shortage in SD leads to enlargement of lysosomes. This is in agreement with our recent immunocytochemical demonstration of larger lysosomes in Au-treated cells (Nagakannan et al., 2016). An earlier report (Ono et al., 2003) suggests that enlarged lysosomes are more susceptible to LMP, which results in releasing their contents into cytosol thereby leading to cell death. To investigate whether lysosomal deficiency after TrxR inhibition in our model was associated with LMP induction, we used acridine orange staining (Erdal et al., 2005) that detects the acidic lysosomes and endosomes. Acridine orange emits red fluorescence in acidic pH, but in neutral and slightly basic pH such as those found in cytosol, it is green (Erdal et al., 2005). Any damage to lysosomal integrity will cause the release of acridine orange into the cytosol which can be detected by an increase in green fluorescence and indication of LMP (Turk et al., 2012). In Fig. 3.1B, acidic lysosomes in control cells are shown in red. A prominent increase in number and lysosomal size is observed after SD, indicating a normal enhanced autophagy. However, the acidophilic lysosomes were visibly decreased in Au-treated

cells confirming the lysosomal deficiency as we reported previously. Additionally, Au-treated cells showed a robust increase in green fluorescence staining suggestive of LMP induction after TrxR inhibition. To further confirm loss of lysosomal integrity and LMP induction after TrxR inhibition, we used cathepsin B (CTSB) immunostaining. No evidence of lysosomal destabilization was found after 6 hr of SD, whereas addition of Au caused a general increase in CTSB protein and CTSB leakage into the cytoplasm around the lysosomes (marked by LAMP2 staining) (Fig. 3.1C).

Figure 3.1. Inhibition of TrxR by auranofin causes lysosomal membrane permeabilization (LMP) in SH-SY5Y cells during serum deprivation (SD).

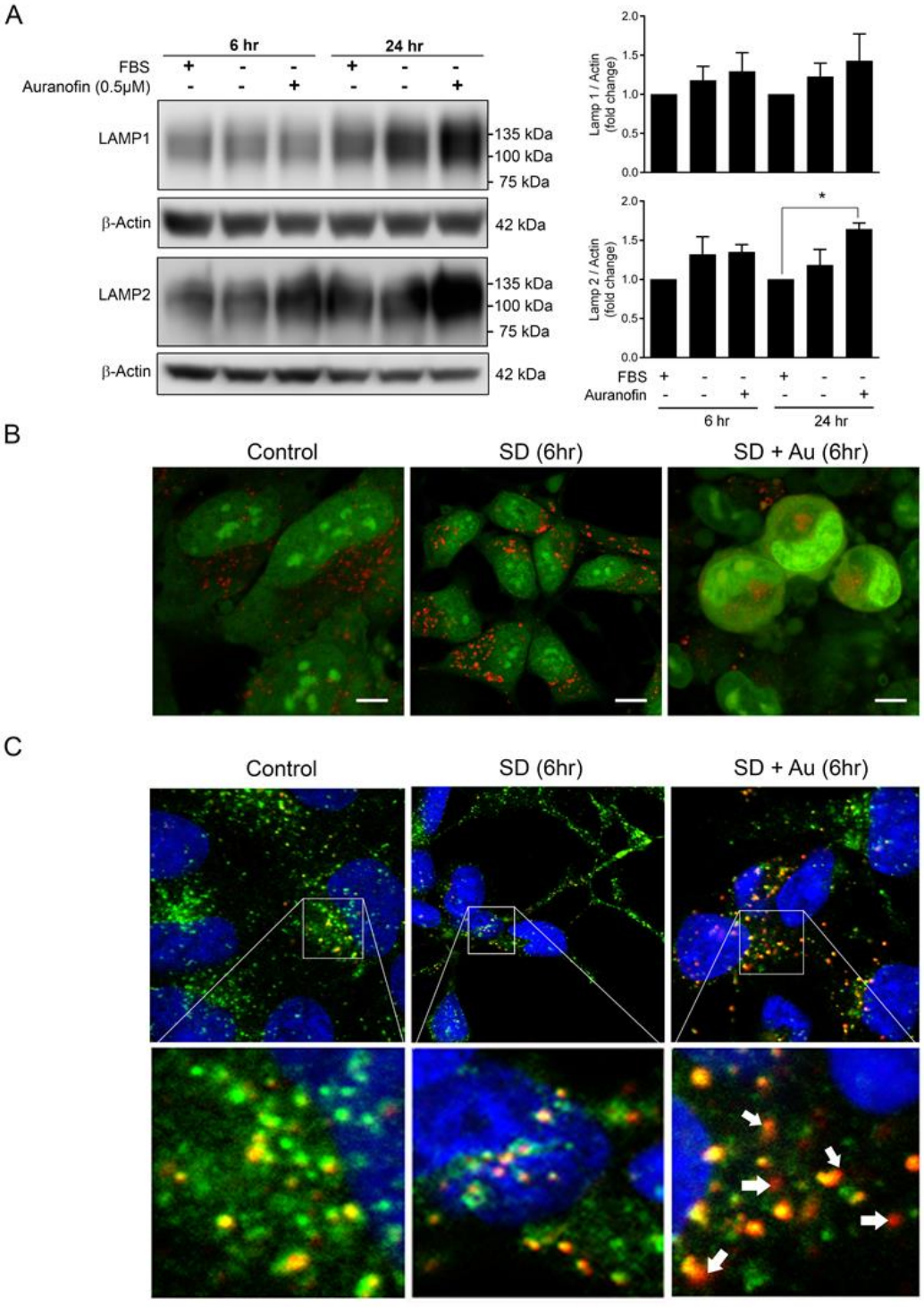

Figure 3.1. Inhibition of TrxR by auranofin causes lysosomal membrane permeabilization (LMP) in SH-SY5Y cells during serum deprivation (SD). (A) Representative western blots showing LAMP1 and LAMP2 levels in lysates extracted from SH-SY5Y cells subjected to different durations of SD in the presence or absence of auranofin. Densitometric analysis of proteins normalized to β-actin is shown. Values represent mean ± S.E.M., n=4; *$p<0.05$. **(B)** SH-SY5Y cells were subjected to 6 hr of SD in the presence or absence of auranofin, stained with 2 μg/ml acridine orange for 15 min and imaged under confocal microscope. **(C)** SH-SY5Y cells were treated with complete FBS medium (control) or serum free medium (SD) for 6 hr or in the presence of auranofin (SD+Au), fixed with paraformaldehyde and stained for lysosomes (LAMP2, green) and cathepsin B (red). DAPI was used to mark the nuclei (blue). Higher magnification images of the inserts are shown in the lower panel. Arrows indicate cathepsin B signal. Note the diffused cathepsin B signal (outside the lysosomes) only in auranofin treated SH-SY5Y cells subjected to SD.

3.4.2 Auranofin causes differential regulation of Cathepsin B and L protein and activity in nutritionally stressed SH-SY5Y cells

To determine the effect of TrxR inhibition on lysosomal proteases, we examined the changes in protein and enzymatic activity of CTSB, and CTSL; the pro-apoptotic and pro-autophagy enzymes (Schwertassek et al., 2014; de Castro et al., 2016; Li et al., 2016a), respectively. Western blotting was used to detect the active form of CTSB (24 and 27kDa) in this study. Our results showed that the level of CTSB protein was not significantly upregulated after SD or Au treatment (Fig. 3.2A and B) during the early (6 hr) or late (24 hr) time points. However, using the commercially available enzymatic activity assay kits, we observed that Au-treatment robustly increased the enzymatic activity of CTSB; 5 and 3.3-fold increase in CTSB activity (Fig. 3.2C) at both 6 and 24 hr, respectively. This suggests that increased CTSB activity is independent of new protein synthesis. We therefore examined the changes in CTSB gene expression using RT-qPCR. Our results (Fig. 3.2D) confirmed that the changes in CTSB activity is not associated with new mRNA expression.

To investigate whether the level of endogenous cystatin C (CysC), a general inhibitor of CTSB and CTSL was affected after TrxR inhibition, we used western blotting. On subjecting SH-SY5Y cells to SD, CysC protein was significantly elevated ($p<0.05$) (Fig 3.2C), perhaps explaining the lack of activation of CTSB during this period. The increase in CysC levels was completely inhibited in Au+SD treated cells ($p<0.05$), that coincided with the significant upregulation of CTSB activity (Fig. 3.2C). This clearly indicates that under SD conditions, upregulation of CysC inhibits cathepsin activation, however excessive oxidative stress condition after inhibition of TrxR overpowers the CysC machinery and therefore unleashes the pro-apoptotic CTSB activation.

In our recent work (Nagakannan et al., 2016) we showed that elevated oxidative stress is a major player after TrxR inhibition in this model, we therefore asked whether cellular reducing capacity may play a role in regulation of Cathepsin: CysC cross talk. N-Acetyl-L- cysteine (NAC) is a precursor of cysteine, the rate limiting amino acid for GSH synthesis. Administration of NAC moderately increased Cystatin C levels (Fig. 3.2A and B) which correlated well with the decrease in cathepsin activity by NAC (Fig. 3.2C) confirming that upregulation of cellular reducing capacity can prevent activation of CTSB-mediated apoptosis. This also implies that induction of oxidative stress unleashes the CTSB activity and apoptotic cell death.

To examine the fate of CTSL, the pro-autophagy member of lysosomal enzymes, western blotting and specific enzymatic activity was performed. Interestingly, here we observed a different profile than CTSB in our experimental model; during the early time points of SD (6 hr) the levels of mature CTSL protein (27kDa) remained unchanged in comparison with those of control conditions, but was significantly increased ($p<0.05$) in SD+Au treated samples (Fig. 3.2A and B). Interestingly there was no significant increase in CTSL activity in these conditions. In contrast, CTSL mature form was moderately elevated at 24 hr SD treated cells, but not in SD+Au group (Fig. 3.2A and B). However, a modest but statistically significant rise in CTSL activity (1.2-fold) was observed by 24 hr of SD, which was further enhanced after Au-treatment (1.4-fold) (Fig. 3.2C). Similar to the CTSL protein levels, we observed an increasing trend (not significant) for CTSL mRNA during the early hours of SD (Fig. 3.2D). This may suggest the pro-autophagy role of CTSL. Similar to CTSB, NAC co-treatment in Au-treated cells significantly abrogated the increase in CTSL protein levels ($p<0.01$ [6 hr], $p<0.05$ [24 hr] vs SD+Au) and enzymatic activity at 24 hr ($p<0.05$) indicating the regulatory role of redox environment on cathepsins.

Figure 3.2. Auranofin causes differential regulation of Cathepsin B and L in serum deprived SH-SY5Y cells.

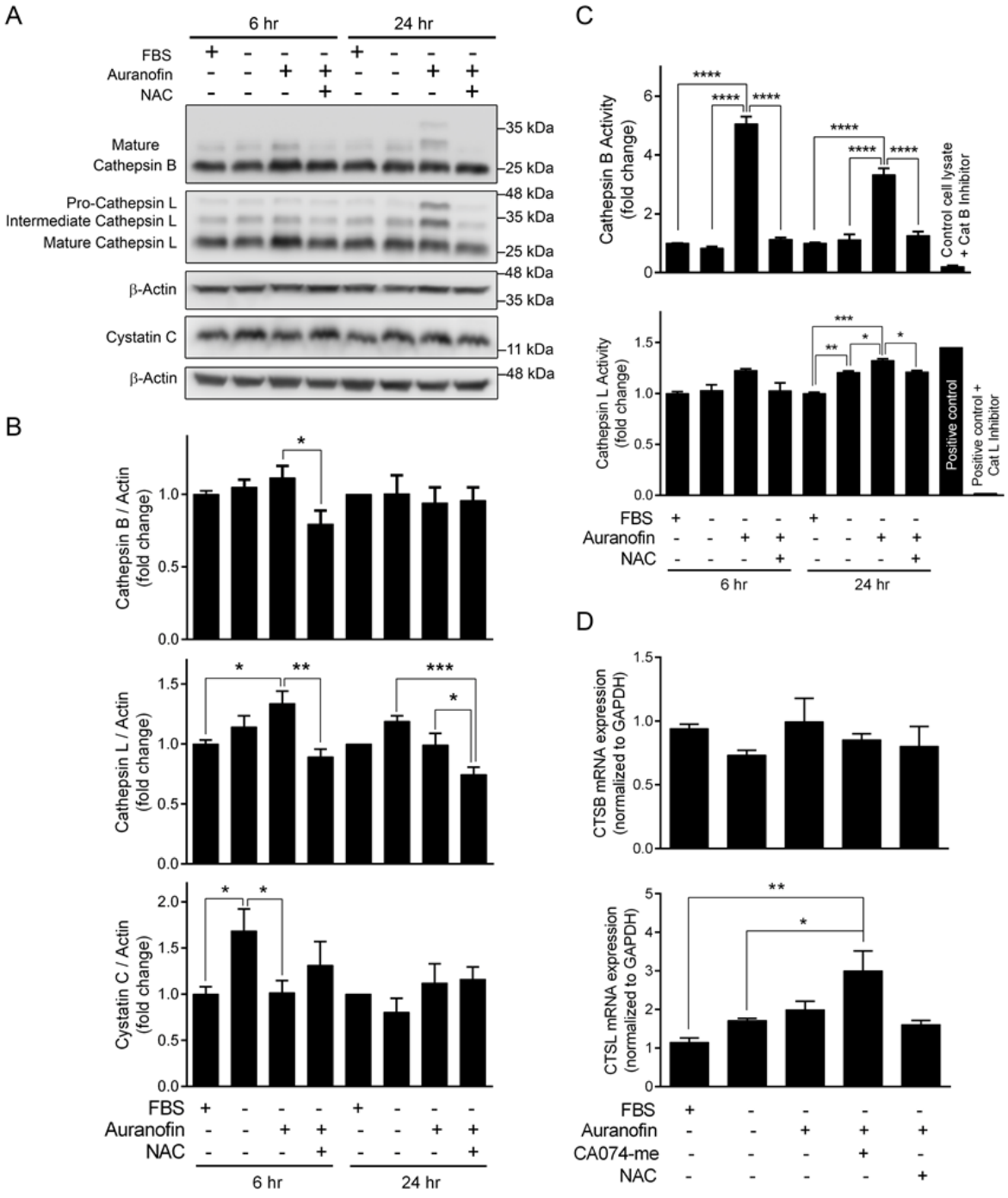

Figure 3.2. Auranofin causes differential regulation of Cathepsin B and L in serum deprived SH-SY5Y cells. SH-SY5Y cells were subjected to serum deprivation for 6 and 24 hr in the presence or absence of auranofin with or without NAC. The lysates were analysed for cathepsin B and L and cystatin C protein levels by western blotting **(A** and **B)** and the activities were measured by fluorometric method using commercially available kits **(C).** Control cell lysates incubated with cathepsin B inhibitor and recombinant human cathepsin L (positive control) with or without cathepsin L inhibitor were used as assay controls. All values are represented as mean ± S.E.M. n=6-10 for protein and n=2-4 for activity. *p<0.05, **p<0.01, ***p<0.001, ****p<0.0001. **(D)** SH-SY5Y cells were pretreated with CA-074-me overnight and were treated with auranofin in serum free media for 6 hr; NAC was added along with auranofin. Total RNAs were extracted and mRNA levels of CTSL and CTSB were quantified using RT-PCR. Bars indicate mean ± S.E.M., n=4; *p<0.05, **p<0.01.

3.4.3 CTSL and CTSB show differential redox sensitivity to auranofin induced oxidative stress

To explain the lack of CTSL enzymatic activity despite the elevated levels of its mature form at 6 hr, we postulated that Au-mediated oxidative stress in our model was responsible for oxidative inactivation of CTSL protein. We used a thiol trapping method that is used for identification of redox sensitive proteins [21]. In this method, after entrapping free thiols using NEM, oxidized proteins move slower in a non-reducing gel and therefore the oxidized and reduced protein can be separated. To establish the method, we added H_2O_2 and DTT (dithiothreitol) to induce protein oxidation and reduction, respectively. As shown in Fig. 3.3A, control cells (lanes 1 and 2) and DTT-treated samples display a prominent band at 25kDa (mature form) and additional heavier bands at ~35-48 kDa representing the intermediate and pro-CTSL. Addition of H_2O_2 (for 10 min) (lane 4) caused a dramatic increase in signal intensity of the pro-CTSL band and decreased the mature form. This confirmed that pro-cathepsin L processing is sensitive to oxidation and reduction. Subjecting the cells to 6 hr of FBS-medium (lane 5), starvation (lane 6) and Au (lanes 7-8), also caused a similar effect as observed with H_2O_2, however addition of NAC to Au treated cells (lane 9) prevented this effect, confirming the role of oxidative stress in CTSL processing.

This was additionally confirmed using a different anti-CTSL antibody and using another thiol trapping method. In this method, AMS is used for thiol trapping, as shown previously (Jakob et al., 1999). Similar to NEM method, we observed that H_2O_2 treatment resulted in increased protein oxidation of pro-CTSL (~48kDa) (Fig. 3.3B, lane 4). Similarly, a prominent accumulation of oxidized pro-CTSL was observed with increasing level of stress (Fig. 3.3B, lanes 6-8). Incidentally, an additional heavy band (~75kDa) was detected in Au-treated samples that may represent dimers or over-oxidized CTSL. Our experiments also showed that increased levels of pro-CTSL correlated with decreased levels of intermediate and mature CTSL. Administration of

NAC rescued protein oxidation as is attested by robust decrease in pro-CTSL levels and increase in intermediate and mature CTSL (Fig 3.3B, lane 9). The additional heavy band (~75kDa) was also resolved after NAC treatment. Using this technique for examining the impact of oxidative stress on CTSB, we did not observe any substantial change in oxidation of pro-CTSB (Fig. 3.3C). These data suggest that CTSL and CTSB are differentially affected/regulated by redox status of the cell.

Figure 3.3. CTSL and CTSB are differentially regulated by the redox status of the cell.

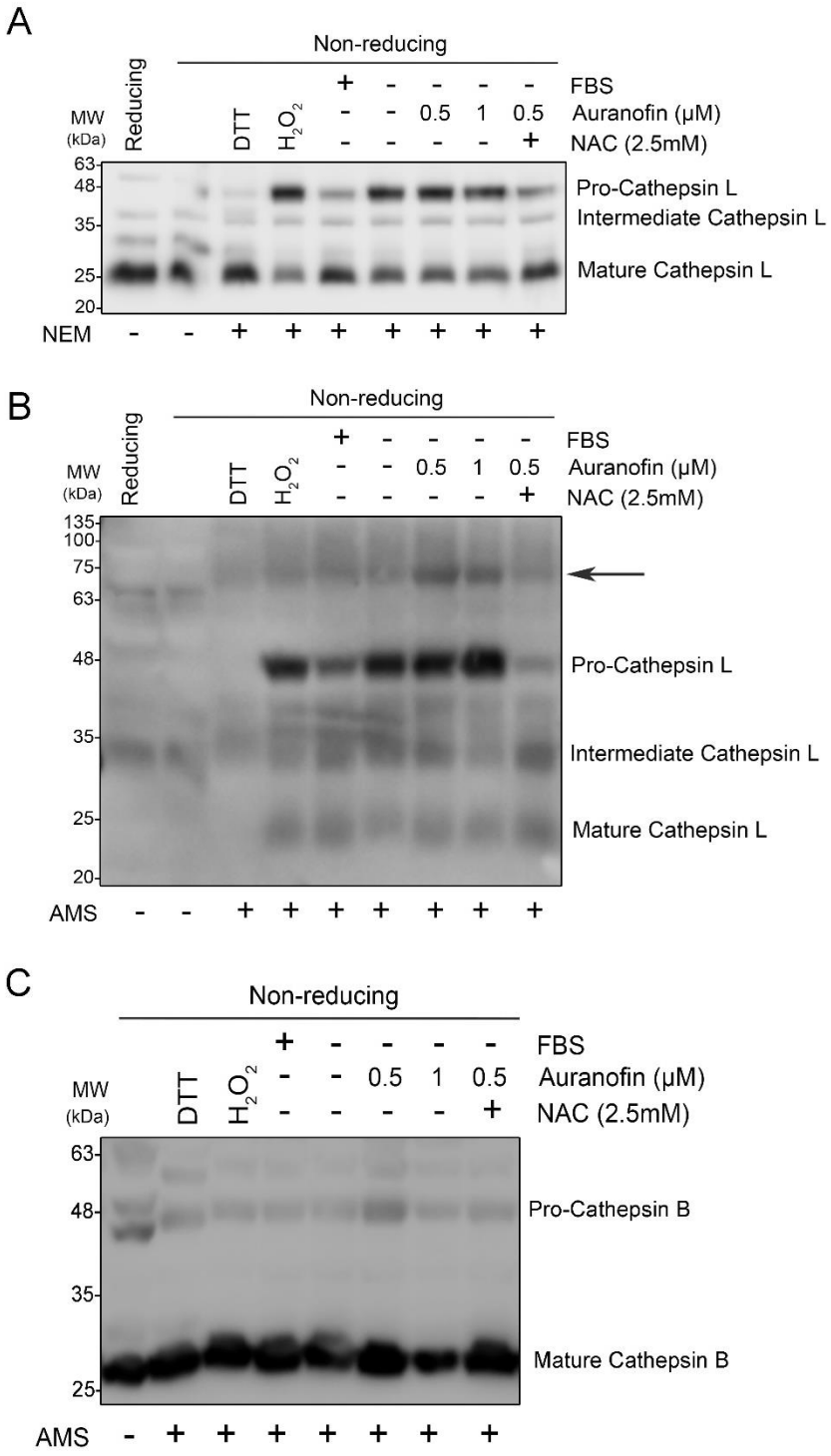

Figure 3.3. CTSL and CTSB are differentially regulated by the redox status of the cell. SH-SY5Y cells were exposed to serum free conditions with or without auranofin or NAC or both for 6 hr. The free thiols were blocked by treating the cell lysates with NEM to prevent any structural modification during processing and the samples were run on non-reducing SDS-PAGE. Cells treated with Dithiothreitol (DTT, 5mM) or Hydrogen Peroxide (H_2O_2, 0.5mM) for 10 minutes in serum free media were used as controls **(A)**. SH-SY5Y cells were subjected to serum deprivation with or without auranofin or NAC or both for 6 hr. Then the redox status of cathepsin L **(B)** and cathepsin B **(C)** were assessed using AMS method by non-reducing SDS-PAGE. Cells treated with Dithiothreitol (DTT, 5mM) or Hydrogen Peroxide (H_2O_2, 0.5mM) for 30 minutes were used as controls.

3.4.4 Cathepsin B mediates the activation of apoptosis after TrxR inhibition in starving SH-SY5Y cells

To examine the contribution of cathepsins to cell death induction in this model, we aimed to test the neuroprotective ability of cathepsin inhibitors in this model. Our SD model resulted in a significant loss in cell viability (36%), which was further augmented by the addition of Au (70%, $p<0.0001$). Specific inhibitors of CTSB, CTSL and CTSD (cathepsin D) were used as described in material and methods. Overnight pre-treatment of SH-SY5Y cells with CTSB inhibitor (CA-074-me) significantly ($p<0.0001$) protected the cells from the cytotoxic effect of Au, however CTSL inhibitor (Z-FY-CHO) and CTSD inhibitor (Pepstatin A) failed to show any improvement in cell viability (Fig. 3.4A). The role of CTSB in induction of apoptosis was assessed using immunoblotting for apoptotic markers in our model. As we showed previously, inhibition of TrxR in starving- SH-SY5Y cells induced PARP-1 and Caspase-3 cleavage (Nagakannan et al., 2016); in these experiments overnight pre-treatment of cells with CTSB inhibitor (CA-074-me) abrogated the increase in these apoptotic markers levels (Fig. 3.4B). Similarly, rescue effect of NAC in prevention of apoptosis further confirmed the involvement of ROS after TrxR inhibition. The protective role of CA-074-me was also reflected in the level of cathepsins message level; as CA-074-me treated cells showed significantly lower CTSB and higher CTSL mRNA levels (Fig. 3.2D). The involvement of cathepsins in cell death and protective role of CysC was additionally confirmed by administration of recombinant CysC in Au-treated cells. This resulted in a significant increase ($p<0.001$) in cell viability in Au-treated starving SH-SY5Y cells, supporting the notion that failure of CTSB: CysC ratio might be another cause for autophagy dysfunction and enhanced apoptosis under TrxR inhibition. These results are in agreement with a recent report that showed the protective capacity of a Cystatin protein against Au-treatment (Oh et al., 2017).

Figure 3.4. Cathepsin B mediates the autophagy to apoptosis switch after TrxR inhibition in starving SH-SY5Y cells.

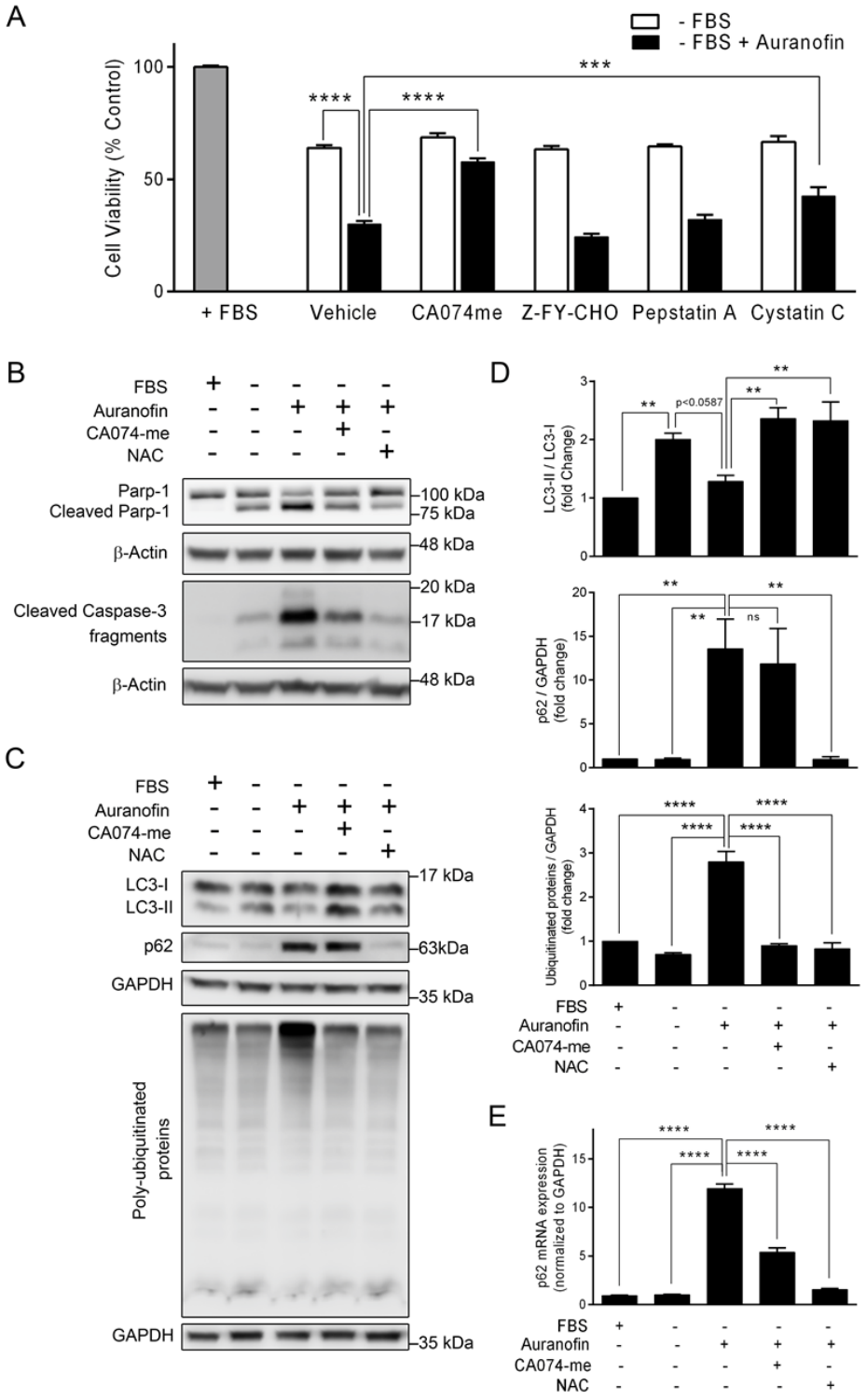

Figure 3.4. Cathepsin B mediates the autophagy to apoptosis switch after TrxR inhibition in starving SH-SY5Y cells. (A) Cells were pretreated with CA-074-me (15 µM), Z-FY-CHO (10 µM) or Pepstatin A (50 µM) overnight and were treated with auranofin in serum free media for 24 hr except for Cystatin C (1.25 µM), which was co-incubated with auranofin. After 24 hr, cell viability was determined by CCK-8 assay. Values represent mean ± S.E.M., n=6-12; ***p<0.001, ****p<0.0001. SH-SY5Y cells were pretreated with CA-074-me overnight and were treated with auranofin in serum free medium; NAC was treated along with auranofin for 6hr and the cell lysates were analysed for apoptosis **(B)** and autophagy **(C)** markers by western blotting. **(D)** Densitometric analysis of proteins normalized to GAPDH is shown. **(E)** mRNA levels of p62 were quantified using RT-PCR is shown. Bars indicate mean ± S.E.M., n=4-6; **p<0.01, ****p<0.0001.

3.4.5 Cathepsin B inhibition prevents accumulation of ubiquitinated proteins and improves lysosomal acidification

Protein homeostasis, or proteostasis, is the sum of multiple systems that control biosynthesis, folding and degradation. Autophagy, protein ubiquitination and proteasome activity regulate the protein turnover. We have previously shown that Au-treatment results in accumulation of ubiquitinated proteins, decreased proteasome activity and autophagy failure. These were successfully prevented when cells were co-treated with NAC (Nagakannan et al., 2016), as these cells displayed a significant increase in LC3-II/LC3-I ratio, decrease in p62 and ubiquitinated protein levels. This indicate an active involvement of oxidative stress in autophagy and Ubiquitin Proteasome System failure (Fig. 3.4C and D). Protective effect of CTSB inhibitor on proteostasis was evident by a robust decrease in protein ubiquitination ($p<0.0001$) indicating improved protein clearance in these cells (Fig. 3.4C). Our recent report showed that Au causes both transcriptional induction and accumulation of p62 protein that was mediated by lysosomal deficiency (Nagakannan et al., 2016). To examine whether inhibition of CTSB can affect markers of autophagy, the classic approach is to measure p62 and LC3-II levels, however since both p62 and LC3-II must be degraded in lysosome, application of CTSB inhibitor will be detrimental to the lysosomal turnover of these proteins (Mizushima and Yoshimori, 2007). Therefore, the protein levels of p62 and LC3-II cannot be used to determine any changes in autophagy when lysosomal proteases are involved. However, we detected a significant decrease in p62 transcription in CTSB inhibitor and in NAC treated groups (Fig. 3.4E). The levels of p62 protein is a reflection of oxidative stress severity and is regulated by Nrf2 level (Jain et al., 2010). Therefore, our results suggest that CA-074-me treatment is associated with decreased levels of oxidative stress. Additionally, using acridine orange staining we observed that lysosomal acidification was

substantially improved in CTSB inhibitor treated cells (Fig. 3.5A), suggesting better lysosomal function. Although these results may not confirm whether lysosomal deficiency were improved after inhibition of CTSB, lower p62 transcription, proper lysosomal acidification and improved protein ubiquitination are clear signs of cellular recovery.

3.4.6 Cathepsin B inhibition prevents LMP induced by Auranofin

Recent findings suggest that upon induction of LMP, CTSB is translocated into cytosol and can further cause lysosomal membrane damage and exacerbate LMP through multiple mechanisms (Hristov et al., 2014; Gorojod et al., 2015). To test whether inhibition of CTSB using CA-074-me can diminish the severity of LMP after Au-mediated TrxR inhibition, we checked the lysosomal integrity with acridine orange staining and cell fractionation. We observed that specific inhibition of CTSB resulted in a significant reduction ($p<0.0001$) in acridine orange green fluorescence when compared to SD+Au group, suggestive of CTSB involvement in the exacerbated LMP by Au (Fig. 3.5A). This was further confirmed with western blotting for CTSB in cytosolic fractions, where Au increased the leakage of this lysosomal protease into the cytosol. Application of CA-074-me markedly reduced the level of CTSB in comparison to SD+Au treated cells providing evidence that CTSB is involved in LMP induction after TrxR inhibition (Fig. 3.5B). Since LMP and CTSB have been reported to be responsible for cytochrome C release and execution of mitochondrial apoptotic pathways (de Castro et al., 2016), we checked whether CA-074-me may affect cytochrome C release into the cytosol. Our western blotting showed that Au+SD treatment caused a drastic spillage of cytochrome C into the cytosol which was prevented by CA-074me confirming the involvement of CTSB in LMP aggravation and induction of apoptosis (Fig. 3.5B). These results are in agreement with another report showing the involvement of LMP and CTSB-mediated apoptosis after oxidative stress in glial cells (Gorojod et al., 2015). The importance of oxidative

stress in LMP and cytochrome C translocation into cytosol was additionally confirmed by protective role of NAC.

Figure 3.5. Cathepsin B inhibition prevents LMP induced by auranofin.

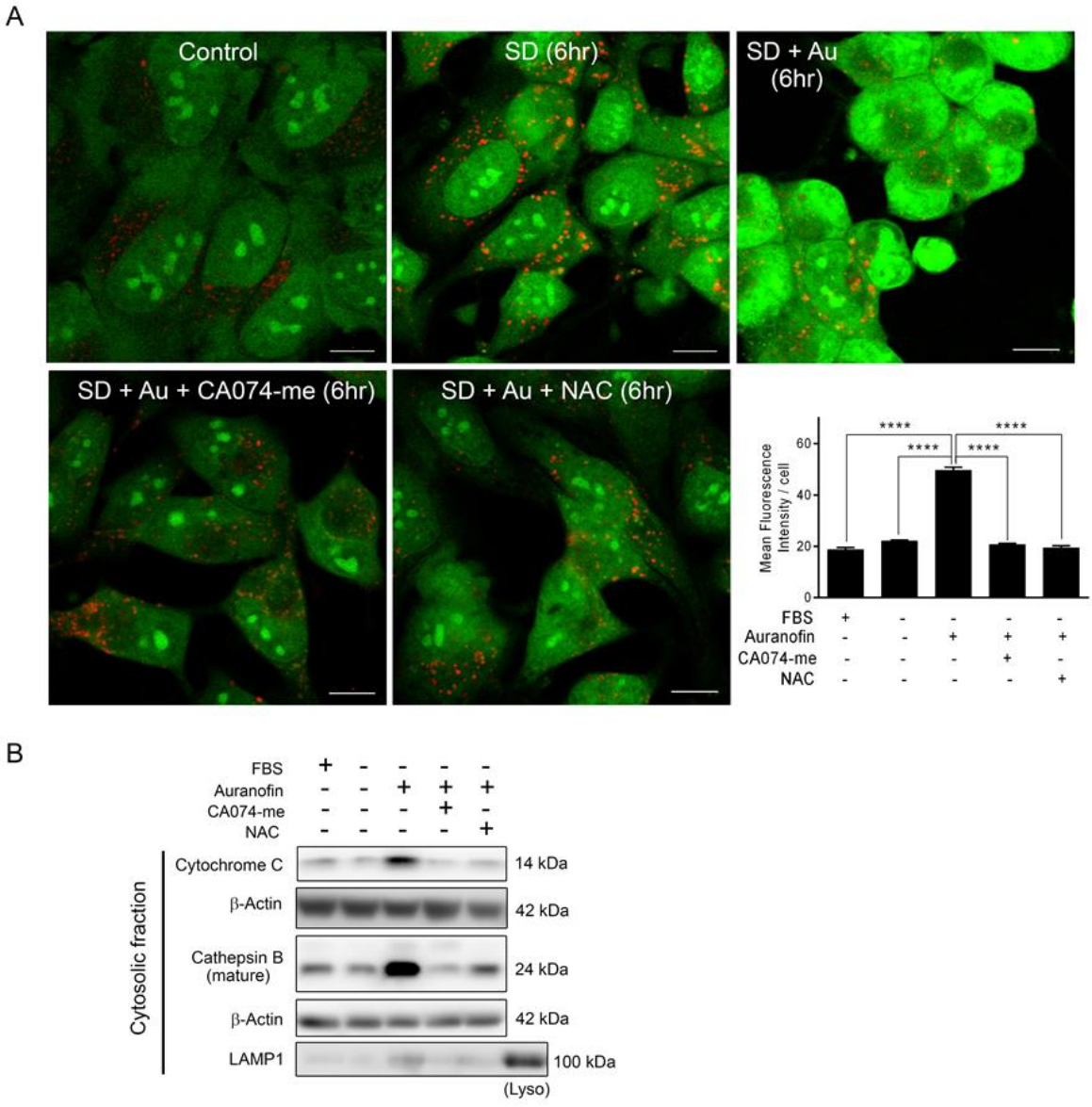

Figure 3.5. Cathepsin B inhibition prevents LMP induced by auranofin. (A) SH-SY5Y cells were pretreated with CA-074-me overnight and were treated with auranofin (whereas NAC was treated along with auranofin) for 6 hr in serum free media and the cells were stained with 2 µg/ml acridine orange for 15 min and imaged under confocal microscope. The mean green fluorescence intensity/cell was measured, and the values are represented as mean ± S.E.M., n ≥100 cells; ****p<0.0001. **(B)** Western blot analysis of cathepsin B and cytochrome C in cytosolic fraction isolated from SH-SY5Y cells treated with auranofin in serum free media for 6 hr. CA-074-me was treated for overnight prior to auranofin treatment and NAC was co-incubated with auranofin. To control fraction purity, β-actin and LAMP1 were used as cytosolic and lysosomal markers, respectively; Lysosome-enriched fraction (Lyso) was used as positive control for LAMP1.

3.4.7 Potential contribution of other antioxidants in this model

Au is a well-characterized inhibitor of TrxR enzyme and has been shown to promote cell death through induction of oxidative stress. TrxR is a member of a wide group of antioxidant proteins such as Thioredoxin, γ-glutamylcysteine synthase and NADPH-quinone reductase that regulate the cellular defence system in response to xenobiotics. The transcription of these proteins is regulated by binding of nuclear factor erythroid 2–related factor 2 (Nrf2) to a major regulatory sequence known as the antioxidant response element (ARE) (Gorrini et al., 2013b). To investigate whether the excessive cell death after Au-treatment was due to a disabled cellular antioxidant machinery in this model, we first examined the level of Nrf2 protein. Under normal conditions low levels of Nrf2 is maintained in the cytosol through binding to Keap1 (Kelch-like ECH-associated protein 1) promoting its ubiquitination and degradation by the proteasome system(Bryan et al., 2013). This maintains a short half-life for Nrf2 protein and a low/basal level of antioxidant protein expression (Reddy, 2008). Accordingly, we detected very low levels of Nrf2 protein in normal and SD conditions (Fig. 3.6A-C). However, addition of Au significantly increased the protein and mRNA levels of Nrf2. Induction of oxidative stress can interfere with the Nrf2-Keap1 interaction by formation of Keap1-p62 complex (Ichimura et al., 2013) that results in Nrf2 stabilization in cytosol followed by its translocation to nucleus and induction of ARE-mediated upregulation of antioxidant systems. Using subcellular fractionation, we observed that Au-treated cells contained significantly upregulated Nrf2 levels in cytosol as well as nucleus indicating that effects of Au on cell viability is not due to failure of Keap1/Nrf2/ARE pathway. Inhibition of CTSB significantly inhibited the accumulation and translocation of Nrf2; similarly, administration of NAC in Au-treated cells completely prevented the changes in Nrf2 levels and subcellular localization (Fig. 3.6D). Peroxiredoxins (Prxs), are a large family of proteins that are

increasingly involved in redox signaling. Prx2 is a major H_2O_2 scavenger that uses Trx as it substrate and has been recently shown to be induced by Nrf2 (Matte et al., 2015). We therefore examined any changes in Prx2 protein levels in our system, however total Prx2 protein levels were not differentially affected in this model (Fig. 3.6A-C). We also used redox western to detect the levels of oxidized/reduced Prx2 proteins, but there were no substantial changes in protein oxidation for Prx2 (data not shown). We then asked whether Au-treatment may result in oxidation of antioxidant thiols; using redox western blotting we recently showed that TrxR deficiency was associated with robust oxidation of Trx(Nagakannan et al., 2016). Here we employed the monochlorobimane assay to examine the overall levels of GSH. Our studies showed that while GSH was modestly increased after SD, administration of Au lowered GSH level (Fig. 3.6E). The GSH levels were further increased after administration of CA-074-me. These data cumulatively indicate that Au-treatment results in inactivation/depletion of Trx and GSH resulting in induction of oxidative stress mediated cell death.

Figure 3.6. Inhibition of TrxR induces Nrf2 activation and causes its nuclear translocation.

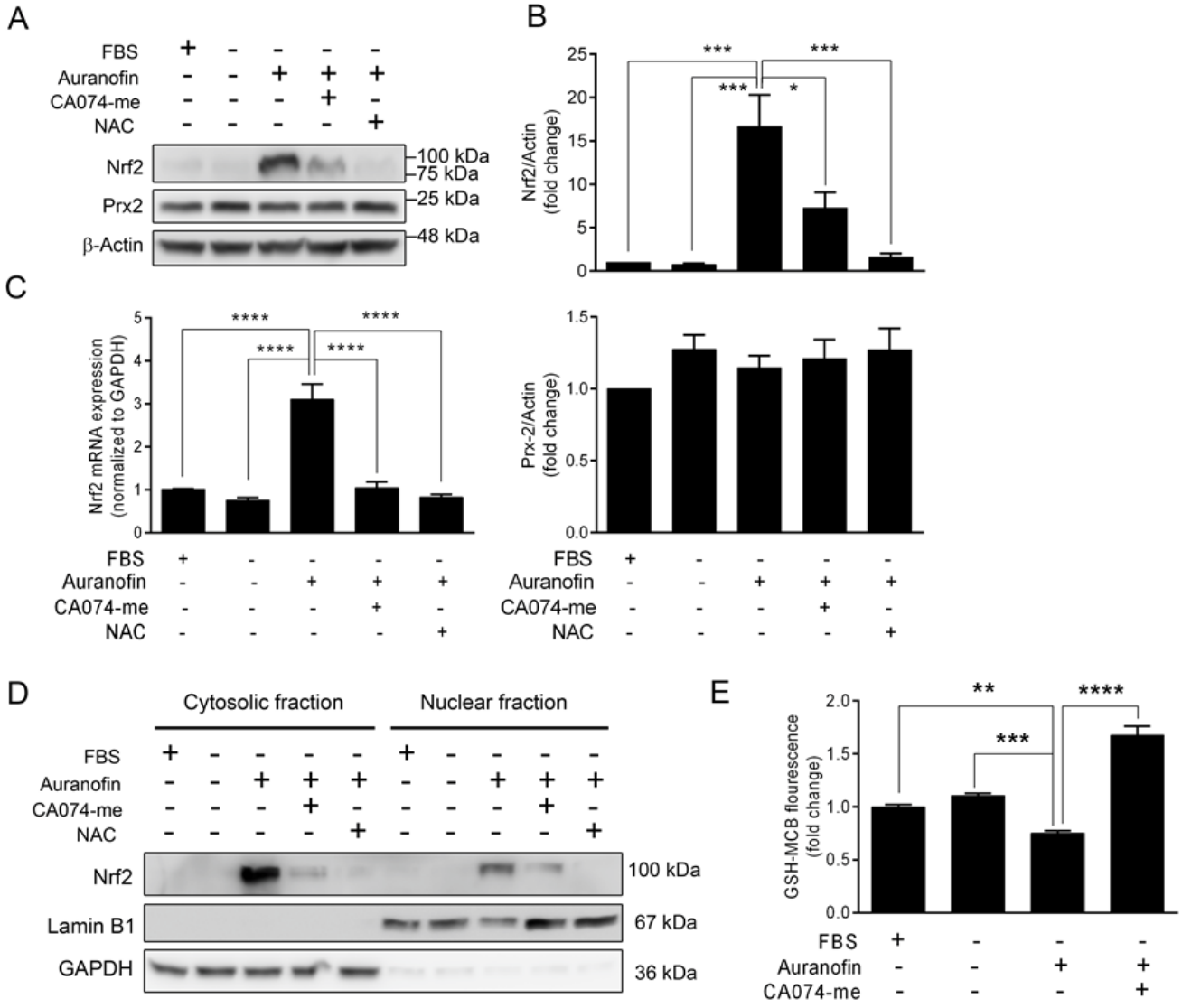

Figure 3.6. Inhibition of TrxR induces Nrf2 activation and causes its nuclear translocation. **(A)** SH-SY5Y cells were pre-treated with CA-074-me overnight and were treated with auranofin in serum free media for 6hr, while NAC was added along with auranofin and the cell lysates were subjected to western blot analysis for Nrf2 and Prx2. Densitometric analysis of proteins normalized to β-actin is shown **(B)**. mRNA levels of Nrf2 quantified using RT-PCR is shown in panel **C**. All values are represented as mean ± S.E.M., n=4. *p<0.05, ***p<0.001, ****p<0.0001. **(D)** Cytosolic and nuclear fractions from SH-SY5Y cells subjected to above mentioned conditions for 6hr were subjected to SDS-PAGE to determine translocation of Nrf2 to nucleus. Lamin B1 and GAPDH were used as nuclear and cytosolic markers, respectively. **(E)** SH-SY5Y cells were subjected to indicated conditions and GSH levels were measured using monochlorobimane method. Bars indicate fold change in GSH-MCB fluorescence normalized to protein, mean ± S.E.M., n=2-4; **p<0.01, ***p<0.001, ****p<0.0001.

3.5 Discussion

We recently reported that inhibition of TrxR using its specific inhibitor Au or RNA editing technology resulted in interruption of protein homeostasis that was associated with increased protein ubiquitination, decreased proteasomal activity and deficient lysosome-mediated autophagy leading to apoptosis(Nagakannan et al., 2016). In the present study we aimed to discover the cause for lysosomal deficiency that signaled conversion of autophagy to apoptosis in this model. Previous reports have shown that SD is associated with significant changes in CTSL and CTSB activity in PC12 cells (Isahara et al., 1999). Authors showed that CTSB activity was significantly decreased while CTSL activity was increased. The pro-appototic effects of CTSB and pro-autophagy effects of CTSL has been well identified (Kaasik et al., 2005; Dennemarker et al., 2010; Wei et al., 2013).

In this study, we hypothesized that lysosomal deficiency and interruption of autophagy and induction of apoptosis might be mediated through differential CTSL and CTSB regulation. Our results confirmed previous reports that activation of CTSB plays a major role in induction of apoptosis (de Castro et al., 2016) and inhibition of CTSB activation prevented cell death that was associated with improved protein degradation. Additionally, we showed that CTSL activation/processing is inhibited in this model. Administration of NAC to enhance the cellular reducing capacity rescued CTSL processing. Here we discuss potential mechanisms that can be responsible for differential CTSB and CTSL activation.

3.5.1 Differential redox sensitivity of CTSL and CTSB in oxidative stress conditions

The intensified ROS levels after inhibition of TrxR has been well documented. The redox western blotting suggested that conversion of CTSL precursor protein to its mature form is affected by oxidizing ROS in this model, but CTSB was not impacted. The observed differential redox

sensitivity and activation paradigm in CTSL and CTSB prompted us to examine the structure of CTSL and CTSB. Using the Universal Protein Resource (UniPort)(2017), we scanned the structure of human CTSB (P07858) and human CTSL1 (P07711). Both enzymes contain a signal peptide, activation peptide (propeptide), and a light and heavy chain. A similar number of thiol groups (cysteine and methionine residues) are present in these molecules (CTSL 22/333, CTSB 21/339), nevertheless upon examination of propeptides (activation peptides) we noted a disproportional distribution of methionine residues in CTSL (8/96) and CTSB (2/69). The CTSB propeptide contains one cysteine residue, while this section of CTSL does not contain any cysteines. The importance of methionine in redox regulation of protein activity is an emerging field in cell biology(Kim et al., 2014a). Our data suggests that higher methionine content in CTSL propeptide may be responsible for redox sensitivity of its processing. However, it must be emphasized that it is not known whether these residues can be accessible to oxidizing ROS. Nonetheless, these data provide a strong rationale for further examination of methionine role in cathepsin biochemistry. To our knowledge, this is the first report addressing the underlying mechanism of cathepsin processing under oxidative stress conditions. Our data support a previous report that showed differential sensitivity of CTSB and CTSL activity to protein hydroperoxides (Headlam et al., 2006). This group showed that CTSL is significantly more sensitive to protein hydroperoxides than CTSB. Although we did not examine the underlying peroxides that may be involved in the observed molecular events, previous reports have shown that inhibition of TrxR by auranofin is associated with increased levels of H_2O_2 originating from mitochondria that can mediate protein oxidation/peroxidation. This results in membrane damage in mitochondria (Munro et al., 2016) and lysosomes and therefore can cause cell death.

3.5.2 Differential response of CTSL and CTSB after TrxR inhibition can be regulated by Cystatin C

In this study we observed that exposing the SH-SY5Y neuroblastoma cells to SD does not induce LMP. Induction of SD resulted in increased levels of CysC, a general cathepsin inhibitor including CTSL and CTSB. Upregulation of CysC has been directly linked to induction of oxidative stress in this model (Nishio et al., 2000). In our study, the upregulated levels of CysC effectively prevented any significant changes in the CTSB and CTSL protein levels and activity during the induction of autophagy in SD. This is in agreement with previous report that links upregulated CysC levels to induction of autophagy (Tizon et al., 2010). Authors in this report showed that pro-autophagy effect of CysC was not caused by inhibition of CTSB activity. In our study, the elevation in CysC levels was prevented after Au administration, which was associated with significant upregulation of CTSB enzymatic activity without any changes in the mature CTSB protein level. Contrary to CTSB, the CTSL protein was significantly upregulated after TrxR inhibition (6hr), however CTSL enzymatic activity remained unchanged.

The differential effect of CysC on CTSB and CTSL activity may be also explained by its differential affinity for CTSB and CTSL; The inhibitor constant (Ki) of CysC for CTSB (Ki=0.27nM) is several times more than CTSL (Ki<0.005nM) indicating that CysC is a much more effective inhibitor for CTSL than CTSB (Turk et al., 2012). This is reflected in our experiments when decreased levels of CysC after TrxR inhibition quickly resulted in increased CTSB activity, but its inhibitory effect remained for CTSL, as despite increased levels of CTSL protein, its enzymatic activity remained unchanged. Interestingly further decrease of CysC at 24 hr samples were correlated with the maximum CTSL enzymatic activity. These results suggest that early *protective* autophagy (6hr) in this model is mediated through CysC upregulation, however

preventing the rise in CysC (by TrxR inhibition) leads to activation of CTSB and execution of apoptosis. Our experiments also show that TrxR inhibition prevents CysC upregulation, suggesting a potential inhibitory role for oxidative stress that is mediated by inhibition of CysC. TrxR deficiency results in Trx oxidation as we showed previously, however the potential interaction of Trx system and CysC remains to be investigated.

3.5.3 Differential effect of cellular pH on CTSB and CTSL activation may be responsible for conversion of autophagy and apoptosis

In the present study we observed that inhibition of TrxR is associated with a sharp increase in CTSB activity, although CTSB protein and message levels were not altered. Activation of CTSB is mediated by its autocatalytic activity by removal of a propeptide sequence in CTSB precursor molecule. The activated CTSB then acts as a catalyzer for activation of more enzyme. This process is especially active in acidic environment of lysosomes (pH~4.0), however it can also occur in normal cytosolic pH=6.5 (Turk et al., 2012). This explains the significant increase in CTSB activity after induction of LMP and the leakage of CTSB into the cytoplasm (pH~7) without the need for new protein synthesis.

Similar to CTSB, CTSL activation is also mediated by removal of its propeptide from the mature cathepsin in acidic environment of the lysosomes (Turk et al., 2012). In contrast to CTSB, increase in pH (from 4-6.5) has been shown to negatively affect the 3D conformation of CTSL propeptide which prevents its activation. Our acridine-orange staining results at 6 hr, confirm that Au-treated cells displayed an elevated level of pH that led to CTSB activation and inactivation of CTSL. Our results suggest that changes in lysosomal pH after TrxR inhibition during the early time points may negatively affect CTSL activation.

3.5.4 CTSB as the master regulator of apoptosis after TrxR inhibition in starving SH-SY5Y cells

Our cumulative results from the present study and the previous report indicate that TrxR inhibition in SD-treated cells results in induction of protective Nrf2/ARE signaling pathway, however lack of Trx reducing capacity and depletion of reduced glutathione after Au-treatment leads to disruption of protein degradation systems including protein ubiquitination, proteasome activity and lysosomal deficiency. CTSB leakage is the downstream event that results in induction of other mechanisms including activation of inflammasome through NLRP3-mediated activation of caspase 11 (Schotte et al., 1998) and 1 (Franchi et al., 2009) resulting in apoptotic cells in glial cells (Terada et al., 2010). Prevention of LMP induction in this study using pre-incubation of cells with CA-074-me prevented CTSB leakage and produced a healthy cellular redox environment as shown by increased level of reduced glutathione and improved protein clearance identified by decreased protein ubiquitination. The Acridine orange staining also showed preserved lysosomal acidification. These data clearly indicate that preventing lysosomal deficiency by inhibition of ectopic CTSB activation can be used as a therapeutic approach for diseases such as neurodegenerative diseases.

In conclusion, we aimed to identify the redox-dependent molecular systems involved in autophagy-apoptosis interplay after inhibition of TrxR in a model of serum deprivation in human neuroblastoma cells. We found that TrxR-deficiency enhances CTSB activity that ensures activation of apoptotic exit in this model. Additionally, we identified novel mechanism by which CTSL, the pro-autophagy cathepsin, is inhibited and therefore guarantees full execution of apoptosis under these conditions. We provide evidence that oxidative stress plays an important part in completion of this scenario. To our knowledge this is the first report indicating the impact of redox balance in CTSB: CTSL cross talk in the context of autophagy-apoptosis conversion.

Chapter 4

Cathepsin B is an executioner of cell death in ferroptosis

Portions of this chapter has been included in the following published article:

Pandian Nagakannan, Md. Imamul Islam, Soheila Karimi-Abdolrezaee, Eftekhar Eftekharpour. Inhibition of VDAC1 protects ggainst glutamate-induced oxytosis and mitochondrial fragmentation in hippocampal HT22 cells. *Cellular and Molecular Neurobiology 2019;39(1):73-85*. © Springer Nature

Author contribution: My contributions in this work includes conceptualization, experimental design, collection and interpretation of data. Dr. Md. Imamul Islam carried out the mitochondrial morphological analysis and critically revised the manuscript. This work was supported through grant funding to SKA and EE. I prepared the manuscript under the guidance of my supervisor.

Acknowledgement: This work was partially supported by grants from Health Sciences Centre Foundation of Winnipeg, Paralyzed Veterans of America and the University of Manitoba (EE). PN is supported by a Research Manitoba/Will-to-Win foundation doctoral studentship award. The authors wish to thank Mr. Khuong Le for his technical assistance.

4.1 Preface

As shown in the previous chapters, failure of antioxidant system induces aggravated oxidative stress and cell death. Similar to thioredoxin system, glutathione is an endogenous thiol antioxidant. In fact, GSH is the most abundant low molecular weight antioxidant in the body and several intracellular processes are dependent on GSH (Wu et al., 2004). Depletion of GSH or inactivation of GSH dependent antioxidant processes are known triggers of cell death. GSH has been shown to either get oxidized or depleted during the progression of apoptosis and necrosis (Canals et al., 2001; Higuchi, 2004; Circu and Aw, 2012).

Recently, failure of GSH system was shown to be involved in a caspase independent mode of regulated cell death, known as "Ferroptosis" (Dixon et al., 2012). Though oxidative stress has been shown to participate in execution of ferroptosis through iron mediated lipid peroxidation, the identification of underlying mechanism/s remain the subject of active research. Recent literatures indicate an active involvement of lysosomes in ferroptosis (Gao et al., 2016; Torii et al., 2016), however the status of lysosomal cathepsins still remains to be examined.

While the previous two chapters of this thesis have identified that lysosomal damage due to failure of antioxidant causes interruption of pro-survival autophagy and promote apoptosis, this chapter investigates the role of oxidative stress on lysosomes and lysosomal cathepsins in the execution of ferroptotic cell death.

4.2 Abstract

Ferroptosis is a necrotic form of cell death caused by inactivation of the glutathione system and uncontrolled iron-mediated lipid peroxidation. Increasing evidence implicates ferroptosis in a wide range of diseases from neurotrauma to cancer, highlighting the importance of identifying an executioner system that can be exploited for clinical applications. In this study, using pharmacological and genetic models of ferroptosis, we observed that lysosomal membrane permeabilization and cytoplasmic leakage of cathepsin B unleashes structural and functional changes in mitochondria and promotes a not previously reported cleavage of histone H3. Inhibition of cathepsin-B robustly rescued cellular membrane integrity and chromatin degradation. We show that these protective effects are independent of glutathione peroxidase-4 but are mediated by preventing lysosomal membrane damage. This was further confirmed when primary fibroblasts derived from cathepsin B knockout mice remained unaffected in response to ferroptosis inducers. Our work identifies new aspects, yet-unrecognized ferroptosis mechanisms and identifies cathepsin B as an executioner of ferroptotic cell death.

4.3 Introduction

Ferroptosis is a non-apoptotic form of cell death that was originally reported in 2012 (Dixon et al., 2012). Several lines of evidence indicate the involvement of autophagy in the execution of ferroptotic cell death (Gao et al., 2016). Autophagy is a naturally occurring and highly regulated process responsible for recycling of damaged proteins and organelles providing metabolic substrates for energy synthesis during stressful conditions. Macroautophagy (hereafter, autophagy) is the most well-studied type of autophagy, during which the autophagic cargo is packaged in a double-membrane vacuole known as the "autophagosome". Fusion of autophagosome and lysosome is the last step leading to digestion of the cargo (Feng et al., 2014). In microphagy and chaperone mediated autophagy (CMA), lysosomes receive their cargo directly or indirectly through an adaptor chaperone protein system, respectively (Kaushik et al., 2011). The involvement of lysosomes as the executioner of ferroptosis has been suggested by a series of reports (Kubota et al., 2010; Torii et al., 2016; Wu et al., 2019; Yang et al., 2019a). In ferroptosis, as the name implies, iron is one of the main contributors of cell death (Dixon et al., 2012). Ferritin, an intracellular protein that sequesters iron, is responsible for its controlled release. Evidence of ferritin degradation by lysosomes, a process known as ferritinophagy, has been reported during ferroptosis (Hou et al., 2016). Free intracellular iron (Fe^{2+}) can initiate the Fenton reaction and generate hydrogen peroxide (H_2O_2), which is quickly converted to the highly reactive hydroxyl radical. These hydroxyl radicals initiates a chain reaction by extracting electrons from the abundant cellular membrane phospholipids and formation of lipid hydroperoxides (Gaschler and Stockwell, 2017), which can be scavenged by glutathione (GSH) and glutathione peroxidase 4 (GPX4) (Conrad et al., 2018; Conrad and Pratt, 2019); however, GPX4 level has been found to be decreased in ferroptosis and this has been mediated by CMA, further implicating lysosomes (Wu et al., 2019).

The involvement of autophagic cell death in ferroptosis is documented by the protective effect of lysosomal blockers including Bafilomycin A1 (Baf-A1), chloroquine and acid neutralizing agent ammonium chloride (Kubota et al., 2010; Hirata et al., 2011; Gao et al., 2016; Torii et al., 2016). Lysosomes, as described originally by Christian de Duve more than five decades ago, are suicidal organelles full of many lytic enzymes including lysosomal cathepsins. These enzymes are affected by oxidative stress and are involved in the execution of other conventional types of cell death such as apoptosis, autophagy and necrosis (Appelqvist et al., 2013). We (Pandian and Eftekharpour, 2017) and others (Gao et al., 2018) have proposed the involvement of cathepsins in execution of ferroptotic cell death; however, the underlying mechanism/s and the status of cathepsins in ferroptosis have remained unclear.

Ferroptosis and oxytosis are seemingly identical twins and are associated with decreased levels of GSH and excessive oxidative stress resulting in a caspase-independent cell death (Lewerenz et al., 2018). Although depletion of glutathione antioxidant defense system and the involvement of lysosome mediated free iron imbalance have been recognized as the underlying mechanism of cell death, the main molecular culprits in execution of ferroptotic cell death remain controversial (Feng and Stockwell, 2018). Using pharmacological inhibitors, gene editing technology and conditional knockout cellular models we now provide comprehensive evidence that while ferroptosis is mediated by lysosomal membrane permeabilization (LMP), cathepsin B (CTSB) but not L (CTSL) or D (CTSD) is the executioner of cell death. Considering the implication of ferroptosis in cancer and neurodegenerative diseases, our findings may have potential therapeutic applications.

4.4 Materials and Methods

4.4.1 Reagents and antibodies

(Z)-4-hydroxy Tamoxifen (#14854), Bafilomycin A1 (#11038), Deferoxamine mesylate (#14595), DPPH (2,2-Diphenyl-1-Picrylhydrazyl) (#14805), FCCP (2-[2-[4-(trifluoromethoxy) phenyl] hydrazinylidene]-propanedinitrile) (#15218), Ferrostatin-1 (#17729), LY294002 (#70920), Pepstatin-A (#9000469) were from Cayman Chemical. Erastin (# 5449) was from Tocris Bioscience. 1,1,3,3-Tetramethoxypropane (#108383), Butylated hydroxytoluene (#W218405), CA074-methyl ester (#C5857), L-Buthionine-sulfoximine (#B2515), L-Glutamic acid monosodium salt hydrate (#G1626), Monochlorobimane (#69899), Trolox ((±)-6-Hydroxy-2,5,7,8-tetramethylchromane-2-carboxylic acid) (#238813) were from Sigma-Aldrich. Cathepsin L substrate (Z-Phe-Arg-7-amido-4-methylcoumarin, Hydrochloride) (#03-32-1501) and Cathepsin B Substrate III, Fluorogenic (Z-Arg-Arg-AMC, 2HCl) (# 219392) were from Calbiochem®. 2-Thiobarbituric acid (#1081800025) was from EMD Millipore. CA074 (#A1926) was from ApexBio. Trichloroacetic acid was from Fisher Scientific. TMRM (Tetramethylrhodamine methyl ester, perchlorate) (#70017) was from Biotium Inc. CellROX™ Deep Red Reagent (#C10422), LysoTracker™ Red DND-99 (#L7528), ATP Determination Kit (#A22066) and Premo™ Autophagy Tandem Sensor RFP-GFP-LC3B Kit (#P36239) were from Invitrogen™. Clarity™ Western ECL Substrate (# 1705061) and Clarity Max™ Western ECL Substrate (#1705062) were from BIO-RAD. Dulbecco's Modified Eagle Medium (DMEM) (#11960-051), Fetal Bovine Serum (#12483-020) and Penicillin-Streptomycin-Neomycin (PSN) Antibiotic Mixture (#15640-055) were from Gibco™. Halt™ Protease and Phosphatase Inhibitor Single-Use Cocktail (# 78442) was from Thermo Scientific™. Recombinant Human Cathepsin B, CF (#953-CY) and Recombinant Human Cathepsin L, CF (#952-CY) proteins were from R & D

Systems. Cell Counting Kit (# CK04) was from Dojindo Molecular Technologies. Pierce™ BCA Protein Assay Kit (# 23225) was from Thermo Scientific. µ-Slide 8 well (#80826) was from ibiTreat, Ibidi. Vivaspin™ 500 MWCO 5000 (#VS0112) was from Sartorius™. Glass cover slips (#72196-12) was from Electron Microscopy Sciences.

The following antibodies were used in this study: AIF (1:1000, #sc-13116), Cathepsin D (1:1000, #sc-377299), Cytochrome C (1:1000, #sc-13156), LAMP-1 (1:1000, #sc-19992), γ-GCSc (1:1000, #sc-390811), γ-GCSm (1:1000, #sc-55586), GAPDH (1:5000, #sc-166574) and β-Actin (1:5000, #sc-47778) from Santa Cruz Biotechnology, USA; Cathepsin B (1:1000, #31718), COX IV (1:1000, #4844) and Ubiquitin (1:1000, #3936) from Cell Signaling Technologies, USA; GPX4 (1:2000, #ab125066) and Histone H3 (1:4000, #ab1791) from abcam, USA; Cathepsin L (1:1500, #AF1515) from R & D Systems, USA; LC3B (1:2500, #L7543) from Sigma-Aldrich, USA.

4.4.2 Cell culture

HT22 (gift from Dr. David Schubert, Salk Institute, San Diego, USA), NIH3T3 (gift from Dr. Afshin Raouf, University of Manitoba, Canada), primary mouse embryonic fibroblasts [Wild-type (WT) and *Ctsb*$^{-/-}$] (generously provided by Dr. Thomas Reinheckel, University of Freiburg, Germany), and 4-hydroxy-tamoxifen-inducible *gpx4*$^{-/-}$ (Pfa1 cells (Seiler et al., 2008), from Dr. Marcus Conrad, Helmholtz Zentrum Munchen, Germany) were used in this study. Cells were cultured in Dulbecco's modified Eagle's medium (DMEM) containing 4.5 g/L glucose, 10 % heat inactivated fetal bovine serum, 2 mM glutamine, 1 mM sodium pyruvate and 1 % PSN (penicillin, streptomycin and neomycin) and maintained in a humidified incubator under 5 % CO_2 at 37 °C.

4.4.3 Treatments and determination of cell viability

HT22 cells were seeded at a density of 8000 cells/well in 96 well plates. After overnight culturing, cells were treated with glutamate or erastin in 100 µl of complete growth media. In experiments

where specific inhibitors were used, cells were pretreated with CA074-me (15 µM), Z-FY-CHO (10 µM) or Pepstatin-A (Pep-A, 50 µM) for 3 hr and then exposed to glutamate or erastin, whereas CA074 (15 µM), ferrostatin-1 (Fer-1, 2 µM) and deferoxamine (DFO, 50 µM) were concomitantly added along with the ferroptosis inducer.

In case of WT and *Ctsb*$^{-/-}$ MEFs, cells were seeded at a density of 2500 cells/well in 96 well plates and were treated at 70% confluency with erastin alone or in combination with Fer-1.

To induce *gpx4* deletion, Pfa1 cells (1000 cells/well) were seeded in 96 well plates and were treated with 1 µM 4-hydroxy-tamoxifen (Tamox) 24 hr after plating. All the inhibitors were added to the cultures at 24 hr after induction of knockout. To determine cell survival, 10 µl of Cell Counting Kit-8 reagent was added to culture medium and incubated for 4 hr at 37°C. Absorbance at 450 nm was measured using Synergy H1 Hybrid Reader (BioTeK Instruments, USA) and the absorbance at 650 nm was used for background correction. The relative cell viability as percentage of control is presented.

4.4.4 Subcellular fractionation

Subcellular fractionation was performed as described previously (Nagakannan and Eftekharpour, 2017b). Briefly, the cells were scraped in culture media, collected by centrifugation at 2000 x g and washed twice with ice-cold PBS. The cells were suspended in ice-cold fractionation buffer [20 mM HEPES (pH 7.4), 250 mM sucrose, 10 mM KCl, 1.5 mM $MgCl_2$, 1 mM EDTA, 1 mM EGTA] with added protease and phosphatase inhibitors and passed through a 25 G needle 20 times to homogenize the cell suspension. The subcellular fractions were obtained by sequential centrifugation of homogenates at 1000 x g (10 min, to pellet out nuclei), 10,000 x g (10 min, to collect mitochondria) and 21,000 x g (2 hr, to collect lysosomes). The supernatant (cytosol) was further concentrated using Vivaspin^{TM} protein concentrating columns with a molecular weight cut-

off of 5 kDa. The pelleted mitochondrial and lysosomal fractions were washed once with fractionation buffer and suspended in RIPA lysis buffer [50 mM Tris HCl (pH 8), 150 mM NaCl, 1 mM EGTA, 1% NP-40, 0.1% SDS, 0.5% sodium deoxycholate, 5% glycerol] with protease and phosphatase inhibitors and were lysed by sonication (2 x 10 s). Modifications to this protocol, if any, are described in the respective method sections.

4.4.5 Western blot analysis

Western blotting was performed following our routine protocol with minor modifications (Nagakannan et al., 2016). Briefly, cells were scraped in culture media, washed twice with ice-cold PBS and collected by centrifugation at 2000 x g. The pelleted cells were lysed in ice-cold NP-40 lysis buffer [1% NP-40 in buffer composed of 50 mM Tris HCl (pH 8), 150 mM NaCl, 5 mM EDTA] with added protease and phosphatase inhibitors. Following sonication (3 x 5 s) on ice, the lysates were centrifuged at 10,000 x g for 15 mins at 4 °C and the clear supernatant was collected and placed on ice. The protein content in whole cell extracts and subcellular fractions (as described above) was quantified using Pierce BCA Protein Assay Kit. The samples were resolved on SDS-PAGE at constant voltage and transferred to PVDF membranes using the Trans-Blot® Turbo™ Transfer Buffer and System. The membranes were blocked with 5 % non-fat dry milk in Tris-buffered saline containing 0.2 % Tween 20 (TBST) for 1 hr at room temperature and incubated with primary antibodies in 1% non-fat dry milk in TBST overnight at 4°C. The membranes were then probed with appropriate HRP - conjugated secondary antibodies and the target proteins were visualized using Clarity™ and Clarity Max™ ECL Western blotting Substrates (Bio-Rad Laboratories). Densitometric measurements of the target proteins were done using AlphaEaseFC (version 6.0.0, Alpha Innotech, USA) or Image J software (version 1.51j8, NIH) and were normalized to appropriate loading controls.

4.4.6 Chemical cross-linking

The oligomeric status of VDAC1 was detected using a membrane permeable cross-linker based approach as described previously (Keinan et al., 2010). Briefly, HT22 cells were harvested after appropriate treatments, washed with PBS and resuspended in PBS (pH 7.4) containing 0.5 mM EGS (ethylene glycol bis(succinimidyl succinate)) and incubated at 30 °C for 20 min. The excess of EGS was quenched by adding appropriate volumes of 1.5 M Tris HCl, pH 7.8 to a final concentration of 20 mM and incubated for further 5 min. The samples were centrifuged at 10,000×g for 5 min and the pellets were lysed in NP-40 lysis buffer by sonication on ice. Samples (50 µg) were diluted in sample loading buffer and subjected to SDS-PAGE and western blotting using anti-VDAC1 antibody.

4.4.7 In-vitro free radical scavenging assay

The intrinsic antioxidant potential of protease inhibitors was examined using 2,2-diphenyl-1-picrylhydrazyl (DPPH) method (Blois, 1958; Dixon et al., 2012). A final concentration of 50 µM of test compounds in DMSO was incubated with 1 ml of DPPH (50 µM) solution in methanol. The samples were vortex mixed and incubated at room temperature for 30 min. Then, 100 µl of each sample was transferred to clear bottom 96-well plate and the absorbance at 517 nm was measured on a microplate reader. The results were normalized to DMSO control and the relative fold change is reported.

4.4.8 Determination of ATP content

Cells were treated as indicated, harvested and lysed in NP-40 buffer by sonication and the ATP content in the cell lysates was quantified by bioluminescence method using ATP determination kit following the manufacturer's protocol.

4.4.9 Lipid peroxidation assay

The degree of lipid peroxidation was determined by measuring the amount of malondialdehyde (MDA) in the samples (Williamson et al., 2003). Lysosomal or mitochondrial fractions [lysed in 50 mM Tris HCl (pH 8), 150 mM NaCl, 1 mM EGTA, 1% NP-40, 0.1% SDS, 3% glycerol] or cell lysates were transferred to microcentrifuge tubes containing 5 µl of 0.5 M butylated hydroxytoluene. Then, 200 µl of MDA detection reagent [1:1:1 mixture of 0.375 % thiobarbituric acid:15 % trichloroacetic acid:0.25 N hydrochloric acid] was added and heated at 95 °C for 1 hr. The reaction mixture was centrifuged at 10,000 x g for 5 min and the supernatants were transferred to black walled 96-well plate. The fluorescence intensity at excitation/emission wavelengths of 532/558 nm was measured on a microplate reader. The MDA concentration was determined from a standard curve plotted using 1,1,3,3-Tetramethoxy propane and were normalized to protein content.

4.4.10 Determination of cellular glutathione

To determine the intracellular levels of reduced glutathione (GSH), cells were incubated with the cell permeable dye monochlorobimane (MCB, 50 µM) in the dark at 37 °C for 30 min (Baxter et al., 2015). Cells were scraped in the culture media and collected by centrifugation at 2000 x g and the cell pellets were washed twice with PBS. Then, the cells were lysed in NP-40 lysis buffer and centrifuged at 12,500 x g for 15 min at 4°C and the supernatants were transferred to a black walled 96-well plate. The fluorescence emitted by GSH bound MCB was measured at excitation/emission wavelengths of 380/480 nm using a microplate reader and the results were normalized to protein content in the lysates.

4.4.11 Detection of reactive oxygen species

Cells were seeded on glass coverslips and treated as indicated. At the termination of study, cells were incubated with CellROX^{TM} Deep Red reagent (5 µM) in phenol red free media for 30 min at 37 °C. Following PBS washes, the cells were fixed with 3% paraformaldehyde in PBS and stained with DAPI (1:10,000) to label nuclei. Images were visualized on a confocal microscope at excitation/emission wavelengths of 633/697 nm.

4.4.12 Assessment of mitochondrial membrane potential (ΔΨm)

Cells were seeded on a µ-slide 8-well chamber (Ibidi GmbH, Germany) and were treated as indicated. To examine the response of mitochondrial membrane potential in these conditions, cells were treated with a 100 nM final concentration of TMRM (Tetramethylrhodamine methyl ester) in phenol red free medium for 30 min at 37 °C (Voronina et al., 2004). Then, the medium was replaced with fresh medium and the images were acquired immediately at excitation/emission wavelengths of 514/610 nm using a confocal microscope.

4.4.13 Lysotracker staining

Cells were grown on glass coverslips and were subjected to the indicated treatments. Cell were treated with Lysotracker^{TM} Red DND-99 solution at a final concentration of 100 nM in phenol red free media for 30 min at 37 °C. Subsequently, cells were washed twice with PBS, fixed with 3% paraformaldehyde in PBS and were stained with DAPI. The images were acquired using a confocal microscope.

4.4.14 Autophagy assessment

To monitor the rate of autophagic flux, Pfa1 cells were treated as indicated and bafilomycin A1 (25 nM) was added to the cells 4 hr prior to sample harvesting. At the termination of experiment, cell lysates were subjected to regular western blotting to determine LC3-II levels.

Alternatively, Pfa1 cells were seeded onto glass coverslips and subjected to respective treatments. Cells were transduced with Premo^{TM} Autophagy Tandem Sensor (2 µl/10,000 cells) during the last 16 hr of the treatment. Then, the cells were imaged using a confocal microscope to visualize GFP and RFP punctas. The number of GFP+RFP (autophagosomes) and RFP alone (autolysosomes) punctas per cell were counted and the percentage of each is presented.

4.4.15 Immunostaining

Cells were seeded onto glass coverslips and at the termination of experiments, cells were washed with PBS, fixed with 3% paraformaldehyde in PBS, permeabilized with 0.3% Triton X-100 and incubated with appropriate primary antibodies overnight at 4 °C. The following day, the coverslips were washed with PBS and incubated with respective Alexa flour conjugated secondary antibodies for 1 hr at room temperature. Following washes with PBS, nuclei were stained with DAPI and the coverslips were mounted onto glass slides.

4.4.16 Image analysis

All the images (unless otherwise specified) were acquired using LSM710 Zeiss confocal microscope (Zeiss, Germany). Image J software was used to quantify the mean fluorescence intensity per cell where appropriate. To determine the nuclear translocation of apoptosis inducing factor (AIF1), mean fluorescence intensity in the nucleus and cytosol (whole cell intensity – nuclear intensity) were measured using Image J software (version 1.51j8, NIH) and the ratio of nuclear to cytosolic AIF1 was shown after correction for background. For lysosomal area analysis,

the lysotracker stained single channel images were converted to 8-bit images and the particle size was determined using the "Analyze Particles" option in Image J software. The following parameters were set to filter the particles for analysis: Threshold = Auto (Triangle method); Size = 0.1 – 1.5 μm^2, Circularity = 0.05-1.00.

4.4.17 Measurement of cathepsin B and L activity

Cathepsin B and L activities were measured by fluorometric method as described previously (Zhang et al., 2003) with minor modifications. After the treatments, cells were washed twice with PBS and were lysed in NP-40 buffer or subjected to subcellular fractionation in the absence of protease and phosphatase inhibitors. All the substrates and inhibitors were diluted in reaction buffer (25 mM MES, 5 mM DTT, pH 5.0) and were pre-warmed at 37 °C. To measure cathepsin B activity, samples were diluted in 50 µL reaction buffer in a black walled 96-well plate and 50 µl of 100 µM Z-Arg-Arg-AMC was added to each well to start the reaction. To measure cathepsin L activity, 10 µl of 100 µM CA074 was added to each sample diluted in 40 µl reaction buffer and 50 µl of 200 µM Z-Phe-Arg-AMC was added. Upon cleavage of the substrates by the respective cathepsins, the release of free AMC was monitored at excitation/emission wavelengths of 360/480 nm for 1 hr using a microplate reader. Results are expressed as relative fluorescence units (RFU) or fold change relative to control.

4.4.18 In-vitro nuclear histone cleavage assay

The nuclei were isolated from control HT22 cells following the protocol described previously (Islam et al., 2019). Briefly, cells were washed twice with PBS and re-suspended in TM buffer (10 mM Tris-HCl, pH 7.4, 2 mM $MgCl_2$) supplemented with 0.5 % Triton X-100 (v/v) and incubated on ice for 10 min. The cells were mechanically sheared by intermittent vortexing and the intact nuclei were pelleted by centrifugation at 1000 x g for 2 min. To remove traces of Triton X-100,

the nuclear pellet was washed twice with TM buffer. For histone cleavage assay, isolated nuclei were incubated in a reaction buffer [20 mM HEPES-KOH (pH 7.4), 20 mM NaCl, 1.5 mM $MgCl_2$, 0.1 mM EDTA, 0.1 mM EGTA, 5 mM DTT] with either recombinant cathepsins alone or in combination with their respective inhibitors at 37°C. After indicated incubation periods, the reaction mixtures were subjected to SDS-PAGE and western blotting using anti-histone H3 antibody.

4.4.19 Data analysis and presentation

All the results are expressed as mean ± S.E.M. Statistical differences among multiple experimental groups were compared by one-way analysis of variance (ANOVA) followed by Tukey's or Dunnett's post-hoc test using GraphPad Prism Software (version 6.07, California, USA). To determine statistical differences between two groups, two tailed unpaired t-test were used. Differences in means were considered statistically significant at p values less than 0.05. Figures were constructed using Photoshop CS5.1 (Adobe Systems, San Jose, CA).

4.5 Results

4.5.1 Lipid peroxidation of lysosomal and mitochondrial membranes in ferroptosis

Inhibition of the cystine/glutamate antiporter system x_c^- with glutamate, erastin or sulfasalazine blocks cystine uptake into cells thereby leading to depletion of intracellular GSH. This in turn leads to inactivation of GPX4, thereby causing uncontrolled lipid peroxidation and ultimately ferroptotic cell death (Yang and Stockwell, 2016). A dose response study was performed to determine the effective concentration of glutamate and erastin for induction of 70-80% cell death in HT22 cells. Cell viability was measured using CCK-8 after 12 hr administration of glutamate and erastin. A dose of 4-5 mM glutamate or 500 nM erastin were chosen for further cell viability assessments (Suppl. Fig. 4.1, A and B). This is in agreement with previous reports for this model (Kang et al., 2014; Neitemeier et al., 2017).

Apart from the general notion that lipid peroxidation takes place in the plasma membrane, which is suspected to be the reason for loss of membrane integrity, the possibility of lipid peroxidation in other intracellular organelles is still a matter of debate (Feng and Stockwell, 2018), although lipid peroxidation of mitochondrial membranes has been recently reported in ferroptosis (Yuan et al., 2016; Fang et al., 2019). To assess the status of lysosomes and to validate previous reports during ferroptosis, glutamate treated HT22 cells were subjected to subcellular fractionation and the extent of lipid peroxidation was assessed by measuring malondialdehyde (MDA) content in mitochondrial and lysosomal fractions. After 12 hr of glutamate treatment, MDA content was markedly increased in lysosomal (~2–fold, Fig. 4.1, A and B) and mitochondrial fractions (~1.5–fold, Fig. 4.1, C and D). This increase in lipid peroxidation of organelle fractions was completely prevented by the ferroptosis inhibitor Fer-1 and the iron chelator DFO (Fig. 4.1, B and D). Lysosomes and mitochondria are known to be the storage compartments for intracellular iron

(Kurz et al., 2011) and in conditions including ferroptosis, the iron stored in these organelles is mobilized and may trigger lipid peroxidation (Dixon et al., 2012). The observation that iron chelation using DFO totally abolished the increase in MDA content in the fractions, indicates the active involvement of iron in the lipid peroxidation of lysosomal and mitochondrial fractions in ferroptosis.

4.5.2 Lysosomal and mitochondrial membrane permeabilization in ferroptosis

Membrane lipid peroxidation is known to alter membrane fluidity, lipid-lipid interactions, ionic gradients, membrane thickness and permeability (Gaschler and Stockwell, 2017). To test whether increased lipid peroxidation during ferroptosis affects the membrane integrity of lysosomes, we exposed HT22 cells to glutamate and performed subcellular fractionation at 6 and 10 hrs. In response to glutamate treatment, we observed a time dependent increase in the levels of lysosomal proteases, CTSB and CTSL, in the cytosol suggesting the induction of lysosomal membrane permeabilization (LMP) during ferroptosis (Fig. 4.1 E). Furthermore, using a fluorescence-based activity assay, we observed a time dependent increase in CTSB and CTSL activities in whole cell lysates harvested at corresponding time points indicating a correlation between cathepsin protein levels and their activities (Fig. 4.1 F). As shown previously (Sanderson et al., 2015), a time dependent increase of mitochondrial proteins such as apoptosis inducing factor (AIF) and cytochrome C (cyto C), were also observed in cytosol indicating mitochondrial membrane permeability (MMP) after glutamate treatment (Fig. 4.1 E). Despite cytosolic translocation of cyto C, minimal or no activation of caspases has been reported in cells undergoing ferroptosis (Yagoda et al., 2007; Fukui et al., 2009). Accordingly, we did not observe any significant activation of caspase-3 in response to glutamate in HT22 cells (Suppl. Fig. 4.1 C).

4.5.3 Glutamate and erastin induce VDAC1 oligomerization in HT22 cells

To further evaluate the status of mitochondrial integrity during ferroptosis, we assessed the status of voltage-dependent anion-selective channel 1 (VDAC1), a major component of the outer mitochondrial membrane which undergoes oligomerization in response to excessive oxidative stress leading to the formation of a transition pore in the outer mitochondrial membrane resulting in the release of cyto C and AIF (Shoshan-Barmatz et al., 2013). HT22 cells were treated with glutamate or erastin for increasing time durations (8, 12 and 16 hr) and the protein expression levels of VDAC1 was assessed by western blotting. Using our routine reducing SDS-PAGE western blotting, a time dependent increase in the expression of VDAC1 protein levels was observed (Suppl. Fig. 4.2 A-D). Interestingly, under non-reducing conditions, the intensity of 35 kDa VDAC1 band (known as VDAC1 monomer) was not notably increased; however, a second band was detected using anti-VDAC1 antibody, which was more pronounced with increasing exposure time of the cells to glutamate and erastin (Suppl. Fig. 4.2 A and B). Using cross-linking agents like BMOE (bis(maleimido)ethane) or EGS (ethylene glycol bis(succinimidyl succinate)) earlier studies have shown the appearance of this faster migrating monomeric form of VDAC1 band upon induction of an apoptotic stimuli (Keinan et al., 2013). This band is proposed to be the result of an intra-molecular bond formation between a single cysteine in the N-terminal region and another amino group, possibly a lysine residue (Geula et al., 2012). However, in this experiment shown in Suppl. Fig. 4.2 A and D, no such cross-linkers were utilized. Cysteine groups in VDACs have been shown to be the target for oxidation by ROS and therefore it is possible that faster migrating anti-VDAC1 antibody reactive band is a result of intra-molecular disulfide bond formation. Although the contribution of this intra-molecular disulfide bond in either pore-conductance or apoptotic induction remains unclear (De Pinto et al., 2016).

To seek further insights into the effect of oxidative stress induced by glutamate and erastin on oligomeric status of VDAC1, we performed cross-linking experiments using EGS to capture the oligomeric states of VDAC1 by western blotting. As shown in Suppl. Fig. 4.2 E, glutamate induced a time dependent induction in VDAC1 oligomerization evident by the higher molecular weight bands corresponding to the dimeric, trimeric and multimeric states of VDAC1. Similar results were obtained with erastin treatment (Suppl. Fig. 4.2 F). The intra-molecular cross-linked monomeric VDAC1 band (indicated by asterisk) with altered electrophoretic migration was also detected in glutamate and erastin treated HT22 cells (Suppl. Fig. 4.2 E and F).

To rule out potential cell type specific effects in induction of LMP and MMP during ferroptosis, we performed similar subcellular fractionation experiments with NIH3T3 cells, where exposure to erastin (3 μM) for 8 hr increased the levels of lysosomal proteases and mitochondrial proteins in the cytosolic fraction (Fig. 4.1 G), demonstrating that LMP and MMP may not be cell specific effects but of general relevance for ferroptosis. This was associated with a corresponding increase in lipid peroxidation of associated organelle membranes as shown by increased MDA content in mitochondrial and lysosomal fractions in NIH3T3 cells exposed to erastin (Suppl. Fig. 4.3 A).

4.5.4 Cathepsins are induced in response to glutamate treatment in HT22 cells

We have previously shown a differential expression and activation pattern for CTSL and CTSB (Nagakannan and Eftekharpour, 2017b) under oxidative stress; while CTSB activity can be increased robustly without detectable changes in its protein levels, increased CTSL activity always correlated with a rise in its protein levels. To examine whether such differential expression pattern of lysosomal proteases exists during ferroptosis, HT22 cells were exposed to glutamate for increasing times and the protein expression of major cathepsins in the cell lysates were assessed by western blotting. As shown in Fig 4.1 H and I, glutamate caused a moderate rise in pro-CTSB

and mature-CTSB levels; however, the level of pro-CTSL was significantly elevated indicating a significant increase in its synthesis. This was further corroborated by upregulated levels of intermediate forms of CTSL; however, no significant change in the level of mature-CTSL was observed. An augmented level of intermediate CTSL was also noted in cytosolic fraction, while the mature form was not altered (Fig. 4.1 E). Previous studies have identified and characterized the intermediate (truncated) form of CTSL as the cytosolic variant resulting from an alternative translation mechanism (Reiser et al., 2010). The higher protein level for the intermediate form was correlated well with an increase in enzymatic activity indicating that indeed it is the intermediate CTSL that is active in ferroptosis. We also assessed the status of CTSD, another major lysosomal protease in the cell lysates. Although a non-significant moderate decrease in the pro form of CTSD was observed, no active fragments were detected (Suppl. Fig. 4.3 B).

Figure 4.1. Lysosomal and mitochondrial membrane permeabilization in ferroptosis induced by system x_c^- inhibition.

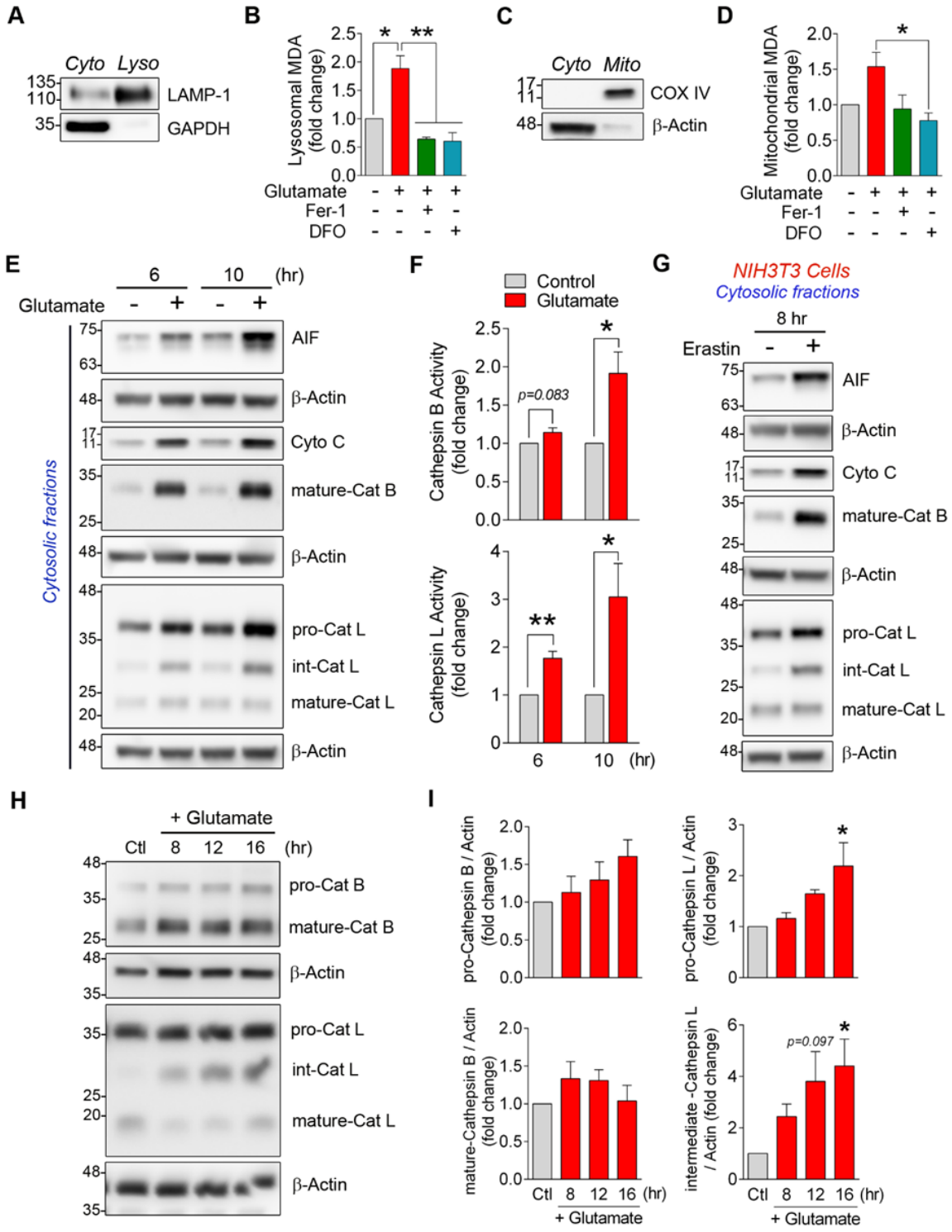

Figure 4.1. Lysosomal and mitochondrial membrane permeabilization in ferroptosis induced by system x_c^- inhibition. HT22 cells were cultured in the presence or absence of glutamate (4 mM) with or without Fer-1 (2 μM) or DFO (50 μM) for 12 hr and were subjected to subcellular fractionation. **(A** and **C)** The purity of different subcellular fractions was validated by western blotting against specific markers for each cellular compartment: lysosomes (LAMP-1), mitochondria (COX-IV) and cytosol (GAPDH / β-Actin). The amount of malondialdehyde (MDA) in lysosomal **(B)** and mitochondrial **(D)** fractions were determined as a measure of extent of lipid peroxidation. The bars in graphs indicate mean ± S.E.M. of averages from n =2-4 independent experiments, *p < 0.05 and **p < 0.01 by one-way ANOVA followed by Tukey's post-hoc test. **(E)** Western blot analysis of cytosolic fractions from vehicle or glutamate (4 mM)-treated HT22 cells isolated at indicated time points are shown. **(F)** Protease activities of cathepsins B and L were measured using fluorogenic substrates in cell lysates obtained from HT22 cells cultured in the presence or absence of glutamate (4 mM). The bars represent mean ± S.E.M. of averages from n =3 independent experiments, *p < 0.05 and **p < 0.01 by unpaired two-tailed *t*-test. **(G)** NIH3T3 cells were treated with vehicle or erastin (3 μM) for 8 hr and the isolated cytosolic fractions were analyzed by western blotting using indicated antibodies. **(H)** HT22 cells were treated with glutamate (4 mM) for indicated time points and the cell lysates were subjected to western blotting. **(I)** Densitometric analysis of proteins normalized to β-Actin are shown as fold change of control (Ctl). The bars in graphs indicate mean ± S.E.M. of averages from n=3-4 independent experiments, *p < 0.05 by one-way ANOVA followed by Dunnett's post-hoc test.

4.5.5 Cathepsin B mediates ferroptotic cell death

Cathepsins B, L and D are known to play important roles in other forms of regulated cell death such as apoptosis, autophagy and necrosis (Mrschtik and Ryan, 2015; Wang et al., 2018a). Based on the results described in the foregoing, we used pharmacological inhibitors to block the different cathepsins to establish a role of individual cathepsins in ferroptosis. CA074-me is an irreversible specific small molecule inhibitor with cell permeating properties that can inhibit CTSB. Pretreatment of HT22 cells with CA074-me offered significant (~85%) protection against glutamate induced cell death, while inhibitors targeting other cathepsin isoforms such as CTSL (Z-FY-CHO) or CTSD (Pepstatin-A, Pep-A) failed to protect from glutamate induced cell death. As expected, treatment with anti-ferroptotic agents, Fer-1 and DFO, completely suppressed glutamate induced cell death (Fig. 4.2 A). HT22 cells exposed to glutamate for 12 hr exhibited a rounded and shrunken morphology. Conversely, cells pretreated with CA074-me exhibited a moderately normal morphology that was comparable with Fer-1 and DFO treated cells exposed to glutamate (Suppl. Fig. 4.3 C). Secretion of CTSB into the extracellular space, especially during inflammatory responses, has been reported to induce apoptotic cell death (Rodriguez-Franco et al., 2012; Hook et al., 2015). To distinguish the roles of intracellular and extracellular CTSB in ferroptosis, we compared the efficacy of CA074 and CA074-me against glutamate induced cytotoxicity. The extracellular inhibitor of CTSB, CA074, failed to protect cells against glutamate induced cell death confirming that intracellular CTSB mediates ferroptotic cell death (Fig. 4.2 A). Validating these results, CA074-me showed significant improvement in cell survival in HT22 cells exposed to erastin, while the CTSL inhibitor Z-FY-CHO failed to do so (Suppl. Fig. 4.3 D). Cognate anti-ferroptotic compounds like Fer-1 and liproxstatin-1 are known to possess radical-trapping ability and are suggested to protect against ferroptosis by inhibiting lipid autoxidation

(Zilka et al., 2017). We therefore performed DPPH radical scavenging assay to test whether cathepsin inhibitors have any antioxidant activity and specifically to exclude the potential radical-trapping capability of CA074-me. In this assay, a decrease in absorbance of DPPH solution by the test compound indicates its trapping activity. Trolox was used as a positive control that showed a robust radical trapping activity by decreasing the DPPH absorbance. Similarly, Fer-1 and DFO displayed potent antioxidant capacity; however, none of the tested cathepsin inhibitors decreased the DPPH absorbance indicating that specific ferroptosis inhibitory effect of CTSB inhibitor is related to its biologic activity and not its direct role as a free radical scavenger (Suppl. Fig. 4.3 E). To further characterize the potential differential effect of classical ferroptosis inhibitors Fer-1 and DFO with that of CTSB inhibitor, we examined the effect of these compounds on lysosomal enzymes CTSB and CTSL isoforms. Similar to our previous report (Nagakannan and Eftekharpour, 2017b), HT22 cells treated with glutamate displayed significant rise in CTSB activity that was not associated with increased CTSB protein level. As expected, treatment with CA074-me completely inhibited the increased CTSB activity, but these CA074-me treated cells displayed significantly higher levels of mature-CTSB protein when compared to control and glutamate treated cells, indicating that CA074-me inhibits the activity of mature form of CTSB, and not its maturation (Fig. 4.2 B-D). Interestingly, Fer-1 significantly inhibited the increase in CTSB activity in response to glutamate, whereas DFO did not (Fig. 4.2 D). However, both Fer-1 and DFO did not have any significant effect on maturation of CTSB protein (Fig. 4.2 B and C). Inhibition of CTSB resulted in an increase in CTSL enzymatic activity in CA074-me pre-treated cells in response to glutamate. This correlated with a significant increase in intermediate form of CTSL protein when compared to glutamate treated cells. Interestingly, CA074-me treatment did not have any effect on glutamate induced upregulation of pro-CTSL protein. Anti-ferroptotic

agents Fer-1 and DFO exhibited a similar effect as CA074-me in terms of CTSL activity. In glutamate treated cells, addition of Fer-1 and DFO significantly decreased the pro-CTSL protein but did not affect the increase in intermediate CTSL protein (Fig. 4.2 B-D).

Using subcellular fractionation, we determined the effect of CTSB inhibitor and other classic anti-ferroptotic agents on lysosomal and mitochondrial membrane integrity in glutamate induced ferroptosis. We used the cytoplasmic level of AIF1 also known as apoptosis inducing mitochondrial factor (AIFM1), and cytochrome C (cyto C) as indicators of mitochondrial membrane damage. CA074-me, Fer-1 and DFO markedly decreased the cytosolic levels of AIF and cyto C indicating preservation of mitochondrial membrane integrity (Fig. 4.2 E). Although the role of AIF1 in apoptosis has been shown before, this protein is not involved in execution of ferroptosis (Doll et al., 2019). In accordance with reports from our lab and others showing that CTSB can exacerbate LMP once translocated to cytoplasm (Jacobson et al., 2013; Katsnelson et al., 2016; Nagakannan and Eftekharpour, 2017b), in the present study, inhibition of intracellular CTSB with CA074-me also strongly decreased the levels of CTSB and pro-CTSL in the cytosol confirming better lysosomal membrane integrity and abrogation of LMP. In case of both Fer-1 and DFO treated cells, dramatically lower cytosolic levels of CTSB and L were detected, indicating that lipid peroxidation and iron mobilization are upstream of LMP. Interestingly, the intermediate form of CTSL was not affected by CA074-me pretreatment, while Fer-1 and DFO markedly decreased this isoform when compared to the cytosolic fraction from glutamate treated cells (Fig. 4.2 E). Since intermediate CTSL is the cytosolic variant of CTSL, it is possible that upregulation of intermediate CTSL was a stress response to induction of oxidative stress and inhibition of lipid peroxidation (Fer-1), and chelation of iron (DFO) were able to inhibit its upregulation, while CA074-me did not.

The involvement of autophagy in induction of ferroptosis was previously reported (Gao et al., 2016). In accordance, we detected a significant increase in LC3-II/LC3-I ratio and LMAP1 protein level, confirming upregulated autophagy, lysosomal enlargement and increased lysosomal synthesis in response to autophagy induction. The LC3-II/LC3-I ratio and LAMP1 levels were significantly reduced by Fer-1 and DFO when compared to glutamate treated cells (Suppl. Fig. 4.4 A and B). On the contrary, the protective effect offered by inhibition of CTSB by CA074-me did not have any major effect on LC3-II/LC3-I ratio and LAMP1 levels. Inhibition of lysosomal proteases is shown to increase autophagosomes and therefore one would expect to see an increase in the levels of LC3-II after inhibition of CTSB; however, we did not observe an additional increase in LC3-II levels after inhibition of CTSB in glutamate treated cells.

Increased oxidative stress and lipid peroxidation, as observed in ferroptosis, is known to induce increased protein damage, which in turn are tagged with ubiquitin for protein degradation (Jung et al., 2014). Ubiquitination acts as a signal to recruit protein degradation machineries such as ubiquitin proteasome system (UPS) or autophagy to clear oxidized proteins and organelles (Cohen-Kaplan et al., 2016). In these experiments we also detected a significant increase in poly-ubiquitinated protein levels in glutamate-treated cells, as detected by western blotting. This was significantly lower in Fer-1 and DFO treated cells, indicating the involvement of oxidative protein damage in ferroptosis. Cells pretreated with CA074-me showed a notable ($p=0.089$) decrease in poly-ubiquitinated proteins in comparison with glutamate treated cells, proposing a role for CTSB in protein damage during ferroptosis (Suppl. Fig. 4.4 A and B). Inhibition of both UPS and autophagy systems have been shown to protect against glutamate toxicity in HT22 cells, suggesting that degradation of pro-survival proteins or essential organelles may be involved in ferroptosis (van Leyen et al., 2005; Kubota et al., 2010; Yang et al., 2019a). Lower levels of protein

ubiquitination in CA074-me also suggests a general decrease in protein oxidation. This is in agreement with a previous report suggesting the regulation of glutamate induced oxidative toxicity by lysosomal ROS generation in HT22 cells (Kubota et al., 2010).

Figure 4.2. Cathepsin B mediates glutamate induced ferroptosis in HT22 cells.

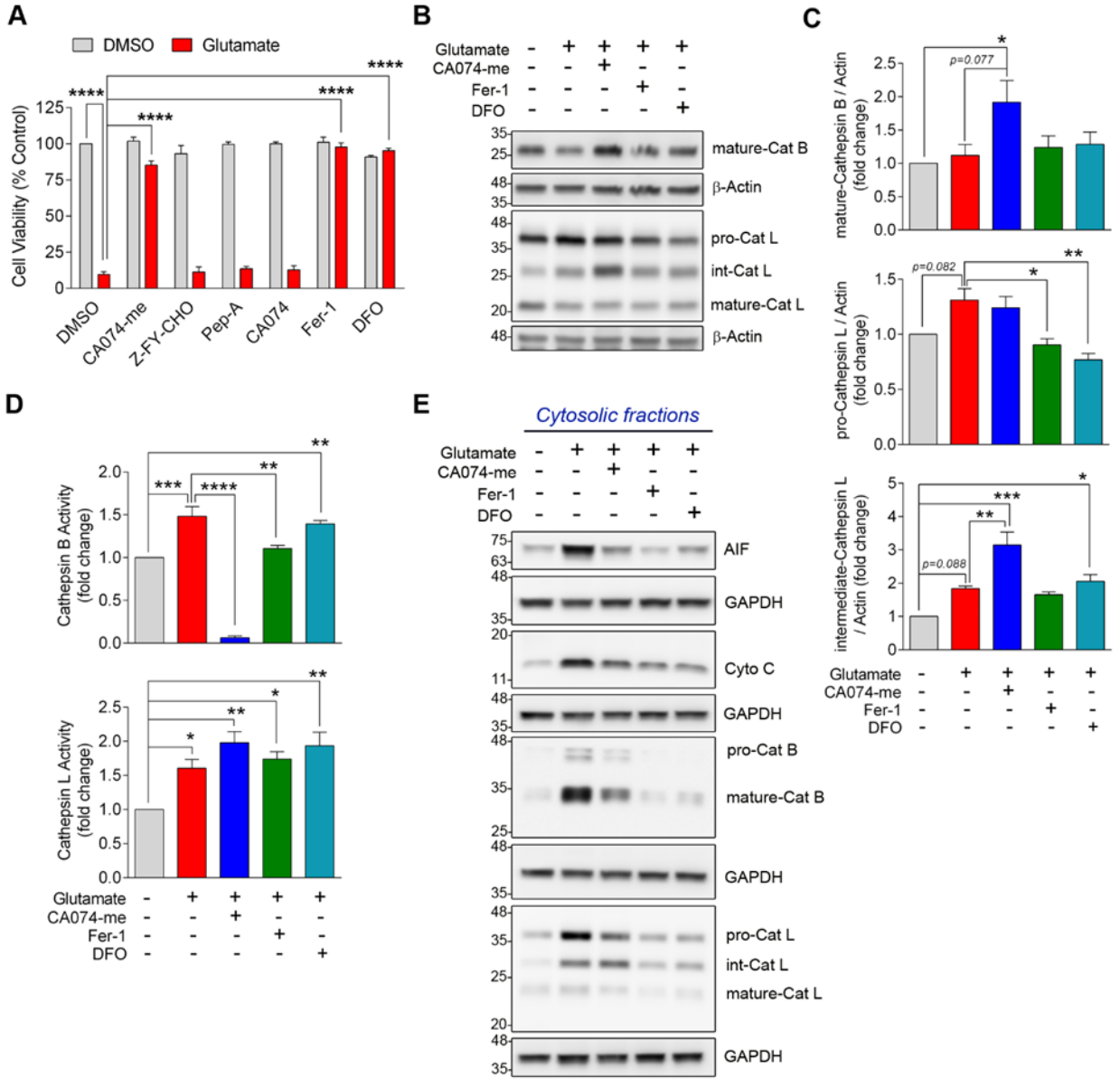

Figure 4.2. Cathepsin B mediates glutamate induced ferroptosis in HT22 cells. (A) HT22 cells were pretreated for 3 hr with CA074-me (15 μM), Z-FY-CHO (10 μM) or Pepstatin A (50 μM) and were treated with glutamate (4 mM) for 12 hr except for CA074 (15 μM), Fer-1 (2 μM) or DFO (50 μM), which were added simultaneously along with glutamate. Cell viability was determined by CCK-8 assay. The bars in graphs indicate mean ± S.E.M. of averages from n=3-6 independent experiments. ****p<0.0001 by one-way ANOVA followed by Tukey's post-hoc test. **(B)** HT22 cells were treated as indicated for 12 hr and the cell lysates were subjected to western blotting to assess the expression of cathepsins B and L. Densitometric analysis of proteins normalized to β-Actin are shown as fold change in **C**. The bars in graphs indicate mean ± S.E.M. of averages from n=3-4 independent experiments. *p < 0.05, **p < 0.01 and ***p<0.001 by one-way ANOVA followed by Tukey's post-hoc test **(D)** The effect of treatments on the protease activities of cathepsins B and L were determined by fluorometric method in cell lysates. The bars in graphs indicate mean ± S.E.M. of averages from n=4 independent experiments. *p < 0.05, **p < 0.01, ***p<0.001 and ****p<0.0001 by one-way ANOVA followed by Tukey's post-hoc test. **(E)** HT22 cells were subjected to indicated treatment conditions for 12 hr and the cytosolic fractions were analyzed by western blotting to determine the effect of inhibitors on glutamate induced lysosomal and mitochondrial membrane permeabilization.

4.5.6 Inhibition of cathepsin B decreases lipid peroxidation and improves mitochondrial functions

Since lipid peroxidation (LPO) is a major driving force in ferroptosis, we sought to examine the role of CTSB in regulation of lipid peroxidation during ferroptosis. Inhibition of CTSB significantly ameliorated the increase in MDA content induced by glutamate in HT22 whole cell lysates (Fig. 4.3 A) as well as mitochondrial and lysosomal fractions (Fig. 4.3 B and C). The efficacy of CA074-me in inhibiting LPO by ferroptotic induction was comparable with Fer-1 or DFO, showing that inhibition of CTSB was sufficient to inhibit intracellular organelle lipid peroxidation (Fig. 4.3 A-C).

The mitochondrial membrane damage induced by glutamate in HT22 cells was associated with a strong depletion of ATP content and a significant decrease in mitochondrial membrane potential ($\Delta\Psi m$), as measured by TMRM staining, demonstrating mitochondrial dysfunction (Fig. 4.3 D-F). Both inhibition of CTSB by CA074-me and lipid peroxidation by Fer-1 and DFO improved the ATP content and $\Delta\Psi m$ in cells exposed to glutamate, implying preserved mitochondrial structural integrity in these conditions (Fig. 4.3 D-F). We used FCCP, a mitochondrial uncoupler, as a positive control and observed a rapid decrease in $\Delta\Psi m$ within 15 min of treatment (Fig. 4.3 D and E). To further assess the effect of CA074-me and standard anti-ferroptotic agents on mitochondrial structural integrity, the oligomeric status of VDAC1 was assessed by chemical-crosslinking using EGS. Inhibition of CTSB or treatment with anti-ferroptotic agents Fer-1 and DFO markedly abrogated the induction of VDAC1 oligomerization and intra-molecular cross-link formation (Suppl. Fig. 4.4 C). Previous reports have shown that VDAC1 oligomerization can be inhibited by pro-survival Bcl-2 proteins (Shimizu et al., 2000; Arbel et al., 2012). Accordingly, administration of glutamate resulted in a corresponding decrease in Bcl-2 protein but was prevented prominently

after inhibition of CTSB or application of ferroptosis inducers Fer-1 and DFO (Suppl. Fig. 4.4 D). These data further confirm the impact of lysosomal membrane permeabilization on mitochondrial damage in ferroptosis.

Further to evaluate the significance of mitochondrial damage in ferroptosis, we tested the effect of inhibition of VDAC1 oligomerization in glutamate and erastin induced cell death using a previously reported VDAC1 inhibitor, DIDS (4,4′-Diisothiocyanatostilbene-2,2′- disulfonate) (Head et al., 2015; Ben-Hail and Shoshan-Barmatz, 2016). A dose dependent improvement in cell survival was observed with DIDS treatment in the presence of glutamate and erastin indicating the potential involvement of VDAC1 in the mediation of cell death after system x_c^- inhibition (Suppl. Fig. 4.5 A). Inhibition of VDAC1 has been shown to be detrimental under normal conditions as VDAC1 is involved in several cellular homeostatic functions such as transport of ions and ATP (Shoshan-Barmatz and Mizrachi, 2012; Pamenter et al., 2013). In agreement with previous reports, at higher concentration of 300µM, DIDS alone showed a significant decrease in cell survival under normal conditions. The efficacy of DIDS was confirmed by VDAC1 cross-linking assay. As shown in Suppl. Fig. 4.5 C, DIDS effectively abrogated the induction of VDAC1 oligomerization as evident by the absence of the trimeric and multimeric higher molecular weight bands and a significant decrease in dimeric and intra-molecular cross-linked bands in cells treated with glutamate-DIDS combination. These results were further confirmed with another inhibitor of VDAC1, Itraconazole (Head et al., 2015), which conferred significant protection against glutamate induced cell death (Suppl. Fig. 4.5 D). Taken together these results indicate that oxidative stress induced mitochondrial membrane damage is a feature of ferroptosis and preserving mitochondrial integrity can prevent ferroptotic cell death.

Figure 4.3. Inhibition of cathepsin B mitigates lipid peroxidation and mitochondrial dysfunction in ferroptosis.

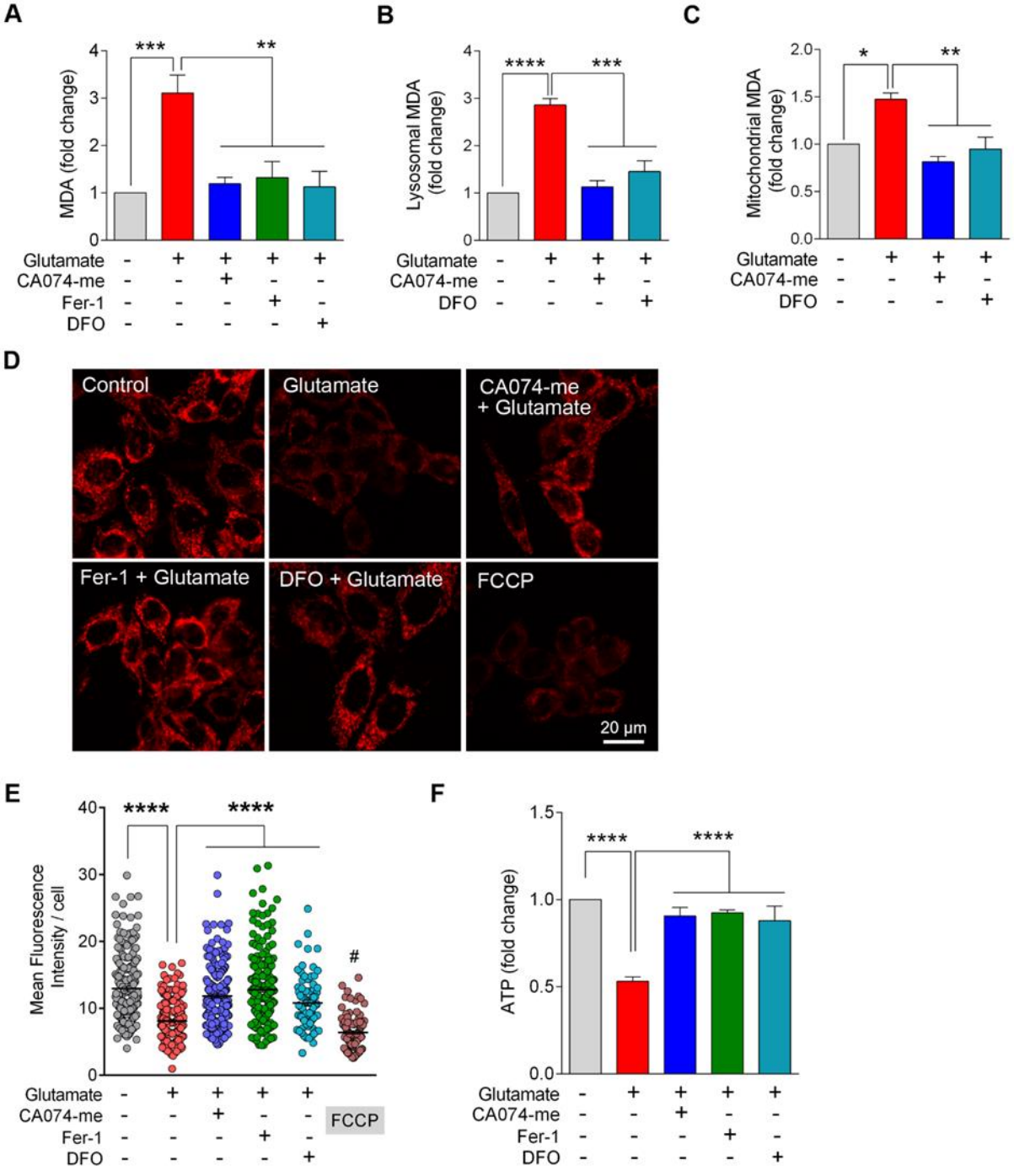

Figure 4.3. Inhibition of cathepsin B mitigates lipid peroxidation and mitochondrial dysfunction in ferroptosis. HT22 cells were treated with glutamate (4 mM) alone or in combination with Fer-1 (2 μM) or DFO (50 μM), except for CA074-me (15 μM), which was pretreated for 3 hr before addition of glutamate. After 12 hr, the extent of lipid peroxidation was determined by measuring the MDA content in whole cell lysates **(A)**, isolated lysosomal **(B)** and mitochondrial **(C)** fractions. The bars in graphs indicate mean ± S.E.M. of averages from n =3 independent experiments. *p < 0.05, **p < 0.01, ***p<0.001 and ****p<0.0001 by one-way ANOVA followed by Tukey's post-hoc test. **(D)** To determine the effect of inhibitors on glutamate-induced disruption of mitochondrial membrane potential, HT22 cells were pretreated with CA074-me for 3 hr and then treated with glutamate (2 mM) for 12 hr, except for Fer-1 and DFO which were added along with glutamate. Cells were then stained with TMRM and the live images were visualized using confocal microscope. Cells incubated with the mitochondrial uncoupler FCCP (for 15 min) served as positive control. The images shown here are representative of three independent experiments. The mean fluorescence intensity per cell in n≥200 cells/condition, except for DFO + glutamate (n=77) and FCCP (n=105), were quantified. The distribution of values is presented as dot plot **(E)** and lines indicate mean ± S.E.M. ****p<0.0001 by one-way ANOVA followed by Tukey's post-hoc test. **(F)** HT22 cells were subjected to indicated treatment conditions for 12 hr and the ATP content in cell extracts was measured. The bars in graphs indicate mean ± S.E.M. of averages from n=5-6 independent experiments. **p < 0.01 and ***p<0.001 by one-way ANOVA followed by Tukey's post-hoc test.

4.5.7 CTSB is essential for ferroptosis induction

To validate our above findings and to ascertain the role of CTSB in ferroptosis, we used primary MEF cells generated from mice lacking CTSB (Fig. 4.4 A). First, we exposed WT and *Ctsb*$^{-/-}$ MEF cells to erastin for 12 hr before the cell survival rates were assessed by the CCK8 assay. Affirming the above findings with pharmacological inhibitors, *Ctsb*$^{-/-}$ cells demonstrated significant resistance towards erastin induced ferroptotic cell death (Fig. 4.4 B). The mitochondrial response of these cells in erastin-mediated ferroptosis was determined by assessment of ATP content. WT MEFs showed a significantly lower ATP content in response to ferroptosis induction whereas, *Ctsb*$^{-/-}$ MEFs showed higher resistance to erastin induced ATP depletion (Fig. 4.4 C). Erastin mediated ferroptosis in WT MEFs was effectively prevented with Fer-1 (Fig. 4.4 B and C).

Similar to the HT22 cells, the WT MEF cells showed a near significant ($p=0.055$) increase in LC3-II/LC3-I ratio and an upregulation of lysosomal LAMP1 protein when treated with erastin. Administration of Fer-1 effectively reversed these changes in these cells. Interestingly, genetic deletion of CTSB prevented the increase in LAMP1 protein but did not affect the LC3-II/LC3-I ratio in response to erastin (Suppl. Fig. 4.6 A and B). WT MEFs exposed to erastin displayed a significant increase in mature-CTSB levels, which was prevented by Fer-1 treatment. Similarly, Fer-1 also abrogated the increase in pro-CTSL protein expression in response to erastin in WT MEFs. *Ctsb*$^{-/-}$ cells showed a comparatively low basal pro-CTSL expression, which was unaffected by erastin. A sharp increase in the intermediate CTSL level was observed in *Ctsb*$^{-/-}$ cells in response to erastin; this was two-fold higher than WT MEFs exposed to erastin. Nonetheless, there was no significant change in mature-CTSL levels observed in either cell types after erastin treatment (Suppl. Fig. 4.6 A and B). These observations are in accordance with a previous report suggesting mutual compensation between lysosomal proteases CTSB and CTSL. Authors reported that *in-*

vivo single gene deletion of either of these cathepsins do not develop lysosomal or autophagosomal accumulations in neurons, while neurons of double knockout (*Ctsb*$^{-/-}$/*Ctsl*$^{-/-}$) mice display excessive autophagosomes (Stahl et al., 2007). The cell-specific role of these cathepsins remains to be further characterized. For instance, in macrophages, prolonged inhibition or knockout of CTSB has been shown to result in accumulation of enlarged lysosomes indicating the involvement of this enzyme in regulation of autophagic flux (Tizon et al., 2010).

Erastin induces ferroptosis through depletion of GSH, which in turn is due to inhibition of the cystine–glutamate antiporter system x_c^- (Dixon et al., 2012). Experimental approaches that limit GSH depletion have been shown to render cells resistant to ferroptosis (Hao et al., 2017). We therefore decided to measure the GSH content in MEF cells in response to erastin. As shown in Fig. 4.4 D, similar to WT MEFs, deletion of cathepsin B (*Ctsb*$^{-/-}$) in MEFs did not prevent erastin-induced GSH depletion comparable to what was reported for Fer-1 (Zilka et al., 2017). To further examine the role of GSH in these cells, WT and *Ctsb*$^{-/-}$ MEF cells were exposed to the GSH synthesis inhibitor L-buthionine sulfoximine (BSO). Administration of BSO induced a dose dependent cell death in WT MEFs after 48 hr, whereas *Ctsb*$^{-/-}$ demonstrated higher resistance to cytotoxicity by BSO (Fig. 4.4 E). GSH depletion by BSO is a well-established model of ferroptosis and hence these results further confirm the key role of CTSB in this mode of cell death.

Although our KO studies conclude that GSH level is not the major player in prevention of ferroptotic cell death in MEF cells, one cannot rule out the potential effect of pharmacological inhibition of CTSB on GSH synthesis. We therefore used our model of glutamate toxicity in HT22 cells to test the effect of CA074-me on GSH levels. As expected, GSH levels were significantly depleted after glutamate treatment, which was not prevented by Fer-1 and DFO. Interestingly, cells pretreated with CA074-me before glutamate administration contained a significantly higher GSH

content when compared to glutamate alone treated cells (Suppl. Fig. 4.7 A). This was not a direct effect of CA074-me treatment, as basal GSH level (pre-glutamate exposure) in these cells (no glutamate) was not increased (0.964 ± 0.019-fold Vs Control). We therefore hypothesized that inhibition of CTSB with CA074-me might be increasing the GSH content by preserving the intracellular GSH synthesis machinery. To test this hypothesis, we performed western blotting to detect the catalytic and modifier subunits of γ-glutamylcysteine synthetase (γ-GCS), γ-GCSc and γ-GCSm, respectively, in cells subjected to various treatments. The de novo synthesis of GSH involves two sequential ATP dependent enzymatic reactions catalyzed by γ-GCS, the rate-limiting step, and GSH synthetase, respectively (Circu and Aw, 2012). Glutamate treatment caused a moderate decrease in both γ-GCSc and γ-GCSm protein levels, indicating impaired GSH synthesis machinery. However, pretreatment with CA074-me induced a significant upregulation in γ-GCSm levels and moderate increase of γ-GCSc when compared to glutamate treated cells indicating that the increase in GSH content after CTSB inhibition by CA074-me in glutamate treated cells could be due to the preservation of GSH synthesis machinery (Suppl. Fig. 4.7 B). Although, Fer-1 and DFO did not increase the GSH content, both inhibitors attenuated the glutamate induced decrease in γ-GCSc and γ-GCSm protein levels (Suppl. Fig. 4.7 A and B). However, no significant change was observed in γ-GCSc and γ-GCSm levels in response to erastin in both WT and *Ctsb*$^{-/-}$ MEF cells (Suppl. Fig. 4.7 C and D).

GSH has numerous functions in the cells, of which most of them are related to its role in scavenging ROS and as a substrate for GSH dependent enzymes (Patlevic et al., 2016). GPX4 is one of the key GSH dependent enzymes reducing phospholipid hydroperoxides to nontoxic lipid alcohols in the presence of GSH. Inactivation of GPX4 either by direct inhibition of its enzymatic activity using inhibitors like RSL3 or by depletion of GSH are known triggers of ferroptosis, as

both these approaches leads to accumulation of potentially toxic lipid peroxidation products resulting in ferroptosis (Friedmann Angeli et al., 2014; Conrad et al., 2016). A recent study suggested that prevention of GPX4 degradation through inhibition of CMA can inhibit ferroptosis (Wu et al., 2019). Considering the crucial role of lysosomes in CMA, we hypothesized that protective effect of CA074-me could be mediated by inhibition of CMA activity thereby preventing GPX4 degradation and eventually leading to prevention of ferroptosis. However, we observed that GPX4 protein degradation in response to glutamate was further augmented after pretreatment with CTSB inhibitor. The protection offered by DFO and Fer-1 in these studies was also independent of GPX4, as none of these treatments prevented GPX4 degradation (Fig. 4.4 F). Likewise, both WT and *Ctsb*$^{-/-}$ MEF cells showed a similar decrease in GPX4 levels in response to erastin (Suppl. Fig. 4.7 C and D). Overall, these results suggest that the resistance to ferroptosis observed after inhibition of CTSB activity or ablation of CTSB protein is not dependent on GPX4. To ascertain these findings on GPX4 dependency and to get further mechanistic insights, we decided to evaluate the effect of CTSB inhibitor on GPX4 ablation induced ferroptosis.

Figure 4.4. Cathepsin B knockout confers resistance to ferroptosis in mouse embryonic fibroblasts.

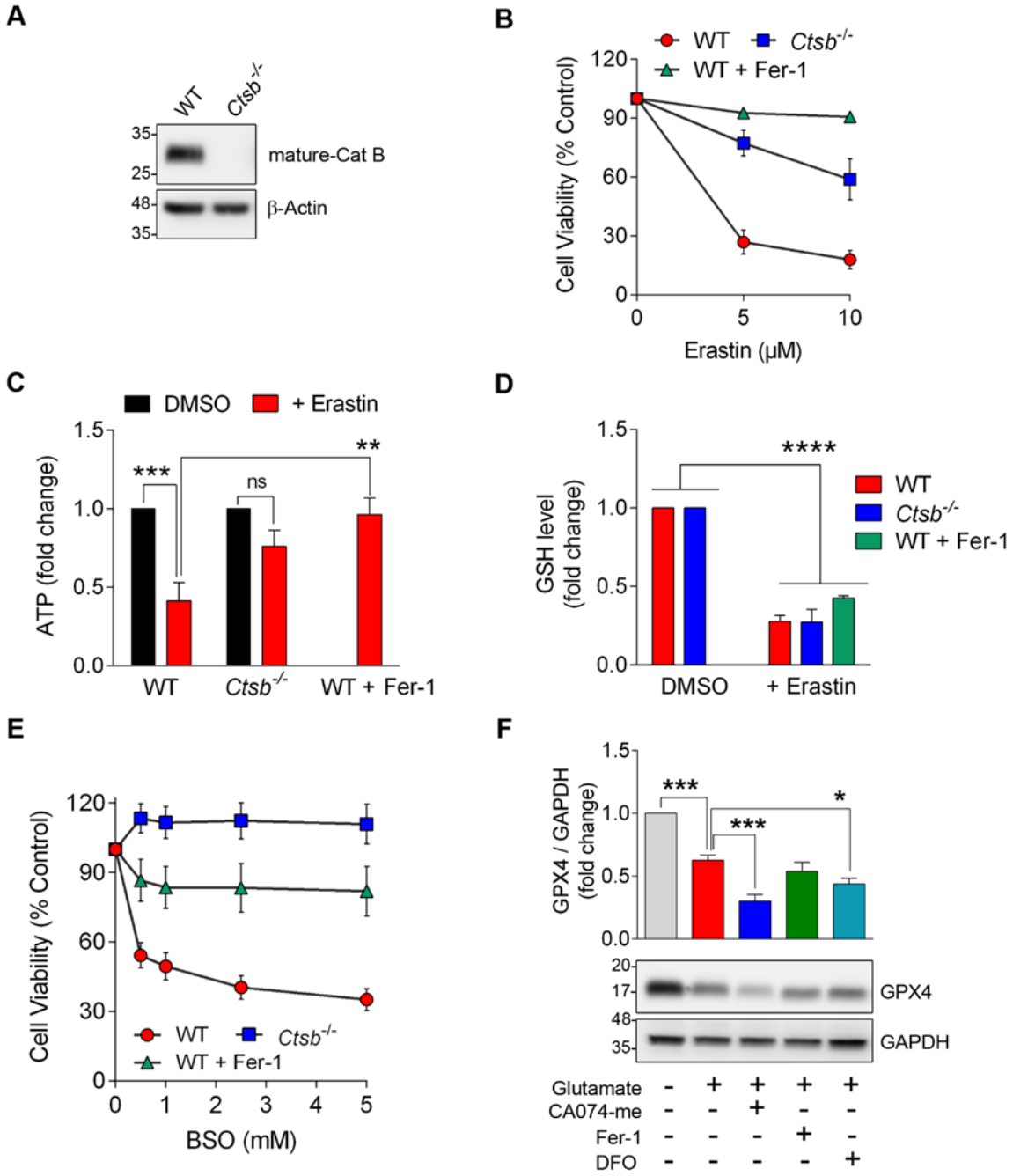

Figure 4.4. Cathepsin B knockout confers resistance to ferroptosis in mouse embryonic fibroblasts. (A) Representative western blots showing knockout of Cathepsin B (*Ctsb*$^{-/-}$) in primary mouse embryonic fibroblasts. **(B)** *Ctsb*$^{-/-}$ MEFs were resistant to erastin induced ferroptosis compared to WT. Fer-1 (2 μM) rescued the WT MEFs from erastin induced ferroptosis. Cell viability was assessed 12 hr after treatment with erastin by CCK8 assay. Data represents mean ± S.E.M. of averages from n =7 independent experiments. **(C)** WT and *Ctsb*$^{-/-}$ MEF cells were treated with erastin (5 μM) alone or in combination with Fer-1 (2 μM) for 12 hr and the ATP content in cell extracts was measured. The bars in graphs indicate mean ± S.E.M. of averages from n=3 independent experiments. **p < 0.01 and ***p<0.001 by one-way ANOVA followed by Tukey's post-hoc test. **(D)** Glutathione (GSH) content was determined by fluorometric method after 12 hr of indicated treatments. The bars in graphs indicate mean ± S.E.M. of averages from n=3 independent experiments. ****p<0.0001 by one-way ANOVA followed by Tukey's post-hoc test. **(E)** *Ctsb*$^{-/-}$ MEFs were resistant to BSO induced ferroptosis compared to WT. Cell death triggered by BSO was rescued by concomitant administration of Fer-1 (2 μM). Cell viability was assessed 48 hr after treatment with BSO by CCK8 assay. Data shown represent mean ± S.E.M. of n=5 independent experiments. **(F)** HT22 cells were pretreated with CA074-me (15 μM) and then exposed to glutamate for 12 hr, while Fer-1 (2 μM) and DFO (50 μM) were added as concomitant treatments along with glutamate. The cell lysates were subjected to western blot analysis for GPX4 protein expression. Densitometric analysis of GPX4 normalized to β-Actin is shown as fold change and the bars indicate mean ± S.E.M. of averages from n=4 independent experiments. *p < 0.05 and ***p<0.001 by one-way ANOVA followed by Tukey's post-hoc test.

4.5.8 GPX4 ablation induces activation of autophagy and lysosomal enlargement

To further examine a potential relationship between GPX4 and lysosomal cathepsins in ferroptosis, we employed the classical model of Pfa1 cells (Seiler et al., 2008), in which addition of Tamox induces a time dependent deletion of GPX4 thereby activating ferroptosis (Fig. 4.5 A). This was accompanied by a concomitant increase in LC3-II/LC3-I ratio indicating an induction of autophagy (Fig. 4.5 A and B), which could be due to increased lipid peroxidation products as a result of genetic *gpx4* deletion. While, a minimal level of ROS is required for induction of autophagy, excessive ROS can however, impair maturation of autophagy (Underwood et al., 2010; Nagakannan et al., 2016). To monitor the status of autophagic flux after GPX4 depletion, we transduced Pfa1 cells with baculovirus expressing LC3 fused with acid-sensitive green fluorescent protein (GFP) and acid-insensitive red fluorescent protein (RFP) (Premo^{TM} Autophagy Tandem Sensor). Using this technique autophagosomes are identified by yellow (GFP+RFP colocalization) and autolysosomes by red, indicating the fusion of autophagosomes with lysosomes (Kimura et al., 2007; Sandilands et al., 2011). Deletion of GPX4 induced a significant decrease in yellow punctas and a corresponding increase in red punctas indicating the increased maturation of autophagosomes to autophagolysosomes. Addition of Baf-A1 that blocks autophagosome-lysosome fusion by decreasing lysosomal acidity completely inhibited the conversion of yellow to red punctas (Suppl. Fig. 4.8 A and B). These findings were further confirmed by western blotting, where the turnover of LC3-II was monitored using Baf-A1 to block the maturation of autophagosome. Deletion of GPX4 in Pfa1 cells induced a four-fold increase in LC3-II protein level, which was further enhanced to 12-fold with addition of Baf-A1 and was comparatively higher than the LC3-II level in control cells treated with Baf-A1. Treatment with Fer-1, however, decreased the accumulation of LC3-II protein levels in both control and GPX4 deleted cells either

in the presence or absence of Baf-A1 (Suppl. Fig. 4.8 C and D). These results collectively support the previous reports (Gao et al., 2016; Wu et al., 2019; Yang et al., 2019a) regarding active autophagic processes during ferroptosis and suggests that induction of lipid peroxidation is upstream of autophagy activation.

Next, we assessed the status of lysosomes in GPX4 ablated cells by western blotting and immunocytochemistry. Deletion of GPX4 induced a time dependent increase in LAMP-1 protein levels (Fig. 4.5 C and D) indicating lysosomal enlargement, which was confirmed by lysosomal immunostaining (Fig. 4.5 E). As shown in Fig. 4.5 E and F, at 48 hr post GPX4 deletion, LAMP-1 positive vesicles were significantly increased and displayed an enlarged morphology. To further assess lysosomal acidity and size, we stained the cells with LysoTracker, an indicator of active lysosomes. Knockout of GPX4 in Pfa1 cells induced a significant increase in lysotracker fluorescence indicating increased lysosomal acidity (Fig. 4.5 E and G). Area distribution analysis of lysotracker stained vesicles revealed a change in lysosomal size when compared to control cells. We categorized the lysosomes according to their size into three groups: small (0-0.499 μm^2), medium (0.5-0.799 μm^2) and large (0.8-1.5 μm^2). We observed that after GPX4 deletion the population of small lysosomes decreased, while the number of medium and large lysosomes increased robustly, confirming an increase in enlarged lysosomes (Fig. 4.5 E and H). The normal size range of lysosomes is reported to be 0.1–1.2 μm^2 (Cai et al., 2017), however as a result of fusion with other membranous structures or activation of autophagy (either macro-autophagy or CMA), the size can increase to 0.5–1.5 μm^2. Accumulation of undigested cargo can also lead to enlarged dysfunctional lysosomes (Walkley and Vanier, 2009; Xu and Ren, 2015). Since, we saw an increase in lysosomal acidity with a corresponding autophagy induction after GPX4 deletion, it is unlikely that the enlargement in lysosomal size is because of lysosomal dysfunction caused by

accumulation of undigested cargo. A comparable lysosomal phenotype has been described earlier in Chediak–Higashi syndrome, where enlarged lysosomes were found to be still functional and were able to fuse with autophagosomes and degrade cargo at normal rate (Holland et al., 2014).

Figure 4.5. GPX4 disruption induces autophagy and lysosomal enlargement.

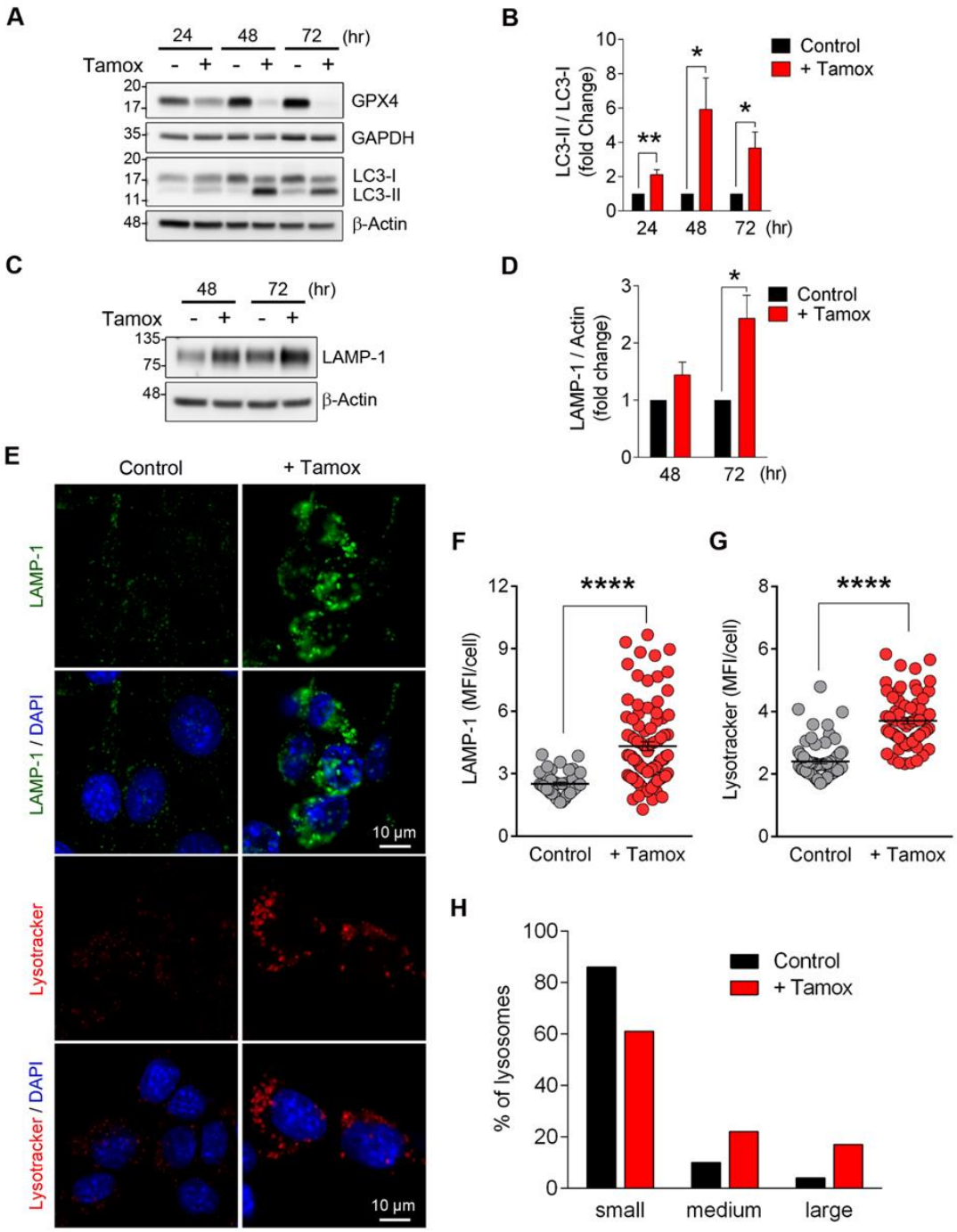

Figure 4.5. GPX4 disruption induces autophagy and lysosomal enlargement. Representative western blots show Tamox (1 μM) induced deletion of GPX4 in Pfa1 cells and the time dependent changes in LC3-I to LC3-II conversion **(A)** and LAMP-1 **(C)** protein levels. Densitometric quantification of LC3-I/LC3-II **(B)** and LAMP-1 **(D)** are shown. The bars represent mean ± S.E.M. of averages from n=4 independent experiments, *$p < 0.05$ and **$p < 0.01$ by unpaired two-tailed *t*-test. **(E)** 48 hr post induction of GPX4 knockout, Pfa1 cells were stained for with LysoTracker red dye or immunostained with antibody against LAMP-1. The mean fluorescence intensity per cell was quantified (LAMP-1, n≥40 and LysoTracker, n≥70 cells/condition) and the distribution of values are represented as dot plot **(F** and **G)**; lines indicate mean ± S.E.M. ****$p < 0.0001$ by unpaired two-tailed *t*-test. Similar results were obtained from experiments performed independently three times. **(H)** Size distribution of lysotracker stained vesicles **(**in **E)** is shown. The lysosomes were categorized according to their size into three groups: small (0-0.499 μm^2), medium (0.5-0.799 μm^2) and large (0.8-1.5 μm^2). Pfa1 cells induced for GPX4 deletion (Tamox, 1 μM) showed an increase in percentage of enlarged lysosomes.

4.5.9 Lysosomal membrane permeabilization after GPX4 ablation

We next investigated the impact of GPX4 deletion on lysosomal proteases. A time dependent increase in the pro form of CTSB and a corresponding significant increase in mature-CTSB was observed after induction of GPX4 deletion in Pfa1 cells. Similarly, both the pro and intermediate forms of CTSL were found to be increased in a time dependent manner, with their expression peaking after 72 hr of induction of GPX4 depletion. Upregulation of mature-CTSL was observed throughout the Tamox-induced ablation of GPX4 (Fig. 4.6 A and B). These results were further confirmed with specific fluorometric enzymatic assays for cathepsins. We detected a significant increase for both CTSB and CTSL enzymatic activities in Tamox-treated Pfa1 cells compared to their time matched controls (Fig. 4.6 C). This was correlated with their protein levels. In case of CTSD, no significant changes were observed in the pro-form until 48 hr after induction of GPX4 knockout however, a moderate, but a significant decrease in pro-CTSD was observed at 72 hr. Nonetheless, no mature forms of CTSD were detected (Suppl. Fig. 4.8 E and F). These results indicate a delayed activation of CTSD, especially at the very last stage of ferroptosis.

Since our results with HT22 cells showed the involvement of LMP in ferroptosis, we next set out to assess the fate of lysosomal membrane integrity after GPX4 deletion. Subcellular fractionation of Tamox-treated Pfa1 cells showed a significant increase in mature-CTSB protein in the cytosolic fraction and a corresponding decrease in lysosomal fraction in response to GPX4 deletion. A similar increase in pro, intermediate and mature forms of CTSL was also observed in the cytosolic fraction; however, contrary to our expectation, a similar increase in pro and mature-CTSL was observed in lysosomes (Fig. 4.6 D and E). Enzymatic activity assays corroborated the protein levels with proportionate enzymatic activity. CTSB activity was found to be four-fold higher in the cytoplasm of GPX4 ablated cells when compared to their untreated counterpart. However, we

could not detect any CTSL enzymatic activity in control cell cytoplasm and only a moderate increase was observed in the cytoplasm of GPX4 deleted cells (Fig. 4.6 F). It is noteworthy that the intermediate form of CTSL was observed only in the cytosolic fraction of GPX4 deleted cells and not control cells (Fig. 4.6 D). Comparing the CTSL enzymatic activity in the cytosol and protein isoforms, it is possible that only the cytosolic/intermediate form of CTSL is active during GPX4 deletion-induced ferroptosis. The observation that only CTSB, but not CTSL was found to be decreased in lysosomal fraction, suggests a possibility of partial or selective LMP in ferroptosis.

Figure 4.6. GPX4 ablation causes lysosomal membrane permeabilization.

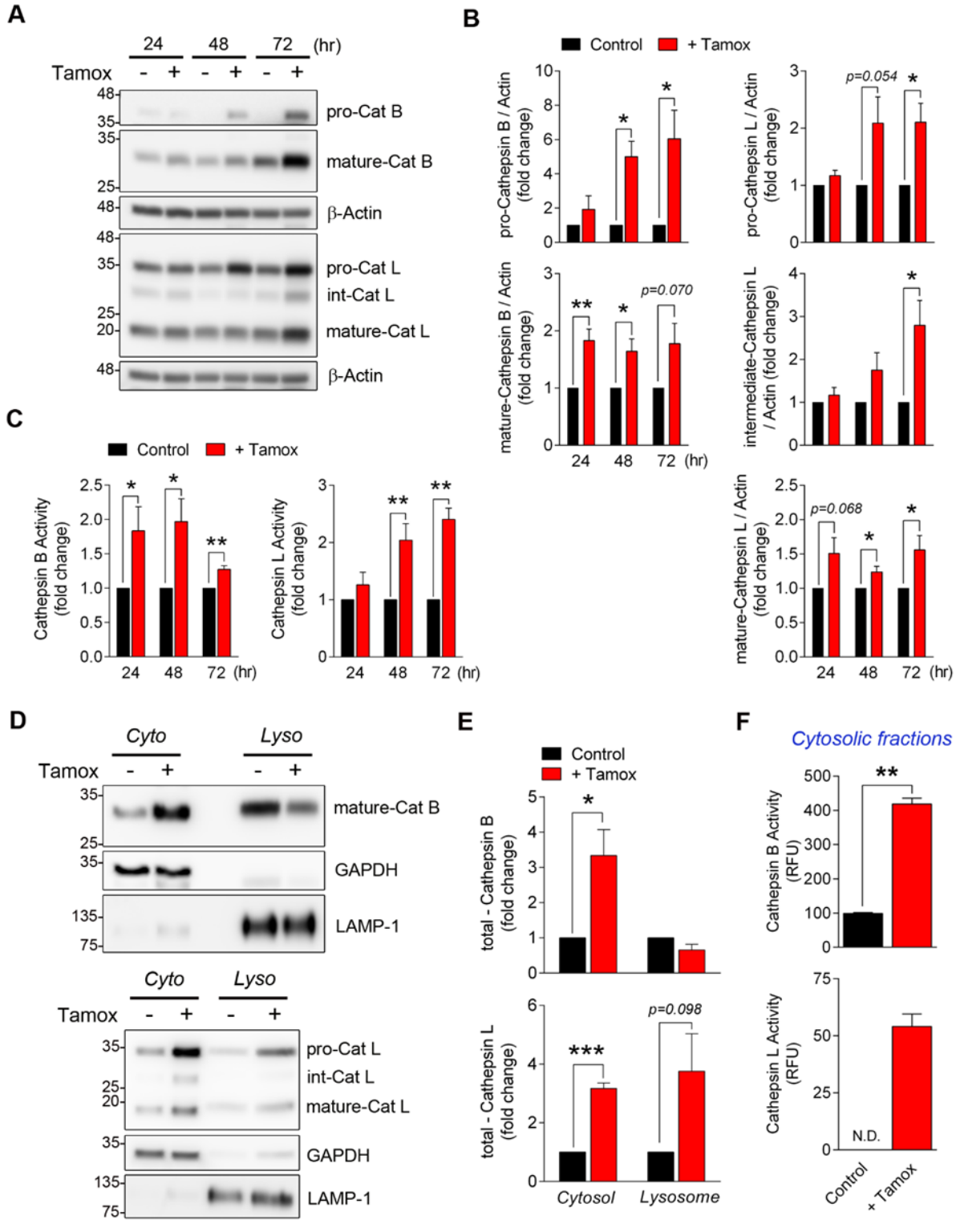

Figure 4.6. GPX4 ablation causes lysosomal membrane permeabilization. (A) Pfa1 cells were harvested at indicated time points after induction of GPX4 disruption with Tamox (1 µM). The cell lysates were subjected to western blot analysis to determine the expression pattern of cathepsins. Densitometric analysis of proteins normalized to β-Actin are shown as fold change **(B)**. The bars in graphs indicate mean ± S.E.M. of averages from n=3-4 independent experiments. *p < 0.05 and **p < 0.01 by unpaired two-tailed *t*-test. **(C)** Enzymatic activities of cathepsins B and L were determined using fluorogenic substrates in Pfa1 cell lysates collected at indicated time points after induction of GPX4 knockout. The bars in graphs indicate mean ± S.E.M. of averages from n=3-5 independent experiments. **(D)** GPX4 was disrupted in Pfa1 cells with Tamox (1 µM) and were subjected to subcellular fractionation after 60 hr of knockout induction. The isolated fractions were analyzed by western blotting to determine the intracellular localization of cathepsin B (upper panel) and cathepsin L (lower panel). Densitometric quantifications of cathepsins normalized to either cytosolic (GAPDH) or lysosomal (LAMP-1) loading control are shown as bar graphs **(E)**. The bars indicate mean ± S.E.M. of averages from n=3 independent experiments. *p < 0.05 and ***p<0.001 by unpaired two-tailed *t*-test. **(F)** Enzymatic activities of cathepsins in cytosolic fractions were determined by fluorometric method. The bars in graphs indicate mean ± S.E.M. of averages from n=2 independent experiments. **p < 0.01 by unpaired two-tailed *t*-test.

4.5.10 Inhibition of CTSB abrogates GPX4 depletion induced ferroptosis

To evaluate the contribution of different lysosomal proteases in GPX4 knockout induced ferroptotic cell death, we used CA074-me, Z-FY-CHO and Pep-A, specific pharmacological inhibitors of CTSB, CTSL and CTSD, respectively. Initially, we screened the efficacy of all the inhibitors with varying durations of pre or concomitant treatment strategies (data not shown). Based on these data, the inhibitors were added 24 hr after the induction of GPX4 deletion. As shown in Fig. 4.7 A, cell death induction after GPX4 ablation was prevented by CA074-me in a dose dependent manner. As shown in Fig. 4.7 B, CA074-me (15μM) showed a marked protection against GPX4 depletion induced changes in cellular morphology. Inhibition of CTSL using Z-FY-CHO (10 and 20 μM) or CTSD with Pep-A (50 μM) did not show any significant improvement in cell viability when compared to Tamox treated cells, whereas lipid peroxidation inhibitor Fer-1 (0.2 μM) displayed a complete protection (Fig. 4.7 A and B).

A previous report has shown that GPX4 deletion by Tamox leads to translocation of AIF1 to nucleus from the mitochondrial compartment shown by a significant increase in nuclear/cytoplasmic ratio of AIF staining (Seiler et al., 2008). To examine the role of CTSB involvement in GPX4 ablation-induced ferroptosis, at the end of experiments we assessed the translocation of AIF to nucleus in Pfa1 cells. Protection mediated by CA074-me in these studies was associated with inhibition of AIF translocation to nucleus. Likewise, Fer-1 completely blocked the nuclear translocation of AIF (Fig. 4.7 C and D). However, a recent report has negated the involvement of AIF1 in ferroptosis (Doll et al., 2019). CSTB inhibition in GPX4-dpeleted cells also diminished the extent of lipid peroxidation by ~ 2 folds as measured by MDA content in Pfa1 cells lysates. This effect was comparable with Fer-1 treatment (Fig. 4.7 E).

Collectively, these results indicate a pivotal role for CTSB in induction of MMP and oxidative stress during ferroptosis. The protection offered by CA074-me against GPX4 deletion induced ferroptosis was independent of GSH content, as CA074-me did not cause any significant increase in GSH content both in normal and GPX4 ablated cells (Suppl. Fig. 4.8 G).

4.5.11 Status of thioredoxin system in ferroptosis

Thioredoxin (Trx) and its reducing enzyme thioredoxin reductase (TrxR) play a major role in maintaining the redox balance of the cells (Holmgren and Lu, 2010). Trx system can also reduce lipid peroxidation indirectly through their redox based control of phospholipid hydroperoxidase peroxiredoxins (Baskin-Bey et al., 2005; Zuo et al., 2018). To assess the status of Trx system during ferroptosis, we assessed the protein expression of Trx1 and TrxR1 in HT22 cells exposed to glutamate and GPX4 disrupted cells (Pfa1). A time dependent decrease in the expression of Trx1 protein, but not TrxR1 was observed in response to glutamate treatment (Suppl. Fig. 4.9 A and B). Similarly, GPX4 disrupted cells showed a significant reduction in Trx1 protein levels, but not TrxR1 (Suppl. Fig. 4.9 C and D). These results indicate a failure of Trx system during ferroptosis. Next, we assessed the impact of CA074-me treatment on Trx system in ferroptotic cells. CA074-me showed non-significant improvement in thioredoxin (Trx) and thioredoxin reductase (TrxR) protein levels further confirming that the protection offered by CA074-me in ferroptosis was independent of Trx system induction (Suppl. Fig. 4.9 C and D).

Figure 4.7. Inhibition of cathepsin B rescues GPX4 deletion-induced ferroptosis.

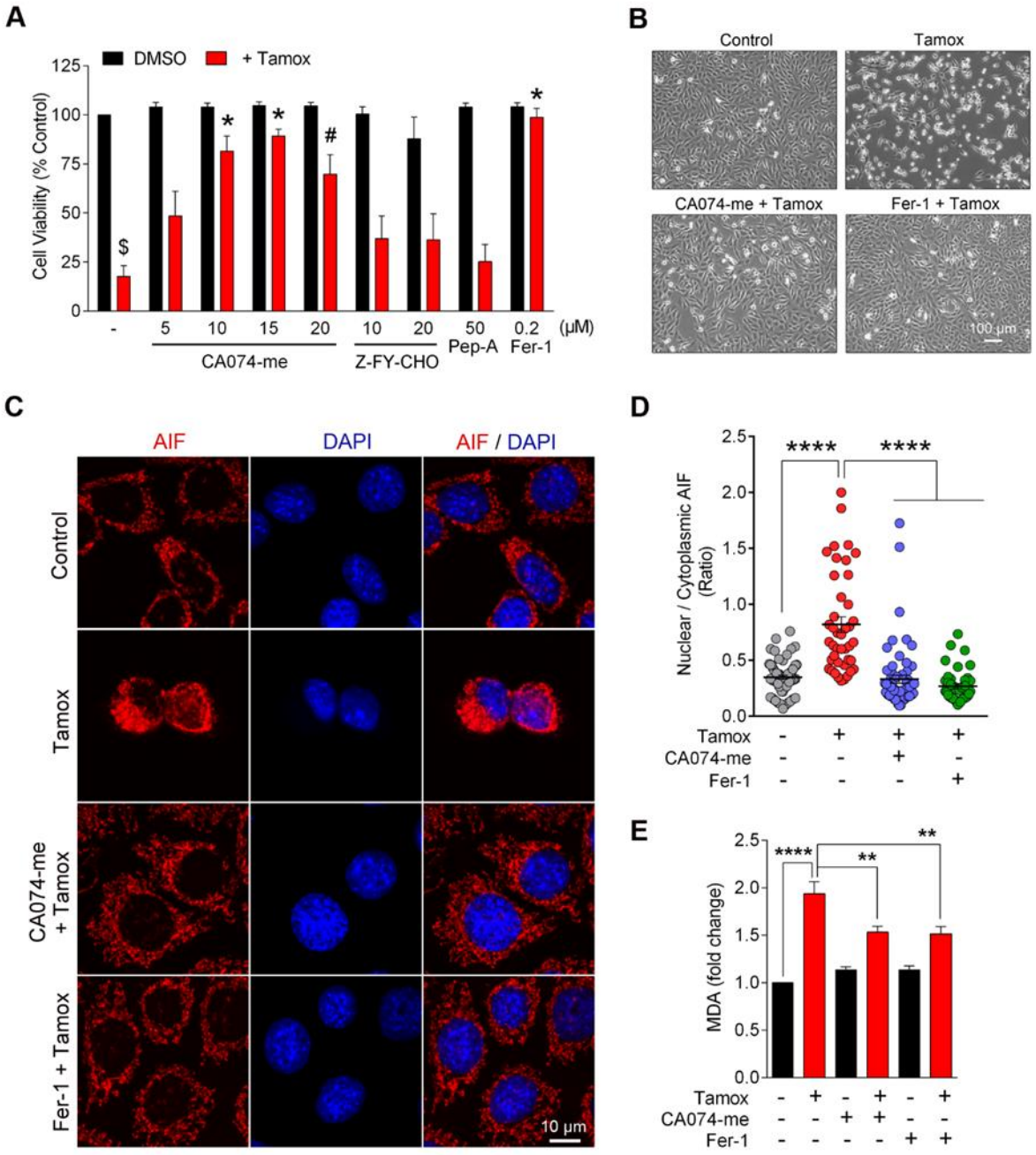

Figure 4.7. Inhibition of cathepsin B rescues GPX4 deletion-induced ferroptosis. **(A)** Pfa1 cells were cultured in the presence of Tamox (1 μM) to disrupt GPX4 and the inhibitors were added 24 hr after knockout induction. Cells grown in normal culture conditions were used to determine the toxicity of inhibitors. Cell viability was assessed 60 hr after knockout induction by CCK8 assay. The bars in graphs indicate mean ± S.E.M. of averages from n=4-5 independent experiments. $ indicates $p<0.0001$ when compared to DMSO treated control; # and * indicate $p<0.001$ and $p<0.0001$, respectively, when compared to Tamox alone treated group. Statistical significance was determined by one-way ANOVA followed by Tukey's post-hoc test. **(B)** CA074-me (15 μM) and Fer-1 (0.2 μM) rescued Pfa1 cells from GPX4 deletion induced ferroptotic cell death. **(C)** Nuclear translocation of AIF was assessed by immunostaining after 48 hr of induction of GPX4 knockout. The mean fluorescence intensity of AIF in nuclear and cytoplasmic compartments were measured in $n \geq 40$ cells/condition and the nuclear / cytoplasmic ratio is presented as dot plot **(D)** and the lines indicate mean ± S.E.M. ****$p<0.0001$ by one-way ANOVA followed by Tukey's post-hoc test. Similar results were obtained from experiments performed independently three times. **(E)** Cells were treated as described in Figure 7A and MDA content in cell lysates were determined by fluorometric method. The bars in graphs indicate mean ± S.E.M. of averages from n=4 independent experiments. **$p < 0.01$ and ****$p<0.0001$ by one-way ANOVA followed by Tukey's post-hoc test.

4.5.12 Blocking cathepsin B activity and lipid peroxidation inhibits autophagy and lysosomal acidity in GPX4 depleted cells

Since CTSB is a major protease in lysosomes, we aimed to determine the effect of loss of CTSB activity on activation of lysosomal autophagy in GPX4 knockout induced ferroptosis. Contrary to our findings with HT22 and MEF cells, blockade of CTSB inhibited the autophagic induction in ferroptotic cells as evidenced by a significant decrease in LC3-II/LC3-I ratio in GPX4 knockout cells treated with CA074-me when compared to vehicle treated control cells. CA074-me did not prevent the upregulation of LAMP1 after *gpx4* deletion. Treatment with Fer-1 elicited a similar effect as CTSB inhibitor in terms of LC3-II/LC3-I ratio and LAMP-1 protein levels (Fig. 4.8 A and B). Fer-1 rescued cells displayed diminished CTSB but enhanced CTSL enzymatic activity. Inhibition of CTSB with CA074-me further enhanced CTSL activity in *gpx4* deleted cells, while completely inhibiting CTSB activity as expected (Fig. 4.8 C). These observations further support the idea that lipid peroxidation acts upstream of autophagy and CTSB activation in ferroptosis and confirmed our findings in HT22 cells. Using lysotracker staining, the effect of CA074-me and Fer-1 on ferroptosis induced increased lysosomal acidity was assessed. Both CA074-me and Fer-1 significantly abolished the multifold increase in lysotracker intensity as a result of GPX4 deletion in Pfa1 cells (Fig. 4.8 D and E), which could be due to reduced autophagy induction by these inhibitors. As positive controls, Baf-A1 treated cells, either with or without *gpx4* deletion, showed a significant decrease in lysotracker intensity. However, neither CA074-me nor Fer-1 showed any significant effects on lysosomal acidity in control cells (Fig. 4.8 D and E).

Figure 4.8. CA074-me and Fer-1 inhibits autophagy induction and lysosomal activity in ferroptosis.

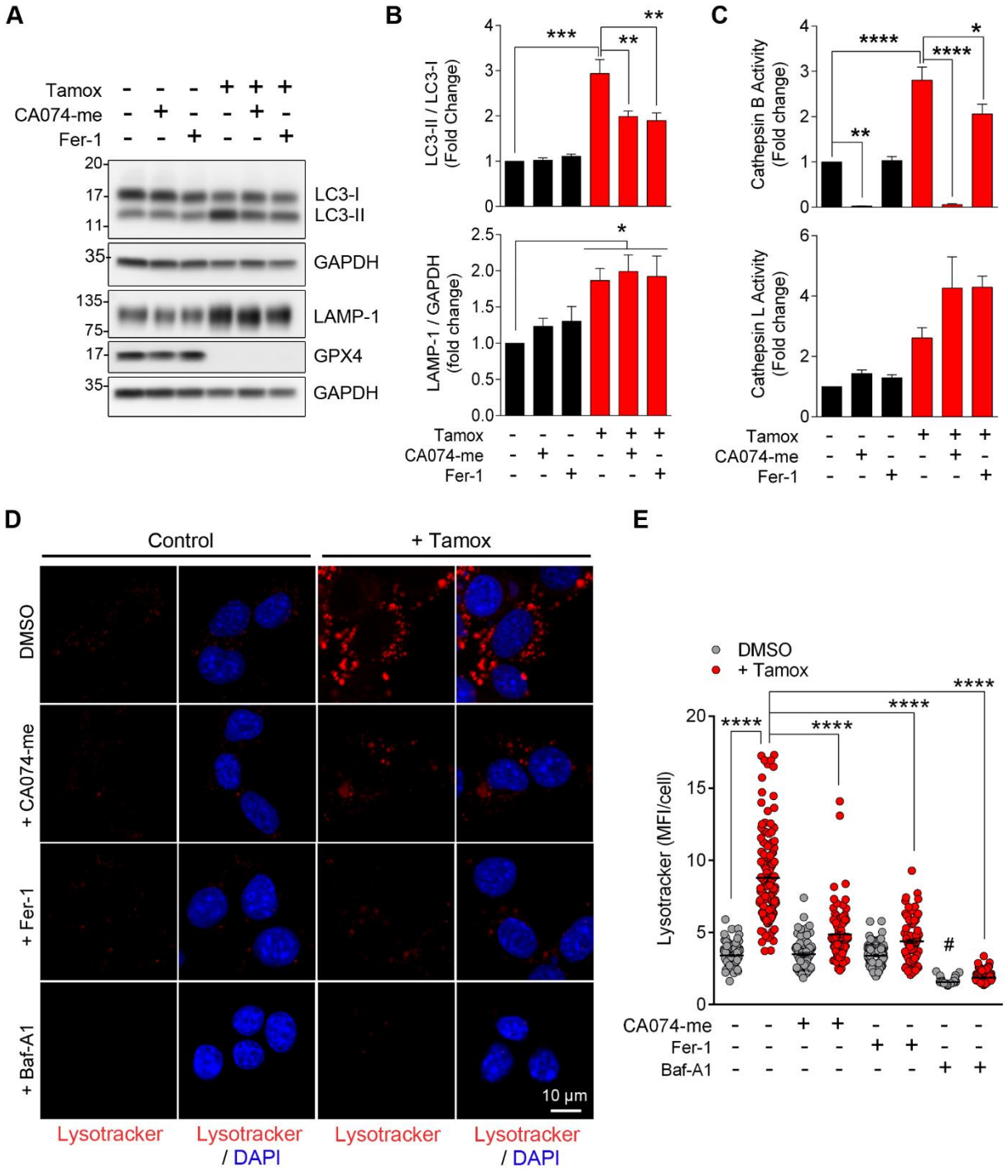

Figure 4.8. CA074-me and Fer-1 inhibits autophagy induction and lysosomal activity in ferroptosis. (A) GPX4 knockout was induced in Pfa1 cells by addition of Tamox (1 μM) and the inhibitors were added 24 hr after knockout induction. The cells were harvested at 60 hr and the cell lysates were subjected to western blot analysis for autophagic markers. Densitometric quantifications of proteins normalized to GAPDH are shown **(B)**. Bars indicate mean ± S.E.M. of averages from n=4 independent experiments. *$p < 0.05$, **$p < 0.01$ and ***$p<0.001$ by one-way ANOVA followed by Tukey's post-hoc test. **(C)** Protease activities of cathepsins B and L in cell lysates were determined by using fluorogenic substrates. The bars in graphs indicate mean ± S.E.M. of averages from n=3 independent experiments. *$p < 0.05$, **$p < 0.01$ and ****$p<0.0001$ by one-way ANOVA followed by Tukey's post-hoc test. **(D)** Pfa1 cells were treated as indicated and stained with LysoTracker dye (red) 48 hr after induction of GPX4 knockout. Counter stained with DAPI to mark nuclei (blue). The mean fluorescence intensity per cell in n≥70 cells/condition were quantified, and the distribution of values is presented as dot plot **(E)**. Similar results were obtained from two experiments performed independently. ****$p<0.0001$ by one-way ANOVA followed by Tukey's post-hoc test.

4.5.13 Histone H3 is cleaved by Cathepsin B in ferroptosis

While DNA fragmentation and chromatic condensation are hallmarks of apoptosis, we observed that nuclear structure and its contents are largely unaffected during ferroptosis. This is similar to a previous report in ferroptotic nuclei in kidney (Friedmann Angeli et al., 2014). Interestingly, we observed that that Histone H3, a core component of chromatin, was cleaved in glutamate treated HT22 neuronal cell line. Several proteases including lysosomal cathepsins are known to digest Histone molecules during cellular differentiation, senescence and death (Yi and Kim, 2018). Since, potent activation of lysosomal proteases is observed during ferroptosis in this study, we attempted to identify the specific protease/s involved in Histone H3 cleavage during ferroptosis. A faster migrating anti-H3 antibody reactive band was detected only in lysates obtained from HT22 cells exposed to glutamate, but not in control cells. Blocking of CTSB activity with CA074-me remarkably inhibited the glutamate induced proteolytic cleavage of H3, whereas CTSL (Z-FY-CHO) and CTSD (Pep-A) inhibitors failed to do so, implying that CTSB is the mediator of H3 cleavage in ferroptosis (Fig. 4.9 A). We noted that inhibition of autophagy during the initiation and maturation stages using LY294002 and Baf-A1, respectively inhibited the H3 cleavage in response to glutamate induced ferroptosis suggesting an active role of lysosomal autophagy in this process. In addition, administration of Fer-1 in glutamate treated cells prevented the cleavage of H3 fragment confirming that H3 cleavage is a ferroptotic process (Fig. 4.9 A).

The involvement of H3 cleavage in ferroptosis was further confirmed in Pfa1 cells, as the cleaved product of H3 was detected only after GPX4 deletion. It is currently unknown whether H3 cleavage is a cell specific event or a general phenomenon in ferroptosis. CA074-me and Fer-1 treatment prevented the H3 cleavage in GPX4 deprived cells suggesting the involvement of CTSB in

cleavage of H3 during GPX4 dependent ferroptosis and is downstream of lipid peroxidation (Fig. 4.9 B).

To further validate the above results, we subjected the whole cell lysates obtained from WT and *CTSB*$^{-/-}$ MEFs grown in the presence or absence of erastin to western blot analysis. We detected the cleaved H3 fragment only in WT cells exposed to erastin, but not in *CTSB*$^{-/-}$ cells upholding our above results. H3 cleavage was completely prevented in WT cells cultured in the presence of Fer-1 and erastin indicating that lipid peroxidation is a trigger for proteolytic cleavage of H3 (Fig. 4.9 C).

To this end, we have shown that CTSB inhibition prevents ferroptotic cell death and cleavage of H3. However, it is not clear whether CTSB causes direct H3 cleavage or facilitates the translocation of other proteases to nucleus that mediate H3 damage in ferroptotic cells. Histone H3 is known to be a substrate of several lysosomal proteases (Yi and Kim, 2018). However, amongst the inhibitors we tested in this study, only CA074-me was able to prevent the ferroptosis induced H3 cleavage (Fig. 4.9 A). To further validate CTSB as a H3 protease in ferroptosis, we used an *in-vitro* histone H3 cleavage assay using isolated nuclei. The assay was performed at pH 7.4 to mimic the cytosolic pH. We observed a higher efficiency in H3 cleavage for CTSL than CTSB, as rh-CTSL (50 ng) caused a severe digestion of H3 that was detectable as early as 30 min. In sharp contrast, similar concentration of rh-CTSB-mediated cleaved products of H3 were not observed until 2 hrs of incubation. As described previously (Duncan et al., 2008), the cleavage of H3 by rh-CTSB was distinctly different when compared to rh-CTSL (Fig. 4.9 D). To determine the potency of CTSB in cleaving H3, we incubated the isolated nuclei with increasing concentrations of rh-CTSB for 2 hrs. In contrast to rh-CTSL, even fourfold higher concentrations of rh-CTSB was unable to completely digest H3 indicating a specific, distinct and controlled

pattern of cleavage of H3 by CTSB. The *in vitro* cleavage of H3 was prevented with inhibitors of their respective cathepsins (Fig. 4.9 E).

Figure 4.9. Cathepsin B cleaves Histone H3 during ferroptosis.

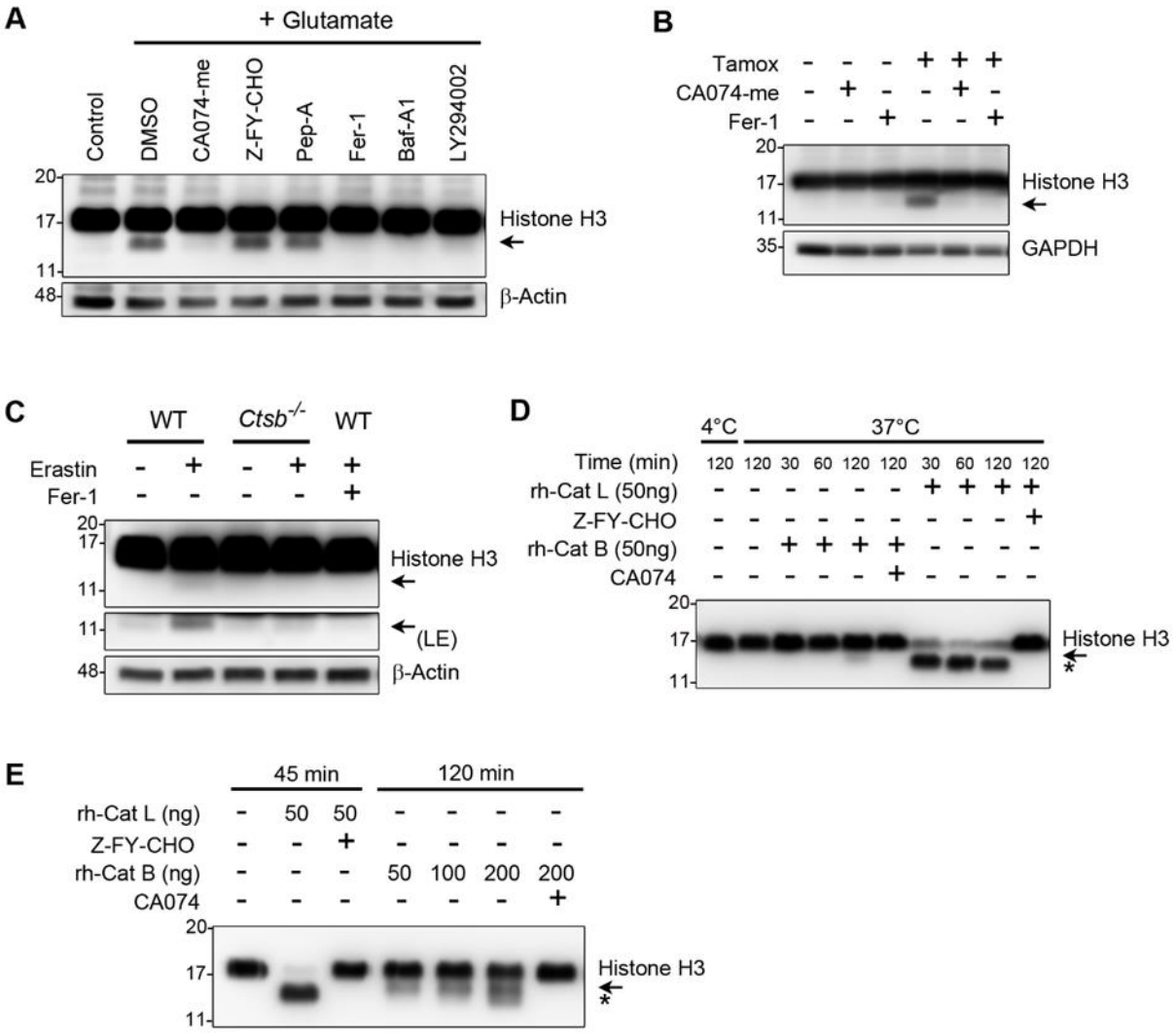

Figure 4.9. Cathepsin B cleaves Histone H3 during ferroptosis. (A) HT22 cells were pretreated for 3 hr with either CA074-me (15 µM), Z-FY-CHO (10 µM) or Pepstatin A (50 µM) prior to exposure to glutamate (4 mM, 12hr). For other groups, Fer-1 (2 µM), Baf-A1 (0.4 µM) or LY294002 (25 µM) were added along with glutamate. The cell lysates were subjected to western blot analysis for Histone H3. Arrow indicates cleaved histone H3. **(B)** GPX4 was disrupted in Pfa1 cells by Tamox (1 µM) treatment and the inhibitors were added 24 hr post knockout induction. The cells were harvested at 60 hr after knockout induction and the status of Histone H3 in cell lysates was assessed by western blotting. Arrow indicates cleaved histone H3. **(C)** WT and *CTSB*$^{-/-}$ MEF cells were exposed to erastin (5 µM) alone or in combination with Fer-1 (2 µM) for 12 hr and the cell lysates were analysed by western blotting. LE=Long Exposure; Arrow indicates cleaved histone H3. **(D** and **E)** Isolated HT22 cell nuclei were incubated with specified concentrations of rh-Cat B or rh-Cat L with or without CA074 (10 µM) or Z-FY-CHO (10 µM) for indicated time durations. The stability of histone H3 was assessed by western blotting. Arrow and asterisk indicate rh-Cat B and rh-Cat L cleaved histone H3 fragments, respectively.

4.6 Discussion

4.6.1 Lipid peroxidation of lysosomal membrane initiates ferroptotic cell death

Our study confirmed the widely accepted role of lipid peroxidation as an important player in completion of ferroptotic cell death; however, the specific cellular compartment of lipid peroxidation and its consequences are controversially debated (Feng and Stockwell, 2018). Previously, the involvement of STAT3 in suppression of ferroptosis by inhibition of ACSL4 has been identified as a therapeutic target in cancer treatment (Brown et al., 2017). STAT3 is an important signaling system in regulation of many vital activities including cell proliferation, inflammation, apoptosis as well as immune system, and therefore inhibition or activation of this system can cause widespread effects (Johnston and Grandis, 2011; Hillmer et al., 2016).

In this study we have further uncovered the cellular and molecular mechanisms in ferroptosis and show that lipid peroxidation of lysosomal membrane in ferroptosis triggers the release of catalytic CTSB, which further damages mitochondrial membrane and promotes cell death. Specific inhibition or genetic deletion of this cysteine protease robustly prevented ferroptotic cell death. Using HT22 immortalized neurons, primary cultures mouse embryonic fibroblasts and NIH3T3 mouse fibroblasts and the standard cellular model of GPX4 deletion in Pfa1 cells, we show that the involvement of CTSB in execution of ferroptotic cell death is not a cell specific phenomenon. The protective role of CTSB in cell protection and aggressiveness of cancer cells has been previously shown (Reinheckel et al., 2012). Additionally, the increasing evidence in implication of glutamate toxicity/oxytosis or ferroptosis in neurodegenerative diseases (Cong et al., 2019; Derry et al., 2019) and neurotrauma (Guan et al., 2019; Yao et al., 2019), demonstrate the suitability of CTSB for therapeutic purposes in these diseases. In our study the protection offered by CA074-me resulted in better lysosomal and mitochondrial membrane integrity, as shown by

decreased membrane damage and cytoplasmic leakage of lysosomal enzymes and mitochondrial proteins resulting in better energy preservation in mitochondria. The requirement of mitochondria for induction of ferroptosis is debated, as few reports had shown an increase in ΔΨm with ferroptosis induction (Gao et al., 2019), while others have noticed a decline (Neitemeier et al., 2017). In the present study, we observed that inhibition of CTSB activity attenuates the decrease in ΔΨm mediated by ferroptosis. Furthermore, inhibition of CTSB was able to inhibit the translocation of AIF from mitochondria to cytosol /nucleus. These results imply that LMP precedes and mediates structural damage in mitochondria, either through CTSB leakage or excessive ROS generation after lysosomal damage.

Mitochondrial membrane damage is a distinguishing feature of ferroptosis in comparison with other forms of regulated cell death (Dixon et al., 2012). Accordingly, we observed that mitochondrial damage in glutamate toxicity is associated with VDAC1 oligomerization and formation of mitochondrial outer membrane pore leading to release of cytochrome C and AIF into the cytoplasm in HT22 cells. Administration of DIDS, an inhibitor of VDAC1, can prevent VDAC1 oligomerization. Using non-reducing gel electrophoresis and chemical cross-linking, we provide evidence of oxidation of VDAC1 in this process as evident by the appearance of a shorter VDAC1-positive band (~30 kDa) representing intramolecular oxidized form. Application of CA074-me prevented formation of this oxidized form, indicating decreased oxidative stress and prevention of mitochondrial membrane damage. Although previous reports have shown that VDAC1 is not a direct target of erastin toxicity unlike VDAC2/3 (Xie et al., 2016), its oligomerization can be considered as a marker of mitochondrial membrane damage in ferroptosis. A seemingly contradictory cell protective role for VDAC1 has been shown in cancer cells; under hypoxic condition, a microfusion of lysosome with mitochondria generates a truncated form of

VDAC1 (VDAC1-ΔC ~25 kDa) by legumain, an endosomal asparaginyl endopeptidase (AEP) (Brahimi-Horn et al., 2015b; Brahimi-Horn et al., 2015a). Formation of this truncated form enhances cell survival for cancer cells in hypoxic conditions (Mazure, 2016). This truncated isoform VDAC1-ΔC has structural properties that are different from the 30 kDa oxidized form of VDAC1 in our experiments. These different isoforms of VDAC1 may imply differential roles for VDAC1 in different conditions.

Similar to previous report from our lab (Nagakannan and Eftekharpour, 2017b), under the oxidative stress conditions, we observed an apparent increase in the intermediate form of CTSL which is known as the cytosolic form of this potent protease. Interestingly, inhibition of CTSL or aspartate protease CTSD did not provide any protection. It has been shown that lack of CTSL in glioblastoma cells increases cellular sensitivity to apoptosis. This is mediated by upregulation of p53 and caspases transcription (Kenig et al., 2011). Inhibition of cysteine uptake and induction of ferroptosis is also attributed to p53 mediated cell death (Jiang et al., 2015). Whether this implies a potential protective function for CTSL under oxidative stress conditions remains to be further examined.

4.6.2 Inhibition of ferroptosis by CTSB inhibitor is independent of glutathione and GPX4 levels

Cellular redox status is a determining factor in ferroptosis or oxytosis. Amongst the different cellular antioxidants only GSH system is well examined as GPX4 has been considered the main antioxidant protein capable of scavenging lipid hydroperoxides (Yang et al., 2014). In our study we provide evidence that despite significant loss of GSH and GPX4 after exposure to ferroptosis inducers, prevention of CTSB activation was sufficient to robustly prevent cell death. These data show that lysosomal damage and lipid peroxidation is downstream of GSH and GPX4 and its inhibition provides an alternative protection mechanism. The protection offered by CA074-me

against ferroptotic inducers was found to be independent of GSH and GPX4 system. Except in glutamate induced ferroptotic model, inhibition or knockout of CTSB did not affect the GSH levels in response to other ferroptosis inducers. Moreover, *ctsb*$^{-/-}$ cells were found to be resistant to GSH depletion (BSO) induced ferroptotic cell death further confirming GSH-independency.

The importance of cellular redox status in execution of ferroptosis has been recently further confirmed with the identification of ferroptosis suppressor protein-1 (FSP-1). This protein is an alternative electron donor system for scavenging lipid peroxide radicals by coenzyme Q (Bersuker et al., 2019; Doll et al., 2019). FSP-1 maintains the reduced form of coenzyme Q by providing reducing equivalents from NADPH.

4.6.3 Contribution of histone modification to induction of ferroptosis

A novel event in nuclear protein damage in ferroptotic cells as demonstrated by cleavage of histone H3 was uncovered in this study. Application of CA074-me in these studies prevented H3 cleavage, suggesting that CTSB can be the protease responsible for this event. To further validate our findings, we performed *in-vitro* histone H3 cleavage assay. Based on our fractionation results, it is evident that CTSB is significantly increased in the cytoplasm and hence we performed this assay at pH7.4, representing the pH of cytosol, which is relatively basic when compared to the pH of lysosomes. CTSL was able to digest H3 relatively faster compared to CTSB. In fact, while CTSL showed ~90% digestion of H3 in *in-vitro* nuclei preparation, CTSB showed a relatively less efficiency and exhibited a distinct cleavage pattern when compared to CTSL.

Histones are an integral part of chromatin and are divided into five major classes, histones H1, H2A, H2B, H3, and H4 (Kamakaka and Biggins, 2005). They are mainly involved in gene regulation which is in turn modulated by wide variety of post-translational modifications of histone proteins including acetylation, methylation, phosphorylation, ubiquitination, sumoylation and

ADP ribosylation (Kouzarides, 2007). Cleavage of histones, especially H3 has been reported in many cellular processes such as during cell cycle, senescence, mouse embryonic stem cell differentiation, infections, osteoclastogenesis, spermatogenesis, and sporulation (Mandal et al., 2012).

H3 cleavage at various amino acid sites has been shown to play a key role in gene activation. For example, matrix metalloproteinase-9 was shown to be necessary for clipping H3 tail near transcription start sites to induce its activation during osteoclast differentiation (Kim et al., 2016). Recently it was reported that under stress conditions that causes DNA damage, Cathepsin L-type protease JMJD5 (a Jumonji C domain-containing protein) mediates the proteolytic cleavage of H3 suggesting a possible role for H3 cleavage in gene regulation (Shen et al., 2017). CTSL was also shown to cleave H3 during mouse embryonic stem cell differentiation and oncogene induced cellular senescence (Duncan et al., 2008; Duarte et al., 2014; Vossaert et al., 2014). Similarly, another lysosomal cathepsin CTSD caused proteolytic cleavage of H3 at its amino terminal during mammary gland involution (Khalkhali-Ellis et al., 2014). These literature evidences indicate the active involvement of lysosomal cathepsins in regulation of histone modifications, however there is no previous report showing CTSB as a histone protease in any cell death model. Notably, in this model of ferroptotic cell death CTSB induced cleavage of H3 is in a different fashion than CTSL; however, the implication and the biological significance of CTSB mediated H3 cleavage is yet to be known and requires further exploration.

In conclusion, we have shown that lysosomal membrane permeabilization and cytoplasmic spillage of CTSB is a major cause of cell death in ferroptosis. Inhibition of CTSB in different cellular models of ferroptosis effectively prevented cell death and this was independent of changes in the GSH/GPX4 axis.

4.7 Supplementary Materials

4.7.1 Supplementary Figures

Supplementary Figure 4.1. Effect of ferroptosis induction on caspase-3 activation in HT22 cells.

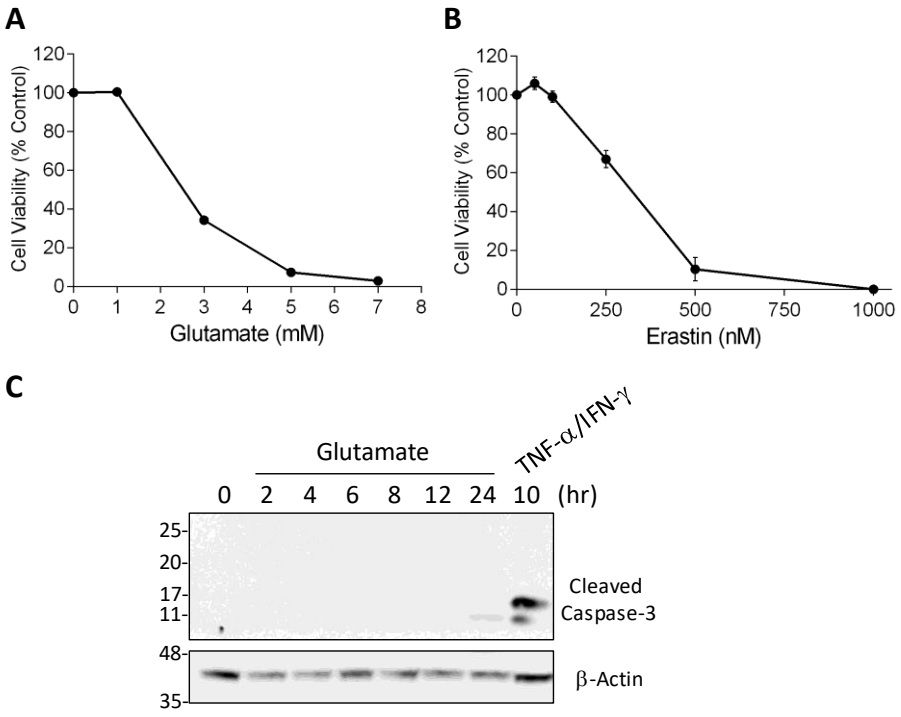

Supplementary Figure 4.1. Effect of ferroptosis induction on caspase-3 activation in HT22 cells. Cytotoxicity of **(A)** glutamate or **(B)** erastin in HT22 cells is shown (12 hr treatment). Values are expressed as mean ± S.E.M. of averages from n=4 (glutamate) and n=3 (erastin) independent experiments. **(C)** HT22 cells were incubated with glutamate (5 mM) or TNF-α (20 ng/ml) and IFN-γ (20ng/ml) for the indicated time durations and the cell extracts were prepared for western blotting of caspase-3 and β-actin. Although HT22 cells are derived from mouse hippocampus, these cells lack ionotropic receptors. Hence, glutamate at mM concentrations inhibits of cysteine transporter x_c^- leading to the depletion of GSH resulting in the induction of ferroptosis. TNF-α/IFN-γ treatment was used as a positive control for induction of caspase activation.

Supplementary Figure 4.2. Glutamate and erastin induce VDAC1 oligomerization.

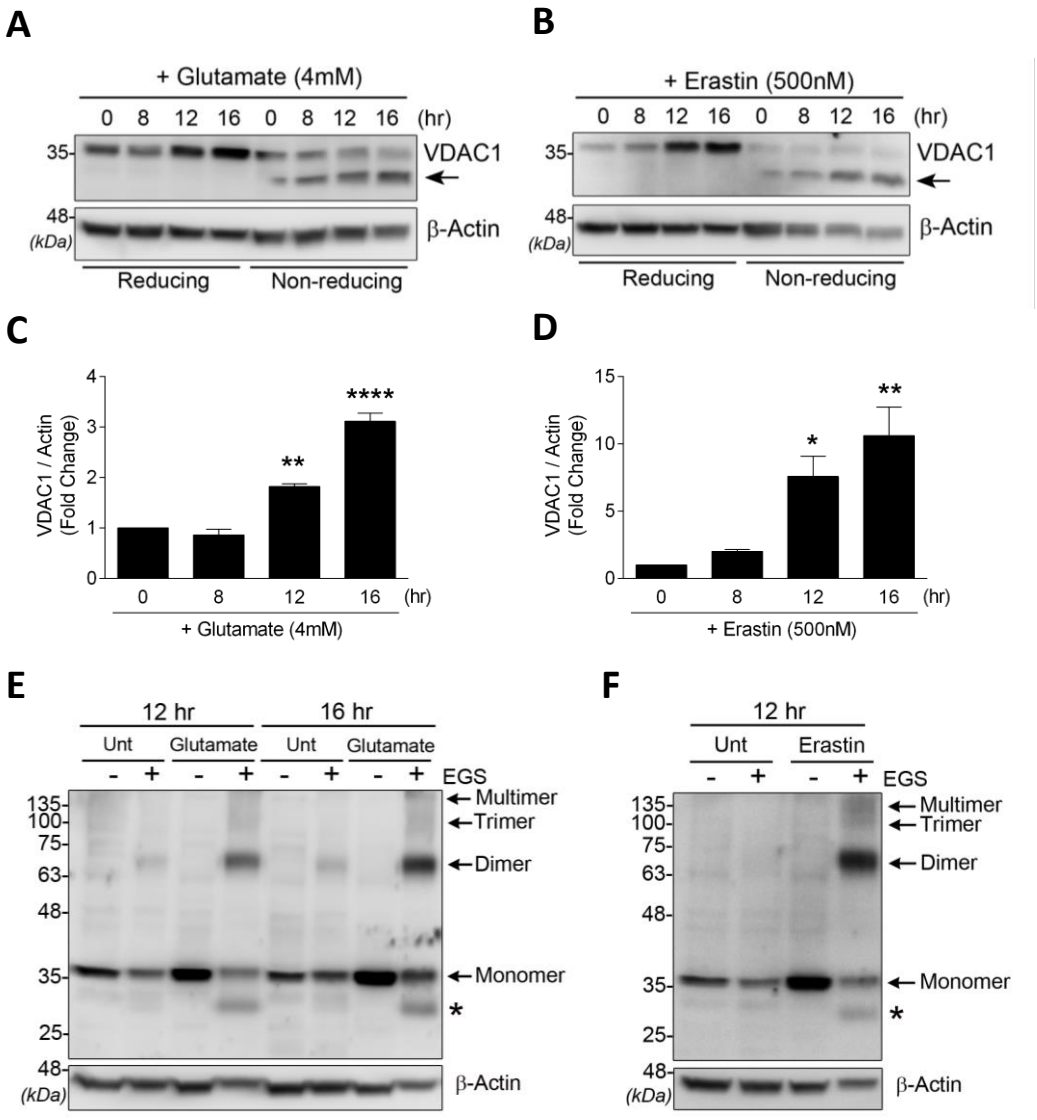

Supplementary Figure 4.2. Glutamate and erastin induce VDAC1 oligomerization. HT22 cells were incubated with (**A**) 4 mM glutamate or (**B**) 500 nM erastin for the indicated time periods and the cell lysates were subjected to SDS-PAGE under reducing and non-reducing conditions and assessed for the expression of VDAC1 protein. Representative western blots are shown in **A** and **B** with corresponding densitometric analysis of VDAC1 (in reducing SDS-PAGE) normalized to β-actin shown in **C** and **D**. Values are expressed as mean ± S.E.M. of averages form n=3 independent experiments, *p<0.05, **p<0.01 and ****p<0.0001. Arrows indicate the faster

migrating monomeric form of VDAC1 band with possible oxidative modification. **(E and F)** HT22 cells were treated with (**E**) 4mM glutamate or (**F**) 500nM erastin for indicated time periods and the cells were harvested and incubated at 30°C for 20 min in the presence or absence of EGS to cross-link the proteins and subjected to western blotting to assess the oligomeric status of VDAC1. Note the multifold increase in dimer, trimer and multimeric forms of VDAC1 in glutamate and erastin treated samples when compared to untreated cells. Asterisk indicates the intra-molecular cross-linked bands. Representative blots are shown here; similar results were observed in two independent experiment

Supplementary Figure 4.3. Cathepsin B inhibitor mitigates ferroptosis in HT22 cells

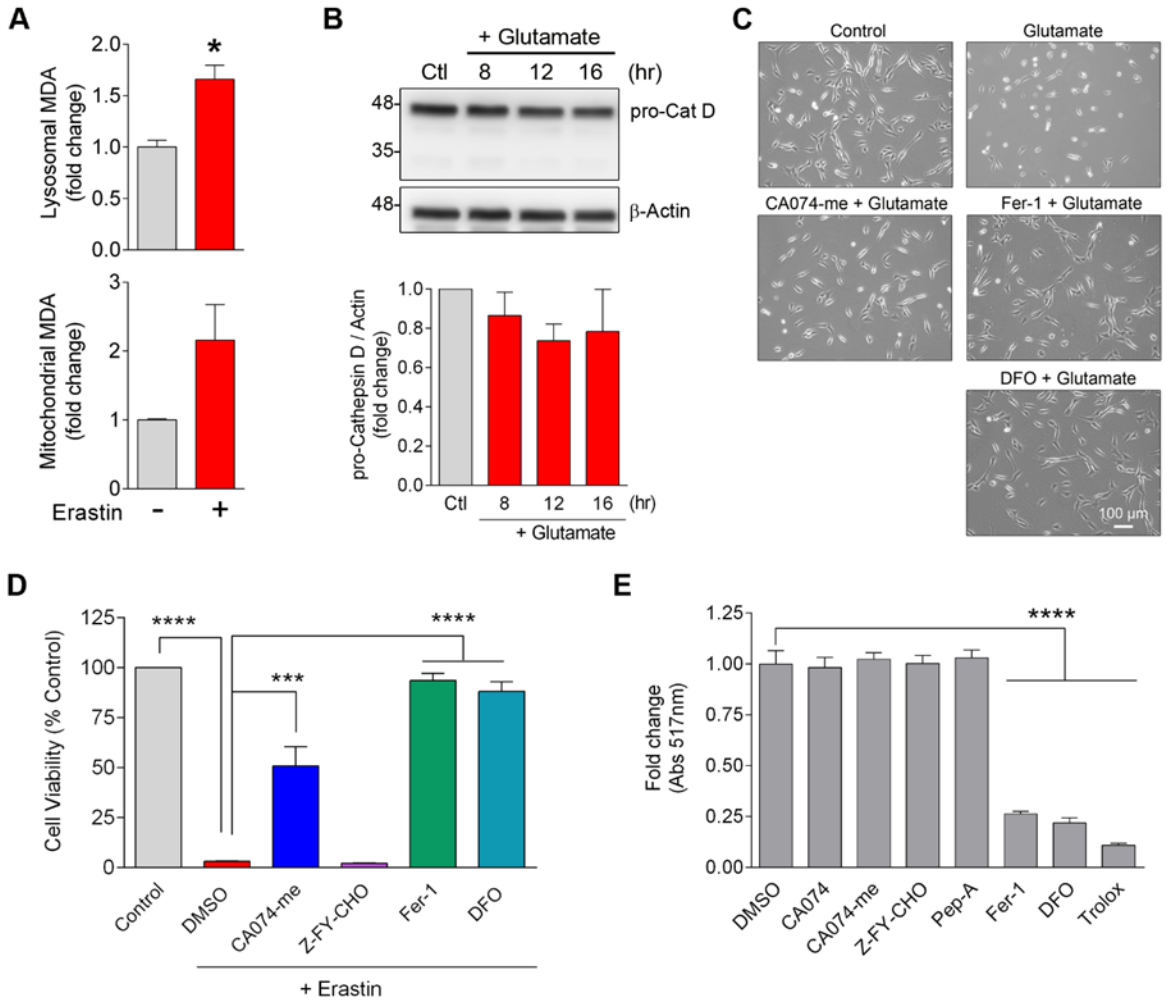

Supplementary Figure 4.3. Cathepsin B inhibitor mitigates ferroptosis in HT22 cells. (A) NIH3T3 cells were treated with erastin (3 μM) for 8 hr and were subjected to subcellular fractionation. The MDA content in isolated lysosomal and mitochondrial fractions were determined by fluorometric method. The bars in graphs indicate mean ± S.E.M. of averages from n=2 independent experiments, *p < 0.05 by unpaired two-tailed *t*-test. **(B)** HT22 cells were exposed to glutamate (4 mM) for indicated time durations and the cell lysates were assessed for cathepsin D (Cat D) by western blotting. Densitometric quantification of Pro-Cat D normalized for β-Actin is shown. The bars in graphs indicate mean ± S.E.M. of averages from n=3 independent

experiments. **(C)** Glutamate (4 mM, 12 hr) caused shrinkage and rounding-off of HT22 cells; inhibition of cathepsin B with CA074-me preserved the morphology, an effect comparable with Fer-1 and DFO treated HT22 cells exposed to glutamate. **(D)** HT22 cells were pretreated for 3 hr with CA074-me (15 μM) or Z-FY-CHO (10 μM) prior to exposure to erastin (0.5 μM) for 12 hr except for Fer-1 (2 μM) or DFO (50 μM), which were added simultaneously along with erastin. Cell viability was determined by CCK-8 assay. The bars in graphs indicate mean ± S.E.M. of averages from n=3 independent experiments. ***$p<0.001$ and ****$p<0.0001$ by one-way ANOVA followed by Tukey's post-hoc test. **(E)** Intrinsic antioxidant activity of the inhibitors was examined using stable DPPH free radical scavenging assay. All the compounds were tested at a final concentration of 50 μM. Bars indicate mean ± S.E.M. of n=3 replicates. Similar results were obtained from four independent experiments. ****$p<0.0001$ by one-way ANOVA followed by Dunnett's post-hoc test.

Supplementary Figure 4.4. Effect of CA074-me and standard ferroptosis inhibitors on glutamate induced changes in autophagy markers, Bcl-2 and mitochondrial transition pore formation in HT22 cells

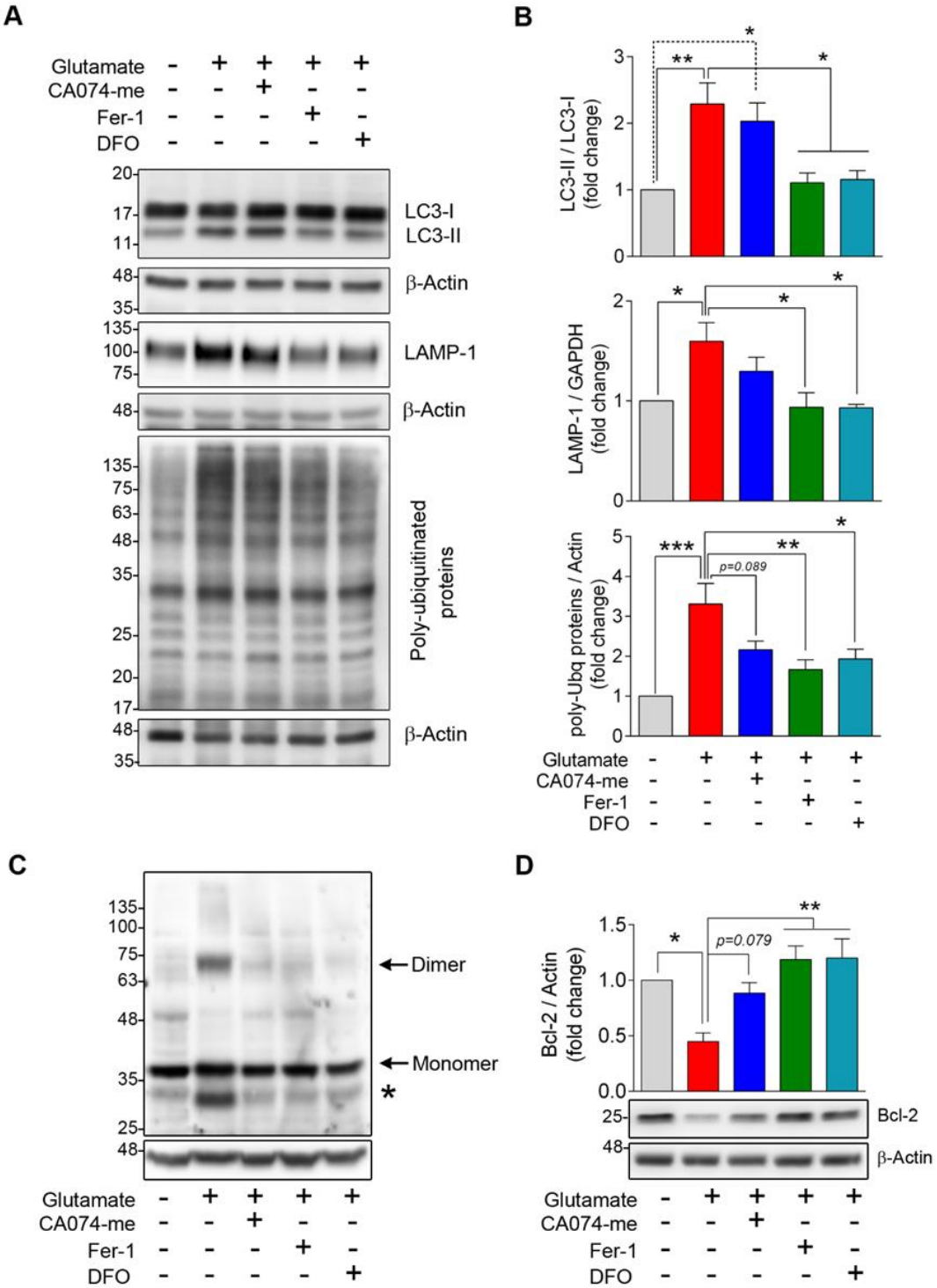

Supplementary Figure 4.4. Effect of CA074-me and standard ferroptosis inhibitors on glutamate induced changes in autophagy markers, Bcl-2 and mitochondrial transition pore formation in HT22 cells (A) HT22 cells were pretreated for 3 hr with CA074-me (15 μM) prior to exposure to glutamate (4 mM) for 12 hr except for Fer-1 (2 μM) or DFO (50 μM), which were added simultaneously along with glutamate. The samples were harvested at the termination of experiment and the cell lysates were subjected to western blot analysis. **(B)** Densitometric quantifications of proteins normalized to β-Actin are shown. The bars in graphs indicate mean ± S.E.M. of averages from n=3-5 independent experiments. *$p < 0.05$, **$p < 0.01$ and ***$p<0.001$ by one-way ANOVA followed by Tukey's post-hoc test. **(C)** HT22 cells were subjected to indicated treatment conditions for 12 hr and the cells were processed for chemical cross-linking with EGS and subjected to SDS-PAGE. Arrow indicates VDAC1 dimer and asterisk indicates intra-molecular cross-linked VDAC1 band. **(D)** Representative western blot and densitometric quantification of Bcl-2 in lysates obtained from HT22 cells subjected to specified treatment conditions are shown. Bars indicate mean ± S.E.M. of averages from n=4 independent experiments. *$p < 0.05$ and **$p < 0.01$ by one-way ANOVA followed by Tukey's post-hoc test.

Supplementary Figure 4.5. Inhibition of VDAC1 abrogates glutamate induced cell death in HT22 cells.

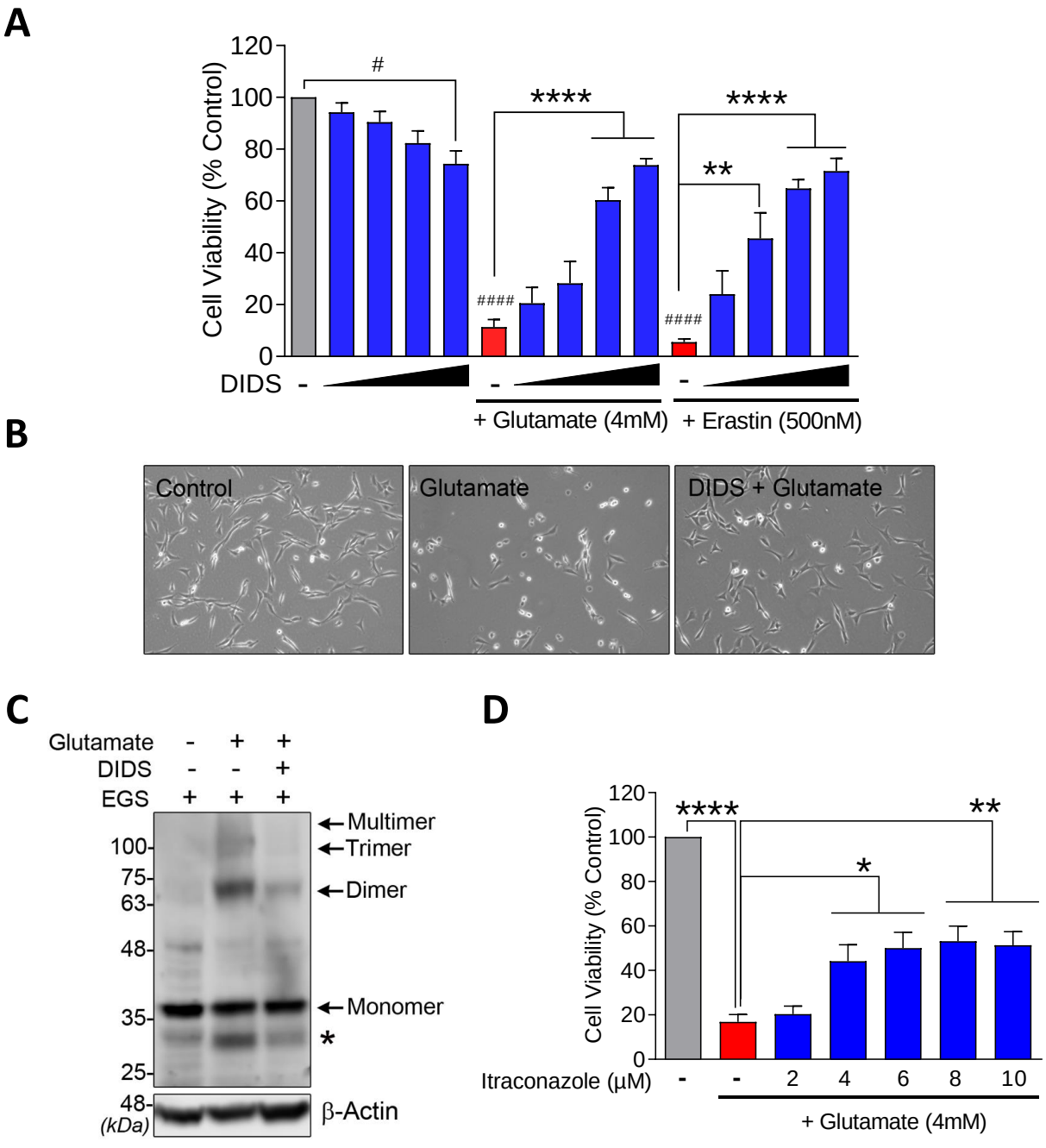

Supplementary Figure 4.5. Inhibition of VDAC1 abrogates glutamate induced cell death in HT22 cells. (**A**) HT22 cells were treated with either glutamate (4mM) or erastin (500nM) in the presence or absence of increasing concentrations of DIDS (50, 100, 200 and 300µM, indicated by black triangle) for 12 hr and cell survival was assessed using CCK-8 assay kit. Values are expressed as mean ± S.E.M. of averages from n=3-4 independent experiments, #p<0.01 and ####p<0.0001 vs. untreated control; **p<0.01 and ****p<0.0001 vs glutamate or erastin alone. (**B**) Bright field images showing the morphological changes (cell shrinkage) and cell loss induced by glutamate (for 12 hr) in HT22 cells; addition of DIDS (250µM) markedly ameliorated the effects of glutamate and preserved the normal morphology of cells. **(C)** HT22 cells were treated with glutamate alone or in combination with DIDS (250µM) for 12 hr and the cells were processed for chemical cross-linking with EGS. DIDS treatment prominently decreased the levels of VDAC1 oligomers and intra-molecular cross-linked band (indicated by asterisk). **(D)** The effect of Itraconazole treatment on glutamate induced cytotoxicity is shown. Values are expressed as mean ± S.E.M. of averages from n=3 independent experiments, *p<0.01, **p<0.01 and ****p<0.0001.

Supplementary Figure 4.6. Effect of Cathepsin B deletion on ferroptosis induced autophagy in mouse embryonic fibroblasts

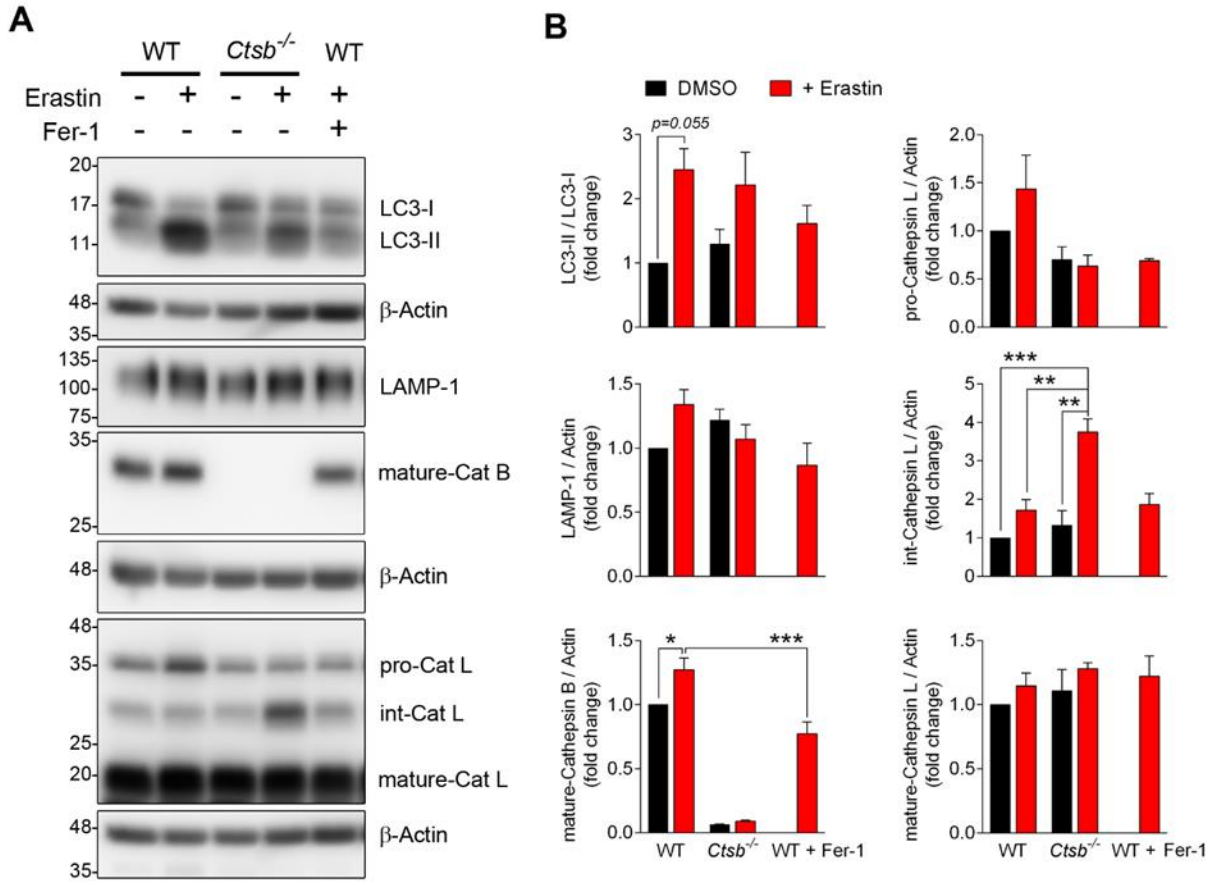

Supplementary Figure 4.6. Effect of Cathepsin B deletion on ferroptosis induced autophagy in mouse embryonic fibroblasts (A) WT and *Ctsb*$^{-/-}$ MEF cells were treated with erastin (5 µM) alone or in combination with Fer-1 (2 µM) for 12 hr and the cell lysates were subjected to western blotting for autophagic markers and cathepsins. Densitometric quantifications of proteins normalized to β-Actin are shown **(B)**. The bars in graphs indicate mean ± S.E.M. of averages from n=3 independent experiments. *p < 0.05, **p < 0.01 and ***p<0.001 by one-way ANOVA followed by Tukey's post-hoc test.

Supplementary Figure 4.7. Effect of cathepsin B inhibition / deletion on the status of glutathione synthesis machinery in ferroptosis.

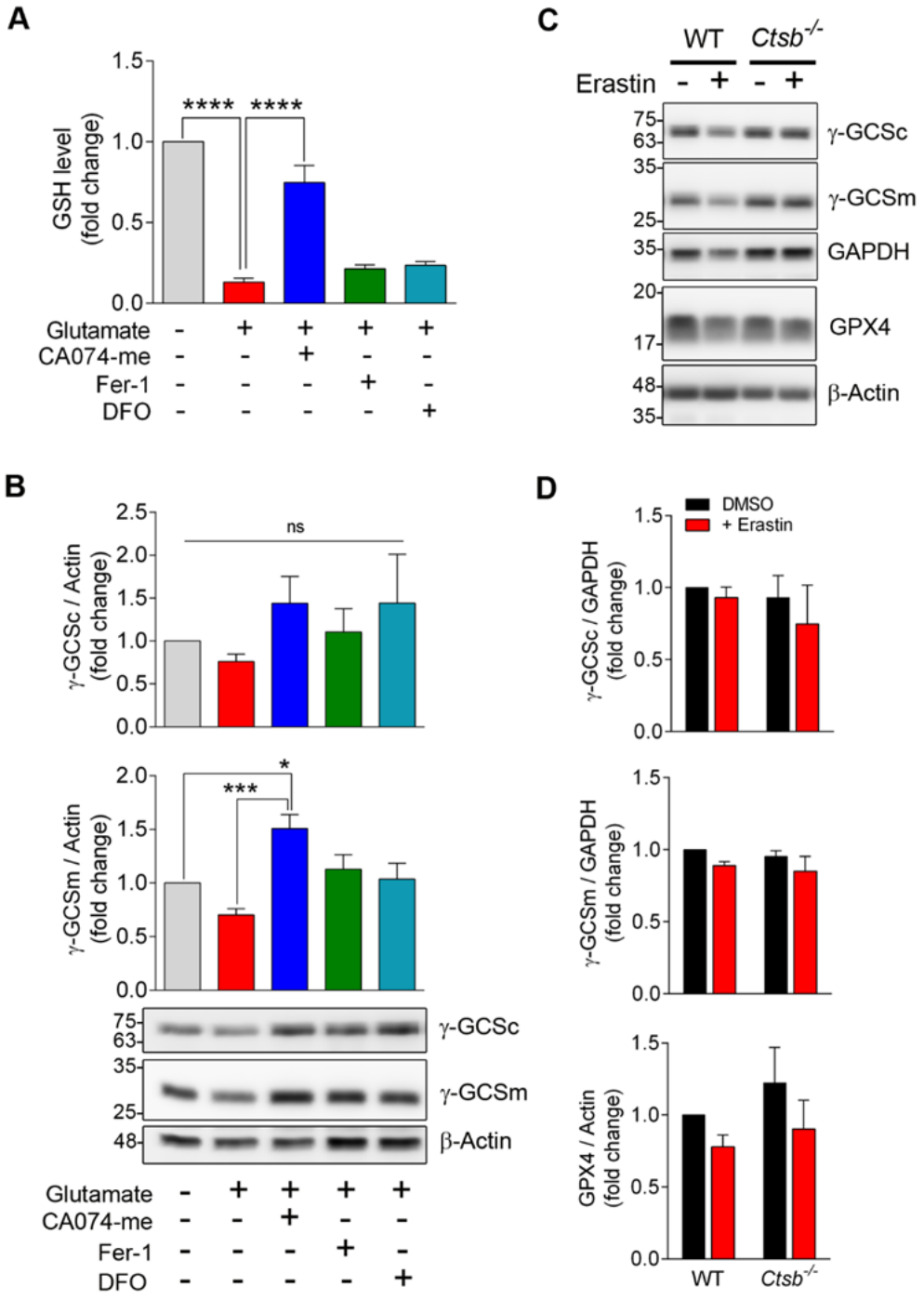

Supplementary Figure 4.7. Effect of cathepsin B inhibition / deletion on the status of glutathione synthesis machinery in ferroptosis. (A) HT22 cells were pretreated for 3 hr with CA074-me (15 μM) prior to exposure to glutamate (4 mM) for 12 hr except for Fer-1 (2 μM) or DFO (50 μM), which were added simultaneously along with glutamate. The Glutathione (GSH) content was determine by monochlorobimane method and the results are presented as bar graphs. Data represents mean ± S.E.M. of averages from n=3 independent experiments. ****p<0.0001 by one-way ANOVA followed by Tukey's post-hoc test. **(B)** Western blot analysis of HT22 cell lysates for γ-GCSc and γ-GCSm are shown. The bars indicate mean ± S.E.M. of averages from n=3-4 independent experiments. *p < 0.05 and ***p < 0.001 by one-way ANOVA followed by Tukey's post-hoc test. **(C)** WT and *Ctsb*$^{-/-}$ cells were treated with erastin (5 μM, 12 hr) and the cell lysates were subjected to western blotting. Densitometric quantifications of proteins normalized to loading controls are shown **(D)**. The bars indicate mean ± S.E.M. of averages from n=3 (γ-GCSc and γ-GCSm) and n=4 (GPX4) independent experiments.

Supplementary Figure 4.8. GPX4 disruption induces autophagy flux.

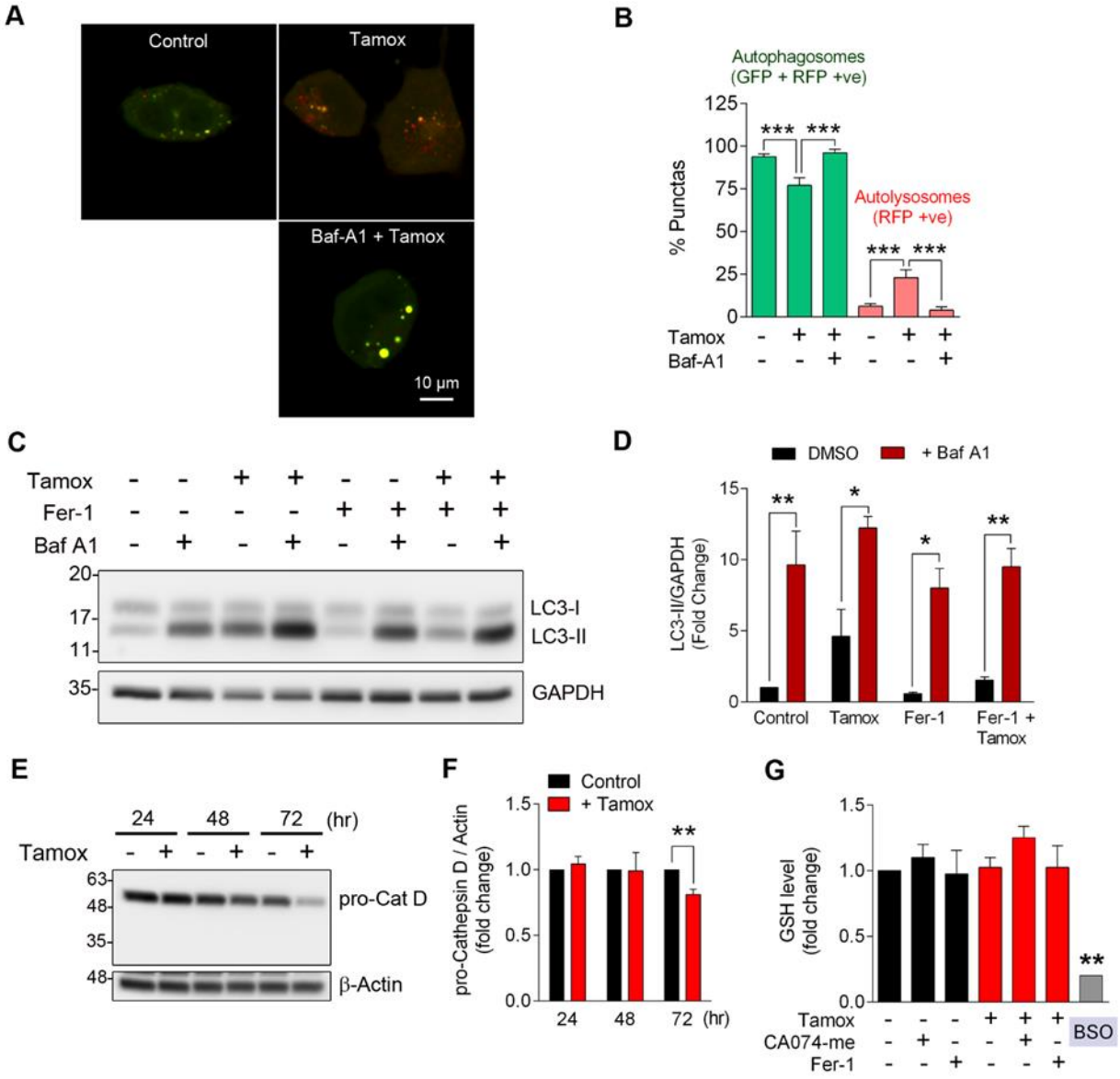

Supplementary Figure 4.8. GPX4 disruption induces autophagy flux. (A) Pfa1 cells induced for GPX4 deletion were transduced with Premo^{TM} Autophagy Tandem Sensor during the last 16 hr of the treatment. 48 hr after GPX4 knockout induction, the cells were imaged on a confocal microscope. The number of GFP + RFP positive (autophagosomes) and RFP alone (autolysosomes) punctas per cell were counted and the percentage of each is presented. Bafilomycin A1 (Baf A1, 25 nM) was added to the cells 4 hr prior to imaging. Mean ± S.E.M. of percentages of punctas is shown **(B)**. ***p<0.001 by ANOVA followed by Tukey's post-hoc test. Similar results were obtained from three independent experiments. **(C)** Pfa1 cells were treated as indicated and bafilomycin A1 (Baf A1, 25 nM) was added to the cells 4 hr prior to sample harvesting. The cells were harvested 48 hr after GPX4 knockout induction and the cell lysates were subjected to western blotting. Densitometric quantifications of LC3-II normalized to GAPDH is shown **(D)**. The bars indicate mean ± S.E.M. of averages from n=4 independent experiments. *p < 0.05, and **p<0.01 by one-way ANOVA followed by Tukey's post-hoc test. **(E)** Pfa1 cells were harvested at indicated time points after induction of GPX4 disruption with Tamox (1 μM). The cell lysates were subjected to western blotting for Cathepsin D (Cat D). Densitometric analysis of Pro-Cat D normalized to β-Actin is shown as fold change **(F)**. The bars indicate mean ± S.E.M. of averages from n=4 independent experiments. **p < 0.01 by unpaired two-tailed *t*-test. **(G)** ***CA074-me inhibits GPX4 deletion induced ferroptosis in a GSH independent manner.*** GPX4 was disrupted in Pfa1 cells by Tamox (1 μM) treatment and the inhibitors were added 24 hr post knockout induction. Glutathione (GSH) content in cell lysates were determined by fluorometric method 48 hr after GPX4 knockout induction. BSO (10 μM, 24 hr) was used as positive control to deplete GSH in Pfa1 cells. The bars indicate mean ± S.E.M. of averages from n=2-4 independent experiments. **p < 0.01 by one-way ANOVA followed by Tukey's post-hoc test.

Supplementary Figure 4.9. Status of Trx and TrxR in ferroptotic cells.

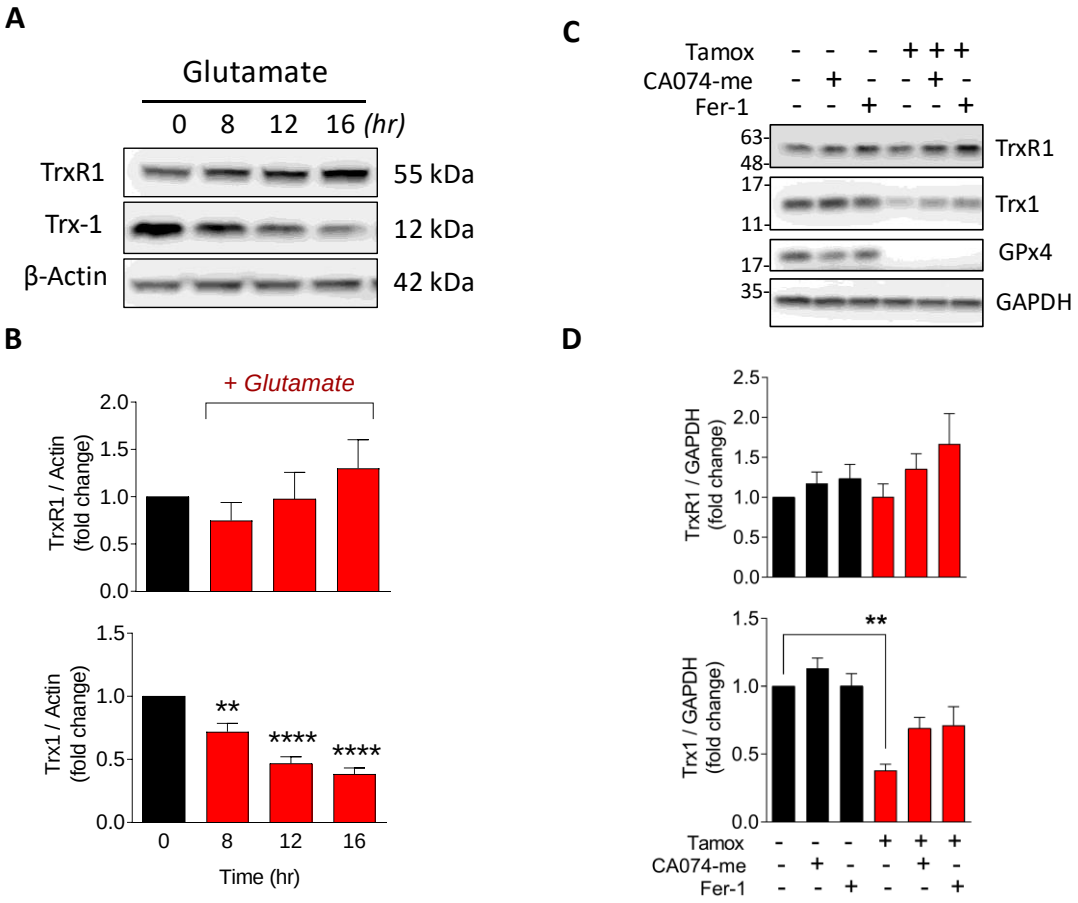

Supplementary Figure 4.9. Status of Trx and TrxR in ferroptotic cells. (A) HT22 cells were exposed to glutamate (4 mM) for indicated time durations and the cell extracts were assessed for Trx1 and TrxR1 by western blotting. **(B)** Densitometric quantification of proteins normalized for β-Actin is shown. The bars in graphs indicate mean ± S.E.M. of averages from n=4 independent experiments. **(C)** GPX4 was depleted in Pfa1 cells by Tamox (1 μM) treatment and the inhibitors were added 24 hr post knockout induction. The cells were harvested at 60 hr after knockout induction and the cell extracts were assessed for the status of Trx1 and TrxR1 by western blotting. **(D)** The bars indicate mean ± S.E.M. of averages from n=3 independent experiments. **p < 0.01 by one-way ANOVA followed by Tukey's post-hoc test.

Chapter 5

General Discussion

5.1 General overview of findings

The overall aim of this thesis was to identify and explore the molecular mechanism/s that contribute to lysosomal dysfunction in oxidative stress induced cell death mechanisms. This thesis demonstrates that inactivation of antioxidant systems as shown by inhibition of Trx system or depletion of glutathione leads to release of lysosomal enzymes resulting in initiation of programed cell death. Specifically, CTSB was identified as an executioner in mediating both apoptotic and non-apoptotic cell death mechanisms in response to aggravated oxidative stress.

5.2 Aggravated oxidative stress impairs autophagy and induces apoptosis

In normal autophagy, a basal level of reactive oxygen species (ROS) is required; however, excessive accumulation of ROS can impair autophagy and cause apoptosis through oxidation of key signaling molecules (Marino et al., 2014). Lysosomes are integral part of the autophagic process and plays a key role in the autophagic turnover of the cargo, any damage to the lysosomes and its components can impact the autophagic process and induce cell death (Boya and Kroemer, 2008). Thioredoxin (Trx) is an antioxidant protein with a unique ability to rescue the oxidized proteins and rejuvenate their functions (Spector et al., 1988b; Fernando et al., 1992). Trx is found in all cells and is upregulated under stress conditions such as ischemia, indicating its potential protective effects. The protective role of Trx is mediated through its ability to donate electrons to its substrates but becomes oxidized in this process and is no longer functional. The oxidized Trx is reduced by Trx Reductase (TrxR). Therefore, Trx and TrxR play a central role in management of oxidative stress and inhibition of either Trx or TrxR leads to accumulation of ROS (Holmgren and Lu, 2010).

To explore the possible involvement of Trx system in autophagy to apoptosis transition, I used the classical model of serum starvation to induce autophagy. Although autophagy is induced during

the early hours of starvation, extended period of nutrient deprivation results in apoptotic cell death (Maiuri et al., 2007a). Interestingly, an early increase in TrxR enzymatic activity was observed, which was inactivated at later time points of starvation despite upregulated proteins levels. It is possible that TrxR was inactivated due to oxidation or non-availability of its electron donor NADPH, since serum starvation can cause a decrease in NADPH/$NADP^+$ ratio (Tian et al., 1998). This observation led us to hypothesize that inactivation of Trx system might be acting as a trigger to induce apoptosis due to severe oxidative damage to cellular macromolecules and organelles.

To explore the impact of aggravated oxidative stress due to dysfunctional antioxidant defense system on the autophagic process, I employed both pharmacological inhibition (using auranofin, Au) and genetic downregulation of TrxR. Redox western blot analysis confirmed that Trx was oxidized and dysfunctional after TrxR deficiency. My results indicate that loss of TrxR activity led to blockade of autophagic flux and proteasome system accompanied by enhanced apoptosis. These changes could be significantly prevented when a cysteine-based antioxidant like NAC was added along with the Au confirming the role of oxidative stress in the transition from autophagy to apoptosis. Both impaired and excessive autophagy can cause cell death (Bialik et al., 2018). Since in my study, I found that inhibition or downregulation of TrxR led to decrease in autophagic progression and accumulation of autophagic cargo proteins, it is obvious of the former scenario. Autophagy can delay apoptosis by sustaining the energy supply to aid cellular repair and survival. For instance, several studies have shown that autophagy can delay the activation of apoptosis by supporting the DNA repair system such as PARP-1 and inhibition of autophagy impaired DNA repair and enhanced cell death (Abedin et al., 2007; Yoon et al., 2012; Hayes et al., 2017). In accordance with these reports, in the current study I observed that genetic or pharmacological interruption of autophagy enhanced apoptotic cell death in nutritionally deprived cells.

Remarkably, deficiency of TrxR further augmented the induction of cell death in starving cells where autophagy was disrupted. On further exploration of the underlying mechanisms, I identified that loss of TrxR activity caused impairment in lysosomal functions in terms of proteolytic ability (decreased DQ BSA degradation) and lysosomal acidity (decreased lysotracker staining). Using a stable oxidant tBHP, I demonstrated the impact of increasing oxidative stress on autophagy to apoptosis transition, where severe accumulation of autophagic cargo (p62) was associated with multifold activation of caspase 3. Taken together, these observations from chapter 2 clearly demonstrate that excessive oxidative stress impairs the pro-survival autophagic process with a possible impairment of lysosomal degradative functions leading to apoptotic cell death.

5.3 Oxidative stress differentially modulates the lysosomal cysteine cathepsins

Oxidative stress can affect the cellular homeostasis in several ways. Accumulation of ROS can oxidatively modify the cellular macromolecules, especially proteins, affecting their structural and/or functional integrity. The oxidative inactivation of essential proteins may lead to defective or blockade of the essential intracellular processes. In addition, severely oxidized proteins can also form aggregates and impair the cellular functions (Dahl et al., 2015). In either scenario, the cells experience an overload of oxidative stress leading to cell death. For instance, oxidative inactivation of several mitochondrial proteins was shown to cause mitochondrial dysfunction and signals cell death and organ damage (Moon et al., 2008). Notably, oxidative inactivation of ATP synthase was shown to cause severe energy depletion (Comelli et al., 1998). Similarly, ROS induced misfolding and aggregation of SOD1 is a well-known hallmark of amyotrophic lateral sclerosis (ALS) (Rakhit et al., 2002).

The key protein in autophagosome biogenesis ATG4 is well documented to be redox sensitive and Trx plays a crucial role in its redox control (Perez-Perez et al., 2014; Perez-Perez et al., 2016).

However, since I observed an impairment in the proteolytic ability of lysosomes (Chapter 2), I hypothesized that lysosomal deficiency and enhanced apoptosis in response to inhibition of TrxR could be due to oxidative inactivation of redox sensitive lysosomal hydrolytic enzymes. Moreover, intra-lysosomal pH plays a key role in facilitating the lysosomal proteolysis of the autophagic cargo since most of the lysosomal enzymes require an acidic pH to be active (Mindell, 2012). In the current study (Chapter 3), using acridine orange staining I observed that inhibition of TrxR caused a marked decrease in acidic lysosomes, which was associated with a corresponding increase in the cytosolic accumulation of the fluorogenic dye. The decrease in lysosomal acidity can result from either actual decrease in intra-lysosomal pH due to dysfunctional lysosomal acidification mechanisms including proton-pump V-type ATPase or loss of lysosomal membrane integrity (Porter et al., 2013; Colacurcio and Nixon, 2016; Song et al., 2017). Although I did not check the status of lysosomal acidification mechanisms, immunostaining for lysosomal membrane marker LAMP2 and lysosomal enzyme cathepsin B showed leakage of lysosomal contents into the cytosol. These observations strongly suggested that lysosomal membrane permeabilization (LMP) is the possible cause for the impairment of lysosomal functions under oxidative stress conditions. However, on investigating the status of lysosomal cathepsins, a differential activation pattern of two cysteine cathepsins – cathepsin B (CTSB) and cathepsin L (CTSL) was detected. Despite no significant increase in the protein content, a dramatic multifold increase in the enzymatic activity of CTSB was observed. In contrast, CTSL showed a delayed increase in activity in spite of significantly upregulated protein levels. On further exploration, a redox dependent inactivation of CTSL was discovered. Using thiol trapping technique, I demonstrated that maturation of CTSL was blocked by uncontrolled ROS accumulation due to the inhibition of TrxR. This led to the inactivation of CTSL during the early hours of starvation, where autophagy is predominantly

induced and requires CTSL in its active state as previous reports have shown the pro-autophagic functions of CTSL (Sun et al., 2013; Wei et al., 2013). In contrast, no such oxidative modification of CTSB was observed.

CTSB and CTSL belong to the class of cysteine proteases, which contains cysteine–histidine–asparagine at their active site. Both the enzymes are synthesized as inactive precursors (or zymogens) containing regulatory prodomain/propeptide and catalytic mature domain. The propeptide hinders the substrates from accessing the active site in the mature domain to prevent unwanted protein degradation. This propeptide is removed by either auto-cleavage (auto-activation) or by other proteases (Coulombe et al., 1996; Verma et al., 2016). Similar to the observations in this study, ROS induced oxidative inactivation of another cysteine cathepsin has been reported earlier. H_2O_2 was shown to inhibit the processing of pro-cathepsin K and inactivate the mature enzyme. However, this inactivation was attributed to the reversible oxidation of Cys25 (sulfenic acid formation) at the active site of cathepsin K (Godat et al., 2008). Though CTSB and CTSL contain similar number of cysteine groups in their structure, surprisingly CTSL does not contain any cysteine residue in its propeptide. However, the number of methionine residues is more abundant in CTSL (8/96) propeptide when compared to CTSB (2/69) (Chapter 3). Thiol amino acids such as cysteine and methionine are highly susceptible to oxidative modifications (Hoshi and Heinemann, 2001a). Since the processing of pro-CTSL was blocked under oxidative stress condition, it seems logical that oxidative modification of methionine could have contributed to the inactivation of CTSL. Importantly, Trx system plays a key role in maintaining the reduced state of methionine by redox recycling of methionine sulfoxide reductase enzyme, which reduces the oxidized methionine (methionine sulfoxide) to reduced methionine (Reeg and Grune, 2015). Another important factor governing the activity of CTSL is the pH of the cytosolic compartment.

Though earlier reports suggested that mature CTSL is unstable and inactivated under neutral or alkaline pH due to irreversible denaturation of the proteins (Turk et al., 1993; Turk et al., 1999), recent reports have shown the presence of active variants of CTSL in cellular compartments with neutral and basic pH like cytosol and nucleus (Reiser et al., 2010; Tamhane et al., 2016). In accordance with these reports, in the present study, I observed a delayed upregulation of intermediate CTSL protein which corresponded with an increase in the enzymatic activity at 24 hr. Since mature CTSL protein level remained unchanged, the observed increase in the activity must be due to the intermediate CTSL. Previous reports have identified this intermediate CTSL as a cytosolic variant of CTSL which is devoid of lysosomal targeting sequence and is produced by alternative translation of CTSL mRNA (Sever et al., 2007). Taken together, it can be concluded that inhibition of TrxR interrupted the auto-activation of CTSL and inhibition of mature CTSL activity.

5.4 Cathepsin B mediates the apoptotic induction under uncontrolled oxidative stress

Under excessive oxidative stress, the lysosomal membrane integrity is weakened leading to the release of lysosomal contents into the cytosol, which can cause cytosolic acidification and proteolytic damage of cytosolic components resulting in cell death (Brunk et al., 1997; Boya and Kroemer, 2008). The major trigger for the induction of apoptosis is the lysosomal proteases such as cathepsins B, D and L. These proteases are known to cause proteolytic cleavage of several pro-survival factors like Bcl-2, Bcl-xl and Mcl-2 thereby enhancing the actions of pro-apoptotic proteins like Bax, Bad and Bak leading to mitochondrial damage and apoptosis (Droga-Mazovec et al., 2008; Brunelle and Letai, 2009). While screening for the cathepsin/s involved in cell death following serum starvation, I identified CTSB as the cell death inducer under TrxR deficiency induced aggravated oxidative stress condition (Chapter 3). In addition to causing mitochondrial

membrane damage and promoting cyto C release, CTSB has been shown to initiate the activation of caspase cascade indirectly through proteolytically degrading XIAP, the endogenous inhibitor of both initiator (caspase-9) and executioner (caspase-3/7) proteases (Guicciardi et al., 2000; Droga-Mazovec et al., 2008; Joy et al., 2010). In accordance with these previous reports, inhibition of CTSB using the chemical inhibitor CA074-me prevented the release of cyto C into the cytosol, activation of caspase-3 and subsequent cleavage of PARP-1. Importantly, CA074-me treatment also reduced the amount of cytosolic CTSB protein indicating preservation of lysosomal integrity. This is in agreement with previous reports showing that CTSB can cause further lysosomal permeabilization (Jacobson et al., 2013; Katsnelson et al., 2016).

Since CTSB is involved in the intra-lysosomal proteolysis, it was expected that inhibition of CTSB would lead to accumulation of proteins. In line, I noted that p62 protein levels were not reduced despite a significant decrease in LC3-II/LC3-I ratio following CA074-me treatment. In contrast, a decrease in the amount of poly-ubiquitinated proteins after CTSB inhibition was observed. This could be due to reduced oxidative stress as LMP and cathepsins can induce oxidative stress, which in turn can cause protein aggregation and accumulation of poly-ubiquitinated proteins (Ghosh et al., 2011; Manohar et al., 2019). In conclusion, this study demonstrates that CTSB mediates the autophagy to apoptosis transition due to excessive oxidative stress, which causes LMP resulting in interruption of autophagic process triggering apoptosis.

5.5 Role of lysosomal membrane damage in ferroptosis

Complementary studies in another model of a recently described cell death mechanism known as ferroptosis further highlights the importance of this thesis identifying CTSB as a major executioner of cell death. Ferroptosis is not a typical apoptotic cell death mechanism and is not prevented by inhibition of caspase pathway indicating a non-caspase dependent cell death mechanism (van

Leyen et al., 2005; Yang and Stockwell, 2008; Fukui et al., 2009; Dixon et al., 2012). In ferroptosis, inhibition of a cysteine transporter (system x_c^-) by erastin or glutamate causes depletion of GSH leading to the inactivation of several GSH dependent cellular processes (Dixon et al., 2012; Fujii et al., 2019). One of the important and crucial antioxidant enzymes affected due to GSH depletion is phospholipid hydroperoxidase GPX4, which reduces hydroperoxides in phospholipid and cholesterol molecules in the cellular membranes (Brigelius-Flohe, 1999; Imai and Nakagawa, 2003). Due to failure of GSH/GPX4 system, lipid molecules in both plasma and intra-cellular membranes undergo excessive lipid peroxidation leading to loss of membrane integrity and cell death (Fujii et al., 2019). Scavenging lipid hydroperoxides and increasing the intracellular GSH content has shown to inhibit ferroptotic cell death. In addition, since iron plays a crucial role in lipid peroxidation through Fenton reaction, iron chelators were also shown to be effective anti-ferroptotic agents (Hao et al., 2017; Conrad et al., 2018; Shah et al., 2018).

Previous reports have shown that lysosomal membrane lipids can be modified by several factors including cholesterol oxidation, degradation of sphingolipids and hydrolysis of phospholipids by phospholipases and can cause LMP and subsequently apoptosis or necrosis (Fong et al., 1973; Li et al., 1998; Wang et al., 2006; Ullio et al., 2012; Zhao et al., 2012). Remarkably, lysosomal membranes can also be permeabilized by the oxidative metabolites of polyunsaturated fatty acids (PUFA) and cholesterol, 4-HNE and oxysterols, respectively (Hughes et al., 1994; Hwang et al., 2008; Chen et al., 2016). Moreover, due to the degradation of several iron-containing macromolecules like ferritin and metallothioneins in the lysosomal compartment, lysosomes contain high amount of labile iron and hence are highly susceptible to iron mediated lipid peroxidation (Hahn et al., 2001; Terman and Kurz, 2013). Although several studies including my previous findings in Chapter 2 have shown that increasing oxidative stress can cause LMP and

result in various types of cell death like apoptosis, necrosis and pyroptosis, not much information is available on the status of lysosomal membrane integrity and the status of lysosomal protease in ferroptosis. In the current study (Chapter 4), I found that depletion of GSH was sufficient to induce lipid peroxidation of lysosomal membranes and translocation of lysosomal proteases CTSB and CTSL to cytosol indicating LMP. This observation was further confirmed by using tamoxifen inducible GPX4 deletion system, where both CTSB and CTSL were increased in cytosolic compartment and were found to be active. Addition of lipid radical scavenger ferrostatin and iron chelator deferoxamine markedly decreased lysosomal membrane lipid peroxidation, LMP and ferroptotic cell death. Although I did not investigate the effect of Trx depletion/inhibition on lysosomal lipid peroxidation, Trx was found to be depleted in ferroptotic cells in a time dependent manner in response to inhibition of cysteine import. This could be because of the non-availability of cysteine for Trx synthesis or possible degradation by certain proteases. However, recent reports have shown that Trx dependent peroxidase, peroxiredoxin 6 to play an important regulatory role in ferroptosis due to their lipid peroxidase functions (Zuo et al., 2018; Lu et al., 2019). This can be well correlated with the observation in chapter 3, where inactivation of Trx system caused severe LMP and cell death.

5.6 Cathepsin B acts as an executioner in ferroptotic cell death

On examining the status of cathepsins in ferroptosis, a time dependent induction of both CTSB and CTSL was noted. In contrast to the observations in chapter 3, where I noticed an impairment in CTSL enzymatic activity no such phenomenon was observed under ferroptotic conditions. This could be due to the differential induction of CTSL variants under diverse conditions. I observed upregulation of mature CTSL at the early time points and intermediate CTSL at later time points in response to TrxR inhibition in chapter 3. Whereas, under ferroptotic conditions such as erastin

induced GSH depletion or GPX4 deletion, a significant induction of intermediate CTSL variant was observed in a time dependent manner.

Though previous works have established an essential role for lysosomes in the progression of ferroptosis (Kubota et al., 2010; Torii et al., 2016; Villalpando-Rodriguez et al., 2019), the identity of the specific executionary protease/s remained elusive. Using small molecule inhibitor screening targeting different cathepsins, I identified CTSB as an executioner in ferroptotic cell death. Pharmacologic and genetic inhibition of CTSB was sufficient to preserve mitochondrial integrity and function as evidenced by decreased cyto C and AIF content in cytosol, improved ATP content and mitochondrial membrane potential. VDAC1 is known to form a major part of mitochondrial permeability transition pore (mPTP) complex along with adenine nucleotide translocator (ANT) and cyclophilin D facilitating the release of mitochondrial contents into cytosol (Shoshan-Barmatz and Mizrachi, 2012; Shoshan-Barmatz et al., 2013). Accordingly, inhibition of VDAC1 oligomerization using small molecule inhibitor can prevent the formation of mPTP and ferroptotic cell death (Nagakannan et al., 2019). In the present study, inhibition of CTSB was able to abrogate the formation of mPTP as shown by VDAC1 oligomerization assay. One of the endogenous inhibitors of VDAC1 oligomerization is Bcl-2, which is well characterized for its anti-apoptotic functions (Shimizu et al., 2000; Arbel et al., 2012). Additionally, a non-canonical role for Bcl-2 in ferroptosis has been suggested recently (Gascon et al., 2016; Lewerenz et al., 2018). I noticed a corresponding decrease in Bcl-2 protein levels with increase in VDAC1 oligomerization indicating that Bcl-2 degradation could be one of the triggers for mitochondrial damage in ferroptosis. Interestingly, inhibition of CTSB prevented the decrease in Bcl-2 and consistently inhibited VDAC1 oligomerization. Bcl-2 has been shown to be proteolytically degraded by number of lysosomal cathepsins. However, CTSB was unable to cleave Bcl-2 in an *in-vitro* system (Droga-

Mazovec et al., 2008). Based on these observations, it appears that CA074-me preserved Bcl-2 level by an indirect pathway. Once released into the cytosolic compartment, cyto C is known to initiate the caspase cascade and apoptosis. However, caspase activation has been shown to be very minimal in ferroptosis and moreover, inhibition of caspases was not able to inhibit ferroptotic cell death (Fukui et al., 2009; Dixon et al., 2012). In accordance with these previous observations, no significant induction of caspase-3 was observed in response to ferroptotic stimuli in the current study. Similarly, AIF was previously shown to mediate cell death after GPX4 ablation (Seiler et al., 2008), however recent studies have revealed that AIF does not participate in ferroptotic execution (Doll et al., 2019). Hence, the reduction in cytosolic cyto C and AIF after CTSB inhibition should be seen as a marker of better mitochondrial integrity and not as prevention of apoptotic pathway in ferroptotic model.

Importantly, similar to the observation in chapter 3, CA074-me treatment was able to improve lysosomal membrane integrity. A second line of evidence using primary fibroblasts derived from cathepsin B knockout (*Ctsb*$^{-/-}$) mice confirmed these above findings, where *Ctsb*$^{-/-}$ MEFs were found to be resistant to ferroptotic inducers such as erastin and BSO. In the same way, CTSB inhibition was able to promote cell survival and improve mitochondrial integrity in GPX4 deletion system affirming the executioner role of CTSB in ferroptosis.

5.7 Role of cathepsin B in degradation of autophagic cargo during ferroptotic cell death

Although autophagy is critical in maintaining cellular homeostasis thereby promoting cell survival, it can also promote cell death through excessive degradation of protective intracellular proteins. For example, during the late oogenesis of *Drosophila melanogaster*, autophagy degrades the anti-apoptotic protein dBruce thereby activating caspases resulting in nurse cell apoptosis (Nezis et al., 2010). Likewise, selective degradation of catalase by autophagy was shown to promote non-

apoptotic programmed cell death (Yu et al., 2006). In case of ferroptosis, autophagic degradation of ferritin, leads to excessive accumulation of intracellular labile iron facilitating lipid peroxidation. Since, autophagosomes/autolysosomes and lysosomes are the sites of ferritin degradation, these structures can act as a major controlling factor in generation of intracellular ROS due to increased intra-lysosomal iron content (Sakaida et al., 1990; Kubota et al., 2010; Quiles Del Rey and Mancias, 2019). Ferritin is selectively sequestered by the autophagic receptor NCOA4 and degraded through a process termed ferritinophagy. Genetic disruption of autophagic process has been demonstrated to prevent ferritin degradation and inhibit ferroptosis (Hou et al., 2016). Even though I have not examined the expression of ferritin after CTSB inhibition in the current study, it is possible that ferritinophagy is reduced as CTSB inhibition was efficient in reducing the extent of lipid peroxidation in both GSH depletion and GPX4 deletion induced ferroptotic models indicating reduced mobilization of intracellular iron. Lipid peroxidation can also be reduced if GSH content or GPX4 expression is increased. Moreover, recently chaperone mediated autophagy was shown to degrade GPX4 during ferroptosis (Wu et al., 2019). Although, an increase in GSH content in CA074-me treated cells was observed, this was not associated with any increase in GPX4 levels. In fact, GPX4 expression was further downregulated in cells where CTSB was inhibited. Furthermore, studies with *Ctsb*$^{-/-}$ MEFs and GPX4 knockout cells confirmed that the resistance towards ferroptotic cell death in CTSB deficient cells was independent of GSH. It is worth noting that CA074-me treatment induced a similar increase in GSH content after TrxR inactivation (Chapter 3), which is possibly due to the preservation of intracellular GSH synthesis machinery as observed in ferroptosis experiments.

5.8 Selective LMP in ferroptosis

Earlier reports have suggested that enlarged lysosomes are more susceptible to LMP (Ono et al., 2003), however, enlarged lysosomes were found to be active and functional in some cases as observed in Chediak–Higashi Syndrome (Holland et al., 2014). Loss of lysotracker staining is indicative of severe LMP as observed in chapter 2 and 3, nonetheless a previous report showed that lysotracker staining was maintained despite LMP that caused cell death by apoptosis indicating selective release of lysosomal enzymes into the cytosol (Bidere et al., 2003). In the present study, although LMP was evident after GPX4 deletion, interestingly, GPX4 deletion in Pfa1 cells caused enlargement of lysosomes which were still be labelled with lysotracker indicating maintained lysosome-cytosol pH gradient. These observations indicate GPX4 deletion causes ferroptotic cell death mediated by selective release of cathepsins, mainly cathepsin B.

5.9 Cathepsin B is a histone H3 protease

Histone proteins are involved in gene regulation and can be modulated through several post-translational modifications (Kouzarides, 2007). Similarly, cellular processes including senescence, embryonic stem cell differentiation and spermatogenesis have been reported to involve the proteolytic cleavage of histone, especially histone H3 (Mandal et al., 2012; Vossaert et al., 2014; Yi and Kim, 2018). Previously Duncan *et al*., had demonstrated that CTSL can cleave H3 protease during mouse embryonic stem cell differentiation. In the same study, CTSB was shown to cleave H3 in a differential pattern in an *in-vitro* setup (Duncan et al., 2008). However, no physiological or pathological relevance has been established yet for CTSB mediated H3 cleavage. In the current study, using multiple experimental approaches I have demonstrated that CTSB is a specific H3 protease in ferroptosis. Importantly, unlike CTSL, H3 is cleaved in a precise manner by CTSB, though the significance of this specific pattern of H3 cleavage is yet to be identified. However, in

the light of recent developments in the identification of several epigenetic changes during ferroptosis, the discovery of CTSB as a specific H3 protease in ferroptosis may advance the understanding of gene regulation in ferroptotic cell death. Notably, KDM3B, a histone H3 lysine 9 demethylase was shown to protect against erastin induced ferroptosis (Wang et al., 2020). However, these findings need to be validated in disease conditions where ferroptosis has been found to play a key regulatory role in the development and progression of the pathology.

Furthermore, although CTSL has been suggested to act as a pro-autophagic factor, CTSL can also induce cell death once translocated into the cytosolic compartment. For instance, CTSL has been shown to promote necrotic cell death by cleaving DNA topoisomerase I (Pacheco et al., 2005). Similarly, LMP followed by cytosolic translocation of CTSL was shown to mediate resveratrol induced apoptosis in cervical cancer cells (Hsu et al., 2009). Correlating our observations in this thesis with previous reports suggesting CTSL as a potent inducer of cell death suggests that preserved protease activity of CTSL inside the lysosomal compartment is the key to promote autophagy whereas, leakage of lysosomal cathepsins including CTSL into the cytosol is detrimental to cell survival based on the cytosolic substrates digested. In this regard, as observed in this thesis and elsewhere (Sever et al., 2007), intermediate CTSL (cytosolic variant) is active in the cytosolic compartment. However, the role of intermediate CTSL in autophagy and cell death mechanisms is yet to be determined.

5.10 Study limitations

One of the limitations of the study was the assessment of autophagic process. Since, the study was focused on the cell death mechanisms, only crucial steps of autophagy were assessed. However, the impact of inactivation of Trx system on autophagosome-lysosomal fusion was not thoroughly assessed. Oxidative stress can impact the transcription and translation of several proteins in

autophagy pathway (Fang et al., 2017; Kosztelnik et al., 2019). Hence, the impact of oxidative stress on the factors involved in autophagosome-lysosome fusion like Rubicon, UVRAG, SNARE complex and others needs to be investigated.

The role of mitochondrial damage is well characterized in apoptotic cell death. However, the role of mitochondria and its components in ferroptosis is still debated as both caspase-dependent and independent mediators of cell death from mitochondria (cyto C and AIF) are shown to have no significant contribution in the execution of ferroptotic cell death. However, few studies including the data presented in this thesis have demonstrated that preserving the mitochondrial membrane integrity could protect against ferroptosis (Krainz et al., 2016; Neitemeier et al., 2017; Nagakannan et al., 2019). This could be possibly due to preservation of ATP content or reduction in mitochondrial ROS generation, which could affect other organelles. Since the present study was focused on lysosomes and its effect on cell death mechanisms, the role of mitochondria on lysosomes was not assessed. Future studies investigating the crosstalk between mitochondria and other organelles especially lysosomes will further the understanding of executioner mechanisms in ferroptosis.

Another limitation of the study is about the assessment of lipid peroxidation in subcellular fractions. The extent of lipid peroxidation in the lysosomal and mitochondrial membranes was analyzed by measuring malondialdehyde (MDA) content in the respective organelle fractions. MDA is a stable end-product formed by peroxidation of PUFAs. Numerous reports have demonstrated that oxidative stress can increase MDA content in subcellular fractions like plasma membrane, mitochondria, nucleus, microsomes and cytosol (Reddy et al., 1999; Kula et al., 2002; Green et al., 2006; Yuan et al., 2016; Fang et al., 2019). However, since MDA is a water-soluble small molecule, it is possible that it can be released into the cytosolic fraction overtime, therefore

measurement of MDA content in membrane fractions can sometimes be misleading. Nevertheless, the findings presented in this thesis were complemented with the measurement of MDA content in whole cell lysates to account for any false positive interpretations. Hence, to get a clear understanding of membrane damage in ferroptosis, mass spectrometry-based analysis of lipids in subcellular organelles can be conducted in future.

An important limitation drawing caution to interpretation of these results is the sole employment of cell lines and primary MEF cells and lack of confirmation in primary cultures or animal models. CTSB has shown both damaging and protective effects in different models. The damaging effects of CTSB refer to its cell death execution in several *in-vivo* models of tissue injury like traumatic brain injury (Luo et al., 2010), experimental stroke (Zuo et al., 2018) and hepatic ischemia (Baskin-Bey et al., 2005). The contribution of oxidative stress and the involvement of CTSB in these studies support our findings. Few studies have shown some neuroprotective effects for CTSB; for instance, modulation of Receptor Protein Tyrosine Phosphatase σ was demonstrated to promote axonal outgrowth after spinal cord injury by enhancing the secretion of CTSB. The secreted CSTB was shown to degrade chondroitin sulfate proteoglycan (CSPG), an extracellular component that inhibits axon regeneration (Tran et al., 2018). These reports indicate possible differential function/s for intracellular and extracellular CTSB in cell survival. Further studies using relevant animal models may shed more light on the differential effects of intracellular vs extracellular CTSB in normal and disease conditions.

5.11 Future directions

The findings presented in this thesis highlights the importance of cellular redox homeostasis and its impact on autophagy-lysosomal system. Any insult to the lysosomes either structural or functional can affect the autophagic process and can lead to cellular stress. Many studies have

noted that complete lysis of lysosomes leads to massive release of its contents into the cytosol resulting in unregulated cell death by necrosis. Contrariwise, the selective or partial damage to lysosomes may release only certain lysosomal contents especially proteases and activate certain specific modes of controlled cell death pathways (Boya and Kroemer, 2008). However, the mechanisms or mediators that regulate selective LMP has not been recognized. The identification of such pathways and mediators will help in better understanding of lysosomal dependent cell death mechanisms and pave the way for development of novel therapeutic approaches.

Contrary to the previous notion that nucleus is largely unaffected in ferroptosis, my thesis had identified that histone H3, a core component of nuclear chromatin being proteolytically digested by cathepsin B in ferroptosis. Interestingly, this proteolytic digestion was found to be highly controlled and precise. Since histones are involved in various gene regulatory functions, identification of the site of cleavage and sequencing of the cleaved histone portion would aid in finding novel gene regulatory mechanisms that decide susceptibility to ferroptosis.

Finally, iron plays an important role in the induction and progression of various types of cell death. Since lysosomes are rich in iron due to continuous degradation of iron-binding proteins, a time dependent kinetics of mobilization of iron during ferroptosis and the impact of cathepsin B inhibition/knockout might be helpful to better understand the role of cathepsin B in cell death mechanisms.

5.12 Conclusions

In conclusion, the findings presented in this thesis aid in better understanding of the role of lysosomes and lysosomal cathepsins in oxidative stress induced cell death mechanisms. While autophagy has been widely considered as a pro-survival process, it can also promote cell death. As shown in Fig. 5.1, the work presented here provide novel evidence that lysosomal damage and

spillage of cathepsin B is the key to execution of both apoptotic and non-apoptotic cell death mechanisms under oxidative stress conditions. Oxidative stress can also differentially regulate lysosomal proteases facilitating diverse cell death mechanisms. Especially, the recent identification of novel cell death mechanism ferroptosis and its contribution to several pathologies have increased the necessity to elucidate the molecular players involved. The identification of cathepsin B as a ferroptotic executioner advances the understanding of ferroptosis. Furthermore, the study has discovered cathepsin B as a histone H3 protease during ferroptosis that was not previously recognized in any physiological or pathological settings. These findings can have implications in several disease conditions including neurodegenerative diseases, traumatic injuries and cancers where oxidative stress mediated macromolecule damage is a key factor in occurrence and development of pathologies.

Figure 5.1. Graphical summary of research findings.

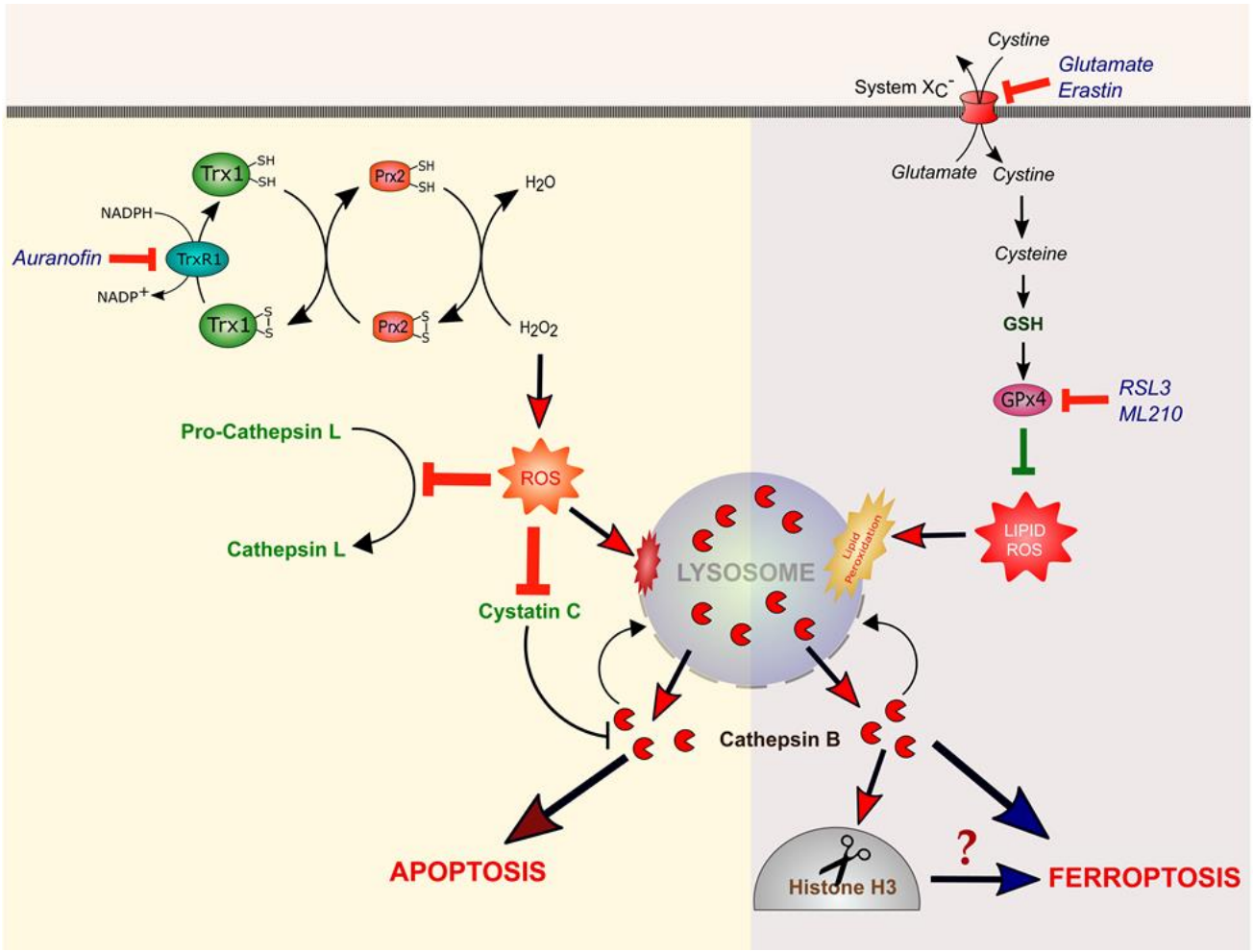

References

(2017) UniProt: the universal protein knowledgebase. Nucleic Acids Res 45:D158-D169.

Abedin MJ, Wang D, McDonnell MA, Lehmann U, Kelekar A (2007) Autophagy delays apoptotic death in breast cancer cells following DNA damage. Cell death and differentiation 14:500-510.

Ahsan MK, Lekli I, Ray D, Yodoi J, Das DK (2009) Redox regulation of cell survival by the thioredoxin superfamily: an implication of redox gene therapy in the heart. Antioxid Redox Signal 11:2741-2758.

Aiken CT, Kaake RM, Wang XR, Huang L (2011) Oxidative Stress-Mediated Regulation of Proteasome Complexes. Molecular & Cellular Proteomics 10.

Alexander A, Cai SL, Kim J, Nanez A, Sahin M, MacLean KH, Inoki K, Guan KL, Shen JJ, Person MD, Kusewitt D, Mills GB, Kastan MB, Walker CL (2010) ATM signals to TSC2 in the cytoplasm to regulate mTORC1 in response to ROS. Proceedings of the National Academy of Sciences of the United States of America 107:4153-4158.

Allison AC, Dingle JT (1966) Role of lysosomes in adrenal necrosis caused by dimethylbenzanthracene. Nature 209:303-304.

Anathy V, Aesif SW, Guala AS, Havermans M, Reynaert NL, Ho YS, Budd RC, Janssen-Heininger YMW (2009) Redox amplification of apoptosis by caspase-dependent cleavage of glutaredoxin 1 and S-glutathionylation of Fas. Journal of Cell Biology 184:241-252.

Andoh T, Chock PB, Chiueh CC (2002) Preconditioning-mediated neuroprotection: role of nitric oxide, cGMP, and new protein expression. Ann N Y Acad Sci 962:1-7.

Apel K, Hirt H (2004) Reactive oxygen species: metabolism, oxidative stress, and signal transduction. Annual review of plant biology 55:373-399.

Appelqvist H, Waster P, Kagedal K, Ollinger K (2013) The lysosome: from waste bag to potential therapeutic target. Journal of molecular cell biology 5:214-226.

Appelqvist H, Nilsson C, Garner B, Brown AJ, Kagedal K, Ollinger K (2011) Attenuation of the lysosomal death pathway by lysosomal cholesterol accumulation. The American journal of pathology 178:629-639.

Appelqvist H, Sandin L, Bjornstrom K, Saftig P, Garner B, Ollinger K, Kagedal K (2012a) Sensitivity to lysosome-dependent cell death is directly regulated by lysosomal cholesterol content. PloS one 7:e50262.

Appelqvist H, Johansson AC, Linderoth E, Johansson U, Antonsson B, Steinfeld R, Kagedal K, Ollinger K (2012b) Lysosome-mediated apoptosis is associated with cathepsin D-specific processing of bid at Phe24, Trp48, and Phe183. Annals of clinical and laboratory science 42:231-242.

Arbel N, Ben-Hail D, Shoshan-Barmatz V (2012) Mediation of the antiapoptotic activity of Bcl-xL protein upon interaction with VDAC1 protein. J Biol Chem 287:23152-23161.

Armstrong JS, Steinauer KK, Hornung B, Irish JM, Lecane P, Birrell GW, Peehl DM, Knox SJ (2002) Role of glutathione depletion and reactive oxygen species generation in apoptotic signaling in a human B lymphoma cell line. Cell death and differentiation 9:252-263.

Arodin L, Miranda-Vizuete A, Swoboda P, Fernandes AP (2014) Protective effects of the thioredoxin and glutaredoxin systems in dopamine-induced cell death. Free radical biology & medicine 73:328-336.

Aslani BA, Ghobadi S (2016) Studies on oxidants and antioxidants with a brief glance at their relevance to the immune system. Life sciences 146:163-173.

Aulak KS, Miyagi M, Yan L, West KA, Massillon D, Crabb JW, Stuehr DJ (2001) Proteomic method identifies proteins nitrated in vivo during inflammatory challenge. Proceedings of the National Academy of Sciences of the United States of America 98:12056-12061.

Ayala A, Munoz MF, Arguelles S (2014) Lipid Peroxidation: Production, Metabolism, and Signaling Mechanisms of Malondialdehyde and 4-Hydroxy-2-Nonenal. Oxid Med Cell Longev.

Bai J, Nakamura H, Kwon YW, Tanito M, Ueda S, Tanaka T, Hattori I, Ban S, Momoi T, Kitao Y, Ogawa S, Yodoi J (2007) Does thioredoxin-1 prevent mitochondria- and endoplasmic reticulum-mediated neurotoxicity of 1-methyl-4-phenyl-1,2,3,6-tetrahydropyridine? Antioxid Redox Signal 9:603-608.

Balce DR, Allan ER, McKenna N, Yates RM (2014) gamma-Interferon-inducible lysosomal thiol reductase (GILT) maintains phagosomal proteolysis in alternatively activated macrophages. The Journal of biological chemistry 289:31891-31904.

Balogh LM, Atkins WM (2011) Interactions of glutathione transferases with 4-hydroxynonenal. Drug Metab Rev 43:165-178.

Bao F, Bailey CS, Gurr KR, Bailey SI, Rosas-Arellano MP, Dekaban GA, Weaver LC (2009) Increased oxidative activity in human blood neutrophils and monocytes after spinal cord injury. Exp Neurol 215:308-316.

Bar-Am O, Weinreb O, Amit T, Youdim MB (2005) Regulation of Bcl-2 family proteins, neurotrophic factors, and APP processing in the neurorescue activity of propargylamine. FASEB J 19:1899-1901.

Basit F, Cristofanon S, Fulda S (2013) Obatoclax (GX15-070) triggers necroptosis by promoting the assembly of the necrosome on autophagosomal membranes. Cell death and differentiation 20:1161-1173.

Baskin-Bey ES, Canbay A, Bronk SF, Werneburg N, Guicciardi ME, Nyberg SL, Gores GJ (2005) Cathepsin B inactivation attenuates hepatocyte apoptosis and liver damage in steatotic livers after cold ischemia-warm reperfusion injury. American journal of physiology Gastrointestinal and liver physiology 288:G396-402.

Bau DT, Wang TS, Chung CH, Wang ASS, Jan KY (2002) Oxidative DNA adducts and DNA-protein cross-links are the major DNA lesions induced by arsenite. Environ Health Persp 110:753-756.

Baxter PS, Bell KF, Hasel P, Kaindl AM, Fricker M, Thomson D, Cregan SP, Gillingwater TH, Hardingham GE (2015) Synaptic NMDA receptor activity is coupled to the transcriptional control of the glutathione system. Nature communications 6:6761.

Bedford L, Hay D, Devoy A, Paine S, Powe DG, Seth R, Gray T, Topham I, Fone K, Rezvani N, Mee M, Soane T, Layfield R, Sheppard PW, Ebendal T, Usoskin D, Lowe J, Mayer RJ (2008) Depletion of 26S proteasomes in mouse brain neurons causes neurodegeneration and Lewy-like inclusions resembling human pale bodies. Journal of Neuroscience 28:8189-8198.

Ben-Hail D, Shoshan-Barmatz V (2016) VDAC1-interacting anion transport inhibitors inhibit VDAC1 oligomerization and apoptosis. Biochimica et biophysica acta 1863:1612-1623.

Benhar M, Forrester MT, Hess DT, Stamler JS (2008) Regulated protein denitrosylation by cytosolic and mitochondrial thioredoxins. Science 320:1050-1054.

Berlett BS, Stadtman ER (1997) Protein oxidation in aging, disease, and oxidative stress. Journal of Biological Chemistry 272:20313-20316.

Bersani NA, Merwin JR, Lopez NI, Pearson GD, Merrill GF (2002) Protein electrophoretic mobility shift assay to monitor redox state of thioredoxin in cells. Methods Enzymol 347:317-326.

Bersuker K, Hendricks JM, Li Z, Magtanong L, Ford B, Tang PH, Roberts MA, Tong B, Maimone TJ, Zoncu R, Bassik MC, Nomura DK, Dixon SJ, Olzmann JA (2019) The CoQ oxidoreductase FSP1 acts parallel to GPX4 to inhibit ferroptosis. Nature 575:688-692.

Bialik S, Dasari SK, Kimchi A (2018) Autophagy-dependent cell death - where, how and why a cell eats itself to death. Journal of cell science 131.

Bidere N, Lorenzo HK, Carmona S, Laforge M, Harper F, Dumont C, Senik A (2003) Cathepsin D triggers Bax activation, resulting in selective apoptosis-inducing factor (AIF) relocation in T lymphocytes entering the early commitment phase to apoptosis. The Journal of biological chemistry 278:31401-31411.

Bielski BHJ, Arudi RL, Sutherland MW (1983) A Study of the Reactivity of Ho2/O2- with Unsaturated Fatty-Acids. Journal of Biological Chemistry 258:4759-4761.

Blois MS (1958) Antioxidant Determinations by the Use of a Stable Free Radical. Nature 181:1199-1200.

Bortolotti P, Faure E, Kipnis E (2018) Inflammasomes in Tissue Damages and Immune Disorders After Trauma. Frontiers in immunology 9.

Bové J, Martínez-Vicente M, Dehay B, Perier C, Recasens A, Bombrun A, Antonsson B, Vila M (2014) BAX channel activity mediates lysosomal disruption linked to Parkinson disease. Autophagy 10:889-900.

Boya P, Kroemer G (2008) Lysosomal membrane permeabilization in cell death. Oncogene 27:6434-6451.

Brahimi-Horn MC, Lacas-Gervais S, Adaixo R, Ilc K, Rouleau M, Notte A, Dieu M, Michiels C, Voeltzel T, Maguer-Satta V, Pelletier J, Ilie M, Hofman P, Manoury B, Schmidt A, Hiller S, Pouyssegur J, Mazure NM (2015a) Local mitochondrial-endolysosomal microfusion cleaves voltage-dependent anion channel 1 to promote survival in hypoxia. Molecular and cellular biology 35:1491-1505.

Brahimi-Horn MC, Giuliano S, Saland E, Lacas-Gervais S, Sheiko T, Pelletier J, Bourget I, Bost F, Feral C, Boulter E, Tauc M, Ivan M, Garmy-Susini B, Popa A, Mari B, Sarry JE, Craigen WJ, Pouyssegur J, Mazure NM (2015b) Knockout of Vdac1 activates hypoxia-inducible

factor through reactive oxygen species generation and induces tumor growth by promoting metabolic reprogramming and inflammation. Cancer & metabolism 3:8.

Bridges KR (1987) Ascorbic-Acid Inhibits Lysosomal Autophagy of Ferritin. Journal of Biological Chemistry 262:14773-14778.

Brigelius-Flohe R (1999) Tissue-specific functions of individual glutathione peroxidases. Free Radical Biology and Medicine 27:951-965.

Brigelius-Flohe R, Muller M, Lippmann D, Kipp AP (2012) The yin and yang of nrf2-regulated selenoproteins in carcinogenesis. Int J Cell Biol 2012:486147.

Broniowska KA, Diers AR, Hogg N (2013) S-Nitrosoglutathione. Bba-Gen Subjects 1830:3173-3181.

Brown CW, Amante JJ, Goel HL, Mercurio AM (2017) The alpha6beta4 integrin promotes resistance to ferroptosis. The Journal of cell biology 216:4287-4297.

Brunelle JK, Letai A (2009) Control of mitochondrial apoptosis by the Bcl-2 family. Journal of cell science 122:437-441.

Brunk UT, Dalen H, Roberg K, Hellquist HB (1997) Photo-oxidative disruption of lysosomal membranes causes apoptosis of cultured human fibroblasts. Free radical biology & medicine 23:616-626.

Brustovetsky T, Li T, Yang YY, Zhang JT, Antonsson B, Brustovetsky N (2010) BAX insertion, oligomerization, and outer membrane permeabilization in brain mitochondria: Role of permeability transition and SH-redox regulation. Bba-Bioenergetics 1797:1795-1806.

Bryan HK, Olayanju A, Goldring CE, Park BK (2013) The Nrf2 cell defence pathway: Keap1-dependent and -independent mechanisms of regulation. Biochem Pharmacol 85:705-717.

Burke MA, Hutter D, Reshamwala RP, Knepper JE (2003) Cathepsin L plays an active role in involution of the mouse mammary gland. Developmental dynamics : an official publication of the American Association of Anatomists 227:315-322.

Cabet E, Batonnet-Pichon S, Delort F, Gausseres B, Vicart P, Lilienbaum A (2015) Antioxidant Treatment and Induction of Autophagy Cooperate to Reduce Desmin Aggregation in a Cellular Model of Desminopathy. PLoS One 10:e0137009.

Cable H, Lloyd JB (1999) Cellular uptake and release of two contrasting iron chelators. The Journal of pharmacy and pharmacology 51:131-134.

Cadet J, Douki T, Ravanat JL (2011) Measurement of oxidatively generated base damage in cellular DNA. Mutat Res-Fund Mol M 711:3-12.

Cadet J, Douki T, Gasparutto D, Ravanat JL (2003) Oxidative damage to DNA: formation, measurement and biochemical features. Mutat Res-Fund Mol M 531:5-23.

Cai Y, Gui C, Samedov K, Su H, Gu X, Li S, Luo W, Sung HHY, Lam JWY, Kwok RTK, Williams ID, Qin A, Tang BZ (2017) An acidic pH independent piperazine-TPE AIEgen as a unique bioprobe for lysosome tracing. Chemical science 8:7593-7603.

Canals S, Casarejos MJ, de Bernardo S, Rodriguez-Martin E, Mena MA (2001) Glutathione depletion switches nitric oxide neurotrophic effects to cell death in midbrain cultures: implications for Parkinson's disease. Journal of neurochemistry 79:1183-1195.

Canuel M, Korkidakis A, Konnyu K, Morales CR (2008) Sortilin mediates the lysosomal targeting of cathepsins D and H. Biochemical and biophysical research communications 373:292-297.

Castino R, Peracchio C, Salini A, Nicotra G, Trincheri NF, Demoz M, Valente G, Isidoro C (2009) Chemotherapy drug response in ovarian cancer cells strictly depends on a cathepsin D-Bax activation loop. Journal of cellular and molecular medicine 13:1096-1109.

Cazanave S, Berson A, Haouzi D, Vadrot N, Fau D, Grodet A, Letteron P, Feldmann G, El-Benna J, Fromenty B, Robin MA, Pessayre D (2007) High hepatic glutathione stores alleviate Fas-induced apoptosis in mice. J Hepatol 46:858-868.

Cernotta N, Clocchiatti A, Florean C, Brancolini C (2011) Ubiquitin-dependent degradation of HDAC4, a new regulator of random cell motility. Mol Biol Cell 22:278-289.

Chang CJ, Hsu HC, Ho WJ, Chang GJ, Pang JS, Chen WJ, Huang CC, Lai YJ (2019) Cathepsin S promotes the development of pulmonary arterial hypertension. American journal of physiology Lung cellular and molecular physiology 317:L1-L13.

Chen J, Saxena G, Mungrue IN, Lusis AJ, Shalev A (2008a) Thioredoxin-interacting protein - A critical link between glucose toxicity and beta-cell apoptosis. Diabetes 57:938-944.

Chen S, Zhou C, Yu H, Tao L, An Y, Zhang X, Wang Y, Xiao R (2019) 27-Hydroxycholesterol Contributes to Lysosomal Membrane Permeabilization-Mediated Pyroptosis in Co-cultured SH-SY5Y Cells and C6 Cells. Frontiers in molecular neuroscience 12:14.

Chen W, Li N, Chen T, Han Y, Li C, Wang Y, He W, Zhang L, Wan T, Cao X (2005) The lysosome-associated apoptosis-inducing protein containing the pleckstrin homology (PH) and FYVE domains (LAPF), representative of a novel family of PH and FYVE domain-

containing proteins, induces caspase-independent apoptosis via the lysosomal-mitochondrial pathway. The Journal of biological chemistry 280:40985-40995.

Chen W, Zhao MJ, Zhao SZ, Lu QY, Ni LS, Zou C, Lu L, Xu X, Guan HJ, Zheng Z, Qiu QH (2017) Activation of the TXNIP/NLRP3 inflammasome pathway contributes to inflammation in diabetic retinopathy: a novel inhibitory effect of minocycline. Inflamm Res 66:157-166.

Chen X, He WT, Hu LC, Li JX, Fang Y, Wang X, Xu XZ, Wang Z, Huang K, Han JH (2016) Pyroptosis is driven by non-selective gasdermin-D pore and its morphology is different from MLKL channel-mediated necroptosis. Cell research 26:1007-1020.

Chen Y, McMillan-Ward E, Kong J, Israels SJ, Gibson SB (2008b) Oxidative stress induces autophagic cell death independent of apoptosis in transformed and cancer cells. Cell Death Differ 15:171-182.

Cheng SB, Nakashima A, Huber WJ, Davis S, Banerjee S, Huang ZP, Saito S, Sadovsky Y, Sharma S (2019) Pyroptosis is a critical inflammatory pathway in the placenta from early onset preeclampsia and in human trophoblasts exposed to hypoxia and endoplasmic reticulum stressors. Cell death & disease 10.

Chung HS, Wang SB, Venkatraman V, Murray CI, Van Eyk JE (2013) Cysteine Oxidative Posttranslational Modifications Emerging Regulation in the Cardiovascular System. Circ Res 112:382-392.

Ciechanover A, Stanhill A (2014) The complexity of recognition of ubiquitinated substrates by the 26S proteasome. Biochimica et biophysica acta 1843:86-96.

Ciechomska IA, Goemans GC, Skepper JN, Tolkovsky AM (2009) Bcl-2 complexed with Beclin-1 maintains full anti-apoptotic function. Oncogene 28:2128-2141.

Circu ML, Aw TY (2012) Glutathione and modulation of cell apoptosis. Biochimica et biophysica acta 1823:1767-1777.

Cirman T, Oresic K, Mazovec GD, Turk V, Reed JC, Myers RM, Salvesen GS, Turk B (2004) Selective disruption of lysosomes in HeLa cells triggers apoptosis mediated by cleavage of Bid by multiple papain-like lysosomal cathepsins. The Journal of biological chemistry 279:3578-3587.

Cohen-Kaplan V, Livneh I, Avni N, Cohen-Rosenzweig C, Ciechanover A (2016) The ubiquitin-proteasome system and autophagy: Coordinated and independent activities. The international journal of biochemistry & cell biology 79:403-418.

Colacurcio DJ, Nixon RA (2016) Disorders of lysosomal acidification-The emerging role of v-ATPase in aging and neurodegenerative disease. Ageing research reviews 32:75-88.

Comelli M, Londero D, Mavelli I (1998) Severe energy impairment consequent to inactivation of mitochondrial ATP synthase as an early event in cell death: a mechanism for the selective sensitivity to H2O2 of differentiating erythroleukemia cells. Free radical biology & medicine 24:924-932.

Cong L, Dong X, Wang Y, Deng Y, Li B, Dai R (2019) On the role of synthesized hydroxylated chalcones as dual functional amyloid-beta aggregation and ferroptosis inhibitors for potential treatment of Alzheimer's disease. European journal of medicinal chemistry 166:11-21.

Conrad M, Pratt DA (2019) The chemical basis of ferroptosis. Nature chemical biology 15:1137-1147.

Conrad M, Angeli JP, Vandenabeele P, Stockwell BR (2016) Regulated necrosis: disease relevance and therapeutic opportunities. Nature reviews Drug discovery 15:348-366.

Conrad M, Kagan VE, Bayir H, Pagnussat GC, Head B, Traber MG, Stockwell BR (2018) Regulation of lipid peroxidation and ferroptosis in diverse species. Genes & development 32:602-619.

Conus S, Perozzo R, Reinheckel T, Peters C, Scapozza L, Yousefi S, Simon HU (2008) Caspase-8 is activated by cathepsin D initiating neutrophil apoptosis during the resolution of inflammation. The Journal of experimental medicine 205:685-698.

Costa V, Quintanilha A, Moradas-Ferreira P (2007) Protein oxidation, repair mechanisms and proteolysis in Saccharomyces cerevisiae. IUBMB life 59:293-298.

Coulombe R, Grochulski P, Sivaraman J, Menard R, Mort JS, Cygler M (1996) Structure of human procathepsin L reveals the molecular basis of inhibition by the prosegment. The EMBO journal 15:5492-5503.

Coutinho MF, Prata MJ, Alves S (2012a) Mannose-6-phosphate pathway: a review on its role in lysosomal function and dysfunction. Molecular genetics and metabolism 105:542-550.

Coutinho MF, Prata MJ, Alves S (2012b) A shortcut to the lysosome: the mannose-6-phosphate-independent pathway. Molecular genetics and metabolism 107:257-266.

Cox AG, Brown KK, Arner ES, Hampton MB (2008) The thioredoxin reductase inhibitor auranofin triggers apoptosis through a Bax/Bak-dependent process that involves peroxiredoxin 3 oxidation. Biochem Pharmacol 76:1097-1109.

D'Alessio M, De Nicola M, Coppola S, Gualandi G, Pugliese L, Cerella C, Cristofanon S, Civitareale P, Ciriolo MR, Bergamaschi A, Magrini A, Ghibelli L (2005) Oxidative Bax dimerization promotes its translocation to mitochondria independently of apoptosis. FASEB journal : official publication of the Federation of American Societies for Experimental Biology 19:1504-1506.

D'Autreaux B, Toledano MB (2007) ROS as signalling molecules: mechanisms that generate specificity in ROS homeostasis. Nat Rev Mol Cell Bio 8:813-824.

Dahl JU, Gray MJ, Jakob U (2015) Protein quality control under oxidative stress conditions. Journal of molecular biology 427:1549-1563.

Dalle-Donne I, Giustarini D, Colombo R, Rossi R, Milzani A (2003) Protein carbonylation in human diseases. Trends Mol Med 9:169-176.

Dannenmann B, Lehle S, Hildebrand DG, Kubler A, Grondona P, Schmid V, Holzer K, Froschl M, Essmann F, Rothfuss O, Schulze-Osthoff K (2015) High Glutathione and Glutathione Peroxidase-2 Levels Mediate Cell-Type-Specific DNA Damage Protection in Human Induced Pluripotent Stem Cells. Stem Cell Rep 4:886-898.

Davies KJ (2001) Degradation of oxidized proteins by the 20S proteasome. Biochimie 83:301-310.

de Castro MA, Bunt G, Wouters FS (2016) Cathepsin B launches an apoptotic exit effort upon cell death-associated disruption of lysosomes. Cell Death Discov 2:16012.

de Duve C (2005) The lysosome turns fifty. Nature cell biology 7:847-849.

De Pinto V, Reina S, Gupta A, Messina A, Mahalakshmi R (2016) Role of cysteines in mammalian VDAC isoforms' function. Biochimica et biophysica acta 1857:1219-1227.

Debelder AJ, Macallister R, Radomski MW, Moncada S, Vallance PJT (1994) Effects of S-Nitroso-Glutathione in the Human Forearm Circulation - Evidence for Selective-Inhibition of Platelet Activation. Cardiovasc Res 28:691-694.

Dedon PC, Tannenbaum SR (2004) Reactive nitrogen species in the chemical biology of inflammation. Archives of biochemistry and biophysics 423:12-22.

Deffieu M, Bhatia-Kissova I, Salin B, Galinier A, Manon S, Camougrand N (2009) Glutathione Participates in the Regulation of Mitophagy in Yeast. Journal of Biological Chemistry 284:14828-14837.

Deng D, Jiang N, Hao SJ, Sun H, Zhang GJ (2009) Loss of membrane cholesterol influences lysosomal permeability to potassium ions and protons. Biochimica et biophysica acta 1788:470-476.

Deng F, Sharma I, Dai Y, Yang M, Kanwar YS (2019) Myo-inositol oxygenase expression profile modulates pathogenic ferroptosis in the renal proximal tubule. The Journal of clinical investigation 129:5033-5049.

Dennemarker J, Lohmuller T, Muller S, Aguilar SV, Tobin DJ, Peters C, Reinheckel T (2010) Impaired turnover of autophagolysosomes in cathepsin L deficiency. Biol Chem 391:913-922.

Deosaran E, Larsen KB, Hua R, Sargent G, Wang YQ, Kim S, Lamark T, Jauregui M, Law K, Lippincott-Schwartz J, Brech A, Johansen T, Kim PK (2013) NBR1 acts as an autophagy receptor for peroxisomes. Journal of cell science 126:939-952.

Derry PJ, Hegde ML, Jackson GR, Kayed R, Tour JM, Tsai AL, Kent TA (2019) Revisiting the intersection of amyloid, pathologically modified tau and iron in Alzheimer's disease from a ferroptosis perspective. Progress in neurobiology:101716.

Desideri E, Filomeni G, Ciriolo MR (2012) Glutathione participates in the modulation of starvation-induced autophagy in carcinoma cells. Autophagy 8:1769-1781.

Dewson G, Kluck RM (2009) Mechanisms by which Bak and Bax permeabilise mitochondria during apoptosis. Journal of cell science 122:2801-2808.

Di Bartolomeo S, Corazzari M, Nazio F, Oliverio S, Lisi G, Antonioli M, Pagliarini V, Matteoni S, Fuoco C, Giunta L, D'Amelio M, Nardacci R, Romagnoli A, Piacentini M, Cecconi F, Fimia GM (2010) The dynamic interaction of AMBRA1 with the dynein motor complex regulates mammalian autophagy. Journal of Cell Biology 191:155-168.

Di Stefano A, Frosali S, Leonini A, Ettorre A, Priora R, Di Simplicio FC, Di Simplicio P (2006) GSH depletion, protein S-glutathionylation and mitochondrial transmembrane potential hyperpolarization are early events in initiation of cell death induced by a mixture of isothiazolinones in HL60 cells. Bba-Mol Cell Res 1763:214-225.

Dickinson DA, Forman HJ (2002) Cellular glutathione and thiols metabolism. Biochem Pharmacol 64:1019-1026.

Dikic I, Elazar Z (2018) Mechanism and medical implications of mammalian autophagy. Nature reviews Molecular cell biology 19:349-364.

Dixon SJ, Lemberg KM, Lamprecht MR, Skouta R, Zaitsev EM, Gleason CE, Patel DN, Bauer AJ, Cantley AM, Yang WS, Morrison B, 3rd, Stockwell BR (2012) Ferroptosis: an iron-dependent form of nonapoptotic cell death. Cell 149:1060-1072.

Doll S et al. (2019) FSP1 is a glutathione-independent ferroptosis suppressor. Nature 575:693-698.

Doulias PT, Kotoglou P, Tenopoulou M, Keramisanou D, Tzavaras T, Brunk U, Galaris D, Angelidis C (2007) Involvement of heat shock protein-70 in the mechanism of hydrogen peroxide-induced DNA damage: the role of lysosomes and iron. Free radical biology & medicine 42:567-577.

Drazic A, Winter J (2014) The physiological role of reversible methionine oxidation. Bba-Proteins Proteom 1844:1367-1382.

Droga-Mazovec G, Bojic L, Petelin A, Ivanova S, Romih R, Repnik U, Salvesen GS, Stoka V, Turk V, Turk B (2008) Cysteine cathepsins trigger caspase-dependent cell death through cleavage of bid and antiapoptotic Bcl-2 homologues. The Journal of biological chemistry 283:19140-19150.

Du Y, Zhang H, Lu J, Holmgren A (2012) Glutathione and glutaredoxin act as a backup of human thioredoxin reductase 1 to reduce thioredoxin 1 preventing cell death by aurothioglucose. J Biol Chem 287:38210-38219.

Du YT, Zhang HH, Zhang X, Lu J, Holmgren A (2013) Thioredoxin 1 Is Inactivated Due to Oxidation Induced by Peroxiredoxin under Oxidative Stress and Reactivated by the Glutaredoxin System. Journal of Biological Chemistry 288:32241-32247.

Duarte LF, Young AR, Wang Z, Wu HA, Panda T, Kou Y, Kapoor A, Hasson D, Mills NR, Ma'ayan A, Narita M, Bernstein E (2014) Histone H3.3 and its proteolytically processed form drive a cellular senescence programme. Nature communications 5:5210.

Dubuisson M, Stricht DV, Clippe A, Etienne F, Nauser T, Kissner R, Koppenol WH, Rees JF, Knoops B (2004) Human peroxiredoxin 5 is a peroxynitrite reductase. FEBS letters 571:161-165.

Duewell P, Kono H, Rayner KJ, Sirois CM, Vladimer G, Bauernfeind FG, Abela GS, Franchi L, Nunez G, Schnurr M, Espevik T, Lien E, Fitzgerald KA, Rock KL, Moore KJ, Wright SD, Hornung V, Latz E (2010) NLRP3 inflammasomes are required for atherogenesis and activated by cholesterol crystals. Nature 464:1357-1361.

Duncan EM, Muratore-Schroeder TL, Cook RG, Garcia BA, Shabanowitz J, Hunt DF, Allis CD (2008) Cathepsin L proteolytically processes histone H3 during mouse embryonic stem cell differentiation. Cell 135:284-294.

Edman MC, Janga SR, Meng Z, Bechtold M, Chen AF, Kim C, Naman L, Sarma A, Teekappanavar N, Kim AY, Madrigal S, Singh S, Ortiz E, Christianakis S, Arkfeld DG, Mack WJ, Heur M, Stohl W, Hamm-Alvarez SF (2018) Increased Cathepsin S activity associated with decreased protease inhibitory capacity contributes to altered tear proteins in Sjogren's Syndrome patients. Scientific reports 8:11044.

Eftekharpour E, Holmgren A, Juurlink BH (2000) Thioredoxin reductase and glutathione synthesis is upregulated by t-butylhydroquinone in cortical astrocytes but not in cortical neurons. Glia 31:241-248.

Eiberger W, Volkmer B, Amouroux R, Dherin C, Radicella JP, Epe B (2008) Oxidative stress impairs the repair of oxidative DNA base modifications in human skin fibroblasts and melanoma cells. DNA Repair 7:912-921.

Erdal H, Berndtsson M, Castro J, Brunk U, Shoshan MC, Linder S (2005) Induction of lysosomal membrane permeabilization by compounds that activate p53-independent apoptosis. Proceedings of the National Academy of Sciences of the United States of America 102:192-197.

Erlich S, Mizrachy L, Segev O, Lindenboim L, Zmira O, Adi-Harel S, Hirsch JA, Stein R, Pinkas-Kramarski R (2007) Differential interactions between Beclin 1 and bcl-2 family members. Autophagy 3:561-568.

Eskes R, Desagher S, Antonsson B, Martinou JC (2000) Bid induces the oligomerization and insertion of Bax into the outer mitochondrial membrane. Molecular and cellular biology 20:929-935.

Esteve JM, Mompo J, De La Asuncion JG, Sastre J, Asensi M, Boix J, Vina JR, Vina J, Pallardo FV (1999) Oxidative damage to mitochondrial DNA and glutathione oxidation in apoptosis: studies in vivo and in vitro. Faseb Journal 13:1055-1064.

Ewanchuk BW, Yates RM (2018) The phagosome and redox control of antigen processing. Free radical biology & medicine 125:53-61.

Fang C, Gu L, Smerin D, Mao S, Xiong X (2017) The Interrelation between Reactive Oxygen Species and Autophagy in Neurological Disorders. Oxidative Medicine and Cellular Longevity 2017:8495160.

Fang X, Wang H, Han D, Xie E, Yang X, Wei J, Gu S, Gao F, Zhu N, Yin X, Cheng Q, Zhang P, Dai W, Chen J, Yang F, Yang HT, Linkermann A, Gu W, Min J, Wang F (2019) Ferroptosis as a target for protection against cardiomyopathy. Proceedings of the National Academy of Sciences of the United States of America 116:2672-2680.

Farnsworth CC, Seabra MC, Ericsson LH, Gelb MH, Glomset JA (1994) Rab Geranylgeranyl Transferase Catalyzes the Geranylgeranylation of Adjacent Cysteines in the Small Gtpases Rab1a, Rab3a, and Rab5a. Proceedings of the National Academy of Sciences of the United States of America 91:11963-11967.

Felbor U, Kessler B, Mothes W, Goebel HH, Ploegh HL, Bronson RT, Olsen BR (2002) Neuronal loss and brain atrophy in mice lacking cathepsins B and L. Proceedings of the National Academy of Sciences of the United States of America 99:7883-7888.

Feldstein AE, Werneburg NW, Li Z, Bronk SF, Gores GJ (2006) Bax inhibition protects against free fatty acid-induced lysosomal permeabilization. American journal of physiology Gastrointestinal and liver physiology 290:G1339-1346.

Feldstein AE, Werneburg NW, Canbay A, Guicciardi ME, Bronk SF, Rydzewski R, Burgart LJ, Gores GJ (2004) Free fatty acids promote hepatic lipotoxicity by stimulating TNF-alpha expression via a lysosomal pathway. Hepatology 40:185-194.

Feng H, Stockwell BR (2018) Unsolved mysteries: How does lipid peroxidation cause ferroptosis? PLoS biology 16:e2006203.

Feng Y, He D, Yao Z, Klionsky DJ (2014) The machinery of macroautophagy. Cell research 24:24-41.

Fernandez AF, Lopez-Otin C (2015) The functional and pathologic relevance of autophagy proteases. The Journal of clinical investigation 125:33-41.

Fernando MR, Nanri H, Yoshitake S, Nagata-Kuno K, Minakami S (1992) Thioredoxin regenerates proteins inactivated by oxidative stress in endothelial cells. European journal of biochemistry 209:917-922.

Finley D (2009) Recognition and Processing of Ubiquitin-Protein Conjugates by the Proteasome. Annu Rev Biochem 78:477-513.

Fong KL, McCay PB, Poyer JL, Keele BB, Misra H (1973) Evidence that peroxidation of lysosomal membranes is initiated by hydroxyl free radicals produced during flavin enzyme activity. The Journal of biological chemistry 248:7792-7797.

Fouchier F, Mego JL, Dang J, Simon C (1983) Thyroid lysosomes: the stability of the lysosomal membrane. European journal of cell biology 30:272-278.

Franchi L, Eigenbrod T, Munoz-Planillo R, Nunez G (2009) The inflammasome: a caspase-1-activation platform that regulates immune responses and disease pathogenesis. Nat Immunol 10:241-247.

Franco R, Cidlowski JA (2009) Apoptosis and glutathione: beyond an antioxidant. Cell death and differentiation 16:1303-1314.

Franco R, Panayiotidis MI, Cidlowski JA (2007) Glutathione depletion is necessary for apoptosis in lymphoid cells independent of reactive oxygen species formation. Journal of Biological Chemistry 282:30452-30465.

Franco R, Bortner CD, Schmitz I, Cidlowski JA (2014) Glutathione depletion regulates both extrinsic and intrinsic apoptotic signaling cascades independent from multidrug resistance protein 1. Apoptosis : an international journal on programmed cell death 19:117-134.

Franco R, DeHaven WI, Sifre MI, Bortner CD, Cidlowski JA (2008) Glutathione Depletion and Disruption of Intracellular Ionic Homeostasis Regulate Lymphoid Cell Apoptosis. Journal of Biological Chemistry 283:36071-36087.

Friedmann Angeli JP et al. (2014) Inactivation of the ferroptosis regulator Gpx4 triggers acute renal failure in mice. Nature cell biology 16:1180-1191.

Friesen C, Kiess Y, Debatin KM (2004) A critical role of glutathione in determining apoptosis sensitivity and resistance in leukemia cells. Cell death and differentiation 11:S73-S85.

Friguet B, Szweda LI (1997) Inhibition of the multicatalytic proteinase (proteasome) by 4-hydroxy-2-nonenal cross-linked protein. FEBS letters 405:21-25.

Friguet B, Stadtman ER, Szweda LI (1994) Modification of Glucose-6-Phosphate-Dehydrogenase by 4-Hydroxy-2-Nonenal - Formation of Cross-Linked Protein That Inhibits the Multicatalytic Protease. Journal of Biological Chemistry 269:21639-21643.

Fujii J, Homma T, Kobayashi S (2019) Ferroptosis caused by cysteine insufficiency and oxidative insult. Free Radic Res:1-12.

Fujita N, Itoh T, Omori H, Fukuda M, Noda T, Yoshimori T (2008) The Atg16L complex specifies the site of LC3 lipidation for membrane biogenesis in autophagy. Molecular biology of the cell 19:2092-2100.

Fukae J, Takanashi M, Kubo S, Nishioka K, Nakabeppu Y, Mori H, Mizuno Y, Hattori N (2005) Expression of 8-oxoguanine DNA glycosylase (OGG1) in Parkinson's disease and related neurodegenerative disorders. Acta neuropathologica 109:256-262.

Fukui M, Song JH, Choi J, Choi HJ, Zhu BT (2009) Mechanism of glutamate-induced neurotoxicity in HT22 mouse hippocampal cells. Eur J Pharmacol 617:1-11.

Gallogly MM, Starke DW, Leonberg AK, Ospina SME, Mieyal JJ (2008) Kinetic and mechanistic characterization and versatile catalytic properties of mammalian glutaredoxin 2: Implications for intracellular roles. Biochemistry-Us 47:11144-11157.

Ganley IG, Lam DH, Wang JR, Ding XJ, Chen S, Jiang XJ (2009) ULK1 center dot ATG13 center dot FIP200 Complex Mediates mTOR Signaling and Is Essential for Autophagy. Journal of Biological Chemistry 284:12297-12305.

Gao H, Bai Y, Jia Y, Zhao Y, Kang R, Tang D, Dai E (2018) Ferroptosis is a lysosomal cell death process. Biochemical and biophysical research communications 503:1550-1556.

Gao M, Monian P, Pan Q, Zhang W, Xiang J, Jiang X (2016) Ferroptosis is an autophagic cell death process. Cell research 26:1021-1032.

Gao M, Yi J, Zhu J, Minikes AM, Monian P, Thompson CB, Jiang X (2019) Role of Mitochondria in Ferroptosis. Molecular cell 73:354-363 e353.

Garcia SC, Grotto D, Bulcao RP, Moro AM, Roehrs M, Valentini J, de Freitas FA, Paniz C, Bubols GB, Charao MF (2013) Evaluation of lipid damage related to pathological and physiological conditions. Drug Chem Toxicol 36:306-312.

Gaschler MM, Stockwell BR (2017) Lipid peroxidation in cell death. Biochemical and biophysical research communications 482:419-425.

Gaschler MM et al. (2018) FINO2 initiates ferroptosis through GPX4 inactivation and iron oxidation. Nature chemical biology 14:507-515.

Gascon S, Murenu E, Masserdotti G, Ortega F, Russo GL, Petrik D, Deshpande A, Heinrich C, Karow M, Robertson SP, Schroeder T, Beckers J, Irmler M, Berndt C, Angeli JP, Conrad M,

Berninger B, Gotz M (2016) Identification and Successful Negotiation of a Metabolic Checkpoint in Direct Neuronal Reprogramming. Cell Stem Cell 18:396-409.

Gasdaska JR, Kirkpatrick DL, Montfort W, Kuperus M, Hill SR, Berggren M, Powis G (1996) Oxidative inactivation of thioredoxin as a cellular growth factor and protection by a Cys(73)->Ser mutation. Biochem Pharmacol 52:1741-1747.

Gault CR, Obeid LM, Hannun YA (2010) An overview of sphingolipid metabolism: from synthesis to breakdown. Advances in experimental medicine and biology 688:1-23.

Gentile F, Pizzimenti S, Arcaro A, Pettazzoni P, Minelli R, D'Angelo D, Mamone G, Ferranti P, Toaldo C, Cetrangolo G, Formisano S, Dianzani MU, Uchida K, Dianzani C, Barrera G (2009) Exposure of HL-60 human leukaemic cells to 4-hydroxynonenal promotes the formation of adduct(s) with alpha-enolase devoid of plasminogen binding activity. Biochemical Journal 422:285-294.

Geula S, Ben-Hail D, Shoshan-Barmatz V (2012) Structure-based analysis of VDAC1: N-terminus location, translocation, channel gating and association with anti-apoptotic proteins. The Biochemical journal 444:475-485.

Ghavami S, Cunnington RH, Gupta S, Yeganeh B, Filomeno KL, Freed DH, Chen S, Klonisch T, Halayko AJ, Ambrose E, Singal R, Dixon IM (2015) Autophagy is a regulator of TGF-beta1-induced fibrogenesis in primary human atrial myofibroblasts. Cell Death Dis 6:e1696.

Ghavami S, Shojaei S, Yeganeh B, Ande SR, Jangamreddy JR, Mehrpour M, Christoffersson J, Chaabane W, Moghadam AR, Kashani HH, Hashemi M, Owji AA, Los MJ (2014) Autophagy and apoptosis dysfunction in neurodegenerative disorders. Prog Neurobiol 112:24-49.

Ghosh M, Carlsson F, Laskar A, Yuan XM, Li W (2011) Lysosomal membrane permeabilization causes oxidative stress and ferritin induction in macrophages. FEBS Lett 585:623-629.

Giorgio M, Trinei M, Migliaccio E, Pelicci PG (2007) Hydrogen peroxide: a metabolic by-product or a common mediator of ageing signals? Nature reviews Molecular cell biology 8:722-728.

Girotti AW (1998) Lipid hydroperoxide generation, turnover, and effector action in biological systems. Journal of lipid research 39:1529-1542.

Glick D, Barth S, Macleod KF (2010) Autophagy: cellular and molecular mechanisms. J Pathol 221:3-12.

Godat E, Herve-Grvepinet V, Veillard F, Lecaille F, Belghazi M, Bromme D, Lalmanach G (2008) Regulation of cathepsin K activity by hydrogen peroxide. Biological chemistry 389:1123-1126.

Gordy C, He YW (2012) The crosstalk between autophagy and apoptosis: where does this lead? Protein Cell 3:17-27.

Gorojod RM, Alaimo A, Porte Alcon S, Pomilio C, Saravia F, Kotler ML (2015) The autophagic-lysosomal pathway determines the fate of glial cells under manganese- induced oxidative stress conditions. Free Radic Biol Med 87:237-251.

Gorrini C, Harris IS, Mak TW (2013a) Modulation of oxidative stress as an anticancer strategy. Nature Reviews Drug Discovery 12:931-947.

Gorrini C et al. (2013b) BRCA1 interacts with Nrf2 to regulate antioxidant signaling and cell survival. J Exp Med 210:1529-1544.

Goulet B, Truscott M, Nepveu A (2006) A novel proteolytically processed CDP/Cux isoform of 90 kDa is generated by cathepsin L. Biological chemistry 387:1285-1293.

Goulet B, Baruch A, Moon NS, Poirier M, Sansregret LL, Erickson A, Bogyo M, Nepveu A (2004) A cathepsin L isoform that is devoid of a signal peptide localizes to the nucleus in S phase and processes the CDP/Cux transcription factor. Molecular cell 14:207-219.

Green RM, Graham M, O'Donovan MR, Chipman JK, Hodges NJ (2006) Subcellular compartmentalization of glutathione: correlations with parameters of oxidative stress related to genotoxicity. Mutagenesis 21:383-390.

Grimm S, Hohn A, Grune T (2012) Oxidative protein damage and the proteasome. Amino Acids 42:23-38.

Grimsrud PA, Xie HW, Griffin TJ, Bernlohr DA (2008) Oxidative stress and covalent modification of protein with bioactive aldehydes. Journal of Biological Chemistry 283:21837-21841.

Gruber F, Ornelas CM, Karner S, Narzt MS, Nagelreiter IM, Gschwandtner M, Bochkov V, Tschachler E (2015) Nrf2 deficiency causes lipid oxidation, inflammation, and matrix-protease expression in DHA-supplemented and UVA-irradiated skin fibroblasts. Free Radical Biology and Medicine 88:439-451.

Grune T, Reinheckel T, Davies KJA (1996) Degradation of oxidized proteins in K562 human hematopoietic cells by proteasome. Journal of Biological Chemistry 271:15504-15509.

Gu Z, Nakamura T, Yao D, Shi ZQ, Lipton SA (2005) Nitrosative and oxidative stress links dysfunctional ubiquitination to Parkinson's disease. Cell Death Differ 12:1202-1204.

Guan X, Li X, Yang X, Yan J, Shi P, Ba L, Cao Y, Wang P (2019) The neuroprotective effects of carvacrol on ischemia/reperfusion-induced hippocampal neuronal impairment by ferroptosis mitigation. Life sciences 235:116795.

Gudipaty SA, Conner CM, Rosenblatt J, Montell DJ (2018) Unconventional Ways to Live and Die: Cell Death and Survival in Development, Homeostasis, and Disease. Annual review of cell and developmental biology 34:311-332.

Guicciardi ME, Bronk SF, Werneburg NW, Gores GJ (2007) cFLIPL prevents TRAIL-induced apoptosis of hepatocellular carcinoma cells by inhibiting the lysosomal pathway of apoptosis. American journal of physiology Gastrointestinal and liver physiology 292:G1337-1346.

Guicciardi ME, Bronk SF, Werneburg NW, Yin XM, Gores GJ (2005) Bid is upstream of lysosome-mediated caspase 2 activation in tumor necrosis factor alpha-induced hepatocyte apoptosis. Gastroenterology 129:269-284.

Guicciardi ME, Deussing J, Miyoshi H, Bronk SF, Svingen PA, Peters C, Kaufmann SH, Gores GJ (2000) Cathepsin B contributes to TNF-alpha-mediated hepatocyte apoptosis by promoting mitochondrial release of cytochrome c. The Journal of clinical investigation 106:1127-1137.

Guinec N, Dalet-Fumeron V, Pagano M (1993) "In vitro" study of basement membrane degradation by the cysteine proteinases, cathepsins B, B-like and L. Digestion of collagen IV, laminin, fibronectin, and release of gelatinase activities from basement membrane fibronectin. Biological chemistry Hoppe-Seyler 374:1135-1146.

Guo HQ, Lin W, Zhang XY, Zhang XH, Hu ZJ, Li LY, Duan ZP, Zhang J, Ren F (2017) Kaempferol induces hepatocellular carcinoma cell death via endoplasmic reticulum stress-CHOP-autophagy signaling pathway. Oncotarget 8:82207-82216.

Gursahani HI, Schaefer S (2004) Acidification reduces mitochondrial calcium uptake in rat cardiac mitochondria. American journal of physiology Heart and circulatory physiology 287:H2659-2665.

Gutierrez EM, Seebacher NA, Arzuman L, Kovacevic Z, Lane DJ, Richardson V, Merlot AM, Lok H, Kalinowski DS, Sahni S (2016) Lysosomal membrane stability plays a major role in the cytotoxic activity of the anti-proliferative agent, di-2-pyridylketone 4, 4-dimethyl-3-

thiosemicarbazone (Dp44mT). Biochimica et Biophysica Acta (BBA)-Molecular Cell Research 1863:1665-1681.

Gwinn DM, Shackelford DB, Egan DF, Mihaylova MM, Mery A, Vasquez DS, Turk BE, Shaw RJ (2008) AMPK phosphorylation of raptor mediates a metabolic checkpoint. Molecular cell 30:214-226.

Gyrd-Hansen M, Farkas T, Fehrenbacher N, Bastholm L, Hoyer-Hansen M, Elling F, Wallach D, Flavell R, Kroemer G, Nylandsted J, Jaattela M (2006) Apoptosome-independent activation of the lysosomal cell death pathway by caspase-9. Molecular and cellular biology 26:7880-7891.

Haga S, Ozawa T, Yamada Y, Morita N, Nagashima I, Inoue H, Inaba Y, Noda N, Abe R, Umezawa K, Ozaki M (2014) p62/SQSTM1 plays a protective role in oxidative injury of steatotic liver in a mouse hepatectomy model. Antioxid Redox Signal 21:2515-2530.

Hahn SH, Yoo OJ, Gahl WA (2001) Effect of metal ions on the stability of metallothionein in the degradation by cellular fractions in vitro. Exp Mol Med 33:32-36.

Halle A, Hornung V, Petzold GC, Stewart CR, Monks BG, Reinheckel T, Fitzgerald KA, Latz E, Moore KJ, Golenbock DT (2008) The NALP3 inflammasome is involved in the innate immune response to amyloid-beta. Nature immunology 9:857-865.

Hamer I, Van Beersel G, Arnould T, Jadot M (2012) Lipids and lysosomes. Current drug metabolism 13:1371-1387.

Hampton MB, Orrenius S (1997) Dual regulation of caspase activity by hydrogen peroxide: implications for apoptosis. FEBS Lett 414:552-556.

Hankin JA, Jones DNM, Murphy RC (2003) Covalent binding of leukotriene A(4) to DNA and RNA. Chemical research in toxicology 16:551-561.

Hanschmann EM, Godoy JR, Berndt C, Hudemann C, Lillig CH (2013) Thioredoxins, glutaredoxins, and peroxiredoxins--molecular mechanisms and health significance: from cofactors to antioxidants to redox signaling. Antioxid Redox Signal 19:1539-1605.

Hao S, Yu J, He W, Huang Q, Zhao Y, Liang B, Zhang S, Wen Z, Dong S, Rao J, Liao W, Shi M (2017) Cysteine Dioxygenase 1 Mediates Erastin-Induced Ferroptosis in Human Gastric Cancer Cells. Neoplasia 19:1022-1032.

Hao SJ, Hou JF, Jiang N, Zhang GJ (2008) Loss of membrane cholesterol affects lysosomal osmotic stability. General physiology and biophysics 27:278-283.

Haratake K, Sato A, Tsuruta F, Chiba T (2016) KIAA0368-deficiency affects disassembly of 26S proteasome under oxidative stress condition. J Biochem 159:609-618.

Hashemy SI, Holmgren A (2008) Regulation of the catalytic activity and structure of human thioredoxin 1 via oxidation and S-nitrosylation of cysteine residues. Journal of Biological Chemistry 283:21890-21898.

Hayes HL, Peterson BS, Haldeman JM, Newgard CB, Hohmeier HE, Stephens SB (2017) Delayed apoptosis allows islet beta-cells to implement an autophagic mechanism to promote cell survival. PloS one 12:e0172567.

Head SA, Shi W, Zhao L, Gorshkov K, Pasunooti K, Chen Y, Deng Z, Li RJ, Shim JS, Tan W, Hartung T, Zhang J, Zhao Y, Colombini M, Liu JO (2015) Antifungal drug itraconazole targets VDAC1 to modulate the AMPK/mTOR signaling axis in endothelial cells. Proc Natl Acad Sci U S A 112:E7276-7285.

Headlam HA, Gracanin M, Rodgers KJ, Davies MJ (2006) Inhibition of cathepsins and related proteases by amino acid, peptide, and protein hydroperoxides. Free Radic Biol Med 40:1539-1548.

Hensley K, Harris-White ME (2015) Redox regulation of autophagy in healthy brain and neurodegeneration. Neurobiol Dis 84:50-59.

Hershko A, Ciechanover A (1998) The ubiquitin system. Annu Rev Biochem 67:425-479.

Higuchi Y (2004) Glutathione depletion-induced chromosomal DNA fragmentation associated with apoptosis and necrosis. Journal of cellular and molecular medicine 8:455-464.

Hillmer EJ, Zhang H, Li HS, Watowich SS (2016) STAT3 signaling in immunity. Cytokine & growth factor reviews 31:1-15.

Hindupur SK, Gonzalez A, Hall MN (2015) The Opposing Actions of Target of Rapamycin and AMP-Activated Protein Kinase in Cell Growth Control. Csh Perspect Biol 7.

Hintze KJ, Wald KA, Zeng H, Jeffery EH, Finley JW (2003) Thioredoxin reductase in human hepatoma cells is transcriptionally regulated by sulforaphane and other electrophiles via an antioxidant response element. J Nutr 133:2721-2727.

Hirata Y, Yamamoto H, Atta MS, Mahmoud S, Oh-hashi K, Kiuchi K (2011) Chloroquine inhibits glutamate-induced death of a neuronal cell line by reducing reactive oxygen species through sigma-1 receptor. Journal of neurochemistry 119:839-847.

Hishita T, Tada-Oikawa S, Tohyama K, Miura Y, Nishihara T, Tohyama Y, Yoshida Y, Uchiyama T, Kawanishi S (2001) Caspase-3 activation by lysosomal enzymes in cytochrome c-independent apoptosis in myelodysplastic syndrome-derived cell line P39. Cancer research 61:2878-2884.

Ho YS, Xiong Y, Ma WC, Spector A, Ho DS (2004) Mice lacking catalase develop normally but show differential sensitivity to oxidant tissue injury. Journal of Biological Chemistry 279:32804-32812.

Holland P, Torgersen ML, Sandvig K, Simonsen A (2014) LYST affects lysosome size and quantity, but not trafficking or degradation through autophagy or endocytosis. Traffic 15:1390-1405.

Holmes RP, Yoss NL (1984) 25-Hydroxysterols increase the permeability of liposomes to Ca2+ and other cations. Biochimica et biophysica acta 770:15-21.

Holmgren A (1979a) Thioredoxin catalyzes the reduction of insulin disulfides by dithiothreitol and dihydrolipoamide. J Biol Chem 254:9627-9632.

Holmgren A (1979b) Reduction of disulfides by thioredoxin. Exceptional reactivity of insulin and suggested functions of thioredoxin in mechanism of hormone action. J Biol Chem 254:9113-9119.

Holmgren A (1985) Thioredoxin. Annu Rev Biochem 54:237-271.

Holmgren A, Lu J (2010) Thioredoxin and thioredoxin reductase: current research with special reference to human disease. Biochemical and biophysical research communications 396:120-124.

Hook G, Jacobsen JS, Grabstein K, Kindy M, Hook V (2015) Cathepsin B is a New Drug Target for Traumatic Brain Injury Therapeutics: Evidence for E64d as a Promising Lead Drug Candidate. Frontiers in neurology 6:178.

Hornung V, Bauernfeind F, Halle A, Samstad EO, Kono H, Rock KL, Fitzgerald KA, Latz E (2008) Silica crystals and aluminum salts activate the NALP3 inflammasome through phagosomal destabilization. Nature immunology 9:847-856.

Hoshi T, Heinemann S (2001a) Regulation of cell function by methionine oxidation and reduction. The Journal of physiology 531:1-11.

Hoshi T, Heinemann SH (2001b) Regulation of cell function by methionine oxidation and reduction. J Physiol-London 531:1-11.

Hosokawa N, Hara T, Kaizuka T, Kishi C, Takamura A, Miura Y, Iemura S, Natsume T, Takehana K, Yamada N, Guan JL, Oshiro N, Mizushima N (2009) Nutrient-dependent mTORC1 Association with the ULK1-Atg13-FIP200 Complex Required for Autophagy. Molecular biology of the cell 20:1981-1991.

Hou W, Han J, Lu CS, Goldstein LA, Rabinowich H (2010) Autophagic degradation of active caspase-8 A crosstalk mechanism between autophagy and apoptosis. Autophagy 6:891-900.

Hou W, Xie Y, Song X, Sun X, Lotze MT, Zeh HJ, 3rd, Kang R, Tang D (2016) Autophagy promotes ferroptosis by degradation of ferritin. Autophagy 12:1425-1428.

Hristov G, Marttila T, Durand C, Niesler B, Rappold GA, Marchini A (2014) SHOX triggers the lysosomal pathway of apoptosis via oxidative stress. Hum Mol Genet 23:1619-1630.

Hsu KF, Wu CL, Huang SC, Wu CM, Hsiao JR, Yo YT, Chen YH, Shiau AL, Chou CY (2009) Cathepsin L mediates resveratrol-induced autophagy and apoptotic cell death in cervical cancer cells. Autophagy 5:451-460.

Huai J, Vogtle FN, Jockel L, Li Y, Kiefer T, Ricci JE, Borner C (2013) TNFalpha-induced lysosomal membrane permeability is downstream of MOMP and triggered by caspase-mediated NDUFS1 cleavage and ROS formation. Journal of cell science 126:4015-4025.

Huang Z, Pinto JT, Deng H, Richie JP (2008) Inhibition of caspase-3 activity and activation by protein glutathionylation. Biochem Pharmacol 75:2234-2244.

Huang Z, Cheng Y, Chiu PM, Cheung FM, Nicholls JM, Kwong DL, Lee AW, Zabarovsky ER, Stanbridge EJ, Lung HL, Lung ML (2012) Tumor suppressor Alpha B-crystallin (CRYAB) associates with the cadherin/catenin adherens junction and impairs NPC progression-associated properties. Oncogene 31:3709-3720.

Hughes H, Mathews B, Lenz ML, Guyton JR (1994) Cytotoxicity of oxidized LDL to porcine aortic smooth muscle cells is associated with the oxysterols 7-ketocholesterol and 7-hydroxycholesterol. Arteriosclerosis and thrombosis : a journal of vascular biology 14:1177-1185.

Hwang J, Suh HW, Jeon YH, Hwang E, Nguyen LT, Yeom J, Lee SG, Lee C, Kim KJ, Kang BS, Jeong JO, Oh TK, Choi I, Lee JO, Kim MH (2014) The structural basis for the negative regulation of thioredoxin by thioredoxin-interacting protein. Nature communications 5:10-23.

Hwang JJ, Lee SJ, Kim TY, Cho JH, Koh JY (2008) Zinc and 4-hydroxy-2-nonenal mediate lysosomal membrane permeabilization induced by H2O2 in cultured hippocampal neurons. The Journal of neuroscience : the official journal of the Society for Neuroscience 28:3114-3122.

Iacobini C, Menini S, Ricci C, Scipioni A, Sansoni V, Mazzitelli G, Cordone S, Pesce C, Pugliese F, Pricci F, Pugliese G (2009) Advanced lipoxidation end-products mediate lipid-induced glomerular injury: role of receptor-mediated mechanisms. J Pathol 218:360-369.

Ichimura Y, Kirisako T, Takao T, Satomi Y, Shimonishi Y, Ishihara N, Mizushima N, Tanida I, Kominami E, Ohsumi M, Noda T, Ohsumi Y (2000) A ubiquitin-like system mediates protein lipidation. Nature 408:488-492.

Ichimura Y, Waguri S, Sou YS, Kageyama S, Hasegawa J, Ishimura R, Saito T, Yang Y, Kouno T, Fukutomi T, Hoshii T, Hirao A, Takagi K, Mizushima T, Motohashi H, Lee MS, Yoshimori T, Tanaka K, Yamamoto M, Komatsu M (2013) Phosphorylation of p62 activates the Keap1-Nrf2 pathway during selective autophagy. Mol Cell 51:618-631.

Imai H, Nakagawa Y (2003) Biological significance of phospholipid hydroperoxide glutathione peroxidase (PHGPx, GPx4) in mammalian cells. Free Radical Biology and Medicine 34:145-169.

Inoki K, Zhu TQ, Guan KL (2003a) TSC2 mediates cellular energy response to control cell growth and survival. Cell 115:577-590.

Inoki K, Li Y, Xu T, Guan KL (2003b) Rheb GTPase is a direct target of TSC2 GAP activity and regulates mTOR signaling. Genes & development 17:1829-1834.

Isahara K, Ohsawa Y, Kanamori S, Shibata M, Waguri S, Sato N, Gotow T, Watanabe T, Momoi T, Urase K, Kominami E, Uchiyama Y (1999) Regulation of a novel pathway for cell death by lysosomal aspartic and cysteine proteinases. Neuroscience 91:233-249.

Ishii T, Sakurai T, Usami H, Uchida K (2005) Oxidative modification of proteasome: Identification of an oxidation-sensitive subunit in 26 S proteasome. Biochemistry-Us 44:13893-13901.

Ishisaka R, Utsumi T, Kanno T, Arita K, Katunuma N, Akiyama J, Utsumi K (1999) Participation of a cathepsin L-type protease in the activation of caspase-3. Cell Struct Funct 24:465-470.

Islam MI, Nagakannan P, Ogungbola O, Djordjevic J, Albensi BC, Eftekharpour E (2019) Thioredoxin system as a gatekeeper in caspase-6 activation and nuclear lamina integrity: Implications for Alzheimer's disease. Free radical biology & medicine 134:567-580.

Jacobson LS, Lima H, Jr., Goldberg MF, Gocheva V, Tsiperson V, Sutterwala FS, Joyce JA, Gapp BV, Blomen VA, Chandran K, Brummelkamp TR, Diaz-Griffero F, Brojatsch J (2013) Cathepsin-mediated necrosis controls the adaptive immune response by Th2 (T helper type 2)-associated adjuvants. The Journal of biological chemistry 288:7481-7491.

Jain A, Lamark T, Sjottem E, Larsen KB, Awuh JA, Overvatn A, McMahon M, Hayes JD, Johansen T (2010) p62/SQSTM1 is a target gene for transcription factor NRF2 and creates a positive feedback loop by inducing antioxidant response element-driven gene transcription. J Biol Chem 285:22576-22591.

Jakob U, Muse W, Eser M, Bardwell JC (1999) Chaperone activity with a redox switch. Cell 96:341-352.

Jensen DE, Belka GK, Du Bois GC (1998) S-Nitrosoglutathione is a substrate for rat alcohol dehydrogenase class III isoenzyme. Biochemical Journal 331:659-668.

Jiang L, Kon N, Li T, Wang SJ, Su T, Hibshoosh H, Baer R, Gu W (2015) Ferroptosis as a p53-mediated activity during tumour suppression. Nature 520:57-62.

Johansson AC, Appelqvist H, Nilsson C, Kagedal K, Roberg K, Ollinger K (2010) Regulation of apoptosis-associated lysosomal membrane permeabilization. Apoptosis : an international journal on programmed cell death 15:527-540.

Johansson C, Lillig CH, Holmgren A (2004) Human mitochondrial glutaredoxin reduces S-glutathionylated proteins with high affinity accepting electrons from either glutathione or thioredoxin reductase. Journal of Biological Chemistry 279:7537-7543.

Johnston PA, Grandis JR (2011) STAT3 signaling: anticancer strategies and challenges. Molecular interventions 11:18-26.

Joy B, Sivadasan R, Abraham TE, John M, Sobhan PK, Seervi M, T RS (2010) Lysosomal destabilization and cathepsin B contributes for cytochrome c release and caspase activation in embelin-induced apoptosis. Molecular carcinogenesis 49:324-336.

Joza N, Susin SA, Daugas E, Stanford WL, Cho SK, Li CY, Sasaki T, Elia AJ, Cheng HY, Ravagnan L, Ferri KF, Zamzami N, Wakeham A, Hakem R, Yoshida H, Kong YY, Mak

TW, Zuniga-Pflucker JC, Kroemer G, Penninger JM (2001) Essential role of the mitochondrial apoptosis-inducing factor in programmed cell death. Nature 410:549-554.

Ju Y, Wu L, Yang G (2016) Thioredoxin 1 regulation of protein S-desulfhydration. Biochemistry and biophysics reports 5:27-34.

Jung CH, Jun CB, Ro SH, Kim YM, Otto NM, Cao J, Kundu M, Kim DH (2009a) ULK-Atg13-FIP200 Complexes Mediate mTOR Signaling to the Autophagy Machinery. Molecular biology of the cell 20:1992-2003.

Jung M, Lee J, Seo HY, Lim JS, Kim EK (2015) Cathepsin inhibition-induced lysosomal dysfunction enhances pancreatic beta-cell apoptosis in high glucose. PLoS One 10:e0116972.

Jung T, Grune T (2008) The Proteasome and its Role in the Degradation of Oxidized Proteins. IUBMB life 60:743-752.

Jung T, Catalgol B, Grune T (2009b) The proteasomal system. Molecular aspects of medicine 30:191-296.

Jung T, Hohn A, Grune T (2014) The proteasome and the degradation of oxidized proteins: Part II - protein oxidation and proteasomal degradation. Redox biology 2:99-104.

Kaasik A, Rikk T, Piirsoo A, Zharkovsky T, Zharkovsky A (2005) Up-regulation of lysosomal cathepsin L and autophagy during neuronal death induced by reduced serum and potassium. Eur J Neurosci 22:1023-1031.

Kagan VE, Bayir HA, Belikova NA, Kapralov O, Tyurina YY, Tyurin VA, Jiang JF, Stoyanovsky DA, Wipf P, Kochanek PM, Greenberger JS, Pitt B, Shvedova AA, Borisenko G (2009) Cytochrome c/cardiolipin relations in mitochondria: a kiss of death. Free Radical Biology and Medicine 46:1439-1453.

Kagan VE, Tyurin VA, Jiang JF, Tyurina YY, Ritov VB, Amoscato AA, Osipov AN, Belikova NA, Kapralov AA, Kini V, Vlasova II, Zhao Q, Zou MM, Di P, Svistunenko DA, Kurnikov IV, Borisenko GG (2005) Cytochrome c acts as a cardiolipin oxygenase required for release of proapoptotic factors. Nature chemical biology 1:223-232.

Kagedal K, Zhao M, Svensson I, Brunk UT (2001) Sphingosine-induced apoptosis is dependent on lysosomal proteases. The Biochemical journal 359:335-343.

Kagedal K, Johansson AC, Johansson U, Heimlich G, Roberg K, Wang NS, Jurgensmeier JM, Ollinger K (2005) Lysosomal membrane permeabilization during apoptosis--involvement of Bax? International journal of experimental pathology 86:309-321.

Kamakaka RT, Biggins S (2005) Histone variants: deviants? Genes & development 19:295-310.

Kang MW, Jang JY, Choi JY, Kim SH, Oh J, Cho BS, Lee CE (2008) Induction of IFN-gamma gene expression by thioredoxin: positive feed-back regulation of Th1 response by thioredoxin and IFN-gamma. Cellular physiology and biochemistry : international journal of experimental cellular physiology, biochemistry, and pharmacology 21:215-224.

Kang Y, Tiziani S, Park G, Kaul M, Paternostro G (2014) Cellular protection using Flt3 and PI3Kalpha inhibitors demonstrates multiple mechanisms of oxidative glutamate toxicity. Nature communications 5:3672.

Karch J, Schips TG, Maliken BD, Brody MJ, Sargent MA, Kanisicak O, Molkentin JD (2017) Autophagic cell death is dependent on lysosomal membrane permeability through Bax and Bak. eLife 6.

Kastle M, Grune T (2011) Proteins bearing oxidation-induced carbonyl groups are not preferentially ubiquitinated. Biochimie 93:1076-1079.

Kasuno K, Nakamura H, Ono T, Muso E, Yodoi J (2003) Protective roles of thioredoxin, a redox-regulating protein, in renal ischemia/reperfusion injury. Kidney Int 64:1273-1282.

Katsnelson MA, Lozada-Soto KM, Russo HM, Miller BA, Dubyak GR (2016) NLRP3 inflammasome signaling is activated by low-level lysosome disruption but inhibited by extensive lysosome disruption: roles for K+ efflux and Ca2+ influx. American journal of physiology Cell physiology 311:C83-C100.

Kaur G, Mohan P, Pawlik M, DeRosa S, Fajiculay J, Che S, Grubb A, Ginsberg SD, Nixon RA, Levy E (2010) Cystatin C rescues degenerating neurons in a cystatin B-knockout mouse model of progressive myoclonus epilepsy. The American journal of pathology 177:2256-2267.

Kaushik S, Bandyopadhyay U, Sridhar S, Kiffin R, Martinez-Vicente M, Kon M, Orenstein SJ, Wong E, Cuervo AM (2011) Chaperone-mediated autophagy at a glance. Journal of cell science 124:495-499.

Kehrer JP (2000) The Haber-Weiss reaction and mechanisms of toxicity. Toxicology 149:43-50.

Keinan N, Tyomkin D, Shoshan-Barmatz V (2010) Oligomerization of the mitochondrial protein voltage-dependent anion channel is coupled to the induction of apoptosis. Molecular and cellular biology 30:5698-5709.

Keinan N, Pahima H, Ben-Hail D, Shoshan-Barmatz V (2013) The role of calcium in VDAC1 oligomerization and mitochondria-mediated apoptosis. Biochimica et biophysica acta 1833:1745-1754.

Kenig S, Frangez R, Pucer A, Lah T (2011) Inhibition of cathepsin L lowers the apoptotic threshold of glioblastoma cells by up-regulating p53 and transcription of caspases 3 and 7. Apoptosis : an international journal on programmed cell death 16:671-682.

Keszler A, Zhang YH, Hogg N (2010) Reaction between nitric oxide, glutathione, and oxygen in the presence and absence of protein: How are S-nitrosothiols formed? Free Radical Biology and Medicine 48:55-64.

Khalkhali-Ellis Z, Goossens W, Margaryan NV, Hendrix MJ (2014) Cleavage of Histone 3 by Cathepsin D in the involuting mammary gland. PloS one 9:e103230.

Kiermayer C, Northrup E, Schrewe A, Walch A, de Angelis MH, Schoensiegel F, Zischka H, Prehn C, Adamski J, Bekeredjian R, Ivandic B, Kupatt C, Brielmeier M (2015) Heart-Specific Knockout of the Mitochondrial Thioredoxin Reductase (Txnrd2) Induces Metabolic and Contractile Dysfunction in the Aging Myocardium. J Am Heart Assoc 4.

Kikuchi A, Takeda A, Onodera H, Kimpara T, Hisanaga K, Sato N, Nunomura A, Castellani RJ, Perry G, Smith MA, Itoyama Y (2002) Systemic increase of oxidative nucleic acid damage in Parkinson's disease and multiple system atrophy. Neurobiology of disease 9:244-248.

Kim EH, Sohn S, Kwon HJ, Kim SU, Kim MJ, Lee SJ, Choi KS (2007) Sodium selenite induces superoxide-mediated mitochondrial damage and subsequent autophagic cell death in malignant glioma cells. Cancer research 67:6314-6324.

Kim G, Weiss SJ, Levine RL (2014a) Methionine oxidation and reduction in proteins. Biochim Biophys Acta 1840:901-905.

Kim HL, Koedrith P, Lee SM, Kim YJ, Seo YR (2013a) Base excision DNA repair defect in thioredoxin-1 (Trx1)-deficient cells. Mutat Res-Fund Mol M 751:1-7.

Kim J, Kundu M, Viollet B, Guan KL (2011) AMPK and mTOR regulate autophagy through direct phosphorylation of Ulk1. Nature cell biology 13:132-U171.

Kim K, Punj V, Kim JM, Lee S, Ulmer TS, Lu W, Rice JC, An W (2016) MMP-9 facilitates selective proteolysis of the histone H3 tail at genes necessary for proficient osteoclastogenesis. Genes & development 30:208-219.

Kim Y, Jeong IG, You D, Song SH, Suh N, Jang SW, Kim S, Hwang JJ, Kim CS (2014b) Sodium meta-arsenite induces reactive oxygen species-dependent apoptosis, necrosis, and autophagy in both androgen-sensitive and androgen-insensitive prostate cancer cells. Anti-Cancer Drug 25:53-62.

Kim Y, Kim YS, Kim DE, Lee JS, Song JH, Kim HG, Cho DH, Jeong SY, Jin DH, Jang SJ, Seol HS, Suh YA, Lee SJ, Kim CS, Koh JY, Hwang JJ (2013b) BIX-01294 induces autophagy-associated cell death via EHMT2/G9a dysfunction and intracellular reactive oxygen species production. Autophagy 9:2126-2139.

Kim YC, Yamaguchi Y, Kondo N, Masutani H, Yodoi J (2003) Thioredoxin-dependent redox regulation of the antioxidant responsive element (ARE) in electrophile response. Oncogene 22:1860-1865.

Kimura S, Noda T, Yoshimori T (2007) Dissection of the autophagosome maturation process by a novel reporter protein, tandem fluorescent-tagged LC3. Autophagy 3:452-460.

Kirisako T, Ichimura Y, Okada H, Kabeya Y, Mizushima N, Yoshimori T, Ohsumi M, Takao T, Noda T, Ohsumi Y (2000) The reversible modification regulates the membrane-binding state of Apg8/Aut7 essential for autophagy and the cytoplasm to vacuole targeting pathway. The Journal of cell biology 151:263-276.

Kissova I, Deffieu M, Samokhvalov V, Velours G, Bessoule JJ, Manon S, Camougrand N (2006) Lipid oxidation and autophagy in yeast. Free Radical Biology and Medicine 41:1655-1661.

Kobayashi T, Stang E, Fang KS, de Moerloose P, Parton RG, Gruenberg J (1998) A lipid associated with the antiphospholipid syndrome regulates endosome structure and function. Nature 392:193-197.

Kobayashi T, Beuchat MH, Chevallier J, Makino A, Mayran N, Escola JM, Lebrand C, Cosson P, Gruenberg J (2002) Separation and characterization of late endosomal membrane domains. The Journal of biological chemistry 277:32157-32164.

Koegl M, Hoppe T, Schlenker S, Ulrich HD, Mayer TU, Jentsch S (1999) A novel ubiquitination factor, E4, is involved in multiubiquitin chain assembly. Cell 96:635-644.

Kohen R, Nyska A (2002) Oxidation of biological systems: oxidative stress phenomena, antioxidants, redox reactions, and methods for their quantification. Toxicologic pathology 30:620-650.

Koike M, Shibata M, Ohsawa Y, Nakanishi H, Koga T, Kametaka S, Waguri S, Momoi T, Kominami E, Peters C, Figura K, Saftig P, Uchiyama Y (2003) Involvement of two different cell death pathways in retinal atrophy of cathepsin D-deficient mice. Molecular and cellular neurosciences 22:146-161.

Kondratskyi A, Yassine M, Slomianny C, Kondratska K, Gordienko D, Dewailly E, Lehen'kyi V, Skryma R, Prevarskaya N (2014) Identification of ML-9 as a lysosomotropic agent targeting autophagy and cell death. Cell Death Dis 5:e1193.

Korolchuk VI, Mansilla A, Menzies FM, Rubinsztein DC (2009) Autophagy inhibition compromises degradation of ubiquitin-proteasome pathway substrates. Mol Cell 33:517-527.

Kosztelnik M, Kurucz A, Papp D, Jones E, Sigmond T, Barna J, Traka MH, Lorincz T, Szarka A, Banhegyi G, Vellai T, Korcsmaros T, Kapuy O (2019) Suppression of AMPK/aak-2 by NRF2/SKN-1 down-regulates autophagy during prolonged oxidative stress. FASEB J 33:2372-2387.

Kouzarides T (2007) Chromatin modifications and their function. Cell 128:693-705.

Krainz T, Gaschler MM, Lim C, Sacher JR, Stockwell BR, Wipf P (2016) A Mitochondrial-Targeted Nitroxide Is a Potent Inhibitor of Ferroptosis. ACS Cent Sci 2:653-659.

Kroemer G, Levine B (2008) Autophagic cell death: the story of a misnomer. Nat Rev Mol Cell Bio 9:1004-1010.

Kruger E, Kloetzel PM, Enenkel C (2001) 20S proteasome biogenesis. Biochimie 83:289-293.

Kryston TB, Georgiev AB, Pissis P, Georgakilas AG (2011) Role of oxidative stress and DNA damage in human carcinogenesis. Mutat Res-Fund Mol M 711:193-201.

Kubota C, Torii S, Hou N, Saito N, Yoshimoto Y, Imai H, Takeuchi T (2010) Constitutive reactive oxygen species generation from autophagosome/lysosome in neuronal oxidative toxicity. The Journal of biological chemistry 285:667-674.

Kula B, Sobczak A, Kuśka R (2002) A study of the effects of static and ELF magnetic fields on lipid peroxidation products in subcellular S1 fractions. Electromagnetic Biology and Medicine 21:161-168.

Kunchithapautham K, Rohrer B (2007) Apoptosis and autophagy in Photoreceptors exposed to oxidative stress. Autophagy 3:433-441.

Kundra R, Kornfeld S (1999) Asparagine-linked oligosaccharides protect Lamp-1 and Lamp-2 from intracellular proteolysis. The Journal of biological chemistry 274:31039-31046.

Kurbanyan K, Nguyen KL, To P, Rivas EV, Lueras AMK, Kosinski C, Steryo M, Gonzalez A, Mah DA, Stemp EDA (2003) DNA-protein cross-linking via guanine oxidation: Dependence upon protein and photosensitizer. Biochemistry-Us 42:10269-10281.

Kurz T, Eaton JW, Brunk UT (2010) Redox activity within the lysosomal compartment: implications for aging and apoptosis. Antioxidants & redox signaling 13:511-523.

Kurz T, Eaton JW, Brunk UT (2011) The role of lysosomes in iron metabolism and recycling. The international journal of biochemistry & cell biology 43:1686-1697.

Kurz T, Terman A, Gustafsson B, Brunk UT (2008) Lysosomes in iron metabolism, ageing and apoptosis. Histochemistry and cell biology 129:389-406.

Lamark T, Kirkin V, Dikic I, Johansen T (2009) NBR1 and p62 as cargo receptors for selective autophagy of ubiquitinated targets. Cell Cycle 8:1986-1990.

Laney JD, Hochstrasser M (1999) Substrate targeting in the ubiquitin system. Cell 97:427-430.

Laurent TC, Moore EC, Reichard P (1964) Enzymatic Synthesis of Deoxyribonucleotides. Iv. Isolation and Characterization of Thioredoxin, the Hydrogen Donor from Escherichia Coli B. The Journal of biological chemistry 239:3436-3444.

Lecker SH, Goldberg AL, Mitch WE (2006) Protein degradation by the ubiquitin-proteasome pathway in normal and disease states. J Am Soc Nephrol 17:1807-1819.

Lee JH, Yu WH, Kumar A, Lee S, Mohan PS, Peterhoff CM, Wolfe DM, Martinez-Vicente M, Massey AC, Sovak G, Uchiyama Y, Westaway D, Cuervo AM, Nixon RA (2010) Lysosomal proteolysis and autophagy require presenilin 1 and are disrupted by Alzheimer-related PS1 mutations. Cell 141:1146-1158.

Lee SH, Elipe MVS, Arora JS, Blair IA (2005) Dioxododecenoic acid: A lipid hydroperoxide-derived bifunctional electrophile responsible for etheno DNA adduct formation. Chemical research in toxicology 18:566-578.

Lefaki M, Papaevgeniou N, Chondrogianni N (2017) Redox regulation of proteasome function. Redox biology 13:452-458.

Lesnefsky EJ, Hoppel CL (2008) Cardiolipin as an oxidative target in cardiac mitochondria in the aged rat. Bba-Bioenergetics 1777:1020-1027.

Levine RL, Moskovitz J, Stadtman ER (2000) Oxidation of methionine in proteins: Roles in antioxidant defense and cellular regulation. IUBMB life 50:301-307.

Levonen AL, Hill BG, Kansanen E, Zhang J, Darley-Usmar VM (2014) Redox regulation of antioxidants, autophagy, and the response to stress: implications for electrophile therapeutics. Free radical biology & medicine 71:196-207.

Lewerenz J, Ates G, Methner A, Conrad M, Maher P (2018) Oxytosis/Ferroptosis-(Re-) Emerging Roles for Oxidative Stress-Dependent Non-apoptotic Cell Death in Diseases of the Central Nervous System. Frontiers in neuroscience 12:214.

Li H, Wang P, Sun QH, Ding WX, Yin XM, Sobol RW, Stolz DB, Yu J, Zhang L (2011) Following Cytochrome c Release, Autophagy Is Inhibited during Chemotherapy-Induced Apoptosis by Caspase 8-Mediated Cleavage of Beclin 1. Cancer research 71:3625-3634.

Li L, Chen YQ, Gibson SB (2013a) Starvation-induced autophagy is regulated by mitochondrial reactive oxygen species leading to AMPK activation. Cell Signal 25:50-65.

Li L, Chen Y, Gibson SB (2013b) Starvation-induced autophagy is regulated by mitochondrial reactive oxygen species leading to AMPK activation. Cell Signal 25:50-65.

Li L, Gao L, Song Y, Qin ZH, Liang Z (2016a) Activated cathepsin L is associated with the switch from autophagy to apoptotic death of SH-SY5Y cells exposed to 6-hydroxydopamine. Biochem Biophys Res Commun 470:579-585.

Li W, Yuan XM, Olsson AG, Brunk UT (1998) Uptake of oxidized LDL by macrophages results in partial lysosomal enzyme inactivation and relocation. Arteriosclerosis, thrombosis, and vascular biology 18:177-184.

Li W, Yuan X, Nordgren G, Dalen H, Dubowchik GM, Firestone RA, Brunk UT (2000) Induction of cell death by the lysosomotropic detergent MSDH. FEBS letters 470:35-39.

Li WW, Li J, Bao JK (2012) Microautophagy: lesser-known self-eating. Cellular and molecular life sciences : CMLS 69:1125-1136.

Li Y, Inoki K, Guan KL (2004) Biochemical and functional characterizations of small GTPase Rheb and TSC2 GAP activity. Molecular and cellular biology 24:7965-7975.

Li Y, Chen B, Zou W, Wang X, Wu Y, Zhao D, Sun Y, Liu Y, Chen L, Miao L, Yang C (2016b) The lysosomal membrane protein SCAV-3 maintains lysosome integrity and adult longevity. The Journal of cell biology 215:167-185.

Lin Y, Epstein DL, Liton PB (2010) Intralysosomal iron induces lysosomal membrane permeabilization and cathepsin D–mediated cell death in trabecular meshwork cells exposed to oxidative stress. Investigative ophthalmology & visual science 51:6483-6495.

Lin YX, Gao YJ, Wang Y, Qiao ZY, Fan G, Qiao SL, Zhang RX, Wang L, Wang H (2015) pH-Sensitive Polymeric Nanoparticles with Gold(I) Compound Payloads Synergistically Induce Cancer Cell Death through Modulation of Autophagy. Mol Pharm 12:2869-2878.

Linard D, Kandlbinder A, Degand H, Morsomme P, Dietz KJ, Knoops B (2009) Redox characterization of human cyclophilin D: Identification of a new mammalian mitochondrial redox sensor? Archives of biochemistry and biophysics 491:39-45.

Lippai M, Low P (2014a) The role of the selective adaptor p62 and ubiquitin-like proteins in autophagy. Biomed Res Int 2014:832704.

Lippai M, Low P (2014b) The Role of the Selective Adaptor p62 and Ubiquitin-Like Proteins in Autophagy. Biomed Res Int.

Liu H, Nishitoh H, Ichijo H, Kyriakis JM (2000) Activation of apoptosis signal-regulating kinase 1 (ASK1) by tumor necrosis factor receptor-associated factor 2 requires prior dissociation of the ASK1 inhibitor thioredoxin. Mol Cell Biol 20:2198-2208.

Liu S, Li Y, Choi HMC, Sarkar C, Koh EY, Wu J, Lipinski MM (2018) Lysosomal damage after spinal cord injury causes accumulation of RIPK1 and RIPK3 proteins and potentiation of necroptosis. Cell death & disease 9:476.

Liu Z, Jing Y, Yin J, Mu J, Yao T, Gao L (2013) Downregulation of thioredoxin reductase 1 expression in the substantia nigra pars compacta of Parkinson's disease mice. Neural regeneration research 8:3275-3283.

Lorincz P, Juhasz G (2019) Autophagosome-Lysosome Fusion. Journal of molecular biology.

Lovell MA, Xie C, Gabbita SP, Markesbery WR (2000) Decreased thioredoxin and increased thioredoxin reductase levels in Alzheimer's disease brain. Free radical biology & medicine 28:418-427.

Lowe J, Blanchard A, Morrell K, Lennox G, Reynolds L, Billett M, Landon M, Mayer RJ (1988) Ubiquitin Is a Common Factor in Intermediate Filament Inclusion-Bodies of Diverse Type

in Man, Including Those of Parkinsons-Disease, Picks Disease, and Alzheimers-Disease, as Well as Rosenthal Fibers in Cerebellar Astrocytomas, Cytoplasmic Bodies in Muscle, and Mallory Bodies in Alcoholic Liver-Disease. J Pathol 155:9-15.

Lu B, Chen XB, Hong YC, Zhu H, He QJ, Yang B, Ying MD, Cao J (2019) Identification of PRDX6 as a regulator of ferroptosis. Acta Pharmacol Sin 40:1334-1342.

Lu J, Chew EH, Holmgren A (2007) Targeting thioredoxin reductase is a basis for cancer therapy by arsenic trioxide. Proc Natl Acad Sci U S A 104:12288-12293.

Lu KF, Psakhye I, Jentsch S (2014) Autophagic Clearance of PolyQ Proteins Mediated by Ubiquitin-Atg8 Adaptors of the Conserved CUET Protein Family. Cell 158:549-563.

Luft JH (1961) Improvements in epoxy resin embedding methods. J Biophys Biochem Cytol 9:409-414.

Luo CL, Chen XP, Yang R, Sun YX, Li QQ, Bao HJ, Cao QQ, Ni H, Qin ZH, Tao LY (2010) Cathepsin B contributes to traumatic brain injury-induced cell death through a mitochondria-mediated apoptotic pathway. Journal of neuroscience research 88:2847-2858.

Lushchak VI (2014) Free radicals, reactive oxygen species, oxidative stress and its classification. Chemico-biological interactions 224:164-175.

Maejima Y, Kyoi S, Zhai PY, Liu T, Li H, Ivessa A, Sciarretta S, Del Re DP, Zablocki DK, Hsu CP, Lim DS, Isobe M, Sadoshima J (2013) Mst1 inhibits autophagy by promoting the interaction between Beclin1 and Bcl-2. Nat Med 19:1478-+.

Mahmood T, Yang PC (2012) Western blot: technique, theory, and trouble shooting. N Am J Med Sci 4:429-434.

Mai TT, Hamaï A, Hienzsch A, Cañeque T, Müller S, Wicinski J, Cabaud O, Leroy C, David A, Acevedo V (2017) Salinomycin kills cancer stem cells by sequestering iron in lysosomes. Nature chemistry 9:1025.

Maiuri MC, Zalckvar E, Kimchi A, Kroemer G (2007a) Self-eating and self-killing: crosstalk between autophagy and apoptosis. Nature reviews Molecular cell biology 8:741-752.

Maiuri MC, Le Toumelin G, Criollo A, Rain JC, Gautier F, Juin P, Tasdemir E, Pierron G, Troulinaki K, Tavernarakis N, Hickman JA, Geneste O, Kroemer G (2007b) Functional and physical interaction between Bcl-X-L and a BH3-like domain in Beclin-1. Embo Journal 26:2527-2539.

Man SM, Kanneganti TD (2016) Regulation of lysosomal dynamics and autophagy by CTSB/cathepsin B. Autophagy 12:2504-2505.

Mancias JD, Wang XX, Gygi SP, Harper JW, Kimmelman AC (2014) Quantitative proteomics identifies NCOA4 as the cargo receptor mediating ferritinophagy. Nature 509:105-+.

Mandal P, Azad GK, Tomar RS (2012) Identification of a novel histone H3 specific protease activity in nuclei of chicken liver. Biochemical and biophysical research communications 421:261-267.

Manohar S, Jacob S, Wang J, Wiechecki KA, Koh HWL, Simoes V, Choi H, Vogel C, Silva GM (2019) Polyubiquitin Chains Linked by Lysine Residue 48 (K48) Selectively Target Oxidized Proteins In Vivo. Antioxid Redox Signal 31:1133-1149.

Marengo B, De Ciucis C, Verzola D, Pistoia V, Raffaghello L, Patriarca S, Balbis E, Traverso N, Cottalasso D, Pronzato MA, Marinari UM, Domenicotti C (2008) Mechanisms of BSO (L-buthionine-S,R-sulfoximine)-induced cytotoxic effects in neuroblastoma. Free radical biology & medicine 44:474-482.

Marino G, Niso-Santano M, Baehrecke EH, Kroemer G (2014) Self-consumption: the interplay of autophagy and apoptosis. Nature reviews Molecular cell biology 15:81-94.

Martina JA, Chen Y, Gucek M, Puertollano R (2012) MTORC1 functions as a transcriptional regulator of autophagy by preventing nuclear transport of TFEB. Autophagy 8:903-914.

Martinez A, Portero-Otin M, Pamplona R, Ferrer I (2010) Protein Targets of Oxidative Damage in Human Neurodegenerative Diseases with Abnormal Protein Aggregates. Brain Pathol 20:281-297.

Marzano C, Gandin V, Folda A, Scutari G, Bindoli A, Rigobello MP (2007) Inhibition of thioredoxin reductase by auranofin induces apoptosis in cisplatin-resistant human ovarian cancer cells. Free radical biology & medicine 42:872-881.

Matsui M, Oshima M, Oshima H, Takaku K, Maruyama T, Yodoi J, Taketo MM (1996) Early embryonic lethality caused by targeted disruption of the mouse thioredoxin gene. Developmental biology 178:179-185.

Matte A, De Falco L, Iolascon A, Mohandas N, An X, Siciliano A, Leboeuf C, Janin A, Bruno M, Choi SY, Kim DW, De Franceschi L (2015) The Interplay Between Peroxiredoxin-2 and Nuclear Factor-Erythroid 2 Is Important in Limiting Oxidative Mediated Dysfunction in beta-Thalassemic Erythropoiesis. Antioxid Redox Signal 23:1284-1297.

Mazure NM (2016) News about VDAC1 in Hypoxia. Frontiers in oncology 6:193.

McNaught KSP, Jenner P (2001) Proteasomal function is impaired in substantia nigra in Parkinson's disease. Neurosci Lett 297:191-194.

Mercer CA, Kaliappan A, Dennis PB (2009) A novel, human Atg13 binding protein, Atg101, interacts with ULK1 and is essential for macroautophagy. Autophagy 5:649-662.

Mindell JA (2012) Lysosomal acidification mechanisms. Annual review of physiology 74:69-86.

Mironczuk-Chodakowska I, Witkowska AM, Zujko ME (2018) Endogenous non-enzymatic antioxidants in the human body. Adv Med Sci-Poland 63:68-78.

Mirzaei H, Regnier F (2006) Creation of allotypic active sites during oxidative stress. J Proteome Res 5:2159-2168.

Mitchell DA, Marletta MA (2005) Thioredoxin catalyzes the S-nitrosation of the caspase-3 active site cysteine. Nature chemical biology 1:154-158.

Mitchell DA, Morton SU, Fernhoff NB, Marletta MA (2007) Thioredoxin is required for S-nitrosation of procaspase-3 and the inhibition of apoptosis in Jurkat cells. Proceedings of the National Academy of Sciences of the United States of America 104:11609-11614.

Mizushima N, Yoshimori T (2007) How to interpret LC3 immunoblotting. Autophagy 3:542-545.

Mizushima N, Yoshimori T, Ohsumi Y (2011) The Role of Atg Proteins in Autophagosome Formation. Annu Rev Cell Dev Bi 27:107-132.

Mobius W, van Donselaar E, Ohno-Iwashita Y, Shimada Y, Heijnen HF, Slot JW, Geuze HJ (2003) Recycling compartments and the internal vesicles of multivesicular bodies harbor most of the cholesterol found in the endocytic pathway. Traffic 4:222-231.

Molaei S, Roudkenar MH, Amiri F, Harati MD, Bahadori M, Jaleh F, Jalili MA, Roushandeh AM (2015) Down-regulation of the autophagy gene, ATG7, protects bone marrow-derived mesenchymal stem cells from stressful conditions. Blood Res 50:80-86.

Moon KH, Hood BL, Mukhopadhyay P, Rajesh M, Abdelmegeed MA, Kwon YI, Conrads TP, Veenstra TD, Song BJ, Pacher P (2008) Oxidative inactivation of key mitochondrial proteins leads to dysfunction and injury in hepatic ischemia reperfusion. Gastroenterology 135:1344-1357.

Mora R, Dokic I, Kees T, Huber CM, Keitel D, Geibig R, Brugge B, Zentgraf H, Brady NR, Regnier-Vigouroux A (2010) Sphingolipid rheostat alterations related to transformation can

be exploited for specific induction of lysosomal cell death in murine and human glioma. Glia 58:1364-1383.

Mrschtik M, Ryan KM (2015) Lysosomal proteins in cell death and autophagy. The FEBS journal 282:1858-1870.

Munro D, Banh S, Sotiri E, Tamanna N, Treberg JR (2016) The thioredoxin and glutathione-dependent H2O2 consumption pathways in muscle mitochondria: Involvement in H2O2 metabolism and consequence to H2O2 efflux assays. Free Radic Biol Med 96:334-346.

Muri J, Heer S, Matsushita M, Pohlmeier L, Tortola L, Fuhrer T, Conrad M, Zamboni N, Kisielow J, Kopf M (2018) The thioredoxin-1 system is essential for fueling DNA synthesis during T-cell metabolic reprogramming and proliferation. Nature communications 9.

Mustacich D, Powis G (2000) Thioredoxin reductase. Biochem J 346 Pt 1:1-8.

Myers BM, Prendergast FG, Holman R, Kuntz SM, Larusso NF (1993) Alterations in hepatocyte lysosomes in experimental hepatic copper overload in rats. Gastroenterology 105:1814-1823.

Nadeau PJ, Charette SJ, Toledano MB, Landry J (2007) Disulfide Bond-mediated multimerization of Ask1 and its reduction by thioredoxin-1 regulate H(2)O(2)-induced c-Jun NH(2)-terminal kinase activation and apoptosis. Molecular biology of the cell 18:3903-3913.

Nagakannan P, Eftekharpour E (2017a) Differential redox sensitivity of cathepsin B and L holds the key to autophagy-apoptosis interplay after Thioredoxin reductase inhibition in nutritionally stressed SH-SY5Y cells. Free Radical Biology and Medicine 108:819-831.

Nagakannan P, Eftekharpour E (2017b) Differential redox sensitivity of cathepsin B and L holds the key to autophagy-apoptosis interplay after Thioredoxin reductase inhibition in nutritionally stressed SH-SY5Y cells. Free radical biology & medicine 108:819-831.

Nagakannan P, Islam MI, Karimi-Abdolrezaee S, Eftekharpour E (2019) Inhibition of VDAC1 Protects Against Glutamate-Induced Oxytosis and Mitochondrial Fragmentation in Hippocampal HT22 Cells. Cellular and molecular neurobiology 39:73-85.

Nagakannan P, Iqbal MA, Yeung A, Thliveris JA, Rastegar M, Ghavami S, Eftekharpour E (2016) Perturbation of redox balance after thioredoxin reductase deficiency interrupts autophagy-lysosomal degradation pathway and enhances cell death in nutritionally stressed SH-SY5Y cells. Free radical biology & medicine 101:53-70.

Nakamura S, Yoshimori T (2017) New insights into autophagosome-lysosome fusion. Journal of cell science 130:1209-1216.

Nakamura T, Tu SC, Akhtar MW, Sunico CR, Okamoto SI, Lipton SA (2013) Aberrant Protein S-Nitrosylation in Neurodegenerative Diseases. Neuron 78:596-614.

Navarro-Yepes J, Burns M, Anandhan A, Khalimonchuk O, del Razo LM, Quintanilla-Vega B, Pappa A, Panayiotidis MI, Franco R (2014) Oxidative stress, redox signaling, and autophagy: cell death versus survival. Antioxid Redox Signal 21:66-85.

Negre-Salvayre A, Coatrieux C, Ingueneau C, Salvayre R (2008) Advanced lipid peroxidation end products in oxidative damage to proteins. Potential role in diseases and therapeutic prospects for the inhibitors. Brit J Pharmacol 153:6-20.

Neitemeier S, Jelinek A, Laino V, Hoffmann L, Eisenbach I, Eying R, Ganjam GK, Dolga AM, Oppermann S, Culmsee C (2017) BID links ferroptosis to mitochondrial cell death pathways. Redox biology 12:558-570.

Nemchenko A, Chiong M, Turer A, Lavandero S, Hill JA (2011) Autophagy as a therapeutic target in cardiovascular disease. Journal of molecular and cellular cardiology 51:584-593.

Nezis IP, Shravage BV, Sagona AP, Lamark T, Bjorkoy G, Johansen T, Rusten TE, Brech A, Baehrecke EH, Stenmark H (2010) Autophagic degradation of dBruce controls DNA fragmentation in nurse cells during late Drosophila melanogaster oogenesis. J Cell Biol 190:523-531.

Nguyen TT, Stevens MV, Kohr M, Steenbergen C, Sack MN, Murphy E (2011) Cysteine 203 of Cyclophilin D Is Critical for Cyclophilin D Activation of the Mitochondrial Permeability Transition Pore. Journal of Biological Chemistry 286:40184-40192.

Nie C, Tian CH, Zhao LX, Petit PX, Mehrpour M, Chen Q (2008) Cysteine 62 of Bax is critical for its conformational activation and its proapoptotic activity in response to H2O2-induced apoptosis. Journal of Biological Chemistry 283:15359-15369.

Nilsson C, Johansson U, Johansson AC, Kagedal K, Ollinger K (2006) Cytosolic acidification and lysosomal alkalinization during TNF-alpha induced apoptosis in U937 cells. Apoptosis : an international journal on programmed cell death 11:1149-1159.

Nishio C, Yoshida K, Nishiyama K, Hatanaka H, Yamada M (2000) Involvement of cystatin C in oxidative stress-induced apoptosis of cultured rat CNS neurons. Brain Res 873:252-262.

Nishiyama A, Masutani H, Nakamura H, Nishinaka Y, Yodoi J (2001) Redox regulation by thioredoxin and thioredoxin-binding proteins. IUBMB life 52:29-33.

Nomura K, Imai H, Koumura T, Kobayashi T, Nakagawa Y (2000) Mitochondrial phospholipid hydroperoxide glutathione peroxidase inhibits the release of cytochrome c from mitochondria by suppressing the peroxidation of cardiolipin in hypoglycaemia-induced apoptosis. Biochemical Journal 351:183-193.

Nonn L, Williams RR, Erickson RP, Powis G (2003) The absence of mitochondrial thioredoxin 2 causes massive apoptosis, exencephaly, and early embryonic lethality in homozygous mice. Molecular and cellular biology 23:916-922.

Oberacker T, Bajorat J, Ziola S, Schroeder A, Roth D, Kastl L, Edgar BA, Wagner W, Gulow K, Krammer PH (2018) Enhanced expression of thioredoxin-interacting-protein regulates oxidative DNA damage and aging. FEBS letters 592:2297-2307.

Oberle C, Huai J, Reinheckel T, Tacke M, Rassner M, Ekert PG, Buellesbach J, Borner C (2010) Lysosomal membrane permeabilization and cathepsin release is a Bax/Bak-dependent, amplifying event of apoptosis in fibroblasts and monocytes. Cell Death Differ 17:1167-1178.

Oh BM, Lee SJ, Cho HJ, Park YS, Kim JT, Yoon SR, Lee SC, Lim JS, Kim BY, Choe YK, Lee HG (2017) Cystatin SN inhibits auranofin-induced cell death by autophagic induction and ROS regulation via glutathione reductase activity in colorectal cancer. Cell Death Dis 8:e2682.

Oku Y, Murakami K, Irie K, Hoseki J, Sakai Y (2017) Synthesized Aβ42 caused intracellular oxidative damage, leading to cell death, via lysosome Rupture. Cell structure and function:17006.

Olsen BN, Schlesinger PH, Ory DS, Baker NA (2012) Side-chain oxysterols: from cells to membranes to molecules. Biochimica et biophysica acta 1818:330-336.

Ono K, Kim SO, Han J (2003) Susceptibility of lysosomes to rupture is a determinant for plasma membrane disruption in tumor necrosis factor alpha-induced cell death. Mol Cell Biol 23:665-676.

Orenstein SJ, Cuervo AM (2010) Chaperone-mediated autophagy: Molecular mechanisms and physiological relevance. Semin Cell Dev Biol 21:719-726.

Orvedahl A, Sumpter R, Xiao GH, Ng A, Zou ZJ, Tang Y, Narimatsu M, Gilpin C, Sun QH, Roth M, Forst CV, Wrana JL, Zhang YE, Luby-Phelps K, Xavier RJ, Xie Y, Levine B (2011) Image-based genome-wide siRNA screen identifies selective autophagy factors. Nature 480:113-117.

Oslowski CM, Hara T, O'Sullivan-Murphy B, Kanekura K, Lu S, Hara M, Ishigaki S, Zhu LJ, Hayashi E, Hui ST, Greiner D, Kaufman RJ, Bortell R, Urano F (2012) Thioredoxin-interacting protein mediates ER stress-induced beta cell death through initiation of the inflammasome. Cell Metab 16:265-273.

Pacheco FJ, Servin J, Dang D, Kim J, Molinaro C, Daniels T, Brown-Bryan TA, Imoto-Egami M, Casiano CA (2005) Involvement of lysosomal cathepsins in the cleavage of DNA topoisomerase I during necrotic cell death. Arthritis and rheumatism 52:2133-2145.

Pagliarini V, Wirawan E, Romagnoli A, Ciccosanti F, Lisi G, Lippens S, Cecconi F, Fimia GM, Vandenabeele P, Corazzari M, Piacentini M (2012) Proteolysis of Ambra1 during apoptosis has a role in the inhibition of the autophagic pro-survival response. Cell death and differentiation 19:1495-1504.

Pajares M, Jimenez-Moreno N, Dias IHK, Debelec B, Vucetic M, Fladmark KE, Basaga H, Ribaric S, Milisav I, Cuadrado A (2015) Redox control of protein degradation. Redox biology 6:409-420.

Pamenter ME, Perkins GA, Gu XQ, Ellisman MH, Haddad GG (2013) DIDS (4,4-diisothiocyanatostilbenedisulphonic acid) induces apoptotic cell death in a hippocampal neuronal cell line and is not neuroprotective against ischemic stress. PloS one 8:e60804.

Pan S, Berk BC (2007) Glutathiolation regulates tumor necrosis factor-alpha-induced caspase-3 cleavage and apoptosis - Key role for glutaredoxin in the death pathway. Circ Res 100:213-219.

Pandey S, Lopez C, Jammu A (2003) Oxidative stress and activation of proteasome protease during serum deprivation-induced apoptosis in rat hepatoma cells; inhibition of cell death by melatonin. Apoptosis 8:497-508.

Pandian N, Eftekharpour E (2017) 98 - Lysosomal Permeabilization Facilitate Mitochondria-mediated Cell Death in Ferroptosis and Oxytosis. Free Radical Biology and Medicine 112:76-77.

Pankiv S, Clausen TH, Lamark T, Brech A, Bruun JA, Outzen H, Overvatn A, Bjorkoy G, Johansen T (2007) p62/SQSTM1 binds directly to Atg8/LC3 to facilitate degradation of ubiquitinated protein aggregates by autophagy. The Journal of biological chemistry 282:24131-24145.

Paradies G, Petrosillo G, Paradies V, Ruggiero FM (2009) Role of cardiolipin peroxidation and Ca2+ in mitochondrial dysfunction and disease. Cell calcium 45:643-650.

Park HA, Khanna S, Rink C, Gnyawali S, Roy S, Sen CK (2009) Glutathione disulfide induces neural cell death via a 12-lipoxygenase pathway. Cell death and differentiation 16:1167-1179.

Park JM, Seo M, Jung CH, Grunwald D, Stone M, Otto NM, Toso E, Ahn Y, Kyba M, Griffin TJ, Higgins L, Kim DH (2018) ULK1 phosphorylates Ser30 of BECN1 in association with ATG14 to stimulate autophagy induction. Autophagy 14:584-597.

Patlevic P, Vaskova J, Svorc P, Jr., Vasko L, Svorc P (2016) Reactive oxygen species and antioxidant defense in human gastrointestinal diseases. Integrative medicine research 5:250-258.

Pattingre S, Tassa A, Qu XP, Garuti R, Liang XH, Mizushima N, Packer M, Schneider MD, Levine B (2005) Bcl-2 antiapoptotic proteins inhibit Beclin 1-dependent autophagy. Cell 122:927-939.

Paulsen M, Ussat S, Jakob M, Scherer G, Lepenies I, Schutze S, Kabelitz D, Adam-Klages S (2008) Interaction with XIAP prevents full caspase-3/-7 activation in proliferating human T lymphocytes. European journal of immunology 38:1979-1987.

Perez-Perez ME, Lemaire SD, Crespo JL (2016) Control of Autophagy in Chlamydomonas Is Mediated through Redox-Dependent Inactivation of the ATG4 Protease. Plant physiology 172:2219-2234.

Perez-Perez ME, Zaffagnini M, Marchand CH, Crespo JL, Lemaire SD (2014) The yeast autophagy protease Atg4 is regulated by thioredoxin. Autophagy 10:1953-1964.

Perez VI, Cortez LA, Lew CM, Rodriguez M, Webb CR, Van Remmen H, Chaudhuri A, Qi WB, Lee S, Bokov A, Fok W, Jones D, Richardson A, Yodoi J, Zhang Y, Tominaga K, Hubbard GB, Ikeno Y (2011) Thioredoxin 1 Overexpression Extends Mainly the Earlier Part of Life Span in Mice. J Gerontol a-Biol 66:1286-1299.

Persson HL, Yu Z, Tirosh O, Eaton JW, Brunk UT (2003) Prevention of oxidant-induced cell death by lysosomotropic iron chelators. Free radical biology & medicine 34:1295-1305.

Peskin AV, Pace PE, Behring JB, Paton LN, Soethoudt M, Bachschmid MM, Winterbourn CC (2016) Glutathionylation of the Active Site Cysteines of Peroxiredoxin 2 and Recycling by Glutaredoxin. The Journal of biological chemistry 291:3053-3062.

Pickering AM, Lehr M, Gendron CM, Pletcher SD, Miller RA (2017) Mitochondrial thioredoxin reductase 2 is elevated in long-lived primate as well as rodent species and extends fly mean lifespan. Aging Cell 16:683-692.

Piper RC, Katzmann DJ (2007) Biogenesis and function of multivesicular bodies. Annual review of cell and developmental biology 23:519-547.

Pirkmajer S, Chibalin AV (2011) Serum starvation: caveat emptor. Am J Physiol Cell Physiol 301:C272-279.

Pirttila TJ, Lukasiuk K, Hakansson K, Grubb A, Abrahamson M, Pitkanen A (2005) Cystatin C modulates neurodegeneration and neurogenesis following status epilepticus in mouse. Neurobiology of disease 20:241-253.

Pizzimenti S, Ciamporcero E, Daga M, Pettazzoni P, Arcaro A, Cetrangolo G, Minelli R, Dianzani C, Lepore A, Gentile F, Barrera G (2013) Interaction of aldehydes derived from lipid peroxidation and membrane proteins. Front Physiol 4.

Pogorzelska A, Zolnowska B, Bartoszewski R (2018) Cysteine cathepsins as a prospective target for anticancer therapies-current progress and prospects. Biochimie 151:85-106.

Porter K, Nallathambi J, Lin Y, Liton PB (2013) Lysosomal basification and decreased autophagic flux in oxidatively stressed trabecular meshwork cells: implications for glaucoma pathogenesis. Autophagy 9:581-594.

Progida C, Bakke O (2016) Bidirectional traffic between the Golgi and the endosomes - machineries and regulation. Journal of cell science 129:3971-3982.

Pucer A, Castino R, Mirkovic B, Falnoga I, Slejkovec Z, Isidoro C, Lah TT (2010) Differential role of cathepsins B and L in autophagy-associated cell death induced by arsenic trioxide in U87 human glioblastoma cells. Biol Chem 391:519-531.

Qiao SX, Dennis M, Song XF, Vadysirisack DD, Salunke D, Nash Z, Yang ZF, Liesa M, Yoshioka J, Matsuzawa S, Shirihai OS, Lee RT, Reed JC, Ellisen LW (2015) A REDD1/TXNIP pro-oxidant complex regulates ATG4B activity to control stress-induced autophagy and sustain exercise capacity. Nature communications 6.

Quiles Del Rey M, Mancias JD (2019) NCOA4-Mediated Ferritinophagy: A Potential Link to Neurodegeneration. Front Neurosci 13:238.

Quinsay MN, Thomas RL, Lee Y, Gustafsson AB (2010) Bnip3-mediated mitochondrial autophagy is independent of the mitochondrial permeability transition pore. Autophagy 6:855-862.

Radi R (2018) Oxygen radicals, nitric oxide, and peroxynitrite: Redox pathways in molecular medicine. Proceedings of the National Academy of Sciences of the United States of America 115:5839-5848.

Rahantaniaina MS, Tuzet A, Mhamdi A, Noctor G (2013) Missing links in understanding redox signaling via thiol/disulfide modulation: how is glutathione oxidized in plants? Front Plant Sci 4.

Rakhit R, Cunningham P, Furtos-Matei A, Dahan S, Qi XF, Crow JP, Cashman NR, Kondejewski LH, Chakrabartty A (2002) Oxidation-induced misfolding and aggregation of superoxide dismutase and its implications for amyotrophic lateral sclerosis. The Journal of biological chemistry 277:47551-47556.

Rastegar M, Hotta A, Pasceri P, Makarem M, Cheung AY, Elliott S, Park KJ, Adachi M, Jones FS, Clarke ID, Dirks P, Ellis J (2009) MECP2 isoform-specific vectors with regulated expression for Rett syndrome gene therapy. PLoS One 4:e6810.

Reczek CR, Chandel NS (2015) ROS-dependent signal transduction. Current opinion in cell biology 33:8-13.

Reczek D, Schwake M, Schroder J, Hughes H, Blanz J, Jin X, Brondyk W, Van Patten S, Edmunds T, Saftig P (2007) LIMP-2 is a receptor for lysosomal mannose-6-phosphate-independent targeting of beta-glucocerebrosidase. Cell 131:770-783.

Reddy SK, Husain K, Schlorff EC, Scott RB, Somani SM (1999) Dose response of ethanol ingestion on antioxidant defense system in rat brain subcellular fractions. Neurotoxicology 20:977-987.

Reddy SP (2008) The antioxidant response element and oxidative stress modifiers in airway diseases. Curr Mol Med 8:376-383.

Reeg S, Grune T (2015) Protein Oxidation in Aging: Does It Play a Role in Aging Progression? Antioxidants & redox signaling 23:239-255.

Reiber DC, Murphy RC (2000) Covalent binding of LTA(4) to nucleosides and nucleotides. Archives of biochemistry and biophysics 379:119-126.

Reichard JF, Motz GT, Puga A (2007) Heme oxygenase-1 induction by NRF2 requires inactivation of the transcriptional repressor BACH1. Nucleic Acids Res 35:7074-7086.

Reiners JJ, Jr., Kleinman M, Kessel D, Mathieu PA, Caruso JA (2011) Nonesterified cholesterol content of lysosomes modulates susceptibility to oxidant-induced permeabilization. Free radical biology & medicine 50:281-294.

Reinheckel T, Ullrich O, Sitte N, Grune T (2000) Differential impairment of 20S and 26S proteasome activities in human hematopoietic K562 cells during oxidative stress. Archives of biochemistry and biophysics 377:65-68.

Reinheckel T, Peters C, Kruger A, Turk B, Vasiljeva O (2012) Differential Impact of Cysteine Cathepsins on Genetic Mouse Models of De novo Carcinogenesis: Cathepsin B as Emerging Therapeutic Target. Frontiers in pharmacology 3:133.

Reinheckel T, Sitte N, Ullrich O, Kuckelkorn U, Davies KJA, Grune T (1998) Comparative resistance of the 20S and 26S proteasome to oxidative stress. Biochemical Journal 335:637-642.

Reiser J, Adair B, Reinheckel T (2010) Specialized roles for cysteine cathepsins in health and disease. The Journal of clinical investigation 120:3421-3431.

Ren XY, Zou LL, Zhang X, Branco V, Wang J, Carvalho C, Holmgren A, Lu J (2017) Redox Signaling Mediated by Thioredoxin and Glutathione Systems in the Central Nervous System. Antioxidants & redox signaling 27:989-1010.

Rinne R, Saukko P, Jarvinen M, Lehesjoki AE (2002) Reduced cystatin B activity correlates with enhanced cathepsin activity in progressive myoclonus epilepsy. Annals of medicine 34:380-385.

Roberg K, Ollinger K (1998) Oxidative stress causes relocation of the lysosomal enzyme cathepsin D with ensuing apoptosis in neonatal rat cardiomyocytes. The American journal of pathology 152:1151-1156.

Roczniak-Ferguson A, Petit CS, Froehlich F, Qian S, Ky J, Angarola B, Walther TC, Ferguson SM (2012) The transcription factor TFEB links mTORC1 signaling to transcriptional control of lysosome homeostasis. Science signaling 5:ra42.

Rodenburg RNP, Snijder J, van de Waterbeemd M, Schouten A, Granneman J, Heck AJR, Gros P (2017) Stochastic palmitoylation of accessible cysteines in membrane proteins revealed by native mass spectrometry. Nature communications 8.

Rodriguez-Franco EJ, Cantres-Rosario YM, Plaud-Valentin M, Romeu R, Rodriguez Y, Skolasky R, Melendez V, Cadilla CL, Melendez LM (2012) Dysregulation of macrophage-secreted cathepsin B contributes to HIV-1-linked neuronal apoptosis. PloS one 7:e36571.

Rousseau A, Bertolotti A (2018) Regulation of proteasome assembly and activity in health and disease. Nat Rev Mol Cell Bio 19:697-712.

Rubinsztein DC, Cuervo AM, Ravikumar B, Sarkar S, Korolchuk V, Kaushik S, Klionsky DJ (2009) In search of an "autophagomometer". Autophagy 5:585-589.

Russell RC, Tian Y, Yuan HX, Park HW, Chang YY, Kim J, Kim H, Neufeld TP, Dillin A, Guan KL (2013) ULK1 induces autophagy by phosphorylating Beclin-1 and activating VPS34 lipid kinase. Nature cell biology 15:741-+.

Saftig P, Hetman M, Schmahl W, Weber K, Heine L, Mossmann H, Koster A, Hess B, Evers M, von Figura K, et al. (1995) Mice deficient for the lysosomal proteinase cathepsin D exhibit progressive atrophy of the intestinal mucosa and profound destruction of lymphoid cells. The EMBO journal 14:3599-3608.

Sakaida I, Kyle ME, Farber JL (1990) Autophagic degradation of protein generates a pool of ferric iron required for the killing of cultured hepatocytes by an oxidative stress. Mol Pharmacol 37:435-442.

Samuel SM, Thirunavukkarasu M, Penumathsa SV, Koneru S, Zhan L, Maulik G, Sudhakaran PR, Maulik N (2010) Thioredoxin-1 gene therapy enhances angiogenic signaling and reduces ventricular remodeling in infarcted myocardium of diabetic rats. Circulation 121:1244-1255.

Sanderson TH, Raghunayakula S, Kumar R (2015) Release of mitochondrial Opa1 following oxidative stress in HT22 cells. Molecular and cellular neurosciences 64:116-122.

Sandilands E, Serrels B, McEwan DG, Morton JP, Macagno JP, McLeod K, Stevens C, Brunton VG, Langdon WY, Vidal M, Sansom OJ, Dikic I, Wilkinson S, Frame MC (2011) Autophagic targeting of Src promotes cancer cell survival following reduced FAK signalling. Nature cell biology 14:51-60.

Sarkar S, Korolchuk VI, Renna M, Imarisio S, Fleming A, Williams A, Garcia-Arencibia M, Rose C, Luo S, Underwood BR, Kroemer G, O'Kane CJ, Rubinsztein DC (2011) Complex inhibitory effects of nitric oxide on autophagy. Molecular cell 43:19-32.

Saxena G, Chen JQ, Shalev A (2010) Intracellular Shuttling and Mitochondrial Function of Thioredoxin-interacting Protein. Journal of Biological Chemistry 285:3997-4005.

Scherrer K, Bey F (1994) The prosomes (multicatalytic proteinases; proteasomes) and their relationship to the untranslated messenger ribonucleoproteins, the cytoskeleton, and cell differentiation. Progress in nucleic acid research and molecular biology 49:1-64.

Scherz-Shouval R, Elazar Z (2007) ROS, mitochondria and the regulation of autophagy. Trends Cell Biol 17:422-427.

Scherz-Shouval R, Shvets E, Fass E, Shorer H, Gil L, Elazar Z (2007a) Reactive oxygen species are essential for autophagy and specifically regulate the activity of Atg4. EMBO J 26:1749-1760.

Scherz-Shouval R, Shvets E, Fass E, Shorer H, Gil L, Elazar Z (2007b) Reactive oxygen species are essential for autophagy and specifically regulate the activity of Atg4. Embo Journal 26:1749-1760.

Schneider C, Boeglin WE, Yin HY, Porter NA, Brash AR (2008) Intermolecular peroxyl radical reactions during autoxidation of hydroxy and hydroperoxy arachidonic acids generate a novel series of epoxidized products. Chemical research in toxicology 21:895-903.

Schneider M, Forster H, Boersma A, Seiler A, Wehnes H, Sinowatz F, Neumuller C, Deutsch MJ, Walch A, de Angelis MH, Wurst W, Ursini F, Roveri A, Maleszewski M, Maiorino M, Conrad M (2009) Mitochondrial glutathione peroxidase 4 disruption causes male infertility. Faseb Journal 23:3233-3242.

Schotte P, Van Criekinge W, Van de Craen M, Van Loo G, Desmedt M, Grooten J, Cornelissen M, De Ridder L, Vandekerckhove J, Fiers W, Vandenabeele P, Beyaert R (1998) Cathepsin B-mediated activation of the proinflammatory caspase-11. Biochem Biophys Res Commun 251:379-387.

Schulze H, Kolter T, Sandhoff K (2009) Principles of lysosomal membrane degradation: Cellular topology and biochemistry of lysosomal lipid degradation. Biochimica et biophysica acta 1793:674-683.

Schwertassek U, Haque A, Krishnan N, Greiner R, Weingarten L, Dick TP, Tonks NK (2014) Reactivation of oxidized PTP1B and PTEN by thioredoxin 1. FEBS J 281:3545-3558.

Seiler A, Schneider M, Forster H, Roth S, Wirth EK, Culmsee C, Plesnila N, Kremmer E, Radmark O, Wurst W, Bornkamm GW, Schweizer U, Conrad M (2008) Glutathione peroxidase 4 senses and translates oxidative stress into 12/15-lipoxygenase dependent- and AIF-mediated cell death. Cell metabolism 8:237-248.

Sekiguchi A, Kanno H, Ozawa H, Yamaya S, Itoi E (2012) Rapamycin promotes autophagy and reduces neural tissue damage and locomotor impairment after spinal cord injury in mice. J Neurotrauma 29:946-956.

Sendler M, Maertin S, John D, Persike M, Weiss FU, Kruger B, Wartmann T, Wagh P, Halangk W, Schaschke N, Mayerle J, Lerch MM (2016) Cathepsin B Activity Initiates Apoptosis via Digestive Protease Activation in Pancreatic Acinar Cells and Experimental Pancreatitis. J Biol Chem 291:14717-14731.

Sengupta R, Billiar TR, Kagan VE, Stoyanovsky DA (2010) Nitric oxide and thioredoxin type 1 modulate the activity of caspase 8 in HepG2 cells. Biochemical and biophysical research communications 391:1127-1130.

Serrano-Puebla A, Boya P (2016) Lysosomal membrane permeabilization in cell death: new evidence and implications for health and disease. Ann N Y Acad Sci 1371:30-44.

Settembre C, Fraldi A, Medina DL, Ballabio A (2013) Signals from the lysosome: a control centre for cellular clearance and energy metabolism. Nature reviews Molecular cell biology 14:283-296.

Settembre C, Di Malta C, Polito VA, Garcia Arencibia M, Vetrini F, Erdin S, Erdin SU, Huynh T, Medina D, Colella P, Sardiello M, Rubinsztein DC, Ballabio A (2011) TFEB links autophagy to lysosomal biogenesis. Science 332:1429-1433.

Sevenich L, Pennacchio LA, Peters C, Reinheckel T (2006) Human cathepsin L rescues the neurodegeneration and lethality in cathepsin B/L double-deficient mice. Biological chemistry 387:885-891.

Sever S, Altintas MM, Nankoe SR, Moller CC, Ko D, Wei C, Henderson J, del Re EC, Hsing L, Erickson A, Cohen CD, Kretzler M, Kerjaschki D, Rudensky A, Nikolic B, Reiser J (2007) Proteolytic processing of dynamin by cytoplasmic cathepsin L is a mechanism for proteinuric kidney disease. J Clin Invest 117:2095-2104.

Sevrioukova IF (2011) Apoptosis-inducing factor: structure, function, and redox regulation. Antioxidants & redox signaling 14:2545-2579.

Shah R, Shchepinov MS, Pratt DA (2018) Resolving the Role of Lipoxygenases in the Initiation and Execution of Ferroptosis. ACS central science 4:387-396.

Shalev A (2014) Minireview: Thioredoxin-interacting protein: regulation and function in the pancreatic beta-cell. Mol Endocrinol 28:1211-1220.

Shan Y, Guan FQ, Zhao XZ, Wang M, Chen Y, Wang QZ, Feng X (2016) Macranthoside B Induces Apoptosis and Autophagy Via Reactive Oxygen Species Accumulation in Human Ovarian Cancer A2780 Cells. Nutr Cancer 68:280-289.

Shang F, Taylor A (1995) Oxidative Stress and Recovery from Oxidative Stress Are Associated with Altered Ubiquitin-Conjugating and Proteolytic Activities in Bovine Lens Epithelial-Cells. Biochemical Journal 307:297-303.

Shao D, Oka SI, Liu T, Zhai P, Ago T, Sciarretta S, Li H, Sadoshima J (2014) A Redox-Dependent Mechanism for Regulation of AMPK Activation by Thioredoxin1 during Energy Starvation. Cell metabolism 19:232-245.

Shao FY, Du ZY, Ma DL, Chen WB, Fu WY, Ruan BB, Rui W, Zhang JX, Wang S, Wong NS, Xiao H, Li MM, Liu X, Liu QY, Zhou XD, Yan HZ, Wang YF, Chen CY, Liu Z, Chen HY (2015) B5, a thioredoxin reductase inhibitor, induces apoptosis in human cervical cancer cells by suppressing the thioredoxin system, disrupting mitochondrion-dependent pathways and triggering autophagy. Oncotarget 6:30939-30956.

Shen J, Xiang X, Chen L, Wang H, Wu L, Sun Y, Ma L, Gu X, Liu H, Wang L, Yu YN, Shao J, Huang C, Chin YE (2017) JMJD5 cleaves monomethylated histone H3 N-tail under DNA damaging stress. EMBO reports 18:2131-2143.

Shimizu S, Konishi A, Kodama T, Tsujimoto Y (2000) BH4 domain of antiapoptotic Bcl-2 family members closes voltage-dependent anion channel and inhibits apoptotic mitochondrial changes and cell death. Proc Natl Acad Sci U S A 97:3100-3105.

Shoshan-Barmatz V, Mizrachi D (2012) VDAC1: from structure to cancer therapy. Front Oncol 2:164.

Shoshan-Barmatz V, Mizrachi D, Keinan N (2013) Oligomerization of the mitochondrial protein VDAC1: from structure to function and cancer therapy. Progress in molecular biology and translational science 117:303-334.

Shuja S, Cai J, Iacobuzio-Donahue C, Zacks J, Beazley RM, Kasznica JM, O'Hara CJ, Heimann R, Murnane MJ (1999) Cathepsin B activity and protein levels in thyroid carcinoma, Graves' disease, and multinodular goiters. Thyroid : official journal of the American Thyroid Association 9:569-577.

Sies H (2015) Oxidative stress: a concept in redox biology and medicine. Redox biology 4:180-183.

Sitte N, Huber M, Grune T, Ladhoff A, Doecke WD, Von Zglinicki T, Davies KJA (2000) Proteasome inhibition by lipofuscin/ceroid during postmitotic aging of fibroblasts. Faseb Journal 14:1490-1498.

Slatter DA, Avery NC, Bailey AJ (2004) Identification of a new cross-link and unique histidine adduct from bovine serum albumin incubated with malondialdehyde. Journal of Biological Chemistry 279:61-69.

Smith WL, Urade Y, Jakobsson PJ (2011) Enzymes of the Cyclooxygenase Pathways of Prostanoid Biosynthesis. Chem Rev 111:5821-5865.

Sobotic B, Vizovisek M, Vidmar R, Van Damme P, Gocheva V, Joyce JA, Gevaert K, Turk V, Turk B, Fonovic M (2015) Proteomic Identification of Cysteine Cathepsin Substrates Shed from the Surface of Cancer Cells. Molecular & cellular proteomics : MCP 14:2213-2228.

Son JH, Shim JH, Kim KH, Ha JY, Han JY (2012) Neuronal autophagy and neurodegenerative diseases. Exp Mol Med 44:89-98.

Song JS, Cho HH, Lee BJ, Bae YC, Jung JS (2011) Role of thioredoxin 1 and thioredoxin 2 on proliferation of human adipose tissue-derived mesenchymal stem cells. Stem cells and development 20:1529-1537.

Song XB, Liu G, Liu F, Yan ZG, Wang ZY, Liu ZP, Wang L (2017) Autophagy blockade and lysosomal membrane permeabilization contribute to lead-induced nephrotoxicity in primary rat proximal tubular cells. Cell death & disease 8:e2863.

Spector A, Yan GZ, Huang RRC, Mcdermott MJ, Gascoyne PRC, Pigiet V (1988a) The Effect of H2o2 Upon Thioredoxin-Enriched Lens Epithelial-Cells. Journal of Biological Chemistry 263:4984-4990.

Spector A, Yan GZ, Huang RR, McDermott MJ, Gascoyne PR, Pigiet V (1988b) The effect of H2O2 upon thioredoxin-enriched lens epithelial cells. The Journal of biological chemistry 263:4984-4990.

Srinivasula SM, Hegde R, Saleh A, Datta P, Shiozaki E, Chai J, Lee RA, Robbins PD, Fernandes-Alnemri T, Shi Y, Alnemri ES (2001) A conserved XIAP-interaction motif in caspase-9 and Smac/DIABLO regulates caspase activity and apoptosis. Nature 410:112-116.

Stadtman ER, Levine RL (2000) Protein oxidation. Ann Ny Acad Sci 899:191-208.

Stahl S, Reinders Y, Asan E, Mothes W, Conzelmann E, Sickmann A, Felbor U (2007) Proteomic analysis of cathepsin B- and L-deficient mouse brain lysosomes. Biochimica et biophysica acta 1774:1237-1246.

Steenken S, Jovanovic SV (1997) How easily oxidizable is DNA? One-electron reduction potentials of adenosine and guanosine radicals in aqueous solution. J Am Chem Soc 119:617-618.

Stoka V, Turk V, Turk B (2016) Lysosomal cathepsins and their regulation in aging and neurodegeneration. Ageing research reviews 32:22-37.

Strappazzon F, Vietri-Rudan M, Campello S, Nazio F, Florenzano F, Fimia GM, Piacentini M, Levine B, Cecconi F (2011) Mitochondrial BCL-2 inhibits AMBRA1-induced autophagy. The EMBO journal 30:1195-1208.

Strickland E, Hakala K, Thomas PJ, DeMartino GN (2000) Recognition of misfolding proteins by PA700, the regulatory subcomplex of the 26 S proteasome. Journal of Biological Chemistry 275:5565-5572.

Suh DH, Kim MK, Kim HS, Chung HH, Song YS (2013) Mitochondrial permeability transition pore as a selective target for anti-cancer therapy. Frontiers in oncology 3:41.

Sun M, Ouzounian M, de Couto G, Chen M, Yan R, Fukuoka M, Li G, Moon M, Liu Y, Gramolini A, Wells GJ, Liu PP (2013) Cathepsin-L ameliorates cardiac hypertrophy through activation of the autophagy-lysosomal dependent protein processing pathways. J Am Heart Assoc 2:e000191.

Sun Y, Zheng YF, Wang CX, Liu YZ (2018) Glutathione depletion induces ferroptosis, autophagy, and premature cell senescence in retinal pigment epithelial cells. Cell death & disease 9.

Taha TA, El-Alwani M, Hannun YA, Obeid LM (2006) Sphingosine kinase-1 is cleaved by cathepsin B in vitro: identification of the initial cleavage sites for the protease. FEBS letters 580:6047-6054.

Taha TA, Kitatani K, Bielawski J, Cho W, Hannun YA, Obeid LM (2005) Tumor necrosis factor induces the loss of sphingosine kinase-1 by a cathepsin B-dependent mechanism. The Journal of biological chemistry 280:17196-17202.

Tai HC, Serrano-Pozo A, Hashimoto T, Frosch MP, Spires-Jones TL, Hyman BT (2012) The Synaptic Accumulation of Hyperphosphorylated Tau Oligomers in Alzheimer Disease Is

Associated With Dysfunction of the Ubiquitin-Proteasome System. American Journal of Pathology 181:1426-1435.

Takagi Y, Mitsui A, Nishiyama A, Nozaki K, Sono H, Gon Y, Hashimoto N, Yodoi J (1999) Overexpression of thioredoxin in transgenic mice attenuates focal ischemic brain damage. Proceedings of the National Academy of Sciences of the United States of America 96:4131-4136.

Talukdar R, Sareen A, Zhu H, Yuan Z, Dixit A, Cheema H, George J, Barlass U, Sah R, Garg SK, Banerjee S, Garg P, Dudeja V, Dawra R, Saluja AK (2016) Release of Cathepsin B in Cytosol Causes Cell Death in Acute Pancreatitis. Gastroenterology 151:747-758 e745.

Tamhane T, Lllukkumbura R, Lu S, Maelandsmo GM, Haugen MH, Brix K (2016) Nuclear cathepsin L activity is required for cell cycle progression of colorectal carcinoma cells. Biochimie 122:208-218.

Tang D, Kang R, Berghe TV, Vandenabeele P, Kroemer G (2019) The molecular machinery of regulated cell death. Cell research 29:347-364.

Tang MZ, Chen Z, Wu D, Chen LX (2018) Ferritinophagy/ferroptosis: Iron-related newcomers in human diseases. J Cell Physiol 233:9179-9190.

Tang P, Hou H, Zhang L, Lan X, Mao Z, Liu D, He C, Du H (2014) Autophagy reduces neuronal damage and promotes locomotor recovery via inhibition of apoptosis after spinal cord injury in rats. Mol Neurobiol 49:276-287.

Taniguchi M, Ogiso H, Takeuchi T, Kitatani K, Umehara H, Okazaki T (2015) Lysosomal ceramide generated by acid sphingomyelinase triggers cytosolic cathepsin B-mediated degradation of X-linked inhibitor of apoptosis protein in natural killer/T lymphoma cell apoptosis. Cell death & disease 6:e1717.

Tedelind S, Poliakova K, Valeta A, Hunegnaw R, Yemanaberhan EL, Heldin NE, Kurebayashi J, Weber E, Kopitar-Jerala N, Turk B, Bogyo M, Brix K (2010) Nuclear cysteine cathepsin variants in thyroid carcinoma cells. Biological chemistry 391:923-935.

Terada K, Yamada J, Hayashi Y, Wu Z, Uchiyama Y, Peters C, Nakanishi H (2010) Involvement of cathepsin B in the processing and secretion of interleukin-1beta in chromogranin A-stimulated microglia. Glia 58:114-124.

Terman A, Kurz T (2013) Lysosomal iron, iron chelation, and cell death. Antioxidants & redox signaling 18:888-898.

Thanan R, Oikawa S, Hiraku Y, Ohnishi S, Ma N, Pinlaor S, Yongvanit P, Kawanishi S, Murata M (2015) Oxidative Stress and Its Significant Roles in Neurodegenerative Diseases and Cancer. Int J Mol Sci 16:193-217.

Thurston TLM, Ryzhakov G, Bloor S, von Muhlinen N, Randow F (2009) The TBK1 adaptor and autophagy receptor NDP52 restricts the proliferation of ubiquitin-coated bacteria. Nature immunology 10:1215-U1103.

Tian L, Nie H, Zhang Y, Chen Y, Peng Z, Cai M, Wei H, Qin P, Dong H, Xiong L (2014) Recombinant human thioredoxin-1 promotes neurogenesis and facilitates cognitive recovery following cerebral ischemia in mice. Neuropharmacology 77:453-464.

Tian WN, Braunstein LD, Pang J, Stuhlmeier KM, Xi QC, Tian X, Stanton RC (1998) Importance of glucose-6-phosphate dehydrogenase activity for cell growth. The Journal of biological chemistry 273:10609-10617.

Tizon B, Sahoo S, Yu H, Gauthier S, Kumar AR, Mohan P, Figliola M, Pawlik M, Grubb A, Uchiyama Y, Bandyopadhyay U, Cuervo AM, Nixon RA, Levy E (2010) Induction of autophagy by cystatin C: a mechanism that protects murine primary cortical neurons and neuronal cell lines. PloS one 5:e9819.

Tobiume K, Matsuzawa A, Takahashi T, Nishitoh H, Morita K, Takeda K, Minowa O, Miyazono K, Noda T, Ichijo H (2001) ASK1 is required for sustained activations of JNK/p38 MAP kinases and apoptosis. EMBO reports 2:222-228.

Tong Y, Song F (2015) Intracellular calcium signaling regulates autophagy via calcineurin-mediated TFEB dephosphorylation. Autophagy 11:1192-1195.

Torii S, Shintoku R, Kubota C, Yaegashi M, Torii R, Sasaki M, Suzuki T, Mori M, Yoshimoto Y, Takeuchi T, Yamada K (2016) An essential role for functional lysosomes in ferroptosis of cancer cells. The Biochemical journal 473:769-777.

Trachootham D, Lu WQ, Ogasawara MA, Valle NRD, Huang P (2008) Redox regulation of cell survival. Antioxidants & redox signaling 10:1343-1374.

Tran AP, Sundar S, Yu M, Lang BT, Silver J (2018) Modulation of Receptor Protein Tyrosine Phosphatase Sigma Increases Chondroitin Sulfate Proteoglycan Degradation through Cathepsin B Secretion to Enhance Axon Outgrowth. The Journal of neuroscience : the official journal of the Society for Neuroscience 38:5399-5414.

Trujillo M, Ferrer-Sueta G, Thomson L, Flohe L, Radi R (2007) Kinetics of peroxiredoxins and their role in the decomposition of peroxynitrite. Sub-cellular biochemistry 44:83-113.

Tumbarello DA, Manna PT, Allen M, Bycroft M, Arden SD, Kendrick-Jones J, Buss F (2015) The Autophagy Receptor TAX1BP1 and the Molecular Motor Myosin VI Are Required for Clearance of Salmonella Typhimurium by Autophagy. Plos Pathog 11.

Turanov AA, Kehr S, Marino SM, Yoo MH, Carlson BA, Hatfield DL, Gladyshev VN (2010) Mammalian thioredoxin reductase 1: roles in redox homoeostasis and characterization of cellular targets. Biochemical Journal 430:285-293.

Turk B, Dolenc I, Turk V, Bieth JG (1993) Kinetics of the pH-induced inactivation of human cathepsin L. Biochemistry 32:375-380.

Turk B, Dolenc I, Lenarcic B, Krizaj I, Turk V, Bieth JG, Bjork I (1999) Acidic pH as a physiological regulator of human cathepsin L activity. European journal of biochemistry 259:926-932.

Turk V, Turk B, Turk D (2001) Lysosomal cysteine proteases: facts and opportunities. EMBO J 20:4629-4633.

Turk V, Stoka V, Vasiljeva O, Renko M, Sun T, Turk B, Turk D (2012) Cysteine cathepsins: from structure, function and regulation to new frontiers. Biochimica et biophysica acta 1824:68-88.

Tyynela J, Sohar I, Sleat DE, Gin RM, Donnelly RJ, Baumann M, Haltia M, Lobel P (2000) A mutation in the ovine cathepsin D gene causes a congenital lysosomal storage disease with profound neurodegeneration. The EMBO journal 19:2786-2792.

Uhlen M et al. (2015) Proteomics. Tissue-based map of the human proteome. Science 347:1260419.

Ullio C, Casas J, Brunk UT, Sala G, Fabriàs G, Ghidoni R, Bonelli G, Baccino FM, Autelli R (2012) Sphingosine mediates TNFα-induced lysosomal membrane permeabilization and ensuing programmed cell death in hepatoma cells. Journal of lipid research 53:1134-1143.

Underwood BR, Imarisio S, Fleming A, Rose C, Krishna G, Heard P, Quick M, Korolchuk VI, Renna M, Sarkar S, Garcia-Arencibia M, O'Kane CJ, Murphy MP, Rubinsztein DC (2010) Antioxidants can inhibit basal autophagy and enhance neurodegeneration in models of polyglutamine disease. Human molecular genetics 19:3413-3429.

Valko M, Leibfritz D, Moncol J, Cronin MT, Mazur M, Telser J (2007) Free radicals and antioxidants in normal physiological functions and human disease. The international journal of biochemistry & cell biology 39:44-84.

van Leyen K, Siddiq A, Ratan RR, Lo EH (2005) Proteasome inhibition protects HT22 neuronal cells from oxidative glutamate toxicity. Journal of neurochemistry 92:824-830.

Vanden Berghe T, Vanlangenakker N, Parthoens E, Deckers W, Devos M, Festjens N, Guerin CJ, Brunk UT, Declercq W, Vandenabeele P (2010) Necroptosis, necrosis and secondary necrosis converge on similar cellular disintegration features. Cell death and differentiation 17:922-930.

Verhoef LGGC, Lindsten K, Masucci MG, Dantuma NP (2002) Aggregate formation inhibits proteasomal degradation of polyglutamine proteins. Human molecular genetics 11:2689-2700.

Verma S, Dixit R, Pandey KC (2016) Cysteine Proteases: Modes of Activation and Future Prospects as Pharmacological Targets. Frontiers in pharmacology 7:107.

Vieira HLA, Belzacq AS, Haouzi D, Bernassola F, Cohen I, Jacotot E, Ferri KF, El Hamel C, Bartle LM, Melino G, Brenner C, Goldmacher V, Kroemer G (2001) The adenine nucleotide translocator: a target of nitric oxide, peroxynitrite, and 4-hydroxynonenal. Oncogene 20:4305-4316.

Villalpando-Rodriguez GE, Blankstein AR, Konzelman C, Gibson SB (2019) Lysosomal Destabilizing Drug Siramesine and the Dual Tyrosine Kinase Inhibitor Lapatinib Induce a Synergistic Ferroptosis through Reduced Heme Oxygenase-1 (HO-1) Levels. Oxidative Medicine and Cellular Longevity 2019:9561281.

Voronina SG, Barrow SL, Gerasimenko OV, Petersen OH, Tepikin AV (2004) Effects of secretagogues and bile acids on mitochondrial membrane potential of pancreatic acinar cells: comparison of different modes of evaluating DeltaPsim. The Journal of biological chemistry 279:27327-27338.

Vossaert L, Meert P, Scheerlinck E, Glibert P, Van Roy N, Heindryckx B, De Sutter P, Dhaenens M, Deforce D (2014) Identification of histone H3 clipping activity in human embryonic stem cells. Stem cell research 13:123-134.

Wagner JR, Cadet J (2010) Oxidation Reactions of Cytosine DNA Components by Hydroxyl Radical and One-Electron Oxidants in Aerated Aqueous Solutions. Accounts Chem Res 43:564-571.

Walkley SU, Vanier MT (2009) Secondary lipid accumulation in lysosomal disease. Biochimica et biophysica acta 1793:726-736.

Walter C, Clemens LE, Muller AJ, Fallier-Becker P, Proikas-Cezanne T, Riess O, Metzger S, Nguyen HP (2016) Activation of AMPK-induced autophagy ameliorates Huntington disease pathology in vitro. Neuropharmacology.

Wang F, Gomez-Sintes R, Boya P (2018a) Lysosomal membrane permeabilization and cell death. Traffic 19:918-931.

Wang JC, Cui DR, Gu SS, Chen XY, Bi YL, Xiong XF, Zhao YC (2018b) Autophagy regulates apoptosis by targeting NOXA for degradation. Bba-Mol Cell Res 1865:1105-1113.

Wang X, Zhao HF, Zhang GJ (2006) Mechanism of cytosol phospholipase C and sphingomyelinase-induced lysosome destabilization. Biochimie 88:913-922.

Wang XR, Yen J, Kaiser P, Huang L (2010) Regulation of the 26S Proteasome Complex During Oxidative Stress. Science signaling 3.

Wang XR, Chemmama IE, Yu C, Huszagh A, Xu Y, Viner R, Block SA, Cimermancic P, Rychnovsky SD, Ye YH, Sali A, Huang L (2017) The proteasome-interacting Ecm29 protein disassembles the 26S proteasome in response to oxidative stress. Journal of Biological Chemistry 292:16310-16320.

Wang Y, Zhao Y, Wang H, Zhang C, Wang M, Yang Y, Xu X, Hu Z (2020) Histone demethylase KDM3B protects against ferroptosis by upregulating SLC7A11. Febs Open Bio 10:637-643.

Wang ZY, Liu WG, Muharram A, Wu ZY, Lin JH (2014) Neuroprotective effects of autophagy induced by rapamycin in rat acute spinal cord injury model. Neuroimmunomodulation 21:257-267.

Watanabe K, Shibuya S, Ozawa Y, Nojiri H, Izuo N, Yokote K, Shimizu T (2014a) Superoxide Dismutase 1 Loss Disturbs Intracellular Redox Signaling, Resulting in Global Age-Related Pathological Changes. Biomed Res Int.

Watanabe S, Hayakawa T, Wakasugi K, Yamanaka K (2014b) Cystatin C protects neuronal cells against mutant copper-zinc superoxide dismutase-mediated toxicity. Cell death & disease 5:e1497.

Watson WH, Pohl J, Montfort WR, Stuchlik O, Reed MS, Powis G, Jones DP (2003) Redox potential of human thioredoxin 1 and identification of a second dithiol/disulfide motif. The Journal of biological chemistry 278:33408-33415.

Wei DH, Jia XY, Liu YH, Guo FX, Tang ZH, Li XH, Wang Z, Liu LS, Wang GX, Jian ZS, Ruan CG (2013) Cathepsin L stimulates autophagy and inhibits apoptosis of ox-LDL-induced endothelial cells: potential role in atherosclerosis. Int J Mol Med 31:400-406.

Wei MC, Lindsten T, Mootha VK, Weiler S, Gross A, Ashiya M, Thompson CB, Korsmeyer SJ (2000) tBID, a membrane-targeted death ligand, oligomerizes BAK to release cytochrome c. Genes & development 14:2060-2071.

Wei Y, Pattingre S, Sinha S, Bassik M, Levine B (2008a) JNK1-mediated phosphorylation of Bcl-2 regulates starvation-induced autophagy. Molecular cell 30:678-688.

Wei YJ, Sinha S, Levine B (2008b) Dual role of JNK1-mediated phosphorylation of Bcl-2 in autophagy and apoptosis regulation. Autophagy 4:949-951.

Werneburg N, Guicciardi ME, Yin XM, Gores GJ (2004) TNF-alpha-mediated lysosomal permeabilization is FAN and caspase 8/Bid dependent. American journal of physiology Gastrointestinal and liver physiology 287:G436-443.

Werneburg NW, Guicciardi ME, Bronk SF, Gores GJ (2002) Tumor necrosis factor-alpha-associated lysosomal permeabilization is cathepsin B dependent. American journal of physiology Gastrointestinal and liver physiology 283:G947-956.

Werneburg NW, Bronk SF, Guicciardi ME, Thomas L, Dikeakos JD, Thomas G, Gores GJ (2012) Tumor necrosis factor-related apoptosis-inducing ligand (TRAIL) protein-induced lysosomal translocation of proapoptotic effectors is mediated by phosphofurin acidic cluster sorting protein-2 (PACS-2). The Journal of biological chemistry 287:24427-24437.

Wilder CL, Park KY, Keegan PM, Platt MO (2011) Manipulating substrate and pH in zymography protocols selectively distinguishes cathepsins K, L, S, and V activity in cells and tissues. Archives of biochemistry and biophysics 516:52-57.

Williams MV, Wishnok JS, Tannenbaum SR (2007) Covalent adducts arising from the decomposition products of lipid hydroperoxides in the presence of cytochrome c. Chemical research in toxicology 20:767-775.

Williamson KS, Hensley K, Floyd RA (2003) Fluorometric and Colorimetric Assessment of Thiobarbituric Acid-Reactive Lipid Aldehydes in Biological Matrices. In: Methods in

Biological Oxidative Stress (Hensley K, Floyd RA, eds), pp 57-65. Totowa, NJ: Humana Press.

Windelborn JA, Lipton P (2008) Lysosomal release of cathepsins causes ischemic damage in the rat hippocampal slice and depends on NMDA-mediated calcium influx, arachidonic acid metabolism, and free radical production. Journal of neurochemistry 106:56-69.

Wirawan E, Vande Walle L, Kersse K, Cornelis S, Claerhout S, Vanoverberghe I, Roelandt R, De Rycke R, Verspurten J, Declercq W, Agostinis P, Vanden Berghe T, Lippens S, Vandenabeele P (2010) Caspase-mediated cleavage of Beclin-1 inactivates Beclin-1-induced autophagy and enhances apoptosis by promoting the release of proapoptotic factors from mitochondria. Cell death & disease 1.

Wold MS, Lim J, Lachance V, Deng ZQ, Yue ZY (2016) ULK1-mediated phosphorylation of ATG14 promotes autophagy and is impaired in Huntington's disease models. Mol Neurodegener 11.

Wong-Ekkabut J, Xu ZT, Triampo W, Tang IM, Tieleman DP, Monticelli L (2007) Effect of lipid peroxidation on the properties of lipid bilayers: A molecular dynamics study. Biophys J 93:4225-4236.

Wong YC, Holzbaur ELF (2014) Optineurin is an autophagy receptor for damaged mitochondria in parkin-mediated mitophagy that is disrupted by an ALS-linked mutation. Proceedings of the National Academy of Sciences of the United States of America 111:E4439-E4448.

Wood ZA, Schroder E, Robin Harris J, Poole LB (2003) Structure, mechanism and regulation of peroxiredoxins. Trends in biochemical sciences 28:32-40.

Wu CG, Parrott AM, Fu CX, Liu T, Marino SM, Gladyshev VN, Jain MR, Baykal AT, Li Q, Oka S, Sadoshima J, Beuve A, Simmons WJ, Li H (2011) Thioredoxin 1-Mediated Post-Translational Modifications: Reduction, Transnitrosylation, Denitrosylation, and Related Proteomics Methodologies. Antioxidants & redox signaling 15:2565-2604.

Wu G, Fang YZ, Yang S, Lupton JR, Turner ND (2004) Glutathione metabolism and its implications for health. J Nutr 134:489-492.

Wu Z, Geng Y, Lu X, Shi Y, Wu G, Zhang M, Shan B, Pan H, Yuan J (2019) Chaperone-mediated autophagy is involved in the execution of ferroptosis. Proceedings of the National Academy of Sciences of the United States of America 116:2996-3005.

Xie Y, Hou W, Song X, Yu Y, Huang J, Sun X, Kang R, Tang D (2016) Ferroptosis: process and function. Cell death and differentiation 23:369-379.

Xiong Y, Uys JD, Tew KD, Townsend DM (2011) S-Glutathionylation: From Molecular Mechanisms to Health Outcomes. Antioxidants & redox signaling 15:233-270.

Xu H, Ren D (2015) Lysosomal physiology. Annual review of physiology 77:57-80.

Xu HD, Wu D, Gu JH, Ge JB, Wu JC, Han R, Liang ZQ, Qin ZH (2013) The pro-survival role of autophagy depends on Bcl-2 under nutrition stress conditions. PLoS One 8:e63232.

Xu L, Sheng J, Tang Z, Wu X, Yu Y, Guo H, Shen Y, Zhou C, Paraoan L, Zhou J (2005) Cystatin C prevents degeneration of rat nigral dopaminergic neurons: in vitro and in vivo studies. Neurobiology of disease 18:152-165.

Yagoda N, von Rechenberg M, Zaganjor E, Bauer AJ, Yang WS, Fridman DJ, Wolpaw AJ, Smukste I, Peltier JM, Boniface JJ, Smith R, Lessnick SL, Sahasrabudhe S, Stockwell BR (2007) RAS-RAF-MEK-dependent oxidative cell death involving voltage-dependent anion channels. Nature 447:864-868.

Yamashima T, Oikawa S (2009) The role of lysosomal rupture in neuronal death. Progress in neurobiology 89:343-358.

Yang M, Liu E, Tang L, Lei Y, Sun X, Hu J, Dong H, Yang SM, Gao M, Tang B (2018) Emerging roles and regulation of MiT/TFE transcriptional factors. Cell communication and signaling : CCS 16:31.

Yang M, Chen P, Liu J, Zhu S, Kroemer G, Klionsky DJ, Lotze MT, Zeh HJ, Kang R, Tang D (2019a) Clockophagy is a novel selective autophagy process favoring ferroptosis. Science advances 5:eaaw2238.

Yang MY, Xu YJ, Heisner JS, Sun J, Stowe DF, Kwok WM, Camara AKS (2019b) Peroxynitrite nitrates adenine nucleotide translocase and voltage-dependent anion channel 1 and alters their interactions and association with hexokinase II in mitochondria. Mitochondrion 46:380-392.

Yang WS, Stockwell BR (2008) Synthetic lethal screening identifies compounds activating iron-dependent, nonapoptotic cell death in oncogenic-RAS-harboring cancer cells. Chem Biol 15:234-245.

Yang WS, Stockwell BR (2016) Ferroptosis: Death by Lipid Peroxidation. Trends in cell biology 26:165-176.

Yang WS, SriRamaratnam R, Welsch ME, Shimada K, Skouta R, Viswanathan VS, Cheah JH, Clemons PA, Shamji AF, Clish CB, Brown LM, Girotti AW, Cornish VW, Schreiber SL, Stockwell BR (2014) Regulation of ferroptotic cancer cell death by GPX4. Cell 156:317-331.

Yao X, Zhang Y, Hao J, Duan HQ, Zhao CX, Sun C, Li B, Fan BY, Wang X, Li WX, Fu XH, Hu Y, Liu C, Kong XH, Feng SQ (2019) Deferoxamine promotes recovery of traumatic spinal cord injury by inhibiting ferroptosis. Neural regeneration research 14:532-541.

Yi SJ, Kim K (2018) Histone tail cleavage as a novel epigenetic regulatory mechanism for gene expression. BMB reports 51:211-218.

Yin DZ (1996) Biochemical basis of lipofuscin, ceroid, and age pigment-like fluorophores. Free Radical Biology and Medicine 21:871-888.

Yin HY, Xu LB, Porter NA (2011) Free Radical Lipid Peroxidation: Mechanisms and Analysis. Chem Rev 111:5944-5972.

Yoon JH, Ahn SG, Lee BH, Jung SH, Oh SH (2012) Role of autophagy in chemoresistance: regulation of the ATM-mediated DNA-damage signaling pathway through activation of DNA-PKcs and PARP-1. Biochemical pharmacology 83:747-757.

You BR, Shin HR, Han BR, Kim SH, Park WH (2015) Auranofin induces apoptosis and necrosis in HeLa cells via oxidative stress and glutathione depletion. Mol Med Rep 11:1428-1434.

Young MM, Takahashi Y, Khan O, Park S, Hori T, Yun J, Sharma AK, Amin S, Hu CD, Zhang JK, Kester M, Wang HG (2012) Autophagosomal Membrane Serves as Platform for Intracellular Death-inducing Signaling Complex (iDISC)-mediated Caspase-8 Activation and Apoptosis. Journal of Biological Chemistry 287:12455-12468.

Yousefi S, Perozzo R, Schmid I, Ziemiecki A, Schaffner T, Scapozza L, Brunner T, Simon HU (2006) Calpain-mediated cleavage of Atg5 switches autophagy to apoptosis. Nature cell biology 8:1124-U1146.

Yu L, Wan FY, Dutta S, Welsh S, Liu ZH, Freundt E, Baehrecke EH, Lenardo M (2006) Autophagic programmed cell death by selective catalase degradation. Proceedings of the National Academy of Sciences of the United States of America 103:4952-4957.

Yu Z, Li W, Hillman J, Brunk UT (2004) Human neuroblastoma (SH-SY5Y) cells are highly sensitive to the lysosomotropic aldehyde 3-aminopropanal. Brain research 1016:163-169.

Yu ZQ, Ni T, Hong B, Wang HY, Jiang FJ, Zou S, Chen Y, Zheng XL, Klionsky DJ, Liang Y, Xie Z (2012) Dual roles of Atg8-PE deconjugation by Atg4 in autophagy. Autophagy 8:883-892.

Yuan H, Li X, Zhang X, Kang R, Tang D (2016) CISD1 inhibits ferroptosis by protection against mitochondrial lipid peroxidation. Biochemical and biophysical research communications 478:838-844.

Yuste VJ, Moubarak RS, Delettre C, Bras M, Sancho P, Robert N, d'Alayer J, Susin SA (2005) Cysteine protease inhibition prevents mitochondrial apoptosis-inducing factor (AIF) release. Cell death and differentiation 12:1445-1448.

Zalckvar E, Berissi H, Mizrachy L, Idelchuk Y, Koren I, Eisenstein M, Sabanay H, Pinkas-Kramarski R, Kimchi A (2009) DAP-kinase-mediated phosphorylation on the BH3 domain of beclin 1 promotes dissociation of beclin 1 from Bcl-XL and induction of autophagy. EMBO reports 10:285-292.

Zdolsek JM, Olsson GM, Brunk UT (1990) Photooxidative damage to lysosomes of cultured macrophages by acridine orange. Photochemistry and photobiology 51:67-76.

Zeldich E, Chen CD, Colvin TA, Bove-Fenderson EA, Liang J, Tucker Zhou TB, Harris DA, Abraham CR (2014) The neuroprotective effect of Klotho is mediated via regulation of members of the redox system. J Biol Chem 289:24700-24715.

Zhang C, Yang L, Wang XB, Wang JS, Geng YD, Yang CS, Kong LY (2013) Calyxin Y induces hydrogen peroxide-dependent autophagy and apoptosis via JNK activation in human non-small cell lung cancer NCI-H460 cells. Cancer Lett 340:51-62.

Zhang DY, Zhao NJ, Ma B, Wang Y, Zhang GL, Yan XL, Hu SQ, Xu T (2016a) Procaspase-9 induces its cleavage by transnitrosylating XIAP via the Thioredoxin system during cerebral ischemia-reperfusion in rats. Scientific reports 6.

Zhang FL, Casey PJ (1996) Protein prenylation: Molecular mechanisms and functional consequences. Annu Rev Biochem 65:241-269.

Zhang H, Zhong C, Shi L, Guo Y, Fan Z (2009) Granulysin induces cathepsin B release from lysosomes of target tumor cells to attack mitochondria through processing of bid leading to Necroptosis. J Immunol 182:6993-7000.

Zhang X, Cheng X, Yu L, Yang J, Calvo R, Patnaik S, Hu X, Gao Q, Yang M, Lawas M, Delling M, Marugan J, Ferrer M, Xu H (2016b) MCOLN1 is a ROS sensor in lysosomes that regulates autophagy. Nature communications 7:12109.

Zhang Y, Spiess E, Groschup MH, Burkle A (2003) Up-regulation of cathepsin B and cathepsin L activities in scrapie-infected mouse Neuro2a cells. The Journal of general virology 84:2279-2283.

Zhao K, Zhou H, Zhao X, Wolff DW, Tu Y, Liu H, Wei T, Yang F (2012) Phosphatidic acid mediates the targeting of tBid to induce lysosomal membrane permeabilization and apoptosis. Journal of lipid research 53:2102-2114.

Zhou J, Tan SH, Nicolas V, Bauvy C, Yang ND, Zhang J, Xue Y, Codogno P, Shen HM (2013) Activation of lysosomal function in the course of autophagy via mTORC1 suppression and autophagosome-lysosome fusion. Cell Res 23:508-523.

Zhou JB, Chng WJ (2013) Roles of thioredoxin binding protein (TXNIP) in oxidative stress, apoptosis and cancer. Mitochondrion 13:163-169.

Zhou KL, Zhou YF, Wu K, Tian NF, Wu YS, Wang YL, Chen DH, Zhou B, Wang XY, Xu HZ, Zhang XL (2015) Stimulation of autophagy promotes functional recovery in diabetic rats with spinal cord injury. Sci Rep 5:17130.

Zhou RB, Tardivel A, Thorens B, Choi I, Tschopp J (2010) Thioredoxin-interacting protein links oxidative stress to inflammasome activation. Nature immunology 11:136-U151.

Zhu YS, Zhao LX, Liu L, Gao P, Tian WL, Wang XH, Jin HJ, Xu HD, Chen Q (2010) Beclin 1 cleavage by caspase-3 inactivates autophagy and promotes apoptosis. Protein Cell 1:468-477.

Zilka O, Shah R, Li B, Friedmann Angeli JP, Griesser M, Conrad M, Pratt DA (2017) On the Mechanism of Cytoprotection by Ferrostatin-1 and Liproxstatin-1 and the Role of Lipid Peroxidation in Ferroptotic Cell Death. ACS central science 3:232-243.

Zuo X, Hou Q, Jin J, Chen X, Zhan L, Tang Y, Shi Z, Sun W, Xu E (2018) Inhibition of Cathepsins B Induces Neuroprotection Against Secondary Degeneration in Ipsilateral Substantia Nigra After Focal Cortical Infarction in Adult Male Rats. Frontiers in aging neuroscience 10:125.